CORRELATION OF HEAT PIPE PARAMETERS

A THESIS

Presented to

The Faculty of the Division of Graduate

Studies and Research

by

Colquitt Lamar Williams

In Partial Fulfillment

of the Requirements for the Degree

Doctor of Philosophy in the

School of Mechanical Engineering

Georgia Institute of Technology

March, 1973

CORRELATION OF HEAT PIPE PARAMETERS

Approved:

G. T. Colwell, Chairman

N. Zuber

W. Z. Black

J. H. Rust

H. C. Ward

Date Approved by Chairman: 2-28-73

ACKNOWLEDGMENTS

The author gratefully acknowledges the assistance of his thesis advisor, Dr. G. T. Colwell, for continual patience and instructive guidance. The author's initial and continued interests in heat pipes stemmed from Dr. Colwell's encouragements.

The author is indebted to Drs. N. Zuber, J. H. Rust, H. C. Ward, W. Z. Black, and A. E. Bergles for their creative suggestions and constructive criticisms in determining thesis scope and methods. Each professor served diligently on the thesis advisory committee or reading committee.

The author extends special thanks to Dr. S. P. Kezios, Director, School of Mechanical Engineering, for providing financial aid with the NDEA Fellowship and graduate teaching assistantships. Special thanks to Mr. L. A. Cavalli for his help and interests in fabricating the heat pipe systems.

TABLE OF CONTENTS

TABLE OF CONTENTS (Continued)

TABLE OF CONTENTS (Continued)

TABLE OF CONTENTS (Continued)

LIST OF TABLES

LIST OF ILLUSTRATIONS

LIST OF ILLUSTRATIONS (Continued)

LIST OF ILLUSTRATIONS (Continued)

NOMENCLATURE

Latin

a	detailed geometry surface parameter
A	area
A_w	total cross sectional wick area
A_L	effective wick cross sectional area for liquid flow
b	width of wick for rectangular heat pipes
Bi	Biot no. defined by Eq. (II. 40)
C_p	specific heat at constant pressure
Ec	Eckert no.
f_i	i^{th} function, nondimensional
$\bar{f}_i$	i^{th} function, dimensional
g	gravitational acceleration
h	specific enthalpy
h'_l	liquid specific enthalpy as averaged over wick cross section
h_{vl}	latent heat of vaporization
H	unit conductance between outer shell wall and surroundings
K_w	wick specific permeability
K	wick friction factor (inverse permeability)
K_1	reference value of wick friction factor
l	total heat pipe length
l_a	design length of adiabatic section
l_c	design length of condenser section
l_e	design length of evaporator section

NOMENCLATURE (Continued)

Latin

ℓ_{eff}	effective frictional length defined by Eq. (V. 4)
L_c	active length of condenser
L_e	active length of evaporator
$\dot{m}$	mass flow rate
M	dimensionless group defined by Eq. (II. 39)
$\vec{n}_1, \vec{n}_2$	unit normal vectors on liquid-vapor interface, see Figure 8
$\vec{n}_i, \vec{n}_e$	unit normal vectors on pipe boundary, see Figure 8
n	number of layers of mesh screen
P	pressure
p	surface coordinate defined by Eq. (III. 66)
q	surface coordinate defined by Eq. (III. 67)
$\vec{q}$	conduction heat flux vector defined by Eq. (III. 15)
$\dot{Q}$	heat transfer rate
r	radial coordinate from heat pipe centerline
r_c	wick pore radius
r_m	evaporator meniscus radius
r_{min}	minimum evaporator meniscus radius
r_p	outer radius of pipe shell
r_s	radial coordinate on liquid-vapor interface,
r_v	vapor space radius from heat pipe centerline
r_w	outer radius of wick
r_{ws}	wick-solid radius, one half wire diameter for mesh screen
Re	Reynolds number

NOMENCLATURE (Continued)

Latin

R_m	variable meniscus radius
R_{ew}	evaporator wick thermal resistance
R_{cw}	condenser wick thermal resistance
R_{ei}	evaporator interface thermal resistance
R_{ci}	condenser interface thermal resistance
R_v	vapor region thermal resistance
S	vapor flow parameter used in Eq. (II. 8)
$\vec{t}_1, \vec{t}_2$	unit tangent vectors
t	tortuosity used in Eq. (II. 4)
T	temperature
T_c	condenser sink temperature
T_H	evaporator source temperature
T_o	heat pipe operating temperature
T_p	outer pipe shell surface temperature
$\bar{T}_{cw}$	condenser average temperature at outer wick surface
$\bar{T}_{ew}$	evaporator average temperature at outer wick surface
U	unit conductance
U_c	unit conductance between outer wick surface and condenser sink
U_H	unit conductance between outer wick surfaces and evaporator source
u	radial velocity
u_v	vapor reference radial velocity defined by Eq. (III. 2)
u_ℓ	liquid reference radial velocity defined by Eq. (III. 3)
v	angular component of velocity

NOMENCLATURE (Continued)

Latin

$\vec{V}$	velocity vector
$\vec{V}_i$	interfacial velocity vector
V_r	radial component of velocity
w	axial velocity
z	axial coordinate

Greek

γ	vapor radial Reynolds no. defined by Eq. (II. 16)
δ	wick thickness
δ_e	evaporator effective wick thickness
ϵ	wick porosity
η	radial coordinate
η_s	radial coordinate, $\eta = \eta(r, \theta)$
θ	angular coordinate, $\eta_s = \eta_s(r, z)$
κ	thermal conductivity
κ_p	pipe shell thermal conductivity
κ_{eff}	effective liquid-wick thermal conductivity
κ_s	wick solid thermal conductivity
λ	second coefficient of viscosity
μ	absolute viscosity
π	number, 3.14159 ...
π_i	i^{th} dimensionless group
ρ	density

NOMENCLATURE (Continued)

Greek

σ	surface tension
$\bar{\bar{\tau}}$	fluid friction tensor
ϕ_o	fluid contact angle

Subscripts

c	condenser
cp	condenser pipe
e	evaporator
eff	effective
E	environment
H	heat source
i	indice
j	indice
k	indice
ℓ	liquid
ℓ,c	liquid-condenser
ℓ,e	liquid-evaporator
o	reference value
p	pipe
r	radial component
s	Surface; surroundings
v	vapor
v,c	vapor-condenser

NOMENCLATURE (Continued)

Subscripts

v,e	vapor-evaporator
ws	wick-solid
z	axial component
θ	angular component
r	radial component

Superscripts and Overscripts

$*$	ratio of model to prototype
$\bar{G}$	average value of variable G
$\hat{G}$	unit vector in G direction
$\vec{G}$	vector of variable G
$+$	limit from above
$-$	limit from below

Special Operators

∇	gradient
$\nabla\cdot$	divergence
∇_s	surface gradient
$\nabla_s\cdot$	surface divergence
$\cdot$	dot product

NOTE: Symbols which cannot be found here are defined in the respective Appendices.

SUMMARY

An analytical and experimental study is conducted for the purpose of identifying and correlating heat pipe parameters. These parameters are studied under three topics, with each section providing new contributions toward the understanding of heat pipe performance.

Dimensional analysis is applied to a general theory, which yields the first nondimensional writing of the detailed field and constitutive equations for the heat pipe vapor and liquid regions. In addition to these equations, boundary conditions at the liquid-vapor interface and the environment are studied. This overall study results in a new listing of twenty four potentially important dimensionless groups. Included is one previously unidentified group which contains the radius of the wick solid (one half wire diameter for mesh screen).

Experiments are conducted on a horizontal, stainless steel heat pipe, with the wick composed of two layers of mesh screen separated by a thin liquid film. The tests use working fluids of water and methanol for a data range of power, 20 - 350 Btu/hr, and operating temperature, 42 - 73°F. Other data are collected for use in evaluating the parameters required for correlation. Independent parameters, those externally controlled during the tests, are determined to be the condenser sink temperature, unit conductance between outer wick wall and condenser sink, and power delivered to the evaporator.

A correlation theory is analysed for simplification of the general theory. This correlation theory yields a system of solvable equations

for heat pipe performance and identification of significant dimensionless groups. Included in the twenty groups are active length ratios of heat pipe condenser and evaporator sections.

The length along which condensation occurs may differ from the design length, depending on the vapor's axial Reynolds number. The length along which evaporation occurs may differ from the design length, depending on the evaporator meniscus radius. These newly identified dependencies and the solved correlation equations yield predictions of the dependent parameters for cases previously untested, experimental values observed in this investigation, and experimental values from the works of others. Comparisons of correlation theory predictions to experimental values indicate agreement to within 10 per cent.

CHAPTER I

INTRODUCTION

1. Relevance of the Problem

The use of heat pipes in source-sink couplings is of interest to various technologies because many engineering operations require devices with high effective thermal conductivities. Examples of such systems include gas turbine blades, spacecraft radiators, nuclear reactors, electronic components, heat exchangers, and thermionic converters.

In order to design a heat pipe for a particular application, all significant parameters governing heat pipe performance must first be identified and then interpretations made as to which variables are independent, i.e. free variables which the designer may select. Examples of the significant parameters include working fluid properties, geometrical factors, operating temperatures, heat transfer rates, and the areas through which heat flows. A failure to consider all parameters may result in inadequate designs.

2. Advances Required

From the discussion of related investigations in Chapter II it can be concluded that the following advances are required:

1) Establish the listing of significant heat pipe variables and a corresponding list of dimensionless groups.

2) Obtain mathematical models which can correctly predict heat pipe performance below the wicking limit.

3) Present results in a parametric form which are useful to researchers and designers.

4) Corroberate the predicted results with experimental data.

3. Description of the Work

The purpose of this investigation is to study the interrelations between the parameters governing heat pipe performance. Goals are divided into three parts.

A. Analytical

Analytical goals are

1) Write the conservation equations of mass, momentum, and energy for the dynamics of vapor and liquid flow in a heat pipe operating with a single working fluid.

2) Write the conservation equations of mass, momentum, and energy for the liquid-vapor interface and external boundary conditions.

3) Write the necessary constitutive equations.

4) Obtain a listing of dimensionless groups from these equations.

B. Experimental

Experimental goals are

1) Operate a single horizontal heat pipe of fixed geometry first with water as the working fluid and then with methanol.

2) Collect performance data necessary for evaluation of the dimensionless groups required for correlation of the groups.

C. Correlation

Correlation goals are

1) Obtain mathematical models which yield the simplified governing equations for heat pipe operation.

2) Indicate the important dimensionless groups.

3) Provide interpretations for distinguishing between independent and dependent variables.

4) Provide predicted solutions of the governing relations for previously untested combinations of heat pipe variables.

5) Compare predicted values to experimental values obtained in this study and the works of others.

CHAPTER II

RELATED INVESTIGATIONS

The heat pipe concept came into open literature in 1964 when Grover, et al. (11)*, published experimental results. Grover demonstrated that a heat pipe could be successfully operated with working fluids of water and sodium. Since Grover's work, many investigations have been conducted on the heat pipe. Source listings and reviews are found in the works of Cheung (4), Winter and Borsch (38), and Shinnick (32). Analytical and experimental investigations directly related to this study concern the topics of Operating Characteristics and Parameter Studies.

1. Operating Characteristics

Understanding the general heat pipe operating characteristics consists of describing the internal dynamics of energy and mass flow and the corresponding limitations. Analytical and experimental studies have been conducted.

A. Theoretical

The work of Cotter (8) provided the first attempt to analyze the heat pipe. Cotter initiated a quantitative engineering theory for the design and performance analysis of heat pipes. Cotter's model, see

*Numbers in parentheses correspond to references listed in the Bibliography.

Figure 1, consists of a simple heat pipe inclined in a gravity field and having only evaporator and condenser sections, i.e. no adiabatic section.

Cotter expressed conservation of mass in steady state by

$$\nabla \cdot (\rho \vec{V}) = 0 \tag{II.1}$$

for both liquid and vapor regions. Taking the velocity of both fluid phases as zero at the evaporator end of the heat pipe, Cotter integrated Equation (II.1) to obtain

$$\dot{m}_v(z) + \dot{m}_l(z) = 0 \tag{II.2}$$

where $\dot{m}_v$ and $\dot{m}_l$ are the net mass flow rates in the axial direction of the vapor and liquid regions respectively.

Conservation of momentum in steady state was expressed by

$$\nabla P = \rho \vec{g} + \mu \nabla \cdot (\nabla \vec{V}) - \rho \vec{V} \cdot (\nabla \vec{V}) \tag{II.3}$$

while assuming constant viscosity and density for each fluid phase. These assumptions were suitable since Cotter defined the heat pipe operation to take place with small changes in temperature and estimated vapor Mach numbers were low.

For liquid flow, Cotter attempted to simplify Equation (II.3) by 1) averaging the terms over a cross sectional area of the wick with dimensions small compared to the wick thickness and shell dimensions but large compared to the average radius of a pore, r_c, and 2) using simple order of magnitude analyses to indicate negligible inertia terms and radial pressure gradient terms. Under these approximations Cotter

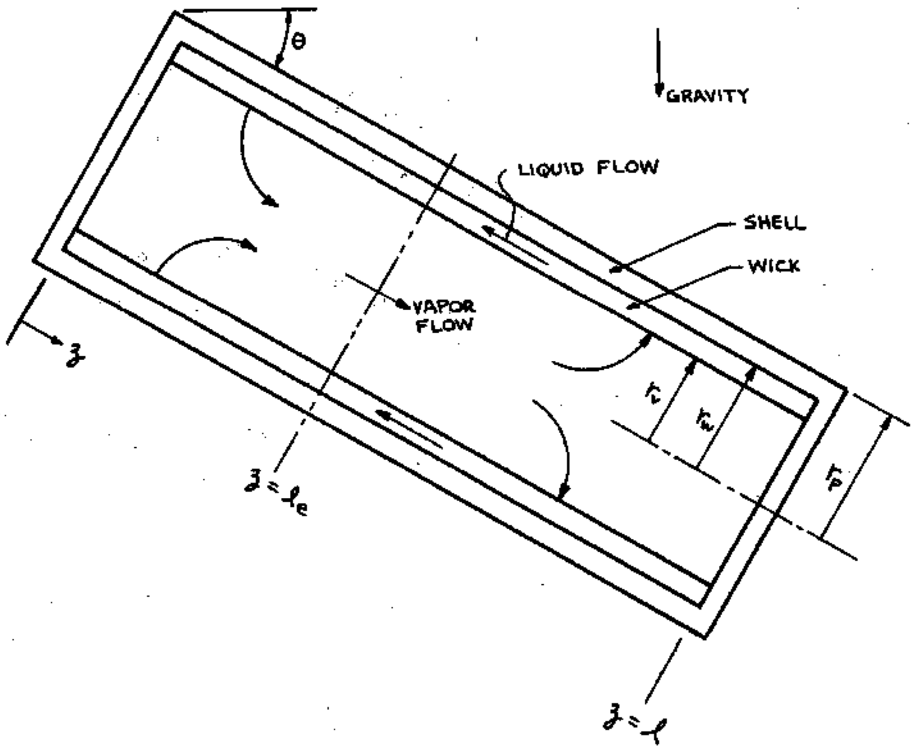

Figure 1. Cotter's Model.

obtained the expression

$$\frac{dP_\ell}{dz} = \rho_\ell g \sin\theta - \frac{t\,\mu_\ell \dot{m}_\ell(z)}{\pi(r_w^2 - r_v^2)\rho_\ell \epsilon r_c^2} \qquad \text{(II.4)}$$

where t and ϵ are dimensionless numbers characterizing the wick geometry by tortuosity and porosity respectively. Cotter referred to Equation (II.4) as a "version of Darcy's law". This was reasonable since Darcy's law for relating the pressure gradient to mass flow rate for flow in a porous media is (27)

$$\frac{dP}{dz} = -\frac{\mu_\ell}{K_w}\frac{\dot{m}_\ell}{\rho_\ell A_\ell} \qquad \text{(II.5)}$$

where K_w is the wick permeability and A_ℓ is the effective flow area of the liquid.

In order to estimate the pressure gradient in the vapor region, Cotter modeled this flow as being dynamically similar to pipe flow with injection or suction through a porous wall. Cotter used the results of Yuan and Finkelstein (39) and Knight and McInteer (15) who studied the problem under the basic assumptions of 1) laminar flow, 2) steady state, 3) constant fluid properties, 4) two dimensional flow, and 5) uniform wall injection or suction velocity. The assumption of uniform wall velocity implies that the wall Reynolds number, γ, defined by

$$\gamma = -\frac{\rho_v r_v V_r}{\mu_v} = \frac{1}{2\pi\mu_v}\frac{d\dot{m}_v}{dz} \qquad \text{(II.6)}$$

is a constant.

For the viscous dominated regime of $|\gamma| \ll 1$ Cotter recommended the expression (39)

$$\frac{dP_v}{dz} = -\frac{8\mu_v \dot{m}_v}{\pi \rho_v r_v^4}\left(1 + \frac{3}{4}\gamma - \frac{11}{270}\gamma^2 + \cdots\right). \qquad \text{(II.7)}$$

This relation had been obtained by a perturbation solution of the momentum and continuity equations under the stated assumptions. In this expression P_v is interpreted as the pressure of the vapor as averaged over the cross section of the heat pipe.

For high evaporation or condensation rates, $|\gamma| \gg 1$, Cotter recommended the expression (15)

$$\frac{dP_v}{dz} = -\frac{S\dot{m}_v}{4\rho_v r_v^4}\frac{d\dot{m}_v}{dz}, \qquad \text{(II.8)}$$

where $S = 1$ for evaporation and $S = 4/\pi^2$ for condensation. This relation had been obtained from an exact solution of the momentum and continuity equations.

Cotter expressed the conservation of energy by the relation

$$\nabla \cdot \vec{q} = 0, \qquad \text{(II.9)}$$

where

$$\vec{q} = h\rho\vec{v} - \kappa\nabla T, \qquad \text{(II.10)}$$

where h and κ are the specific enthalpy and thermal conductivity of the working fluid respectively. Cotter stated that an energy equation, formed by substituting Equation II.10 into II.9, was subject to the assumptions of 1) steady state, 2) no energy sources, and 3) negligible heat exchange by radiation. Cotter's energy equation implies that the work done by pressure and viscous actions are negligible, which is reasonable since low velocities are presumed to be encountered and the corresponding parameter E_c/R_e (3) is much less than unity for typical heat pipes.

Cotter proceeded by defining the total axial heat transfer rate, $\dot{Q}(z)$, of the heat pipe by

$$\dot{Q}(z) = \int_0^{r_p} q_{z}(z,r)\, 2\pi r\, dr \quad , \tag{II.11}$$

where r_p is the outside radius of the heat pipe shell. Cotter stated that heat pipe operation takes place when all temperature gradients are small except for the radial gradient in the wick and shell. This simplifying assumption permitted Cotter to express his energy equation as

$$\dot{Q}(z) = \dot{m}_v(z)\, h_{v\ell}\left[1 + \frac{h_\ell - h'_\ell}{h_{v\ell}}\right] \quad , \tag{II.12}$$

where h_ℓ is the liquid specific enthalpy at the liquid-vapor interface, h'_ℓ is the liquid specific enthalpy as averaged over the wick cross section, and $h_{v\ell}$ is the heat of vaporization. For the low radial heat fluxes encountered in heat pipes, Cotter reasoned that the term $(h_\ell - h'_\ell)/h_{v\ell}$ could be neglected when compared to unity. Thus Cotter's resulting relation was

$$\dot{Q}(z) = \dot{m}_v(z)\, h_{v\ell} \tag{II.13}$$

Later studies by Chi and Cygnarowicz (5) have confirmed this approximation.

In order to couple the internal phenomena of the heat pipe to its external environment, Cotter wrote the energy Equations (II.9) and (II.10) for an annulus, bounded by z and $z + dz$, and radii r_v and r_p, and used Equations (II.12) and (II.13) to obtain the relation

$$2\pi \chi_v \left.\frac{\partial T}{\partial r}\right|_{r_v} = 2\pi r_p \chi_p \left.\frac{\partial T}{\partial r}\right|_{r_p} . \tag{II.14}$$

Cotter reasoned that the coupling could be approximated by the simple thermal conduction result of

$$T_p = T_v + \dot{Q}'/\chi'_{eff} . \tag{II.15}$$

where $\dot{Q}'$ is the rate of heat transfer externally added or withdrawn per unit length and χ'_{eff} is the effective thermal conductivity of the annular rings formed by the wick and solid shell.

Cotter's analysis continued by modeling the external environment as one of uniform heat addition and uniform heat withdrawal with

$$\dot{Q}(z) = \dot{m}_v(z)\, h_{v\ell} = \frac{z}{\ell_e}\, \dot{Q}_e \text{ , for} \tag{II.16}$$

$$0 \le z \le \ell_e \text{ , and} \tag{II.17}$$

$$\dot{Q}(z) = \dot{m}_v(z) h_{v\ell} = \frac{\ell - z}{\ell - \ell_e} \dot{Q}_e \,, \quad \text{for} \tag{II.18}$$

$$\ell_e \leq z \leq \ell \,, \tag{II.19}$$

where $\dot{Q}_e$ is the total heat input rate at the evaporator. Using Equations (II.16) through (II.19), Cotter evaluated the pressure drops in both liquid and vapor regions as determined by Equations (II.4) and (II.7) or (II.8). This gave Cotter expressions of the type

$$\Delta P_\ell = P_\ell(\ell) - P_\ell(0) \quad \text{and} \quad \Delta P_v = P_v(0) - P_v(\ell) \,, \tag{II.20}$$

where ΔP_ℓ and ΔP_v are both positive quantities. In order to relate the pressure distributions of the vapor and the liquid, Cotter recommended the equilibrium expression of

$$P_v - P_\ell = \frac{2\sigma}{r_m} \,, \tag{II.21}$$

where r_m is the characteristic meniscus radius at the liquid-vapor interface. Cotter's Equation (II.21) neglects the inertia term in the jump conditions (14) across the interface. However, typical heat pipes have low radial heat fluxes, thus permitting the inertia term to be validly neglected.

Cotter proceeded by reasoning that at the condenser end of the heat pipe, r_m, is infinite, i.e. a flat surface separates the two phases. This approximation allowed Cotter to obtain from Equation (II.21) the relation

$$P_v(\ell) = P_\ell(\ell) \,, \tag{II.22}$$

which when combined with Equation (II.20) indicated

$$P_v(0) - P_\ell(0) = \left.\frac{2\sigma}{r_m}\right|_{z=0} = \Delta P_\ell + \Delta P_v \geq 0 \; . \tag{II.23}$$

Cotter then reasoned that the maximum heat flux of the heat pipe would be limited by the capillary term $2\sigma/r_m$ at the evaporator, and that this would take place when $r_m = r_c$ where r_c is the characteristic pore radius at the liquid-vapor interface. Thus Cotter obtained expressions for the maximum heat rate, rewritten as

$$\dot{Q}_{max} = \left(\frac{\rho_\ell \sigma h_{v\ell}}{\mu_\ell}\right)\left(\frac{\pi(r_w^2 - r_v^2)}{1}\right)\left(\frac{4\frac{\epsilon}{t} r_c^2 \cos^2\phi}{\ell \, r_c \cos\phi}\right)\left[\frac{1 - \frac{r_c}{\ell}\frac{\rho_\ell \ell^2 g}{\sigma}\frac{\sin\theta}{\cos\phi}}{1 + 2\pi\frac{\epsilon}{t}\frac{r_c^2}{r_v^2}\left(\frac{r_w^2}{r_v^2} - 1\right)\left(\frac{\mu_v}{\rho_v}\frac{\rho_\ell}{\mu_\ell}\right)}\right] . \tag{II.24}$$

The first term, containing $h_{v\ell}$ may be interpreted as a heat pipe parameter of dimensions power / area which characterizes the working fluid. The second factor, $\pi(r_w^2 - r_v^2)$ may be interpreted as the total cross sectional area of the wick in the axial direction. The third term, containing ϵ/t is a dimensionless factor which characterizes the permeability of the wick and the corresponding pressure drop due to liquid flow. The bracketed term containing $g \sin\theta$ reflects the effects of pipe inclination in a gravity field. The bracketed term containing μ_v/ρ_v reflects the effects of pressure drop in the vapor region.

Although the work of Cotter served as only a first approximation for analysis of heat pipes, it did provide a basis for other investigations. The work of Kunz, et al. (17, 18) presented a simplified approach to Cotter's analytical problem of predicting heat pipe performance. Kunz suggested the overall pressure balance equation of

$$(P_{\ell,e}-P_{v,e}) + (P_{v,e}-P_{v,c}) + (P_{v,c}-P_{\ell,c}) + (P_{\ell,c}-P_{\ell,e}) = 0 \quad , \tag{II.25}$$

where the subscripts ℓ and v refer to the liquid and vapor regions respectively, and the subscripts e and c refer to the evaporator and condenser sections respectively. For the low velocity vapor region, Kunz suggested

$$(P_{v,e} - P_{v,c}) = 0 \ . \tag{II.26}$$

Considering the condenser liquid-vapor interface to be flat, Kunz used

$$(P_{v,c} - P_{\ell,c}) = 0 \ . \tag{II.27}$$

Characterizing the evaporator liquid-vapor interface as a spherical shape of meniscus radius r_m, Kunz recommended

$$(P_{\ell,e} - P_{v,e}) = -\frac{2\sigma}{r_m} \ . \tag{II.28}$$

Using Darcy's law for liquid flow through porous media and showing the inertial term to be negligible, Kunz showed

$$(P_{\ell,c}-P_{\ell,e}) = K_1 \frac{\mu_\ell}{\rho_\ell}\frac{1}{b\delta}\frac{\dot{m}_\ell}{1}\frac{l_{eff}}{1} \quad , \tag{II.29}$$

where K_1 is the inverse of specific permeability, $b\delta$ is the product of width and thickness for the total cross sectional area of the wick, $\dot{m}_\ell$ is the total mass flow rate of liquid, and ℓ_{eff} is the effective total length of the heat pipe for computing frictional pressure drop.

Using an analysis similar to Cotter's for uniform radial mass flow along the condenser and evaporator, Kunz recommended

$$\dot{m}_\ell = \frac{\dot{Q}}{h_{v\ell}} \text{ , and} \tag{II.30}$$

$$\ell_{eff} = \tfrac{1}{2}\ell_e + \ell_a + \tfrac{1}{2}\ell_c \text{ ,} \tag{II.31}$$

for heat pipes with an adiabatic section, and

$$\ell_{eff} = \tfrac{1}{2}\ell_e + \tfrac{1}{2}\ell_c = \tfrac{1}{2}\ell \text{ ,} \tag{II.32}$$

for heat pipes without an adiabatic section.

Kunz combined his equations and followed Cotter's reasoning that the capillary limited maximum heat transfer rate would occur when the meniscus radius was at its minimum. The resulting expression was

$$\dot{Q}_{max} = \left(\frac{\rho_\ell \sigma h_{v\ell}}{\mu_\ell}\right)\left(\frac{b\delta}{1}\right)\left(\frac{4}{K_1 \ell r_{min}}\right) \text{ ,} \tag{II.33}$$

where r_{min} is the minimum meniscus radius. Essentially, Cotter's (8) and Kunz's (17, 18) predictions are the same, save vapor effects, with both requiring wick flow characteristics: for Cotter, tortuosity and porosity, for Kunz, permeability.

Other analytical studies on the general operational characteristics of heat pipes include 1) sonic limitations due to the effects of vapor compressibility, Levy (19, 20), 2) time transient performance, Kessler (13) and Biernert (2), and 3) nonconstant fluid properties, Cosgrove, et al. (7). All general theories yield the same form of prediction, that being the maximum heat transfer rate is a function of the physical properties of the working fluid and the detailed wick geometry.

B. Experimental

Caution must be used in selecting experimental results to be used for comparison. Many experimental data have been reported on heat pipe performance; most operating below the maximum power level and a few at the maximum.

The experiments of Kunz, et al. (18) included tests for maximum heat transfer. Tested was a horizontal water heat pipe of rectangular cross section, 1.6 inches high by 6.0 inches wide by 24.0 inches long. Kunz's wick was formed from sintered nickel fibers shaped to a 6.0 inches by 24.0 inches by 0.1 inches sheet. The sheet was bonded to the inner lower surface of the heat pipe. External heat was electrically supplied by a resistance heater over a length of 6.2 inches and was removed by colling water circulation over an adjacent length of 11.6 inches. Maximum heat transfers were described to occur when high temperatures appeared in the evaporator section. Kunz's work also included experimentally determined values of K_1, the friction parameter, for various wicks.

The study by Schwartz (28) also included tests for maximum heat transfer. His system was a horizontal ammonia heat pipe of cylindrical cross section, 15.5 inches long by 0.199 inches inside diameter. The wick was formed by cylindrically wrapping two layers of 100 mesh stainless steel screen. External heat exchange was accomplished by circulating hot water and cold water through jackets around the evaporator and condenser sections respectively. Each section was 3.0 inches long with the central 9.5 inches considered adiabatic.

C. Comparison of Theories to Experiments

Comparison of the theories of Cotter and Kunz to the experiments of Kunz and Schwartz is shown in Figure 2. The agreement is good, with deviations less than 7.0 per cent. The predictions of Cotter and Kunz coincided for all data points since 1) both experiments used horizontal heat pipes (no gravity term in Cotter's equation), 2) secondary experiments of Kunz on permeability, porosity, and pore size were used to evaluate the porosity and tortuosity terms of Cotter's equation, and 3) the vapor flow term of Cotter's equation is negligible for both experiments. Kunz's data indicated that condensation took place over a length of 17.8 inches rather than the design length of 11.6 inches. It is suspected that axial conduction was present in Kunz's thick heat pipe shell beneath the condenser wick.

Other experimental maximum heat rates are reported in the literature for capillary limited heat pipes. Comparison is not made due to 1) lack of complete experimental data - Miller and Holm (24), Cosgrove, et al. (7), and Neal (25), or 2) employment of wick configurations different than the porous media assumed by the theories of Cotter and Kunz

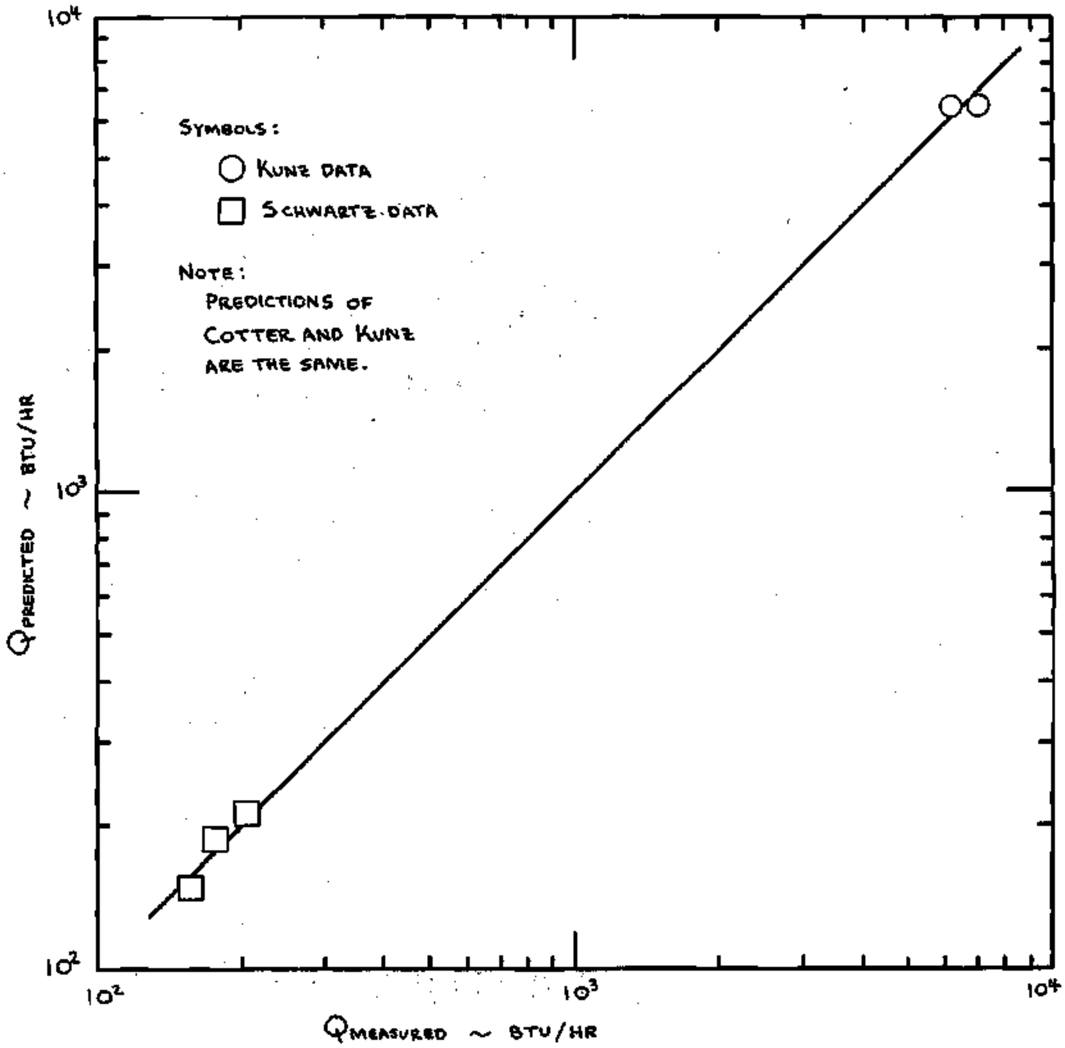

Figure 2. Comparison of Predicted to Measured Values of Maximum Heat Rates.

Kunz - McSweeney (23), grooves, and Kemme (12), grooves covered with screen.

See Appendix V for a calculation of maximum heat transfer rate based on Kunz's theory and parameter values tested in this investigation.

2. Parameter Studies

Studying the effects of varying heat pipe parameters consists of identifying the significant parameters and describing the relations between the parameters. The early works of Cotter (8) and Kunz, et al. (17, 18) served to identify the parameters listed in Table 1. These parameters include only those applied to heat pipes using wicks formed of porous media.

A. Fluid Properties

The work of Neal (25) indicated values of the heat pipe parameter N, where

$$N = \frac{\rho_l \sigma h_{vl}}{\mu_l} , \qquad \text{(II.34)}$$

for various fluids. As seen in Figure 3, the employment of a particular working fluid determines the temperature range suitable for heat pipe operation and the variation of N with temperature.

The parametric analysis by Parker and Hanson (26) on various liquid metals included relative values of surface tension and heat of vaporization, relative values of pressure drop for liquid and vapor flow.

Table 1. Initially Identified Heat Pipe Parameters

Category	Symbol	Name	Remarks
Operating Characteristics	$\dot{Q}_{max}$	heat rate	maximum capillary limit
	T_o	operating temperature	average vapor temperature or pipe wall in adiabatic section
Fluid Properties	σ	surface tension	for liquid contacting solid in presence of vapor
	ρ_ℓ	liquid density	liquid flow
	μ_ℓ	liquid viscosity	
	ρ_v	vapor density	vapor flow
	μ_v	vapor viscosity	
	$h_{v\ell}$	latent heat of vaporization	energy storage in vapor
	$\frac{\rho_\ell \sigma h_{v\ell}}{\mu_\ell}$	heat pipe parameter	fluid capability

(Continued)

Table 1. (Continued)

Category	Symbol	Name	Remarks
Overall Geometry	r_v	radius of vapor space	cylindrical heat pipes
	r_w	outer wick radius	
	r_p	outer shell radius	
	b	wick width	rectangular heat pipes
	δ	wick thickness	
Overall Geometry	ℓ_e	evaporator length	design lengths
	ℓ_c	condenser length	
	ℓ_a	adiabatic length	
	ℓ	total length	
	g	gravitational acceleration	significant only when heat pipe is inclined in a gravity field
	θ	inclination angle	

(Continued)

Table 1. (Continued)

r_m –

Category	Symbol	Name	Remarks
Wick Geometry	r_c	pore radius	wick structure
	ϵ	porosity	
	r_{min}	meniscus radius	liquid-vapor interface
	r_{min}	minimum meniscus radius	
	ϕ_o	contact angle	
	t	tortuosity	liquid pressure drop
	K_l	inverse permeability	
Environmental Coupling	X_{eff}	effective wick thermal conductivity	implied by Cotter (8)
	X_p	pipe shell thermal conductivity	
	T_H	evaporator heat source temperature	

(Continued)

Table 1. (Continued)

Category	Symbol	Name	Remarks
Environmental Coupling	T_c	condenser heat sink temperature	implied by Cotter (8)
	U_H	unit conductance to heat source	
	U_c	unit conductance to heat sink	

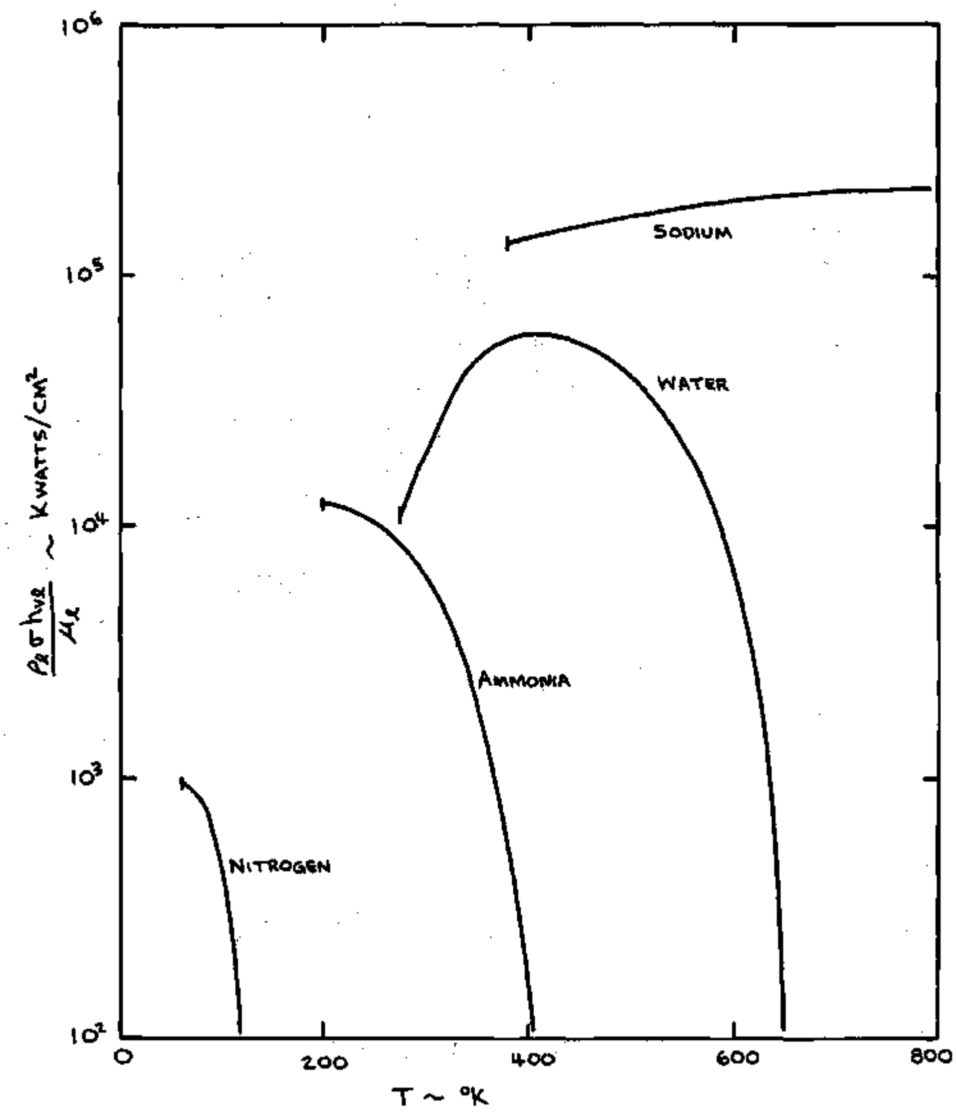

Figure 3. Heat Pipe Fluid Parameter vs. Temperature for Various Fluids.*
*From Neal (25)

The experimental work of Kunz, et al. (17, 18) included tests of the same heat pipe operated with fluids of water and freon 113. The water pipe was capable of higher heat transfer rates than the freon pipe.

B. Geometric Factors

McKinney's (22) work included computer studies for variation of geometric variables with a water heat pipe. Typical results, see Figure 4, indicate variation of maximum heat rate with changes in the overall geometric parameter r_v/r_w and with changes in the wick friction parameter $1/K_1$.

The computer analysis by Watts (35) included techniques for optimizing the capillary pore size and the corresponding maximum heat rate.

Edwards, et al. (9) wrote a computer program which included variations of 1) geometrical factors, 2) working fluids, and 3) environmental factors for a heat pipe operating with the inclusion of inert gases. No graphical results were indicated.

The experimental work of Kunz, et al. (17) included measurements of the wick friction parameter K_1. Their results indicate the validity of assuming K_1 to be a constant for a given wick, see Figure 5.

C. Environmental Coupling

Coupling the internal dynamics of heat pipe operation to the surroundings requires description of the modes and paths of heat exchange.

In his original analysis, Cotter (8) suggested the simple coupling model of

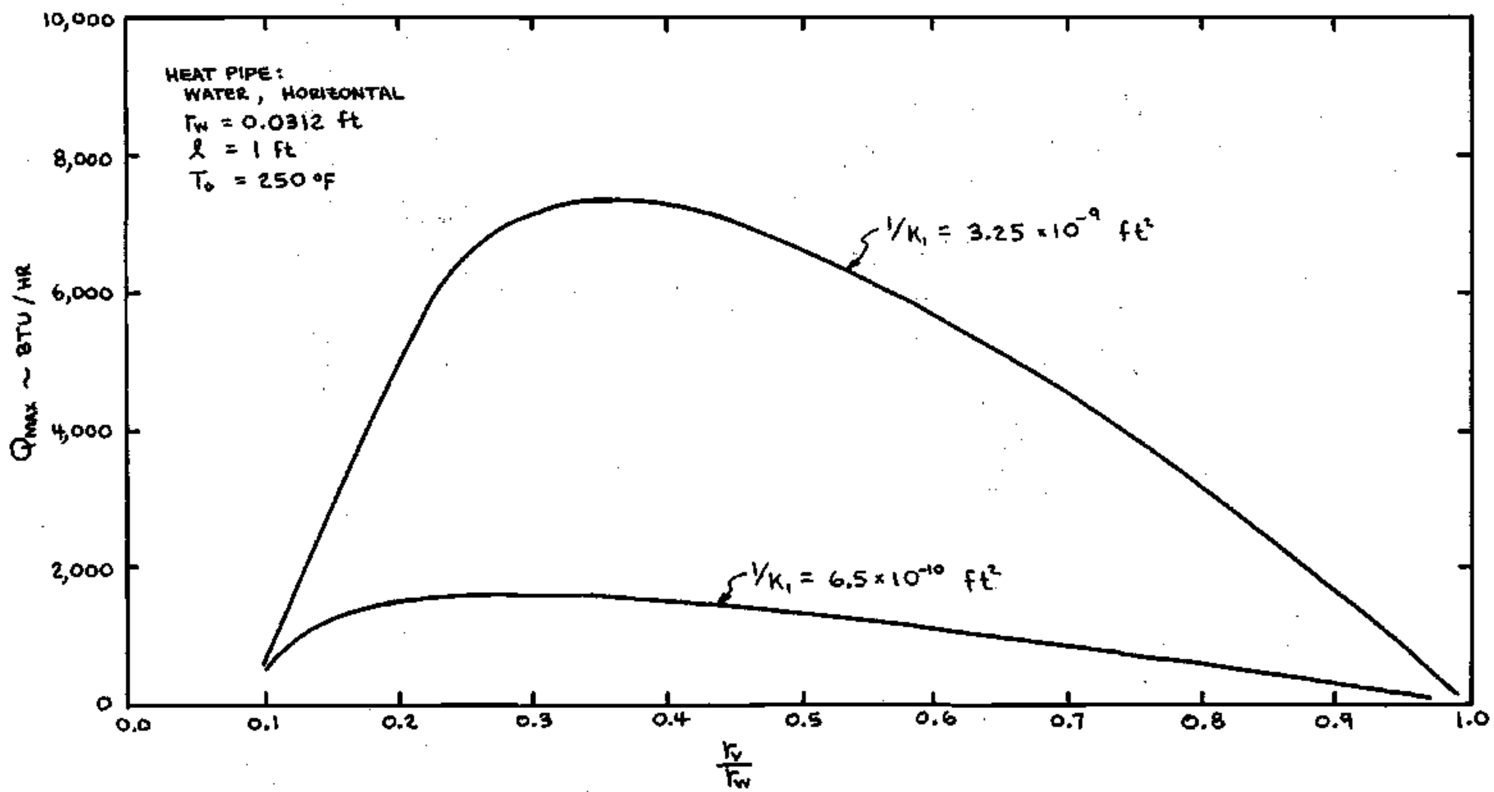

Figure 4. Q_{max} vs. r_v/r_w for Various $1/K_1$.*

*From McKinney (22)

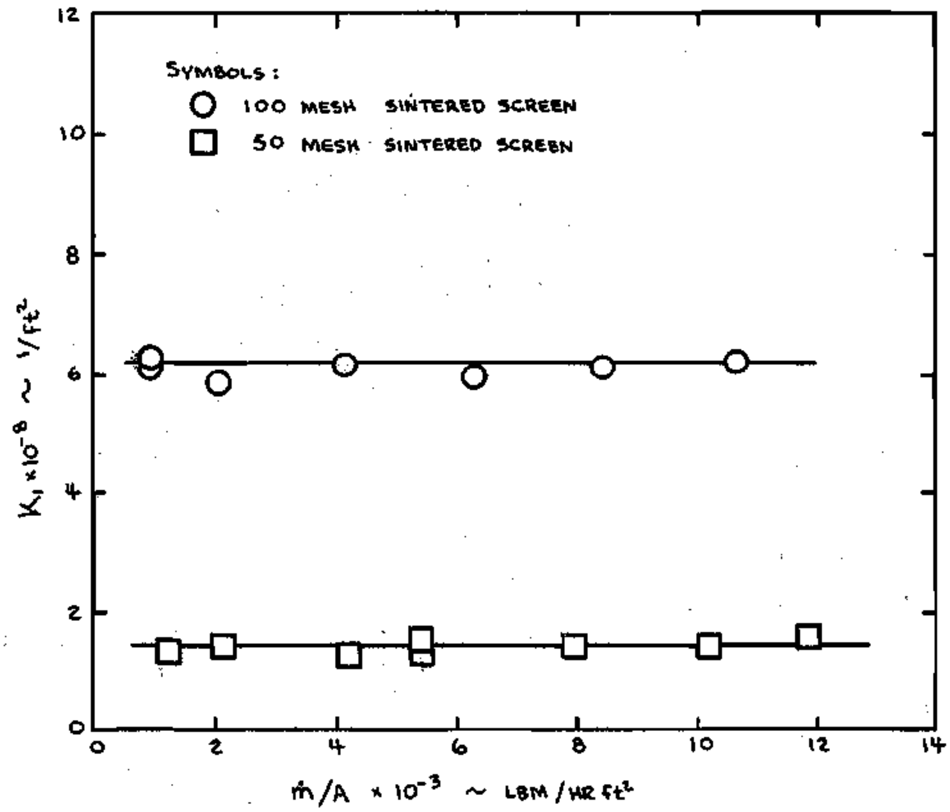

Figure 5. Variation of K_1 with Mass Flux Rate.*

*From Kunz, et al. (17)

1) constant temperature or uniform heat flux at the outer shell radius along the entire evaporator design length,

2) radial conduction through the pipe shell,

3) radial conduction through the wick,

4) evaporation at the evaporator liquid-vapor interface,

5) vapor flow to the condenser section,

6) condensation on the condenser liquid-vapor interface,

7) radial conduction through the wick,

8) radial conduction through the pipe shell, and

9) constant temperature or uniform heat flux at the outer shell radius along the entire condenser design length. Cotter assumed the outer shell to be coupled with sinks and sources by appropriate conductances. Studies of Cotter's simple model and its limitations have been the subjects of many investigations.

The analysis by Lyman and Huang (21) indicated the validity of assuming simple conduction in the heat pipe wick. This conclusion was based on the exclusion of convection since Peclet numbers were small as calculated from typical heat pipes (18, 7). Lyman used the suggestions of Kunz, et al. (18) that the effective wick thermal conductivity be modeled as isotropic by the parallel conduction relation

$$\chi_{eff} = \epsilon \chi_{\ell} + (1-\epsilon)\chi_{s} \quad , \tag{II.35}$$

where χ_{eff} is the effective wick-liquid thermal conductivity, ϵ is the wick porosity, χ_{ℓ} is the liquid thermal conductivity, and χ_{s} is the thermal conductivity of the wick solid.

An experimental study by Seban and Abhat (31) included measurement of effective wick thermal conductivity. Tests were made during the evaporation of water from two separate screen wicks, 150 and 325 mesh. Results, see Figure 6, indicated the observed effective conductivity to be between the values predicted by simple parallel and simple series models. The measured values were much closer to the series predictions. Seban did not attempt to explain this trend.

In their similarity investigation, Miller and Holm (24) attempted to overcome the uncertainties of wick conduction, heat transfer through the pipe shell, and shell boundary conditions. Their concept consisted of using a model heat pipe to predict the performance of a geometrically different prototype heat pipe, both in an environment of thermal radiation. A material preservation analysis was tested in which both model and prototype used the same working fluid (water) and wick material (200 mesh nickel screen). This implied equality of thermal conductivities of the wall and wick, the emittance of the condenser wall surface, and the permeability of the wick. Using starred quantities to indicate the ratio of model values to prototype values of that quantity, the suggested model equations were

$$\left(T_v - T_{cp}\right)^* = \frac{\dot{Q}^* A_w^*}{(L^*)^3} , \tag{II.36}$$

$$T_{cp}^* = \frac{(\dot{Q}^*)^{1/4}}{(L^*)^{1/2}} , \text{ and} \tag{II.37}$$

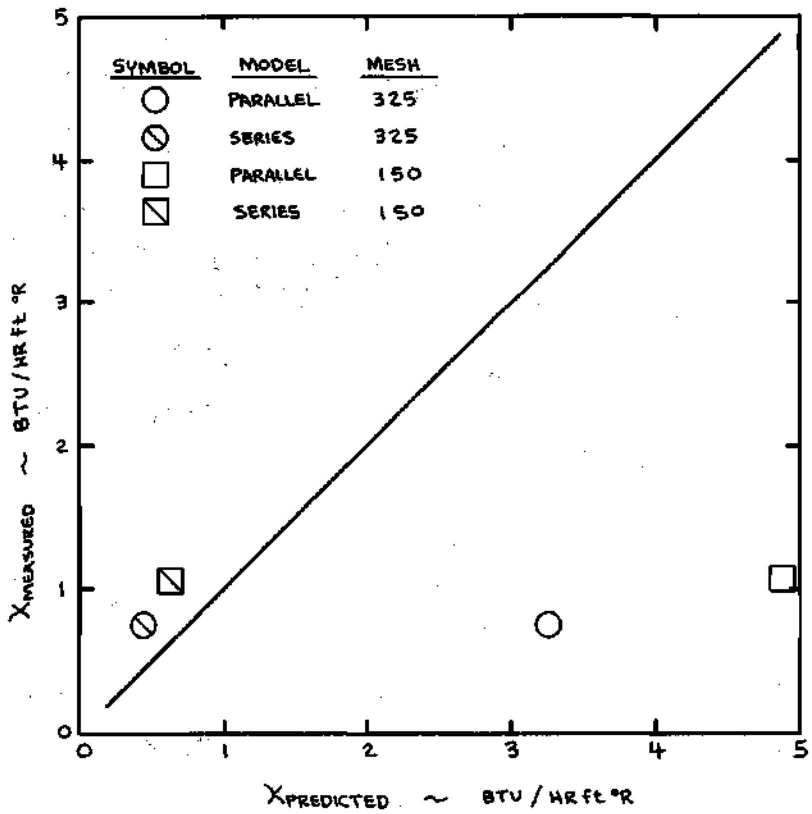

Figure 6. Comparison of Measured and Predicted Values of Effective Wick Thermal Conductivity*.

*From Seban and Abhat (31).

$$\dot{Q}^* = \left(\frac{\rho_\ell \sigma h_{v\ell}}{\mu_\ell}\right)^* \left(\frac{A_w}{L}\right)^* , \qquad \text{(II.38)}$$

where T_v and T_{cp} are the temperatures of the vapor and condenser outside wall respectively, L is the combined length of evaporator and condenser sections, and A_w is the wick cross sectional area. Experimental results indicated the prototype behavior could be predicted from model performance to within 10° F over a temperature range of 140 - 330° F.

In a recent paper, Sun and Tien (34) constructed a simple conduction model for theoretical steady state heat pipe performance. By considering the interaction of axial heat conduction in the shell and wick, the effective lengths of condensation and evaporation were shown to be larger than the design lengths. For a given pipe geometry, these effective lengths and the corresponding overall conductance of the heat pipe were shown to depend significantly on the two dimensionless parameters M and B_i, where

$$M^2 = \frac{2\left(\frac{X_{eff}}{X_p}\right)\left(\frac{\ell}{r_w}\right)^2}{\left[\left(\frac{r_p}{r_w}\right)^2 - 1\right]\ln\left(\frac{r_w}{r_v}\right)} , \text{ and} \qquad \text{(II.39)}$$

$$B_i = \left(\frac{H r_p}{X_{eff}}\right)\ln\left(\frac{r_w}{r_v}\right) . \qquad \text{(II.40)}$$

M has physical interpretations of the ratio of wick to shell wall conductance times the ratio of shell surface area to shell cross sectional area. Bi, the Biot number, has a physical interpretation of the ratio of wick radial temperature drop to the temperature difference between the outer shell wall and the surroundings. Sun recommended that axial conduction be neglected for values of M greater than 100 and Bi less than unity. See Appendix V for a calculation using parameter values tested in this investigation.

Fox, et al. (10) experimentally operated heat pipes with configurations similar to that proposed in this investigation but with different values of the geometric parameters. His system was a horizontal heat pipe of cylindrical cross section, 24 inches long by 1.50 inches outside diameter with 0.028 inch shell thickness. Water was the working fluid. The wicks were formed by cylindrically wrapping mesh screen. Tested were a 100 mesh wick consisting solely of layers of 100 mesh screen and a dual wick consisting of 16 mesh screen layers covered with a single layer of 100 mesh screen. Operating temperatures (incompletely reported) were approximately 200°F with power levels from 400 to 1250 watts.

Schwartz (29) also tested a heat pipe with configurations similar to that proposed in this investigation shell and wick were made of stainless steel with water as the working fluid. Geometries were the shell, 15.5 inches long by 0.199 inch inside radius with 0.020 inch thickness, and wick, two tightly wrapped cylindrical layers of 100 mesh screen. Operating data were collected over the ranges 79 to 153°F and 6.3 to 58 watts.

CHAPTER III

GENERAL THEORY

1. Objective

The purpose of this analysis is to study the general relations which describe the performance of a heat pipe. Results of this study will 1) provide a list of governing field and constitutive equations, 2) provide a list of potentially important dimensionless groups, and 3) provide an analytical basis for future studies.

2. Overall Concepts

The physical model of the heat pipe, see Figure 7, consists of an annular region of porous material bound by a circular cylinder at $r = r_w$ and flat planes at each end. A fluid is distributed within the pipe. The pipe is divided into the following axial sections: 1) a section surrounded by a heat source, the evaporator section, 2) a section surrounded by insulation, the adiabatic section, and 3) a section surrounded by a heat sink, the condenser section. The pipe is divided into the following radial regions: 1) a vapor region, $r < r_{INTERFACE}$, 2) a liquid-wick region, $r_{INTERFACE} < r < r_w$, and 3) an external region, $r > r_w$. The working fluid is modeled as being distributed in the liquid phase solely within the liquid-wick region and the vapor phase solely within the vapor region.

The general formulation is made by separate studies of each region of fluid with appropriate boundary conditions and using reference parameters to obtain dimensionless groups.

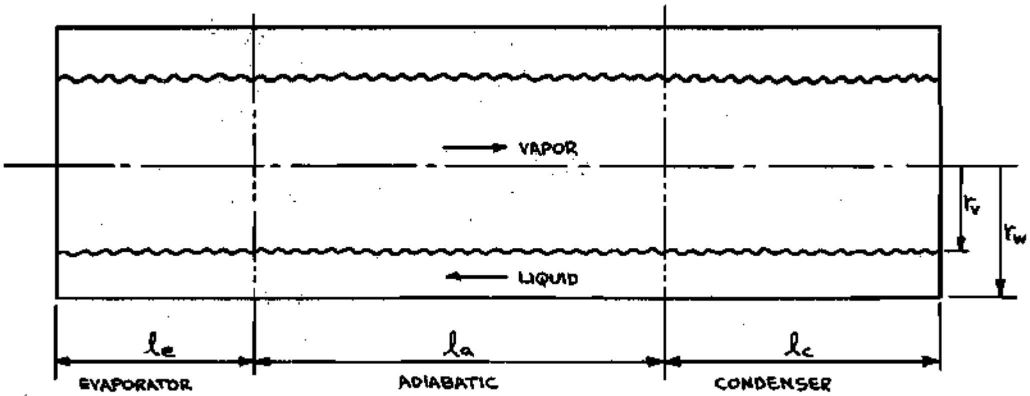

Figure 7. General Theory Heat Pipe Schematic.

3. Reference Parameters

Table 2 indicates the nondimensional parameters as defined in terms of the dimensional parameter and reference parameters. For material properties, the general relation is

$$\text{nondimensional property} = \frac{\text{dimensional property}}{\text{reference property}} \qquad \text{(III.1)}$$

The nondimensional parameter is indicated by the property symbol with a bar drawn over it. The dimensional property is interpreted as the actual value of the property at its local spatial location and temperature. The reference parameter is the value of the dimensional property at temperature T_o, where T_o is defined as the heat pipe operating temperature, interpreted as the average vapor temperature or wall temperature in the adiabatic section. Liquid and vapor reference properties are saturation values evaluated at T_o. Exceptions to this system are 1) vapor enthalpy, and 2) liquid and vapor pressures where specified reference parameters are used.

Geometrical parameters are nondimensionalized by their indicated reference parameters.

Velocity terms are nondimensionalized by the reference velocities of

$$u_v = \frac{\dot{Q}_e}{\rho_v (2\pi r_v \ell_c) h_{v\ell}} \text{, and} \qquad \text{(III.2)}$$

$$u_\ell = \frac{\dot{Q}_e}{\rho_\ell (2\pi r_v \ell_c) h_{v\ell}} . \qquad \text{(III.3)}$$

Table 2. General Theory Reference Relations

Category	Name	Reference Relation
Temperature	temperature	$\bar{T} = \frac{T}{T_c}$
Vapor	density	$\bar{\rho}_v = \frac{\rho}{\rho_v}$
	pressure	$\bar{P}_v = \frac{P}{\rho_v u_v^2}$
	viscosity	$\bar{\mu}_v = \frac{\mu}{\mu_v}$
	thermal conductivity	$\bar{\chi}_v = \frac{\chi}{\chi_v}$
	enthalpy	$\bar{h}_v = \frac{h}{c_{pv} T_c}$
Liquid	density	$\bar{\rho}_\ell = \frac{\rho}{\rho_\ell}$
	pressure	$\bar{P}_\ell = \frac{P}{\rho_\ell u_\ell^2}$
	viscosity	$\bar{\mu}_\ell = \frac{\mu}{\mu_\ell}$

(Continued)

Table 2. (Continued)

Category	Name	Reference Relation
Liquid	thermal conductivity	$\bar{K}_\ell = \frac{K}{K_\ell}$
	surface tension	$\bar{\sigma} = \frac{\sigma}{\sigma_{at\,T_0}}$
	enthalpy	$\bar{h}_\ell = \frac{h}{c_{p\ell} T_c}$
Wick Properties	wick-solid thermal conductivity	$\bar{K}_s = \frac{K}{K_s}$
	wick effective thermal conductivity	$\bar{K}_{eff} = \frac{K_{eff}}{K_{eff\ at\ T_0}}$
	wick friction factor (inverse permeability)	$\bar{\kappa}_1 = \frac{\kappa}{\kappa_1}$
Vapor Velocities	radial velocity	$\bar{u}_v = \frac{u}{u_v}$
	angular velocity	$\bar{v}_v = \frac{v}{u_v}$

(Continued)

Table 2. (Continued)

Category	Name	Reference Relation
Vapor Velocities	axial velocity	$\bar{\omega}_v = \frac{\omega}{2u_v(l_c/r_v)}$
Liquid Velocities	radial velocity	$\bar{u}_l = \frac{u}{u_l}$
	angular velocity	$\bar{v}_l = \frac{v}{u_l}$
	axial velocity	$\bar{\omega}_l = \frac{\omega}{\frac{2}{\epsilon_o}\frac{l_c}{r_v}\left(\frac{1}{\left(\frac{r_w}{r_v}\right)^2-1}\right)u_l}$
Bulk Geometry	radial coordinate	$\bar{r} = \frac{r}{r_v}$
	angular coordinate	$\bar{\theta} = \frac{\theta}{2\pi}$
	axial coordinate	$\bar{z} = \frac{z}{l_c}$
Detail Geometry	radial coordinate	$\bar{r}_s = \frac{r_s}{r_c}$

(Continued)

Table 2. (Continued)

Category	Name	Reference Relation
Detail Geometry	radial coordinate	$\bar{\eta} = \frac{\eta}{r_c}$
	radial coordinate	$\bar{\eta}_s = \frac{\eta_s}{r_c}$
	angular coordinate	$\bar{\theta}_s = \frac{r_v}{r_c}\theta_s$
	axial coordinate	$\bar{z}_s = \frac{z_s}{r_c}$
	surface coordinate	$\bar{p} = \frac{p}{r_c}$
	surface coordinate	$\bar{q} = \frac{q}{r_c}$
	wetting angle	$\bar{\phi} = \frac{\phi}{\phi_o}$
	porosity	$\bar{\epsilon} = \frac{\epsilon}{\epsilon_o}$

(Continued)

Table 2. (Continued)

Category	Name	Reference Relation
Environmental Parameters	heat transfer rate	$\bar{\dot{Q}} = \frac{\dot{Q}}{\dot{Q}_e}$
	unit conductance	$\bar{U} = \frac{U}{U_c}$

Environmental references parameters are 1) T_c, the average temperature of the heat sink, 2) U_c, the average unit conductance between the heat sink and the outer surface of the wick, and 3) $\dot{Q}_e$, the total power delivered to the evaporator section from the heat source.

4. Vapor Region

The vapor region is studied by examining its spatial boundaries, assumptions, field equations, and constitutive equations. Dimensionless groups are obtained.

A. Spatial Boundaries

The spatial boundaries, see Figure 8, are

$$0 \le z < l_e + l_a + l_c \, , \tag{III.4}$$

$$0 \le r < r_v + \eta(\theta, z) \, , \text{ and} \tag{III.5}$$

$$0 \le \theta \le 2\pi \, . \tag{III.6}$$

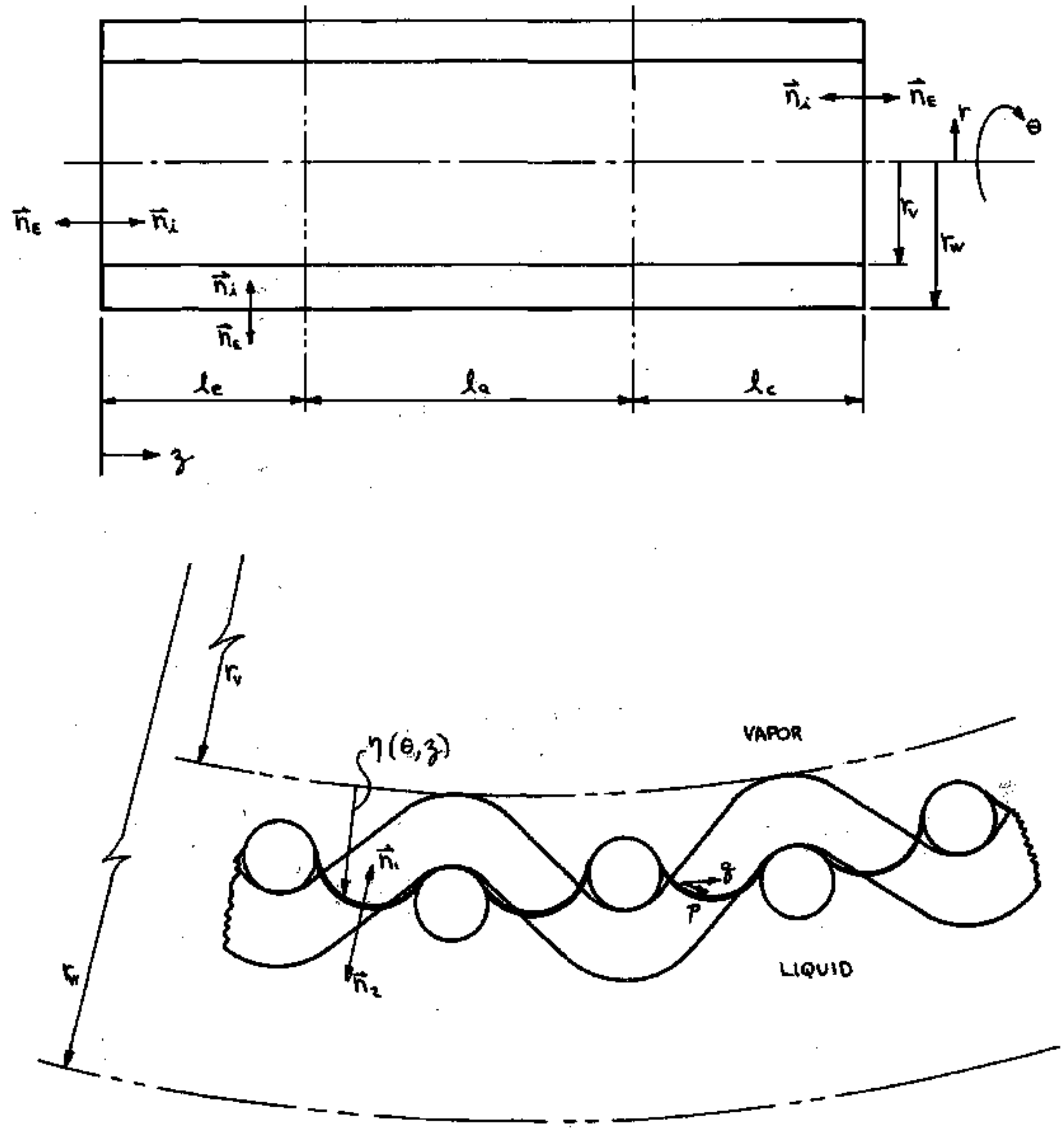

Figure 8. General Theory Spatial Boundaries.

B. Assumptions

The basic assumptions are

1) single species,

2) no body forces,

3) no heat generation,

4) negligible heat exchange by radiation,

5) no phase changes occur within the spatial boundaries,

6) steady state,

7) laminar flow, and

8) negligible viscous dissipation of heat.

C. Field Equations in Vector Form

The field equations in vector form are

equation of continuity

$$\nabla \cdot (\rho \vec{V}) = 0 \quad , \tag{III.7}$$

equation of motion

$$\nabla \cdot (\rho \vec{V} \vec{V}) = -\nabla P - \nabla \cdot \overline{\overline{\tau}} \quad , \text{ and} \tag{III.8}$$

equation of energy

$$\nabla \cdot (\rho \vec{V} h) = -\nabla \cdot \vec{q} + \vec{V} \cdot \nabla P \quad . \tag{III.9}$$

D. Constitutive Equations in General Form

The constitutive equations in general form are

rheological equation

$$\overline{\overline{\tau}} = \overline{\overline{\tau}}\left(\mu, \lambda, u_j, \frac{\partial u_i}{\partial x_k}\right), \text{ for} \tag{III.10}$$

$$j = 1,2,3 \quad \text{and} \quad k = 1,2,3 \quad , \qquad \text{(III.11)}$$

equations of viscosity

$$\mu = \mu(T) \text{ , and} \qquad \text{(III.12)}$$

$$\lambda = \lambda(T) \text{ , where} \qquad \text{(III.13)}$$

$$\lambda = -\tfrac{2}{3}\mu \text{ for monatomic gases ,} \qquad \text{(III.14)}$$

heat conduction equation

$$\vec{q} = -\chi \nabla T \quad , \qquad \text{(III.15)}$$

equation of thermal conductivity

$$\chi = \chi(T) \quad , \qquad \text{(III.16)}$$

thermal equation of state

$$\rho = \rho(P,T) \text{ , and} \qquad \text{(III.17)}$$

caloric equation of state

$$h = h(P,T) \quad . \qquad \text{(III.18)}$$

E. Dimensionless Groups

Writing Equations (III.4) through (III.18) in dimensionless form with the reference parameters, see Appendix A, results in the following seven dimensionless groups for the vapor region

$$\frac{l_e}{l_c} \; , \; \frac{l_a}{l_c} \; , \; \frac{r_v}{l_c} \; , \; \frac{r_c}{r_v} \; , \; \frac{\rho_v u_v r_v}{\mu_v} \; , \; \frac{\mu_v c_{pv}}{\chi_v} \; , \; \frac{u_v^2}{c_{pv} T_c} \quad .$$

5. Liquid Region

The liquid region is studied by examining its spatial boundaries, assumptions, field equations, and constitutive equations. Dimensionless groups are obtained.

A. Spatial Boundaries

The spatial boundaries, see Figure 8, are

$$0 \le z \le l_e + l_a + l_c \,, \tag{III.19}$$

$$r_v + \eta(\theta, z) < r < r_w \quad \text{, and} \tag{III.20}$$

$$0 \le \theta \le 2\pi \quad . \tag{III.21}$$

B. Assumptions

The basic assumptions are

1) single species,
2) no body forces,
3) no heat generation,
4) negligible heat exchange by radiation,
5) no phase changes occur within the spatial boundaries,
6) steady state,
7) constant density,
8) negligible viscous dissipation of heat, and
9) Darcy's law for flow in porous media applies.

C. Field Equations in Vector Form

The field equations in vector form are

equation of continuity

$$\nabla \cdot (\rho \vec{V}) = 0 \,, \tag{III.22}$$

equation of motion

$$\nabla\cdot(\rho\vec{V}\vec{V}) = -\nabla P - \nabla\cdot\overline{\overline{\tau}}, \text{ and} \qquad \text{(III.23)}$$

equation of energy

$$\nabla\cdot(\rho\vec{V}h) = -\nabla\cdot\vec{q} + \vec{V}\cdot\nabla P \quad . \qquad \text{(III.24)}$$

D. Constitutive Equations in General Form

The constitutive equations in general form are

rheological equation

$$\nabla\cdot\overline{\overline{\tau}} = -K\mu\epsilon\vec{V} \ , \qquad \text{(III.25)}$$

equation of viscosity

$$\mu = \mu(T) \qquad \text{(III.26)}$$

equation of wick friction parameter

$$K = K(r_w, r_v, r_{ws}, r_c, \text{ wick configuration}) \ , \qquad \text{(III.27)}$$

equation of porosity

$$\epsilon = \epsilon(r_w, r_v, r_{ws}, r_c, \text{ wick configuration}), \text{ for} \qquad \text{(III.28)}$$

$$\epsilon V_i = \frac{\text{mass flow rate in "}i\text{" direction}}{\text{total cross sectional area in "}i\text{" direction}} \ , \qquad \text{(III.29)}$$

heat conduction equation

$$\vec{q} = -\chi\nabla T \ , \qquad \text{(III.30)}$$

equation of liquid thermal conductivity

$$\chi_\ell = \chi_\ell(T) \ , \tag{III.31}$$

equation of wick-solid thermal conductivity

$$\chi_s = \chi_s(T) \ , \tag{III.32}$$

equation of effective wick thermal conductivity

$$\chi_{eff} = \chi_{eff}(\chi_\ell(T), \chi_s(T), r_w, r_v, r_c, r_{ws}, n) \ , \tag{III.33}$$

thermal equation of state

$$\rho = \text{constant} \ , \ \text{and} \tag{III.34}$$

caloric equation of state

$$h = h(P, T) \ . \tag{III.35}$$

E. Dimensionless Groups

Writing Equations (III.19) through (III.35) in nondimensional form, see Appendix A, results in the following fourteen dimensionless groups for the liquid region

$$\frac{\ell_e}{\ell_c} \ , \ \frac{\ell_a}{\ell_c} \ , \ \frac{r_v}{r_w} \ , \ \frac{r_c}{r_v} \ , \ \frac{r_v}{\ell_c} \ , \ \frac{\chi_s}{\chi_\ell} \ , \ \frac{\chi_\ell}{\chi_{eff}} \ , \ \frac{r_{ws}}{r_c} \ , \ K_1 r_c^2 \ , \ \epsilon_o \ , \ n \ ,$$

$$\frac{\rho_\ell u_\ell r_c}{\mu_\ell} \ , \ \frac{\mu_\ell c_{p\ell}}{\chi_\ell} \ , \ \frac{u_\ell^2}{c_{p\ell} T_c} \ .$$

6. Liquid-Vapor Interface

The liquid-vapor interface, that surface separating the liquid and vapor regions, is studied by examining its spatial location, assumptions, boundary conditions, and constitutive equations. Dimensionless groups are obtained.

A. Spatial Location

The spatial location, see Figure 8, is

$$0 \le z \le l_e + l_a + l_c , \tag{III.36}$$

$$r = r_v + \eta(\theta, z) \quad \text{, and} \tag{III.37}$$

$$0 \le \theta \le 2\pi \quad . \tag{III.38}$$

B. Assumptions

The basic assumptions are

1) steady state,

2) negligible heat exchange by radiation,

3) negligible effects of dilatational and surface shear viscosities,

4) constant liquid density,

5) continuum flow in regions surrounding the surface, and

6) negligible viscous dissipation of heat.

C. Boundary Conditions in Vector Form

The boundary conditions in vector form are

equation of continuity

$$(\rho_v \vec{V}_v)\cdot\vec{n}_2 + (\rho_l \vec{V}_l)\cdot\vec{n}_1 = 0 \quad , \tag{III.39}$$

no slip conditions

$$(\vec{V}_v - \vec{V}_i)\cdot\vec{t}_1 = 0 \quad , \tag{III.40}$$

$$(\vec{V}_v - \vec{V}_i)\cdot\vec{t}_2 = 0 \quad , \tag{III.41}$$

$$(\vec{V}_\ell - \vec{V}_i)\cdot\vec{t}_1 = 0 \quad , \text{ and} \tag{III.42}$$

$$(\vec{V}_\ell - \vec{V}_i)\cdot\vec{t}_2 = 0 \quad , \tag{III.43}$$

equation of motion

$$(\rho_v \vec{V}_v)\cdot\vec{n}_2 \vec{V}_v + (\rho_\ell \vec{V}_\ell)\cdot\vec{n}_1 \vec{V}_\ell = - P_v \vec{n}_2 - \tag{III.44}$$

$$- P_\ell \vec{n}_1 - \bar{\bar{\tau}}_v \cdot \vec{n}_2 - \bar{\bar{\tau}}_\ell \cdot n_1 - \frac{2\sigma}{R_m}\vec{n}_1 - \nabla_s \sigma \quad ,$$

equation of energy

$$\left[\rho_v \vec{V}_v \left(h_v + \frac{V_v^2}{2}\right) + \vec{q}_v + \bar{\bar{\tau}}_v \cdot \vec{V}_v\right]\cdot\vec{n}_2 + \left[\rho_\ell \vec{V}_\ell \left(h_\ell + \frac{V_\ell^2}{2}\right) + \vec{q}_\ell + \right. \tag{III.45}$$

$$\left. + \bar{\bar{\tau}}_\ell \cdot \vec{V}_\ell \right]\cdot\vec{n}_1 + \nabla_s \cdot (\sigma \vec{V}_i) = 0 \quad .$$

D. Constitutive Equations in General Form

The constitutive equations in general form are

rheological equation

$$\bar{\bar{\tau}} = \bar{\bar{\tau}}\left(\mu, u_j, \frac{\partial u_j}{\partial x_k}\right), \text{ for} \tag{III.46}$$

$$j = 1, 2, 3 \text{ and } k = 1, 2, 3 \quad , \tag{III.47}$$

equations of viscosity

$$\mu_v = \mu_v(T) \quad \text{, and} \tag{III.48}$$

$$\mu_\ell = \mu_\ell(T) \quad , \tag{III.49}$$

equation of heat conduction

$$\vec{q} = -\chi \nabla T \quad , \tag{III.50}$$

equations of thermal conductivity

$$\chi_\ell = \chi_\ell(T) \quad , \tag{III.51}$$

$$\chi_v = \chi_v(T) \quad \text{, and} \tag{III.52}$$

$$\chi_s = \chi_s(T) \quad , \tag{III.53}$$

thermal equations of state

$$\rho_v = \rho_v(P,T) \quad \text{, and} \tag{III.54}$$

$$\rho_\ell = \rho_\ell(P,T) \quad , \tag{III.55}$$

caloric equations of state

$$h_v = h_v(P,T) \quad \text{, and} \tag{III.56}$$

$$h_\ell = h_\ell(P,T) \quad , \tag{III.57}$$

equation of latent heat of vaporization

$$h_{v\ell} = h_v - h_\ell \quad \text{at saturation} \quad , \tag{III.58}$$

equation of surface tension

$$\sigma = \sigma(T) \quad , \tag{III.59}$$

unit normal vectors

$$\vec{n}_1 = -\vec{n}_2 = \vec{n}(\text{surface geometry}) , \tag{III.60}$$

unit tangent vectors

$$\vec{t}_1 = \vec{t}_1(\text{surface geometry}) , \text{ and} \tag{III.61}$$

$$\vec{t}_2 = \vec{t}_2(\text{surface geometry}) , \tag{III.62}$$

radius of curvature

$$R_m = R_m(\text{surface geometry}) , \tag{III.63}$$

surface gradient

$$\nabla_s \rightarrow \text{operator based on surface geometry} , \tag{III.64}$$

surface divergence

$$\nabla_s \cdot \rightarrow \text{operator based on surface geometry , and} \tag{III.65}$$

surface coordinates

$$p = p(r_c, r_v, r_{ws}, \phi) , \text{ and} \tag{III.66}$$

$$q = q(r_c, r_v, r_{ws}, \phi) . \tag{III.67}$$

E. Dimensionless Groups

Writing Equations (III.36) through (III.67) in dimensionless form with the reference parameters, see Appendix A, results in the following twenty dimensionless groups for the liquid-vapor interface

$$\frac{l_e}{l_c}, \frac{l_a}{l_c}, \frac{r_w}{r_v}, \frac{r_v}{l_c}, \frac{r_{ws}}{r_c}, \frac{r_c}{r_v}, \frac{\rho_\ell}{\rho_v}, \frac{\rho_v r_v u_v}{\mu_v}, \frac{\rho_\ell r_c u_\ell}{\mu_\ell},$$

$$\frac{\rho_\ell u_\ell^2 r_c}{\sigma}, \frac{u_v^2}{h_{v\ell}}, \frac{\mu_v c_{pv}}{\chi_v}, \frac{\mu_\ell c_{p\ell}}{\chi_\ell}, \frac{u_v^2}{c_{pv} T_c}, \frac{u_\ell^2}{c_{p\ell} T_c}, \frac{\chi_s}{\chi_\ell},$$

$$\frac{c_{pv}}{c_{p\ell}}, \phi_o, \frac{R_m}{r_c}, \epsilon_o .$$

7. Environmental Boundary Conditions

The environmental boundary of the heat pipe, that surface separating the contained working fluid and its surroundings, is studied by examining its spatial location, assumptions, boundary conditions, and constitutive equations. Dimensionless groups are obtained. The boundary is subdivided into the following five sections: evaporator, adiabatic, condenser, evaporator end, and condenser end. These sections are distinguished from each other by their respective spatial locations and their respective constitutive equations of environmental heat transfer.

A. Spatial Location

The spatial location of the heat pipe boundary sections, see Figure 8, are as follows

evaporator

$$r = r_w \tag{III.68}$$

$$0 < z \le l_e \text{ , and} \tag{III.69}$$

$$0 \le \theta \le 2\pi \quad , \tag{III.70}$$

adiabatic

$$r = r_w \quad , \tag{III.71}$$

$$l_e < z < l_e + l_a \quad , \text{ and} \tag{III.72}$$

$$0 \le \theta \le 2\pi \quad , \tag{III.73}$$

condenser

$$r = r_w \, , \tag{III.74}$$

$$l_e + l_a \le z < l_e + l_a + l_c \, , \text{ and} \tag{III.75}$$

$$0 \le \theta \le 2\pi \quad , \tag{III.76}$$

evaporator end

$$0 \le r < r_w \, , \tag{III.77}$$

$$z = 0 \quad , \text{ and} \tag{III.78}$$

$$0 \le \theta \le 2\pi \, , \text{ and} \tag{III.79}$$

condenser end

$$0 \le r < r_w \quad , \tag{III.80}$$

$$z = l_e + l_a + l_c \, , \text{ and} \tag{III.81}$$

$$0 \le \theta \le 2\pi \, . \tag{III.82}$$

B. Assumptions

The basic assumptions which apply to each subdivision of the boundary are

1) steady state,
2) continuum flow on fluid sides of the boundaries,
3) the environment contains no working fluid,
4) the boundary is motionless,
5) negligible heat exchange by radiation, and
6) negligible viscous dissipation of heat.

C. Boundary Conditions in Vector Form

The boundary conditions which apply to each subdivision are

equation of continuity

$$(\rho\vec{V})\cdot\vec{n}_E = 0 \tag{III.83}$$

no slip conditions

$$(\rho\vec{V})\cdot\vec{t}_1 = 0 \text{ , and} \tag{III.84}$$

$$(\rho\vec{V})\cdot\vec{t}_2 = 0 \text{ , and} \tag{III.85}$$

equation of energy

$$\left[\rho\vec{V}\left(h+\frac{V^2}{2}\right)+\vec{q}\right]\cdot\vec{n}_E + \left[\vec{q}_E\right]\cdot\vec{n}_i = 0 \ . \tag{III.86}$$

D. Constitutive Equations in General Form

The constitutive equations which apply to each subdivision are

equation of heat conduction

$$\vec{q} = -\chi\nabla T \ , \tag{III.87}$$

equation of liquid thermal conductivity

$$\chi_\ell = \chi_\ell(T) \, , \tag{III.88}$$

equation of wick-solid thermal conductivity

$$\chi_s = \chi_s(T) \, , \tag{III.89}$$

equation of wick effective thermal conductivity

$$\chi_{eff} = \chi_{eff}\left(\chi_\ell(T), \chi_s(T), r_w, r_v, r_c, r_{ws}, n\right) \, , \tag{III.90}$$

liquid thermal equation of state

$$\rho_\ell = \text{constant} \, , \tag{III.91}$$

liquid caloric equation of state

$$h_\ell = h_\ell(P, T) \, , \tag{III.92}$$

unit normal vectors

$$\vec{n}_i = -\vec{n}_e = \vec{n}(\hat{r}, \hat{z}, \hat{\theta}) \, , \tag{III.93}$$

unit tangent vectors

$$\vec{t}_1 = \vec{t}_1(\hat{r}, \hat{z}, \hat{\theta}) \, , \text{ and} \tag{III.94}$$

$$\vec{t}_2 = \vec{t}_2(\hat{r}, \hat{z}, \hat{\theta}) \, . \tag{III.95}$$

The remaining constitutive equations which apply only to the respective subdivisions are

evaporator section

external heat flux vector

$$\int_0^{2\pi}\int_0^{l_e} \vec{q}_E \cdot (r_w \hat{r})\, dz\, d\theta = \dot{Q}_e \, , \qquad \text{(III.96)}$$

adiabatic section

external heat flux vector

$$\vec{q}_E = 0 \, , \qquad \text{(III.97)}$$

condenser section

external heat flux vector

$$\int_0^{2\pi}\int_{l_e+l_a}^{l_e+l_a+l_c} \vec{q}_E \cdot (r_w \hat{r})\, dz\, d\theta = \int_0^{2\pi}\int_{l_e+l_a}^{l_e+l_a+l_c} U_c\left[T(r=r_w, z, \theta) - T_c\right] r_w\, dz\, d\theta \, , \qquad \text{(III.98)}$$

where U_c and T_c are reference parameters, see Chapter III, Section 3, and

evaporator and condenser end sections

external heat flux vector

$$\vec{q}_E = 0 \, , \qquad \text{(III.99)}$$

equation of vapor thermal conductivity

$$\chi_v = \chi_v(T) \, , \qquad \text{(III.100)}$$

vapor thermal equation of state

$$\rho_v = \rho_v(P, T) \, , \text{ and} \qquad \text{(III.101)}$$

loric

vapor calorie equation of state

$$h_v = h_v(P,T) . \qquad \text{(III.102)}$$

E. Dimensionless Groups

Writing Equations (III.68) through (III.102) in dimensionless form with the reference parameters and substitution of the constitutive equations, see Appendix A, results in the following eleven dimensionless groups for the environmental boundary conditions

$$\frac{l_e}{l_c}, \frac{l_a}{l_c}, \frac{r_v}{l_c}, \frac{r_v}{r_w}, \frac{r_c}{r_v}, \frac{r_{ws}}{r_c}, \frac{\chi_s}{\chi_l}, \frac{\chi_{eff}}{\chi_l}, n, \frac{\chi_l}{r_w U_c}, \frac{\dot{Q}_e}{\chi_{eff} l_c T_c} .$$

8. Heat Pipe Operating Temperature

Temperature, the explicit parameter appearing in various constitutive equations (e.g. equation of thermal conduction), provides the dimensionless group

$$\frac{T(r,z,\theta)}{T_c} ,$$

where T_c is the condenser sink reference parameter. In accordance with the reference parameters, see Chapter III, Section 3, this group is interpreted as

$$\frac{T_o}{T_c} ,$$

where T_o is the heat pipe operating temperature.

9. Summary of Dimensionless Groups

The collection of 24 dimensionless groups obtained from the general theory is shown in Table 3. For groups containing velocity, the defining reference parameters of Equations (III.2) and (III.3) have been substituted, hence velocity does not appear explicitly. All symbols refer to the reference parameters, see Chapter III, Section 3. Details are indicated in Appendix A.

Table 3. Dimensionless Groups of General Theory

Category	Symbol	Remarks
Material Properties	$\frac{\rho_l}{\rho_v}$	$\frac{\text{liquid density}}{\text{vapor density}}$
	$\frac{\mu_v C_{pv}}{\chi_v}$	vapor Prandtl number
	$\frac{\mu_l C_{pl}}{\chi_l}$	liquid Prandtl number
	$\frac{\chi_s}{\chi_l}$	$\frac{\text{wick-solid conductivity}}{\text{liquid conductivity}}$
	$\frac{C_{pv}}{C_{pl}}$	$\frac{\text{vapor specific heat}}{\text{liquid specific heat}}$
	$\frac{h_{vl}}{C_{pl} T_c}$	Kutateladze number
	$\frac{\chi_{eff}}{\chi_l}$	$\frac{\text{wick effective conductivity}}{\text{liquid conductivity}}$
Flow Parameters	$\frac{2}{\pi}\left(\frac{\dot{Q}_e}{h_{vl} r_v \mu_v}\right)$	vapor axial Reynolds number

(Continued)

Table 3. (Continued)

Category	Symbol	Remarks
Flow Parameters	$\frac{1}{c_{p_v} T_c}\left(\frac{\dot{Q}_e}{2\pi r_v \ell_c \rho_v h_{v\ell}}\right)^2$	vapor Eckert number
	$\frac{\rho_\ell r_c}{\sigma}\left(\frac{\dot{Q}_e}{2\pi r_v \ell_c \rho_\ell h_{v\ell}}\right)^2$	Weber number
	$\left(\frac{\pi r_c h_{v\ell} \mu_\ell}{\dot{Q}_e}\right)\left(K_1 r_c^2\right)$	Darcy number
	$\frac{\dot{Q}_e}{\pi r_c h_{v\ell} \mu_\ell}$	liquid pore Reynolds number
Geometry	$\frac{r_v}{r_w}$	vapor radius / wick outer radius
	$\frac{r_v}{\ell_c}$	vapor radius / condenser length
	$\frac{\ell_e}{\ell_c}$	evaporator length / condenser length
	$\frac{\ell_a}{\ell_c}$	adiabatic length / condenser length
	$\frac{r_c}{r_v}$	wick pore radius / vapor radius
	$\frac{r_{ws}}{r_c}$	wick-solid radius / wick pore radius
	n	number of wick screen layers

(Continued)

Table 3. (Continued)

Category	Symbol	Remarks
Geometry	ϕ_o	fluid wetting angle
	$\frac{R_m}{r_c}$	$\frac{\text{evaporator meniscus radius}}{\text{wick pore radius}}$
	ϵ_o	wick porosity
Environment	$\frac{T_o}{T_c}$	$\frac{\text{heat pipe operating temperature}}{\text{condenser sink temperature}}$
	$\frac{U_c l_c}{K_l}$	$\frac{\text{liquid thermal resistance}}{\text{condenser external thermal resistance}}$

CHAPTER IV

EXPERIMENTATION

1. Objective

The purpose of this experimentation is to provide data from an operating heat pipe which will allow correlation of the parameters and further understanding of heat pipe operation. The results of these experiments will yield measured values of temperatures and heat transfer rates for a horizontal heat pipe of fixed geometry with a working fluid of water and methanol, and provide raw data which can be used to evaluate the parameters required for correlation.

2. Equipment

The equipment is comprised of the heat pipe with its attached instrumentation, see Figures 9, 10, and 11, and the auxiliary equipment and instrumentation, see Figure 12.

A. Heat Pipe

The heat pipe shell, see Figure 9, consists of a 3/4 inch diameter by 18.0 inch long tube of 304 stainless steel. The heat pipe wick is composed of two layers of 316 stainless steel screen, 100 mesh and 0.0045 inch wire diameter, mounted concentrically on the inside wall of the pipe shell. See Table 4 for a listing of geometric parameters.

The condenser section is constructed from a 5.0 inch long by 1 inch diameter schedule 40 pipe of 304 stainless steel. The pipe is solder mounted concentric to the heat pipe shell and sealed at each end

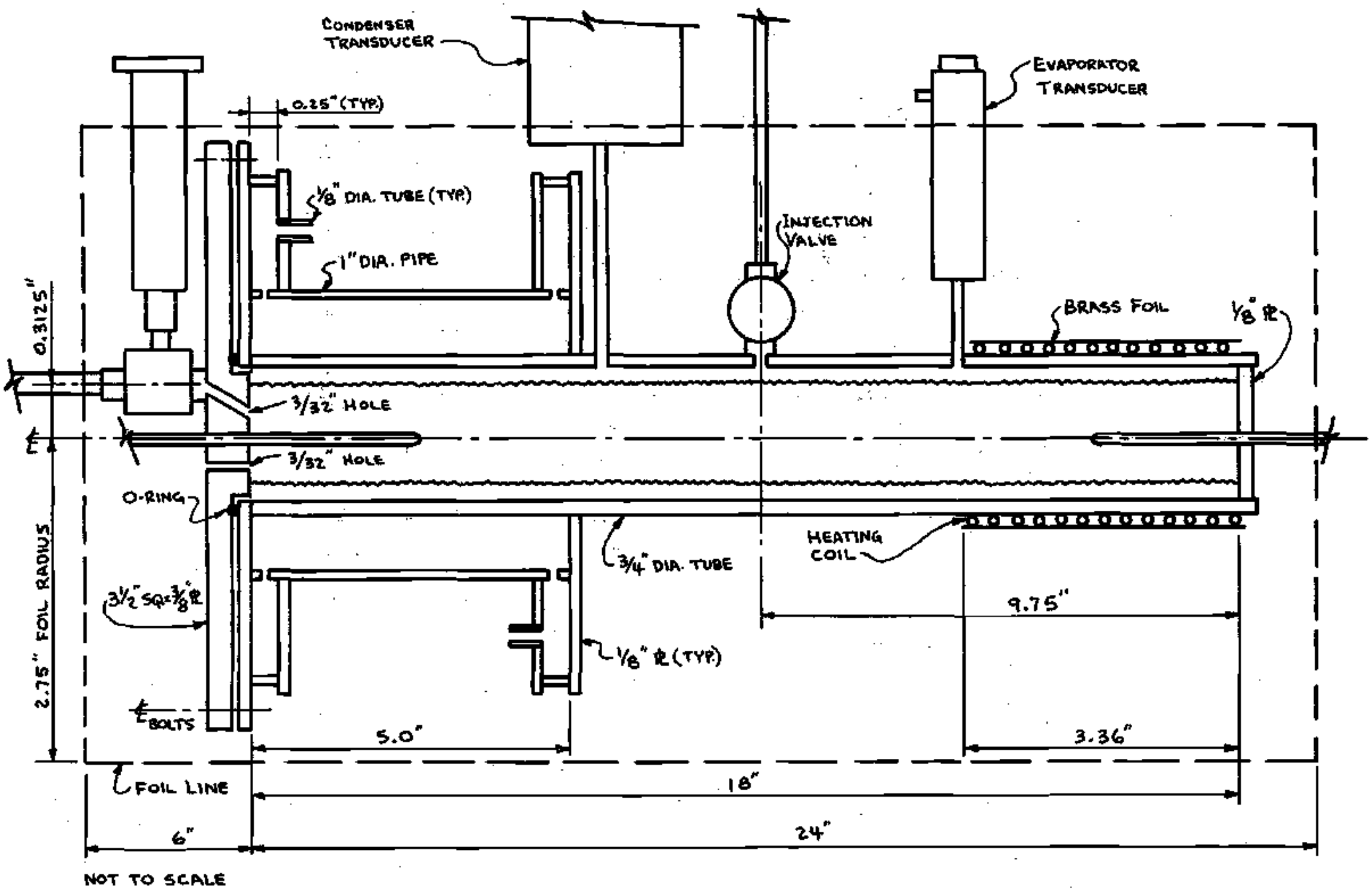

Figure 9. Experimental Heat Pipe Dimensions.

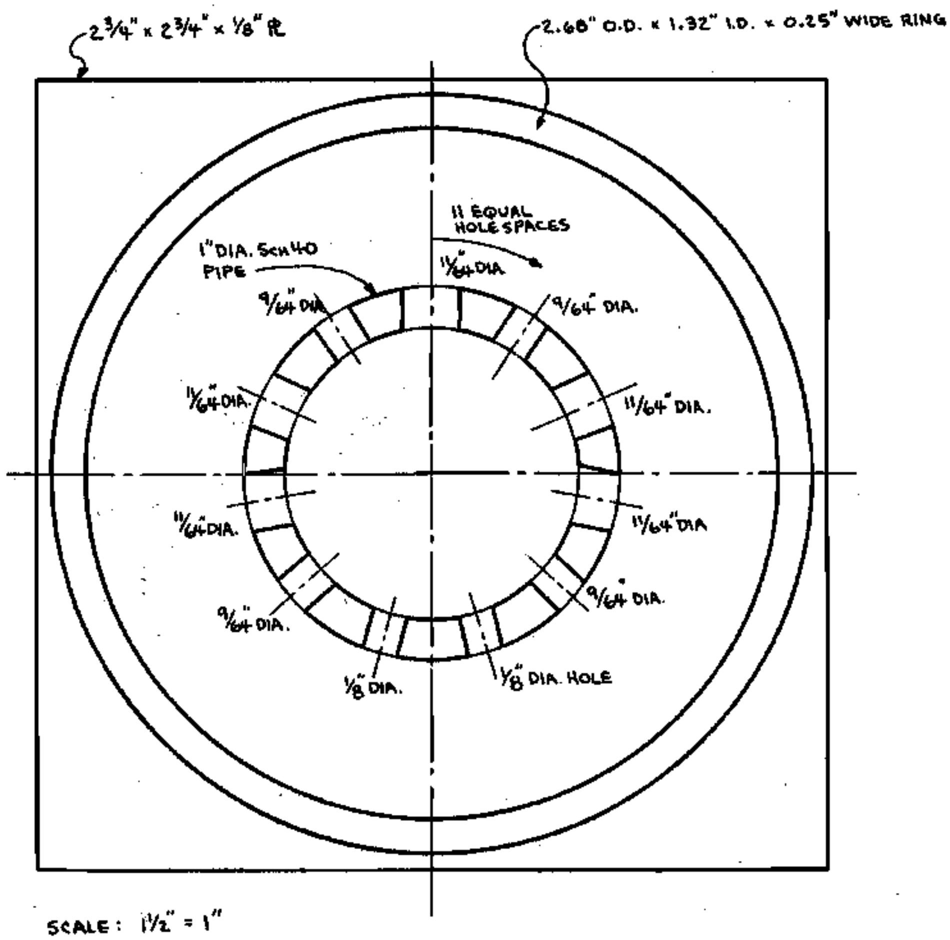

Figure 10. Experimental Heat Pipe Condenser Header.

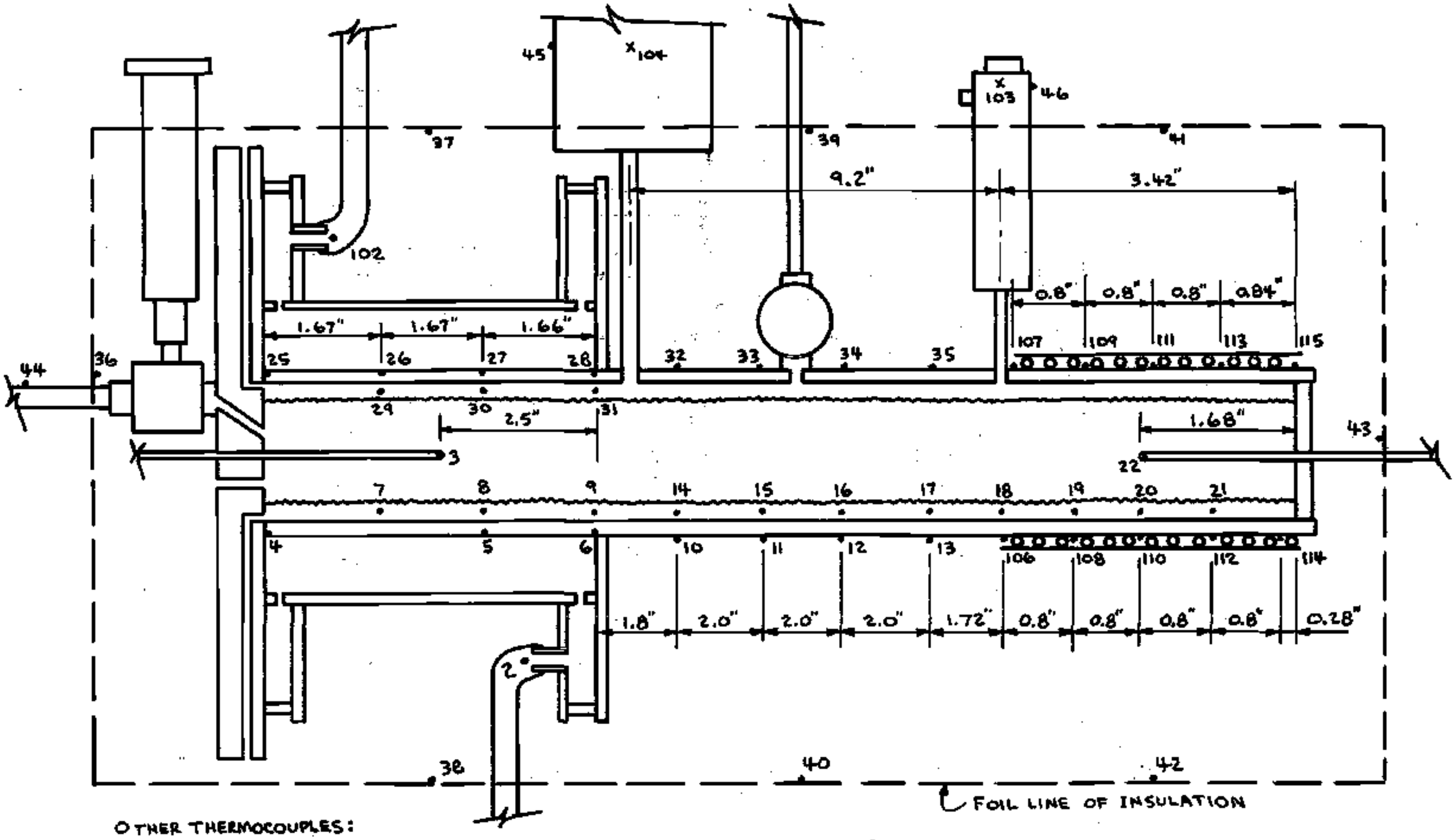

OTHER THERMOCOUPLES:

1	LOW CALIB. FROM ICE	101	HIGH CALIB. TO RECORDER
23	HIGH CALIB. FROM POT.	105	INJECTION PRE-HEAT
24	RELAY SKIP		
47	ROOM TEMPERATURE		
48	RELAY SKIP		

Figure 11. Experimental Heat Pipe Instrument Location.

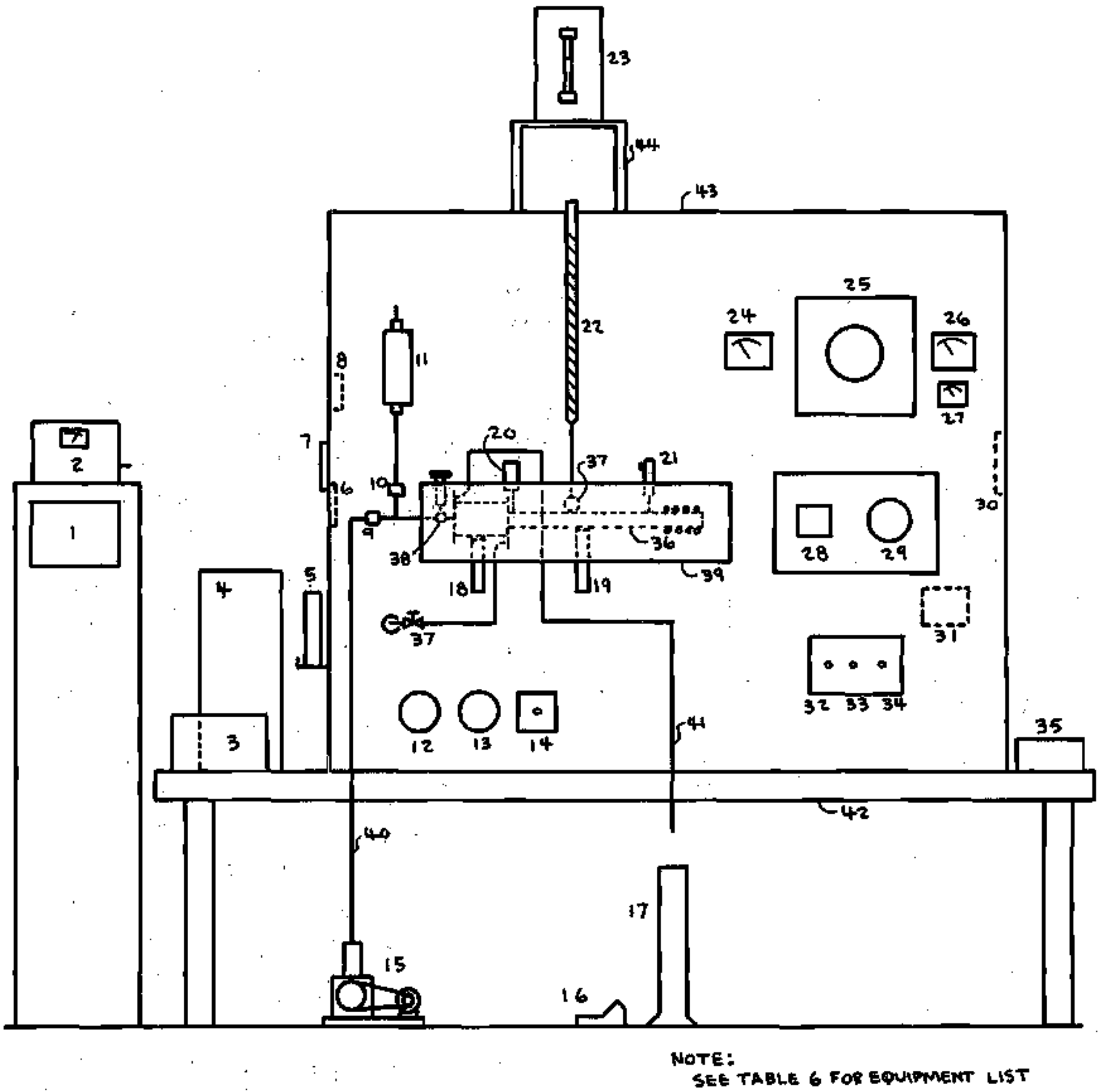

Figure 12, Experimental Auxiliary Equipment Schematic

Table 4. Geometric Parameters of Experimental Heat Pipe.

Name	Symbol	Value inches (u.o.n.)
evaporator length	l_e	3.36
adiabatic length	l_a	9.64
condenser length	l_c	5.00
inside wick radius	r_v	0.298
outside wick radius	r_w	0.326
wick pore radius	r_c	0.00275
wick-solid radius	r_{ws}	0.00225
number of screen layers	n	2 layers

by header chambers. Each header is composed of stainless steel plates separated by a 1/4 inch wide spacer ring. Openings for cooling water flow consist of a single port in one of the plates and multiple holes in the condenser pipe between the plates, see Figure 10. The condenser end of the heat pipe is sealed by an O-ring between the end header plate and a flange.

The evaporator section is formed by an electric resistance heating coil wrapped helically around a 3.36 inch long section of the heat pipe shell. The coil is covered by a sheath of brass foil. The evaporator end of the heat pipe is sealed by a welded plate of 304 stainless steel.

The adiabatic section is covered with fiberglas insulation. The entire heat pipe (condenser, adiabatic, and evaporator) is covered with fiberglas insulation to a diameter of 5.5 inches and is covered with aluminum foil.

Heat pipe instrumentation, that instrumentation attached directly to thehheat pipe test section, consists of two pressure transducers and various thermocouples, see Figure 11. The condenser pressure transducer is mounted to a copper tube positioned on the heat pipe shell in the adiabatic section adjacent to the condenser header. The evaporator pressure transducer is mounted to a copper tube positioned on the heat pipe shell in the adiabatic section and adjacent to the end of the heating coil.

Thermocouples are mounted on the heat pipe in seven different areas, see Figure 11 and Table 5. Wick thermocouples are spot welded between the two layers of screen. These wires extend out of the heat

Table 5. Thermocouple Materials

Category	Junction	Wire Size	Insulation
Condenser Wall	Copper-Constantan	36 ga	enamel
Adiabatic Wall	Copper-Constantan	24 ga	fiberglas
Evaporator Wall	Chromel-Alumel	30 ga	fiberglas
Wick	Copper-Constantan	36 ga	enamel
Cooling Water	Copper-Constantan	30 ga	nylon
Vapor Probe	Copper-Constantan	36 ga	Ceramic in S. S. Sheath
Insulation	Copper-Constantan	24 ga	fiberglas

pipe through an epoxy sealed hole in the condenser flange. Condenser wall thermocouples are mounted in grooves in the outer shell wall. The grooves are sealed with a epoxy of high thermal conductivity. Adiabatic shell wall thermocouples are spot welded to the outer shell wall. Evaporator shell wall thermocouples are spot welded to the outer shell wall between the coils of the heating element. These wires extend out through the brass foil. Vapor thermocouple probes are positioned at the center of the evaporator and condenser sections. The probe sheaths are attached to end plates by silver solder. Insulation thermocouples are mounted on the underside of the aluminum foil. Cooling water thermocouples are epoxy sealed within the tubing attached to the ports of each condenser header.

B. <u>Auxiliary Equipment</u>

The auxiliary equipment is made up of systems for 1) vacuum, 2) condenser cooling water, 3) evaporator electric power, 4) pressure transducer power supply, 5) working fluid injection, and 6) emf measurement, see Figure 12 and Table 6.

The vacuum system consists of the vacuum pump, connecting copper tubing, a valve attached to the condenser end flange, and a top line of copper tubing to the Alphatron pressure sensor.

The condenser cooling water system is composed of a constant head tank supplied with building water, precooling chamber, heat pipe inlet control valve, water collection beaker, and connecting tubing.

The evaporator electric power system is comprised of the alternating current voltage regulator, volt meter, ammeter, and watt meter.

Table 6. Equipment List

Equipment numbers refer to Figure 13.

Item No	Name	Description
1	Recorder	Honeywell Model SY153-89-(C)-II-III-16 24 channel
2	Alphatron Pressure Gage	NRC Equipment Corp., Alphatron Type 530
3	Potentiometer	Leeds & Northrup No. 8686
4	Pre-chiller	Ebco water cooler, D 89031
5	Ice Reference	Dewar Flask
6	Thermocouple Panel	For thermocouple extension wires from relays
7	Thermocouple Panel	For thermocouple extension wires to recorder
8	Relays	48 bank relays, Southern Bell
9	Valve	Nupro Type B-4H
10	Valve	Nupro Type B-4H
11	Alphatron Sensor	For Alphatron Type 530
12	Switch	For 10 Potentiometer thermo-couples
13	Switch	For 10 Potentiometer thermo-couples
14	Switch	From power source to relays
15	Vacuum Pump	Cenco-HYVAC 14, No. 91705
16	Stop Watch	Compass, 1 jewel
17	Collection Water Beaker	Pyrex No. 3042
18	Support	Bar for heat pipe support

(Continued)

Table 6. (Continued)

Item No	Name	Description
19	Support	Bar for heat pipe support
20	Condenser Pressure Transducer	Statham Model PA769-50
21	Evaporator Pressure Transducer	Statham Model PM732TC $\pm$ 25-350
22	Injection Burette	LKMAX Type TD, with nichrome ribbon
23	Constant Head Tank	Shown with sight glass
24	Voltmeter	Simpson, 0-150 AC
25	Voltage Regulator	Powerstat, 0-115V AC, for evaporator coils
26	Ammeter	Simpson, 0-25 AC
27	Wattmeter	Triplet, 0-750 W (not used in tests)
28	Voltage Regulator Power Supply	Lambda Model LCS-2-01, 0-6.5V DC, for excitation to transducers
29	Voltage Regulator	Powerstat, 0-115V AC, for relay
30	Power Panel	For connections to building lines
31	Rectifier	0-30V DC output
32	Switch	To relay bank
33	Switch	To injection burette coil
34	Switch	To evaporator heating coils
35	Wattmeter	Weston Model 310
36	Heat Pipe	Shown with evaporator coil of Chromalox Type TSSM-40, 1120 w.

(Continued)

Table 6. (Continued)

Item No	Name	Description
37	Valve	Nupro Type B-4H
38	Valve	Nupro Type B-4H
39	Insulation	Fiberglas with Aluminum foil cover
40	Vacuum Tubing	Copper, to vacuum pump
41	Cooling Water Tubing	Copper, to collection beaker
42	Table	Wood
43	Test Board	Plywood with angle frame
44	Tank Support	Steel angle

The transducer power supply system is a single direct current power supply for both transducers.

The working fluid injection system utilizes a 50 ml. burette, resistance heating ribbon wrapped around the burette, and an injection valve joining the burette to the heat pipe shell. A 1/16 inch diameter hole in the pipe shell permits the flow of injection fluid.

The thermocouple recording system consists of a 24 channel recorder, 48 channel relay bank with power supply, and an ice reference flask. Direct emf measurement is accomplished with a potentiometer, potentiometer switches, and the same ice reference flask.

3. Procedure

The operational procedures of this study are composed of various stages of construction and testing.

A. Heat Pipe Construction

Construction consists of

1) assembling the parts of the heat pipe shell, cooling water jacket, and evaporator heating coil,

2) attaching the shell wall and vapor thermocouples to the heat-pipe,

3) attaching the pressure transducers,

4) spot welding thermocouples to the wick, forming the wick around a core, spot welding the wick along its seam into its final form, cleaning the wick with acetone, and inserting it into the pipe shell,

5) sealing the condenser end with O-ring and flange, and sealing the wick thermocouple port with high vacuum epoxy, and

6) insulating the entire heat pipe, attaching insulation thermocouples, and foil attachment.

B. Preliminary Testing

Preliminary testing is comprised of instrument calibration and vacuum leak testing.

Each transducer is calibrated by recording the emf signal, measured with potentiometer, and the column height of a mercury monometer. These calibrations are made prior to transducer attachment to the heat pipe.

Thermocouple calibration consists of recording the emf signal, measured with potentiometer, and indication by a standardized thermometer, both in a constant temperature bath. For thermocouples with fiberglas insulation, a sample thermocouple is calibrated. All other thermocouples are individually calibrated. These calibrations are made prior to thermocouple mounting onto the heat pipe.

Vacuum leak testing is composed of drawing a vacuum on the heat pipe interior, closing valves to the surroundings, and recording the internal pressure over a time period, see Appendix B. The Alphatron vacuum gage is used for pressure indication. These tests are repeated until all leak points are sealed either with solder or epoxy. The heat pipe is considered sealed when the leak rate is sufficiently low for only negligible amounts of room air to enter the pipe over the time period required for data taking. These tests are conducted prior to working fluid injection.

C. Start up

Operational start up is begun with vacuum pumping over a 24 hour period. The working fluid is then pre-heated with the resistance ribbon on the burette. Heating takes place for 30 minutes with no boiling. Injection is accomplished by opening the injection valve and permitting liquid to be drawn into the evacuated heat pipe. The amount of fluid injected is that amount estimated to saturate the wick with liquid and fill the vapor region with vapor, see Appendix C. External heat transfer is initiated by first flowing the pre-chilled cooling water through the condenser jacket and then raising the voltage across the evaporator jeating element until the desired power level is reached.

D. Measurements

Data acquisition consists or recording four types of steady state information 1) condenser conditions, 2) evaporator condition, 3) general emf data, and 4) room conditions. The system is considered to be at steady state when no observable changes in any data occurred during the time period (nominal 15 minutes) required for data taking.

The volume flow rate of cooling water is measured by collecting the water in a graduated beaker over a measured time period. Other condenser conditions are the potentiometer readings for inlet temperature and temperature difference between inlet and exit.

The power (wattage) delivered to the evaporator heating coil is recorded.

General temperature and pressure data are comprised of 1) potentiometer readings of transducer emfs, 2) potentiometer readings of evaporator shell wall thermocouples, and 3) recorder printings of emf signals through the relays for both banks of 24 thermocouples.

Room temperature and barometric pressure are recorded.

E. Change of Operating Point

The heat pipe operating point, characterized during testing by adiabatic wall temperature and coil power, is changed in one of three ways. These methods are 1) change the power level delivered to the evaporator heating coil, 2) change the water flow rate through the condenser cooling jacket, or 3) change the cooling water inlet temperature by alteration of the percentage of pre-chilled water flowing into the cooling jacket. Once the change is initiated, the system is permitted to reach steady state, then data taking is repeated.

F. Shut Down

When a series of tests is completed, the evaporator power is turned off. After the evaporator vapor thermocouple reaches room temperature, the condenser cooling water flow is terminated.

G. Terminal Testing

Following heat pipe shut down all thermocouples reach room temperature (nominal 12 hours). The transducer pressures are then measured and recorded. A negligible difference between transducer pressure and interior saturation pressure indicates no gases leaked into the heat pipe during operation.

4. Results

Experimental results are comprised of three parts 1) direct data, those data recorded during heat pipe operation, 2) data reduction, application of calibration and correction factors to direct data, and 3) listing of the reduced data.

A. Direct Data

Direct operational data consists of 1) power delivered to heating coil, 2) volume of cooling water collected, 3) time lapse of collection, see Appendix D, and 4) emf data, see Appendix E.

B. Data Reduction

Data reduction is divided into the three parts of pressure and temperature reduction, evaluation of the heat pipe evaporator heat transfer rates, and evaluation of condenser environment conditions.

Data from pressure transducers and thermocouples are reduced with calibration curves, see Appendices F, G, and H. The heat pipe heat transfer rate is evaluated by estimating the heat loss rate to the surroundings, see Appendix I.

The condenser sink temperature is evaluated from cooling water temperatures, see Appendix J. Evaluation of the unit conductance between the sink and the outer wick wall is accomplished by considering the temperatures, heat rates, and heat flow areas, see Appendices K and Q.

A discussion of the reduction techniques applied to other parameters required for correlation analysis is reserved until those parameters have been identified.

C. Reduced Data

Operating data are tabulated in Table 7. Test values are listed for the independent variables of heat rate $(\dot{Q}_e)$, condenser sink temperature (T_c), and sink unit conductance (U_c). The operating temperature (T_o) is also given. Tables 8 and 9 show pressure and typical temperature data for the water and methanol tests respectively.

Measured pressures of both condenser and evaporator transducer differ from the saturation pressure at the operating temperature (e.g. Test 9, $T_o = 110.25\ °F$, $P_{sat.} = 2.61$ in. Hg). A probable cause for these differences is that each transducer is positioned in a region where temperature differs from the operating value. The condenser transducer measures a pressure corresponding to a saturation temperature which is between the condenser wall and operating temperatures. Similarly, the evaporator transducer measures a pressure corresponding to a saturation temperature between evaporator wall and operating temperatures.

Figure 13 illustrates typical axial temperature distributions for water (Test 9) and methanol (Test 20). Near isothermal conditions are observed along the adiabatic shell wall. Vapor temperatures for Test 9 coincide with values along the adiabatic wall. The condenser vapor temperature of Test 20 agrees with the condenser wall value, suggesting negligible radial heat transfer near the axial position of thermocouple T_3. High evaporator wall temperatures (T_{113}) are observed for both tests. This suggests that wick drying has occurred. If drying exists, it must be a partial drying, since evaporator vapor temperatures are nearly equal to the corresponding adiabatic wall temperatures. For high heat rates (e.g. Tests 4 and 11) increases in the evaporator vapor temperature (T_{22}) over the adiabatic wall temperature suggested a large amount of drying, and testing was terminated to avoid damage to the heat pipe.

Table 7. Reduced Operating Data.

Fluid	Test	$\dot{Q}_e$	T_c	U_c	T_o
		$\frac{BTU}{HR}$	°F	$\frac{BTU}{HR\ FT^2\ °R}$	°F
Water	1	155.0	69.74	236.46	93.55
	2	230.3	70.43	234.89	102.37
	3	331.0	71.30	235.25	111.11
	4	339.6	72.13	219.67	118.14
	5	172.7	70.33	243.23	97.29
	6	249.9	71.15	232.48	103.82
	7	349.9	72.51	220.86	114.56
	8	167.5	70.98	198.70	100.57
	9	247.9	72.90	176.19	110.25
Methanol	10	52.2	67.67	135.61	93.09
	11	90.8	70.30	133.91	104.26
	12	39.0	66.70	229.62	88.54
	13	50.8	67.03	183.53	91.91
	14	68.2	68.07	156.36	97.87
	15	93.7	68.77	146.75	103.72
	16	52.7	54.66	121.28	85.97
	17	71.9	57.60	116.25	93.10
	18	80.8	60.44	140.43	100.29
	19	24.9	46.95	202.59	73.64
	20	66.1	48.81	138.85	86.07
	21	20.6	42.97	186.66	71.51

Table 8. Axial Profile Data Sampling for Water*

	Pressure		Temperature											
			vapor probe		condenser shell wall				adiabatic shell wall			wick		evap. shell wall
	cond. P_{104}	evap. P_{103}	T_3	T_{22}	T_4	T_{26}	T_{27}	T_{28}	T_{10}	T_{11}	T_{12}	T_9	T_{14}	T_{113}
Test	in Hg	in Hg	°F	°F	°F	°F	°F	°F	°F	°F	°F	°F	°F	°F
1	1.21	2.13	93.99	94.08	82.86	80.97	84.06	81.87	94.00	94.00	94.00	80.41	93.55	147.77
2	1.66	2.66	103.12	102.79	88.59	84.07	89.30	86.42	101.40	101.40	101.40	86.26	102.37	210.90
3	2.25	3.33	111.74	111.56	94.36	88.97	94.17	90.42	111.39	111.50	111.50	93.28	111.11	308.97
4	2.81	3.94	118.96	126.09	99.28	92.14	97.16	94.52	117.76	117.58	117.99	100.75	118.45	377.10
5	1.32	2.63	97.70	97.28	85.39	82.82	86.05	84.30	97.12	97.36	97.36	83.18	97.29	174.11
6	1.68	2.90	104.51	103.75	88.90	86.14	90.01	87.80	104.42	104.42	104.42	90.12	103.82	247.20
7	2.35	3.67	114.42	113.47	96.82	90.93	95.60	94.73	114.73	114.73	114.83	98.26	114.56	342.45
8	1.58	2.80	101.12	101.79	88.29	88.07	89.53	88.77	100.78	100.78	100.89	86.04	100.57	169.83
9	2.19	3.58	110.57	110.09	95.24	93.74	95.71	94.87	110.54	110.21	108.40	96.31	110.25	210.50

*Thermocouple numbers refer to locations shown in Figure 11.

Table 9. Axial Profile Data Sampling for Methanol*

	Pressure		Temperature											
			vapor probe		condenser shell wall				adiabatic shell wall			wick		evap. shell wall
Test	cond. P_{104} in Hg	evap. P_{103} in Hg	T_3 °F	T_{22} °F	T_{25} °F	T_{26} °F	T_{27} °F	T_{28} °F	T_{10} °F	T_{11} °F	T_{12} °F	T_9 °F	T_{16} °F	T_{113} °F
10	8.30	9.70	71.07	96.83	73.51	76.35	79.14	77.91	93.34	93.24	93.24	79.61	93.09	130.32
11	11.48	13.21	102.26	123.90	84.04	82.51	84.89	82.50	104.56	104.56	104.56	87.69	104.26	199.00
12	7.22	8.57	67.57	90.67	68.43	71.73	74.96	73.86	88.22	88.22	88.22	73.75	88.54	114.70
13	8.05	9.46	69.97	95.44	71.82	73.09	76.78	75.23	91.78	91.78	91.91	78.02	91.91	130.22
14	9.42	11.05	85.64	103.11	79.74	76.08	79.50	77.49	98.06	97.79	97.79	83.18	97.87	157.95
15	11.11	11.53	100.22	118.10	82.53	79.99	82.70	80.37	103.98	103.63	103.63	86.16	103.72	196.79
16	6.70	7.95	59.48	89.51	61.71	67.00	70.30	68.81	85.55	85.57	85.77	68.90	85.97	123.14
17	8.26	9.78	77.11	98.86	72.16	71.39	74.49	72.74	92.56	92.56	92.45	76.80	93.10	154.31
18	10.19	11.94	95.22	118.10	76.81	77.05	80.26	77.36	100.33	100.33	100.33	80.39	100.29	195.25
19	4.61	5.43	47.63	75.59	48.21	49.58	57.31	57.53	73.87	73.87	73.87	54.89	73.64	86.82
20	6.79	8.06	60.14	91.58	62.05	61.95	65.90	63.41	88.00	88.22	88.22	68.10	86.07	114.58
21	4.35	5.08	43.62	73.60	43.29	44.89	52.79	52.90	71.58	71.81	71.91	50.87	71.50	85.25

*Thermocouple numbers refer to locations shown in Figure 11.

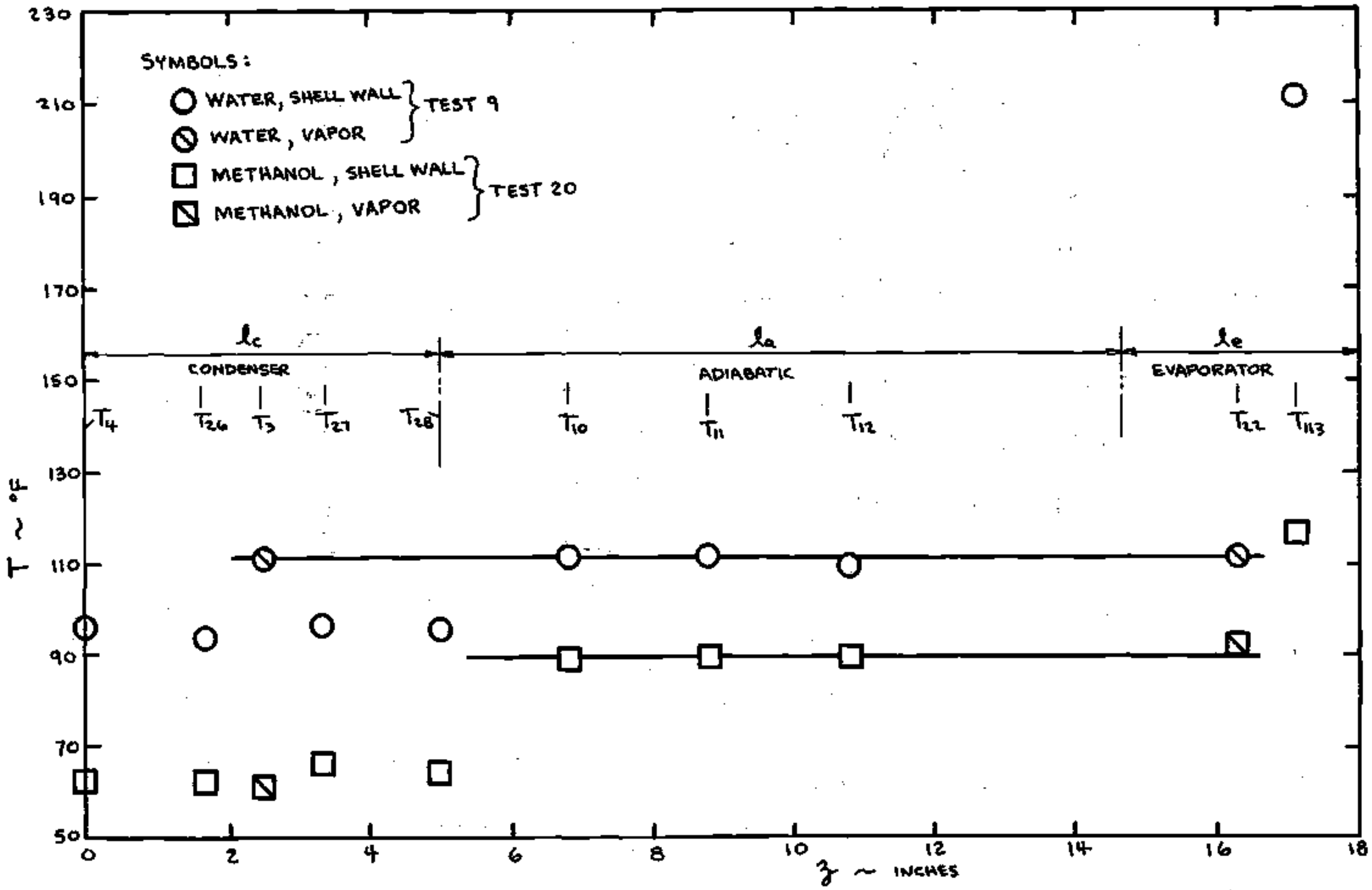

Figure 13. Typical Axial Temperature Distributions*.

*Thermocouple numbers refer to locations shown in Figure 12.

CHAPTER V

CORRELATION THEORY

1. Objective

The purpose of this analysis is to determine the interrelations between the various heat pipe parameters. This study will 1) state the governing simplified equations, 2) identify the parameters required for correlation, 3) demonstrate the data reduction techniques for evaluation of experimental values of the parameters required for correlation, 4) provide interpretations for distinguishing between internal independent and dependent parameters, 5) use the correlations to predict solutions for untested conditions, and 6) compare predictions to experimentally tested conditions.

2. Overall System

The structure of the heat pipe consists of a thin walled circular cylinder and a multiple layer of wire mesh screen lining the inside of the cylinder. A working fluid is distributed within the pipe. The structure is divided into the three axial sections of condenser, adiabatic, and evaporator. The structure is divided into the two radial regions of vapor and liquid. An external region surrounds the liquid region. See Figure 14.

The overall system is studied by considering a pressure balance over the entire cycle of evaporation, vapor flow, condensation, and liquid flow. Using the approach of Kunz, et al, (17, 18) the pressure

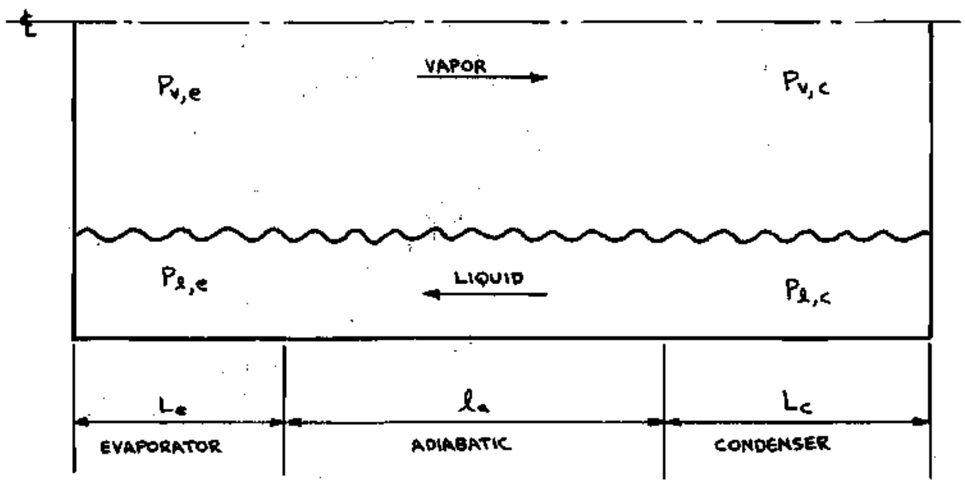

Figure 14. Correlation Theory Heat Pipe Schematic.

balance is made from Figure 14 by writing the identity

$$\left(P_{\ell,e} - P_{v,e}\right) + \left(P_{v,e} - P_{v,c}\right) + \left(P_{v,c} - P_{\ell,c}\right) + \left(P_{\ell,c} - P_{\ell,e}\right) = 0 . \qquad (V.1)$$

The first term is the pressure drop across the liquid-vapor interface in the evaporator section. Neglecting inertial forces, see Appendix L, and characterizing the meniscus by a single radius gives

$$\left(P_{\ell,e} - P_{v,e}\right) = -\frac{2\sigma}{r_m} , \qquad (V.2)$$

where r_m is the meniscus radius at the evaporator end of the pipe.

The second term is the pressure drop along the path of vapor flow which is assumed to be negligible (17, 18), see Appendix M.

The third term is the pressure drop across the liquid-vapor interface in the condenser section. This term is assumed to be negligible (8, 17, 18) which implies this interface to be a flat interface.

The fourth term is the pressure drop along the path of liquid flow. Using Darcy's law for flow in porous media (17, 18, 27) gives

$$\left(P_{\ell,c} - P_{\ell,e}\right) = K_1 \frac{\mu_\ell}{\rho_\ell} \frac{\dot{m}_\ell}{A_w} \left(\ell_{effective}\right) , \qquad (V.3)$$

where K_1 is the wick friction factor, see Appendix N, A_w is the wick cross sectional area, and $\ell_{effective}$ is the effective frictional length of liquid flow. Equation (V.3) is simplified by assuming mass flow to be uniform and radial at the liquid-vapor interfaces of both evaporator and condenser (8, 17, 18). It is further assumed that all heat goes to phase change (5, 8, 17, 18). These assumptions provide the simple relations

$$\ell_{effective} = \frac{1}{2}L_e + \ell_a + \frac{1}{2}L_c \text{ , and} \tag{V.4}$$

$$\dot{m}_\ell = \frac{\dot{Q}_e}{h_{v\ell}} \text{ ,} \tag{V.5}$$

respectively. The inertial term for axial liquid flow is neglected (17), see Appendix O.

Substitution of Equations (V.2), (V.3), (V.4), and (V.5) into Equation (V.1) and neglecting the second and third terms in Equation (V.1) yields

$$\frac{2\sigma}{r_m} = \frac{K_1}{1}\frac{\mu_\ell}{\rho_\ell}\frac{\dot{Q}_e}{h_{v\ell}}\frac{1}{\pi(r_w^2-r_v^2)}\left[\frac{1}{2}L_e + \ell_a + \frac{1}{2}L_c\right] \text{ .} \tag{V.6}$$

Rearranging and using the pore radius r_c to characterize the wire mesh opening size provides the relation

$$\frac{r_m}{r_c} = 2\,\frac{\left(\frac{\rho_\ell \sigma h_{v\ell}}{\mu_\ell}\right)\left(\frac{\pi(r_w^2-r_v^2)}{\dot{Q}_e}\right)}{K_1 r_c\left(\frac{1}{2}L_e + \ell_a + \frac{1}{2}L_c\right)} \text{ .} \tag{V.7}$$

The overall internal heat transfer analysis is made by identifying the various thermal resistances. From Figure 15 the balance is

$$\dot{Q}_e = \frac{(\bar{T}_{ew} - \bar{T}_{cw})}{R_{ew} + R_{cw} + R_{ei} + R_v + R_{ci}} \text{ ,} \tag{V.8}$$

where $\bar{T}_{ew}$ and $\bar{T}_{cw}$ are the average temperatures at r_w along the active lengths of evaporator (L_e) and condenser (L_c) respectively.

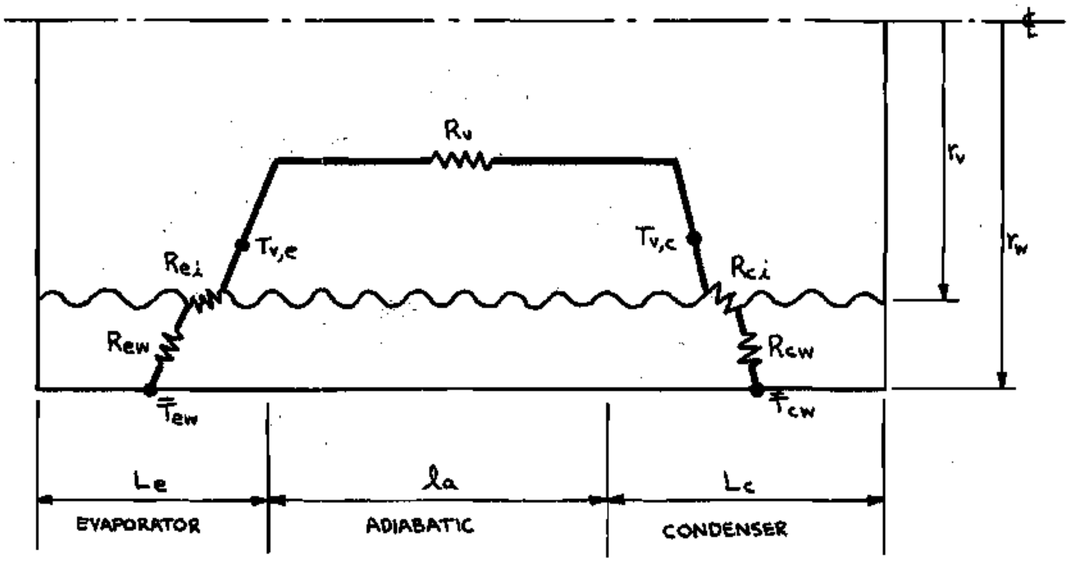

Figure 15. Correlation Theory Thermal Resistances.

Considering the relative magnitudes of the thermal resistances, see Appendix P, Equation (V.8) reduces to

$$\dot{Q}_e = \frac{\bar{T}_{ew} - \bar{T}_{cw}}{R_{ew} + R_{cw}} . \tag{V.9}$$

Since the effect of thermal convection in the wick is small (8, 17, 18, 21), the wick resistances are described by the simple conduction model. Hence

$$\dot{Q}_e = \frac{\bar{T}_{ew} - \bar{T}_{cw}}{\frac{\ln\left(\frac{r_w}{r_{ve}}\right)}{2\pi X_{eff} L_e} + \frac{\ln\left(\frac{r_w}{r_{vc}}\right)}{2\pi X_{eff} L_c}} , \tag{V.10}$$

where X_{eff} is the wick's effective thermal conductivity, and r_{ve} and r_{vc} are the radii, from heat pipe centerline, of the liquid-vapor interfaces in the evaporator and condenser sections respectively. In order to provide interpretations of the parameters of Equation (V.10), the condenser and evaporator sections are considered individually.

3. Condenser

The fluid flow path in the condenser is modeled as that of vapor flowing axially into a long cavity with porous walls. The length of the cavity is divided into two regions, one with vapor flowing, and one with the vapor static, see Figure 16. For small axial inertia entering the cavity, the flow is considered quenched, i.e. the vapor ceases to flow axially before reaching the design length of the condenser. For

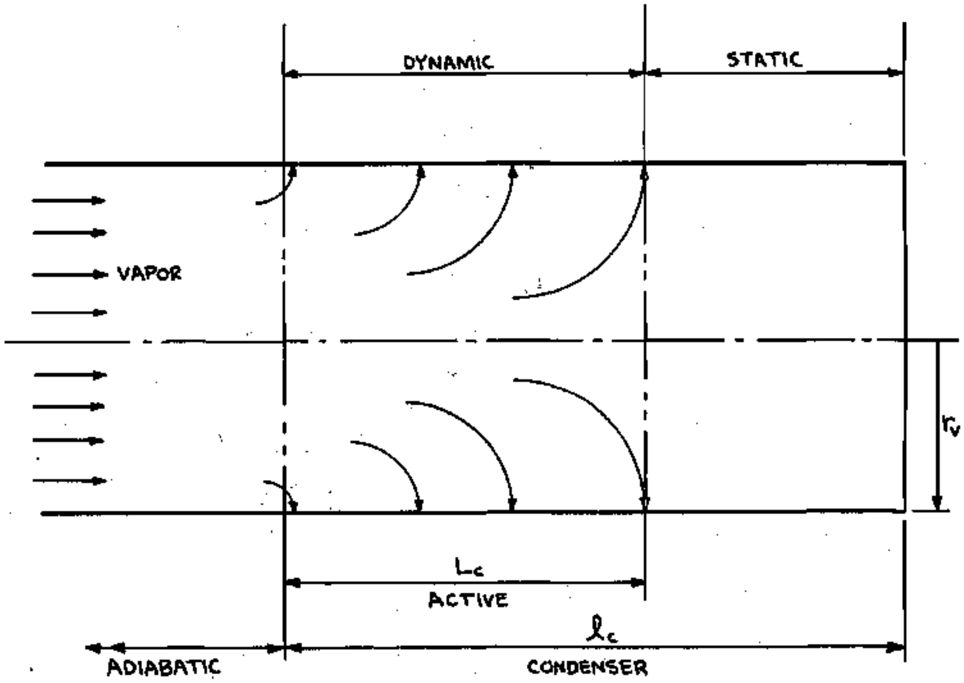

Figure 16. Correlation Model of Condenser Active Length.

high axial inertia, the flow is considered unquenched, i.e. the entire design length is filled with flowing vapor. This model suggests a relation of the form

$$\left(\frac{L_c}{\ell_c}\right) = \text{function}\left(R_e\right) \quad , \tag{V.11}$$

where (L_c/ℓ_c) is the ratio of active to design length of the condenser, and R_e is the vapors axial Reynolds number at the cavity entrance. Using Equation (V.5) for the mass flow rate of the vapor, Equation (V.11) is expressed as

$$\left(\frac{L_c}{\ell_c}\right) = f_1\left(\frac{2}{\pi}\,\frac{Q_e}{r_v\,\mu_v\,h_{v\ell}}\right) \quad . \tag{V.12}$$

Previous investigations on vapor flow dynamics have suggested the possible existence of an active condenser length. Analytical studies by Knight and McInteer (15) and White (36) on the dynamics of axial flow with radial suction indicated singularities or no solutions for various flow conditions. The analytical study by Bankston and Smith (1) suggested flow reversal could occur and stated "Thus, the character of the condenser flow depends upon the evaporator Reynolds number or velocity profile at the entrance to the condenser, the [design] length of the condenser, and the condenser Reynolds number, even for the simplest situation where the condensation rate is uniform".

Evaluation of the measured active length of condensation (L_c) is accomplished by use of a data reduction model based on 1) radial heat conduction through the wick and pipe shell, 2) measured vapor and [illegible] temperatures, and 3) the measured heat pipe heat transouter shell wall temperatures, and 3) the measured heat pipe heat transfer rate. See Appendix Q for reduction details. Consideration of the experimental data taken in this investigation suggests the function f_{1}, see Figure 17, to be

$$\left(\frac{L_c}{\ell_c}\right) = 1.245\left(0.3 \ln\left(\frac{2}{\pi}\frac{\dot{Q}_e}{r_v \mu_v h_{v\ell}}\right) - 1.0\right), \text{ for} \tag{V.13}$$

$$28 < \frac{2}{\pi}\frac{\dot{Q}_e}{r_v \mu_v h_{v\ell}} < 408 \quad , \text{ and} \tag{V.14}$$

$$\left(\frac{L_c}{\ell_c}\right) = 1.0 \quad , \text{ for} \tag{V.15}$$

$$\frac{2}{\pi}\frac{\dot{Q}_e}{r_v \mu_v h_{v\ell}} \geq 408 \; . \tag{V.16}$$

The liquid-vapor interface of the condenser is modeled as a flat interface, see Figure 18. Hence

$$r_{vc} = r_v \; . \tag{V.17}$$

The heat flow path for the condenser is modeled as that of simple radial conduction through the active length of the wick followed by heat transfer to the heat sink which surrounds the entire design length of the condenser, see Figure 19. The wall temperature $\overline{T}_{cw}$ is interpreted as a self adjusting parameter depending on the chosen external conditions of T_c the sink temperature and U_c the unit conductance between the sink and the wick outer surface. Hence the

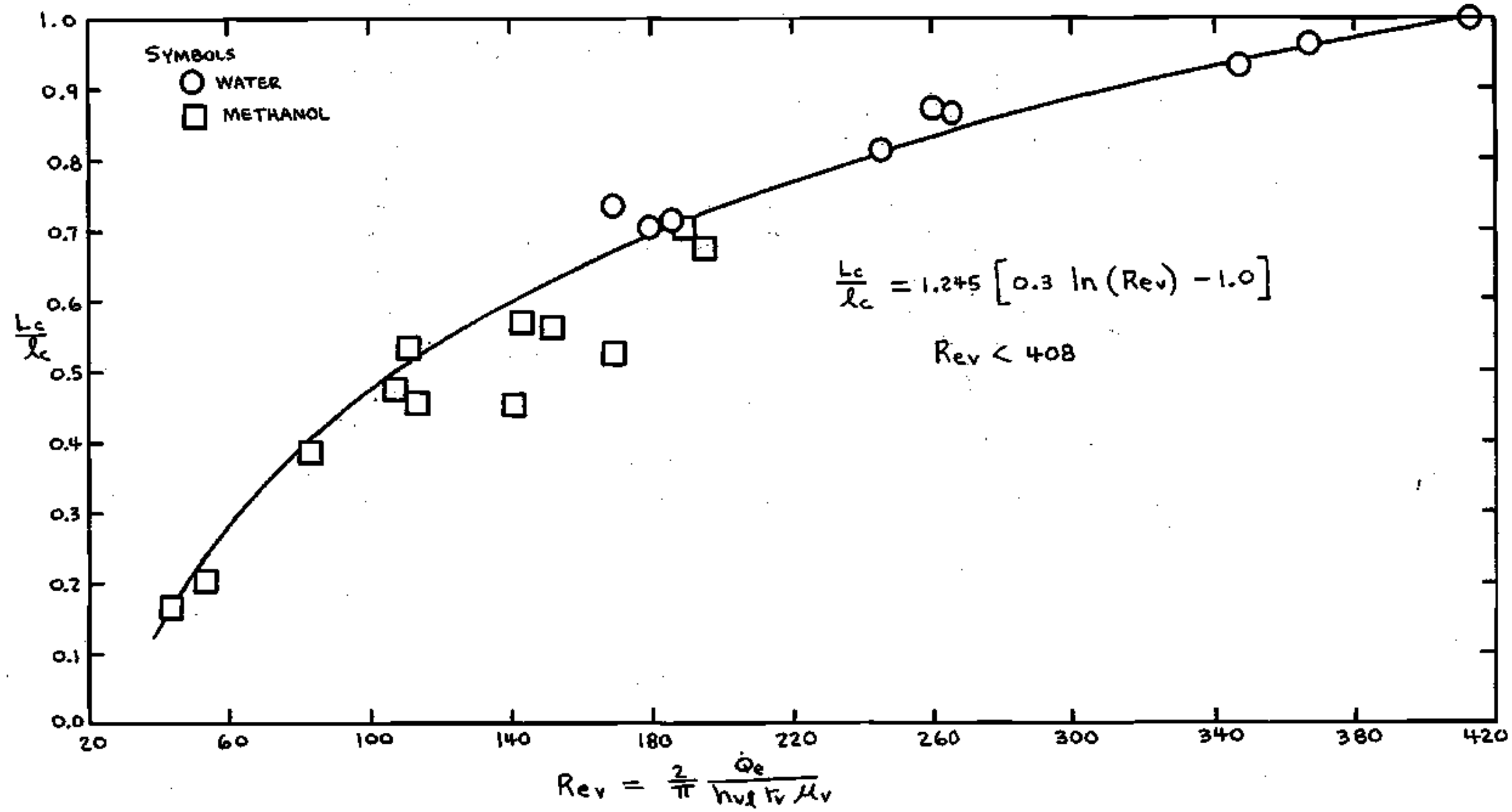

Figure 17. Correlation Data Curve for Condenser Active Length Ratio and Axial Vapor Reynolds Number.

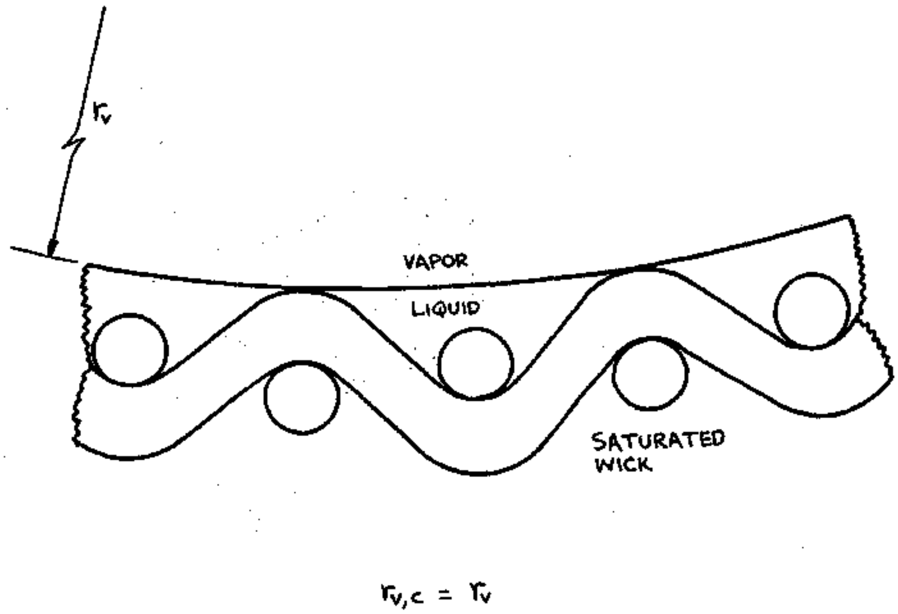

Figure 18. Condenser Liquid-Vapor Interface Schematic.

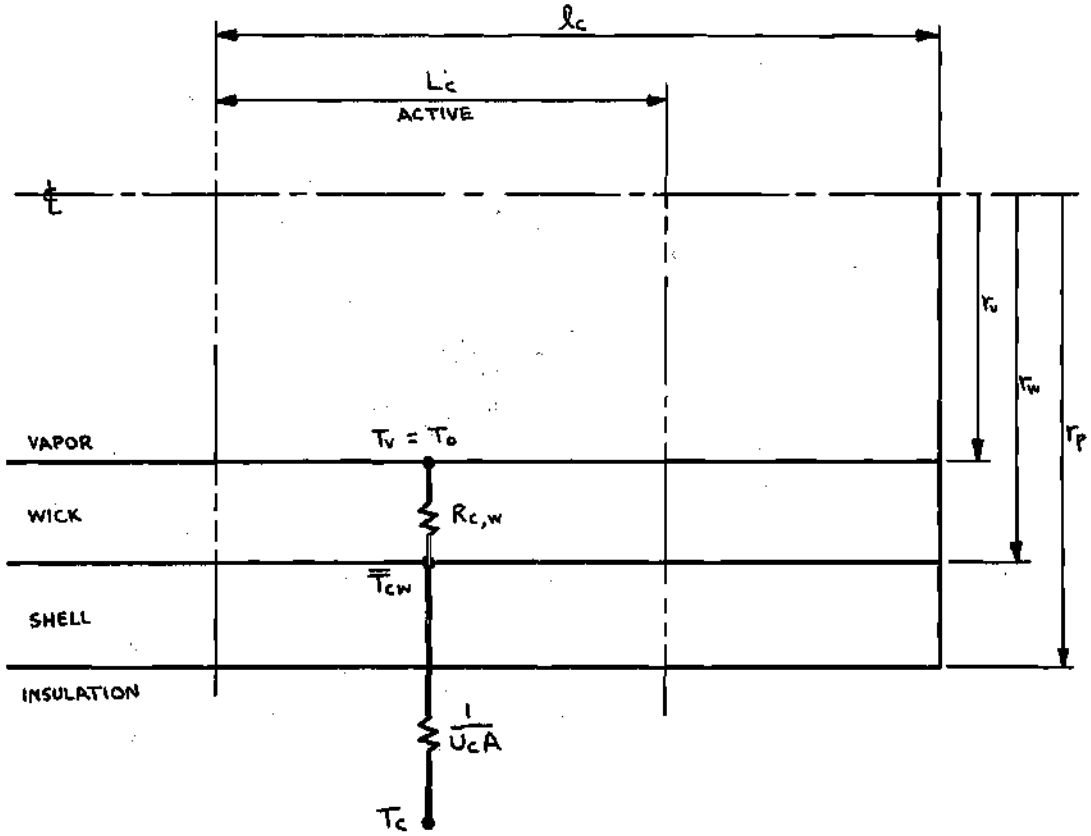

Figure 19. Condenser Thermal Resistance Schematic.

condenser contribution to Equation (V.10) is expressed by

$$\left(T_o - T_c\right) = \dot{Q}_e\left[\frac{\ln\left(\frac{r_w}{r_v}\right)}{2\pi K_{eff} L_c} + \frac{1}{U_c 2\pi r_w L_c}\right] , \tag{V.18}$$

where T_o is the temperature at the liquid-vapor interface along the active length, equal to the heat pipe operating temperature.

The effective thermal conductivity is modeled as a combination of parallel and series conduction through the solid wick-liquid region. For a thin wick consisting of multiple layers of wire mesh screen, each saturated with liquid, and separated by a thin region of liquid, see Appendix R, the effective thermal conductivity is expressed as

$$\frac{K_\ell}{K_{eff}} = \frac{1}{\ln\left(\frac{r_w}{r_v}\right)}\left\{\left[\frac{K_\ell}{K_w}\right]\left[\ln\left(\frac{r_w}{r_w - 2r_c - 2r_{ws}}\right) + \ln\left(\frac{r_v + 2(n-1)r_c\left(1+\frac{r_{ws}}{r_c}\right)}{r_v}\right)\right] + \ln\left(\frac{r_w - 2r_c\left(1+\frac{r_{ws}}{r_c}\right)}{r_v + 2(n-1)r_c\left(1+\frac{r_{ws}}{r_c}\right)}\right)\right\}, \tag{V.19}$$

where

$$\left(\frac{K_\ell}{K_w}\right)^{-1} = \frac{1}{\left(\frac{r_c}{r_{ws}}+1\right)\left(2\frac{K_\ell}{K_s} + \left(\frac{r_c}{r_{ws}}-1\right)\right)} + \frac{2}{\left(\frac{r_c}{r_{ws}}+1\right)\left(\frac{K_\ell}{K_s}\frac{r_{ws}}{r_c}+1\right)} + \frac{1}{\left(\frac{r_{ws}}{r_c}+1\right)^2} . \tag{V.20}$$

4. Evaporator

The fluid flow path in the evaporator is modeled as that of vapor flowing out of a porous wall (wick surface) into a vapor cavity. Make-up liquid is supplied to the porous wick. The length of the wick is divided into two regions, one with liquid flowing in the wick and one with the wick filled with static vapor, see Figure 20. Depending on the particular wick structure and for a given operating meniscus radius, see Equation (V.7), the liquid filled region retreats axially in a manner to change the active length (L_e) This model is studied by considering a pressure balance at the end of the active length, see Figure 21. The pressure balance around the indicated loop is given by

$$(P_{v_1} - P_{v_2}) + (P_{v_2} - P_{\ell_3}) + (P_{\ell_3} - P_{v_4}) + (P_{v_4} - P_{v_1}) = 0 \quad . \tag{V.21}$$

Dynamic pressure drops are negligible since these drops are over a short distance of order r_c. The inertial pressure drops across the liquid-vapor interfaces are also negligible, see Appendix L. Hence the terms of Equation (V.21) are given by the simple relations

$$(P_{v_1} - P_{v_2}) = 0 \;, \tag{V.22}$$

$$(P_{v_2} - P_{\ell_3}) = \left.\frac{2\sigma}{r_m}\right|_{2\text{-}3} \;, \tag{V.23}$$

$$(P_{\ell_3} - P_{v_4}) = -\left.\frac{2\sigma}{r_m}\right|_{3\text{-}4} \;, \text{ and} \tag{V.24}$$

$$(P_{v_4} - P_{v_1}) = 0 \;. \tag{V.25}$$

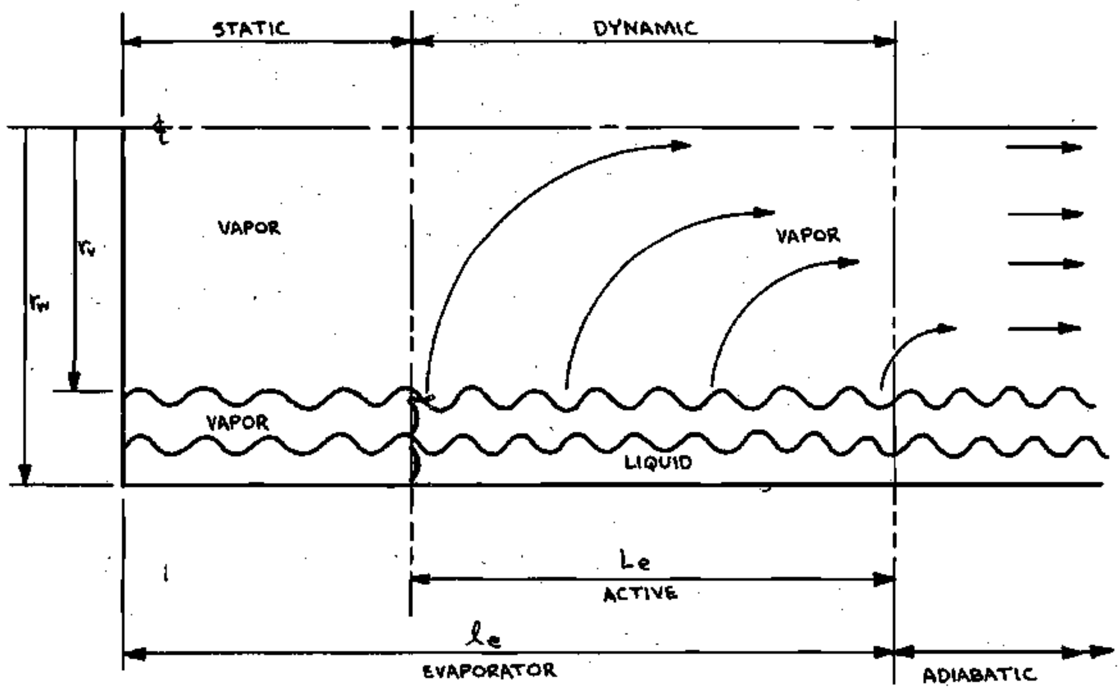

Figure 20. Correlation Model of Evaporator Active Length.

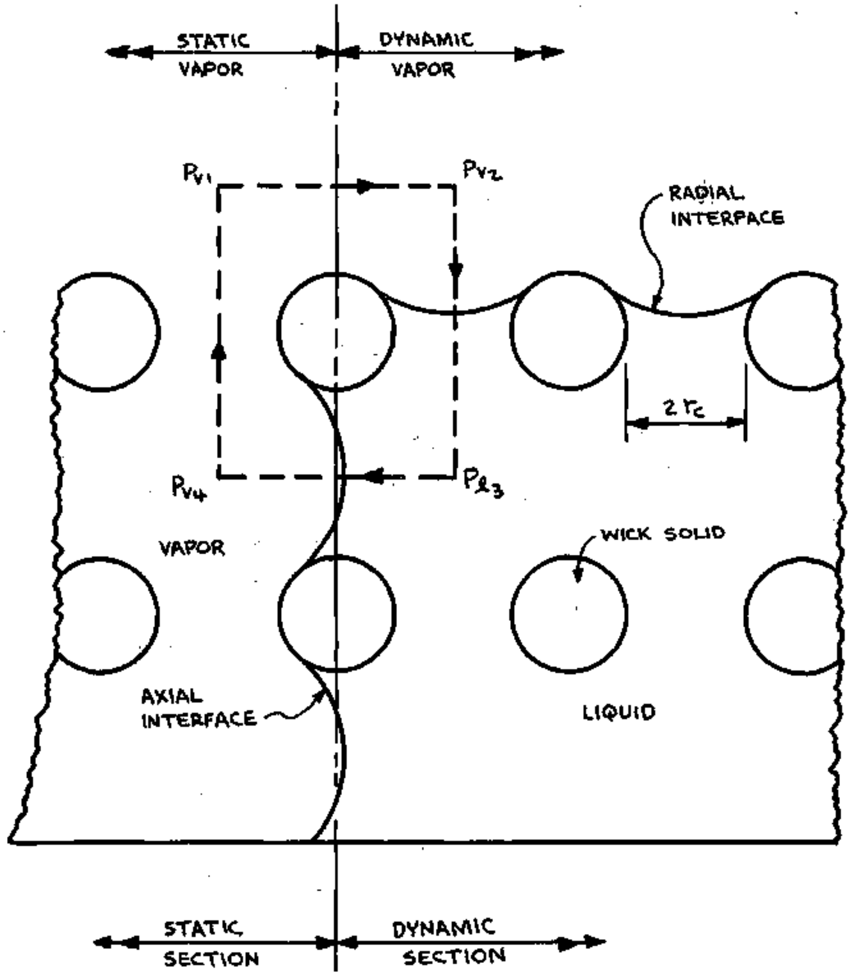

Figure 21. Pressure Balance Loop at End of Active Evaporator.

Substituting Equations (V.22) through (V.25) into Equation (V.21) yields the meniscus radii relation

$$r_m|_{3-4} = r_m|_{2-3} \quad . \tag{V.26}$$

Since the same meniscus radius must be present at two different surfaces, the axial position of attachment, characterized by the active length (L_e), will vary if the pore size in the axial direction is greater than the pore size in the radial direction (r_c) .

This model thus suggests that, for a given wick, the function f_2 exists where

$$\left(\frac{L_e}{\ell_e}\right) = f_2\left(\frac{r_m}{r_c}\right) \quad . \tag{V.27}$$

The measured active length of evaporation (L_e) is evaluated by use of a data reduction model based on 1) radial heat conduction through the active length of the wick, 2) radial and axial heat conduction through the entire length (ℓ_e) of the heat pipe shell, 3) measured vapor and shell wall temperatures, and 4) measured heat pipe heat transfer rate. See Appendix S for reduction details. Equation (V.7) is used for evaluation of (r_m/r_c). Consideration of these experimental data for a wick composed of two layers of wire mesh screen separated by a thin layer of liquid suggests the function f_2, see Figure 22, to be

$$\left(\frac{L_e}{\ell_e}\right) = 0.656\left(\frac{r_m}{r_c} - 1\right)^{0.107} \quad , \text{ for} \tag{V.28}$$

$$r_c|_{radial} < r_c|_{axial} \quad , \text{ and} \tag{V.29}$$

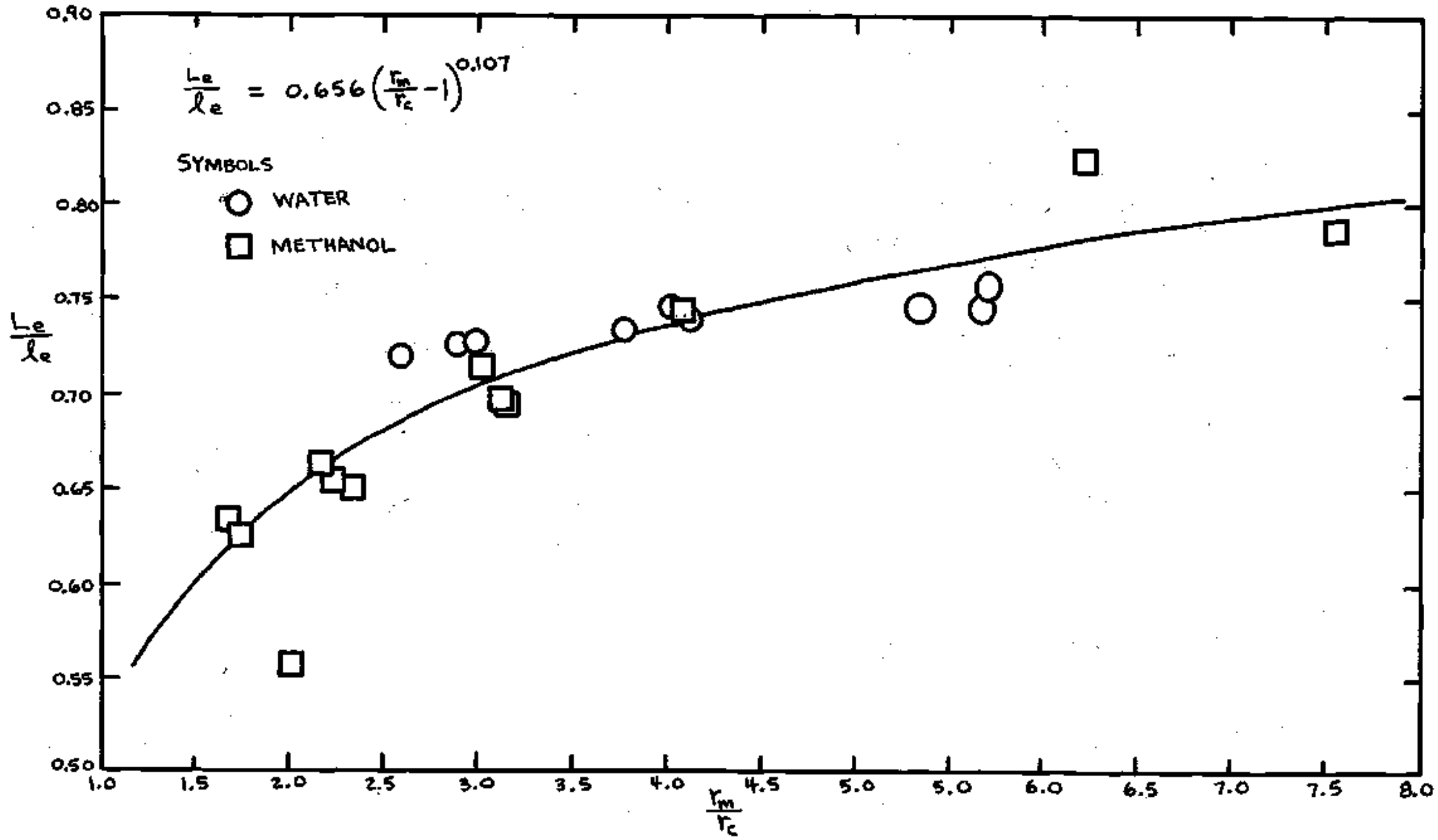

Figure 22. Correlation Data Curve for Evaporator Active Length Ratio and Meniscus Radius Ratio.

$$\frac{L_e}{\ell_e} = 1.0 \text{ , for} \tag{V.30}$$

$$r_c|_{radial} \gg r_c|_{axial} \quad . \tag{V.31}$$

The particular coefficients of Equation (V.28) are interpreted as applying only to the wick tested in this investigation. Although other investigators may use the same wick configuration (i.e. cylindrical wrappings of layers of mesh screen) variations exist in wrapping tightness and provisions of liquid gaps between the screen layers.

The existance of curvature on the evaporator liquid-vapor interface implies a radial retreat of the interface into the wick. This radial retreat is characterized by the effective wick thickness δ_e, see Figure 23. The liquid-vapor interface position as required by Equation (V.10) is given by

$$r_{ve} = r_w - \delta_e , \tag{V.32}$$

where δ_e depends on the operating meniscus radius, the detailed wick geometry, and the fluid contact angle. From Figure 23 and Appendix T, δ_e is seen to be described by

$$\frac{\delta_e}{r_w - r_v} = f_3\left(\frac{r_w}{r_v}, \frac{r_{ws}}{r_c}, \frac{r_c}{r_v}, \frac{r_m}{r_c}, \phi\right) \quad . \tag{V.33}$$

Typical plots of δ_e based on the geometric values used in Experimentation are indicated in Figure 24.

The heat flow path for the evaporator is modeled as that of simple radial conduction through the active length of wick and the [illegible]

[illegible]

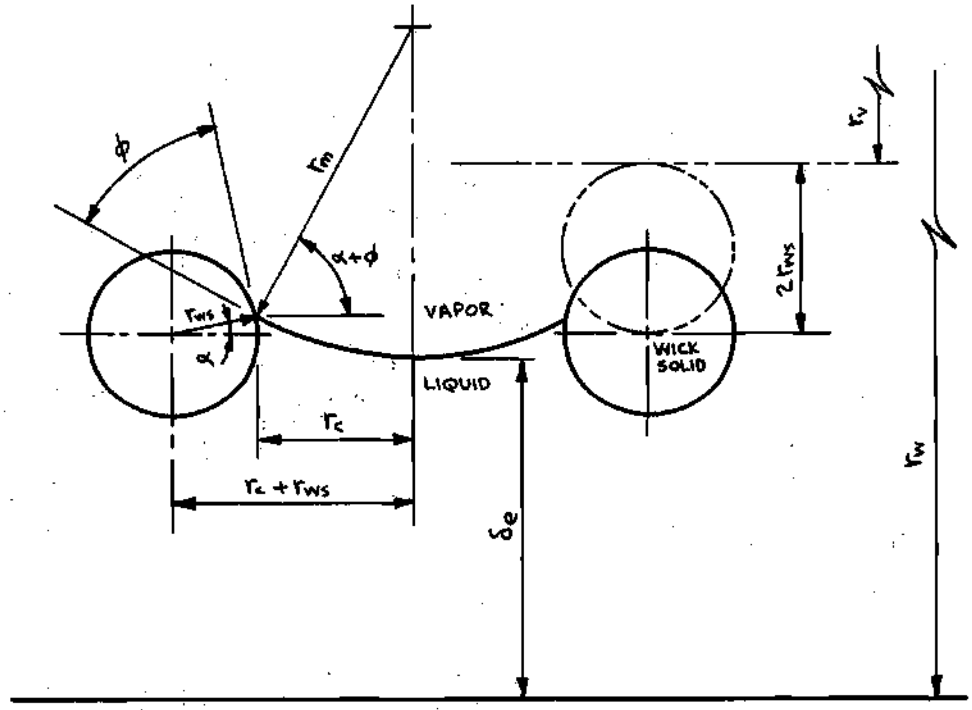

PARAMETER VALUES (THIS INVESTIGATION)

r_w = 0.326 in.
r_v = 0.298 in.
r_c = 0.00275 in.
r_{ws} = 0.00225 in.

Figure 23. Evaporator Effective Wick Thickness Schematic.

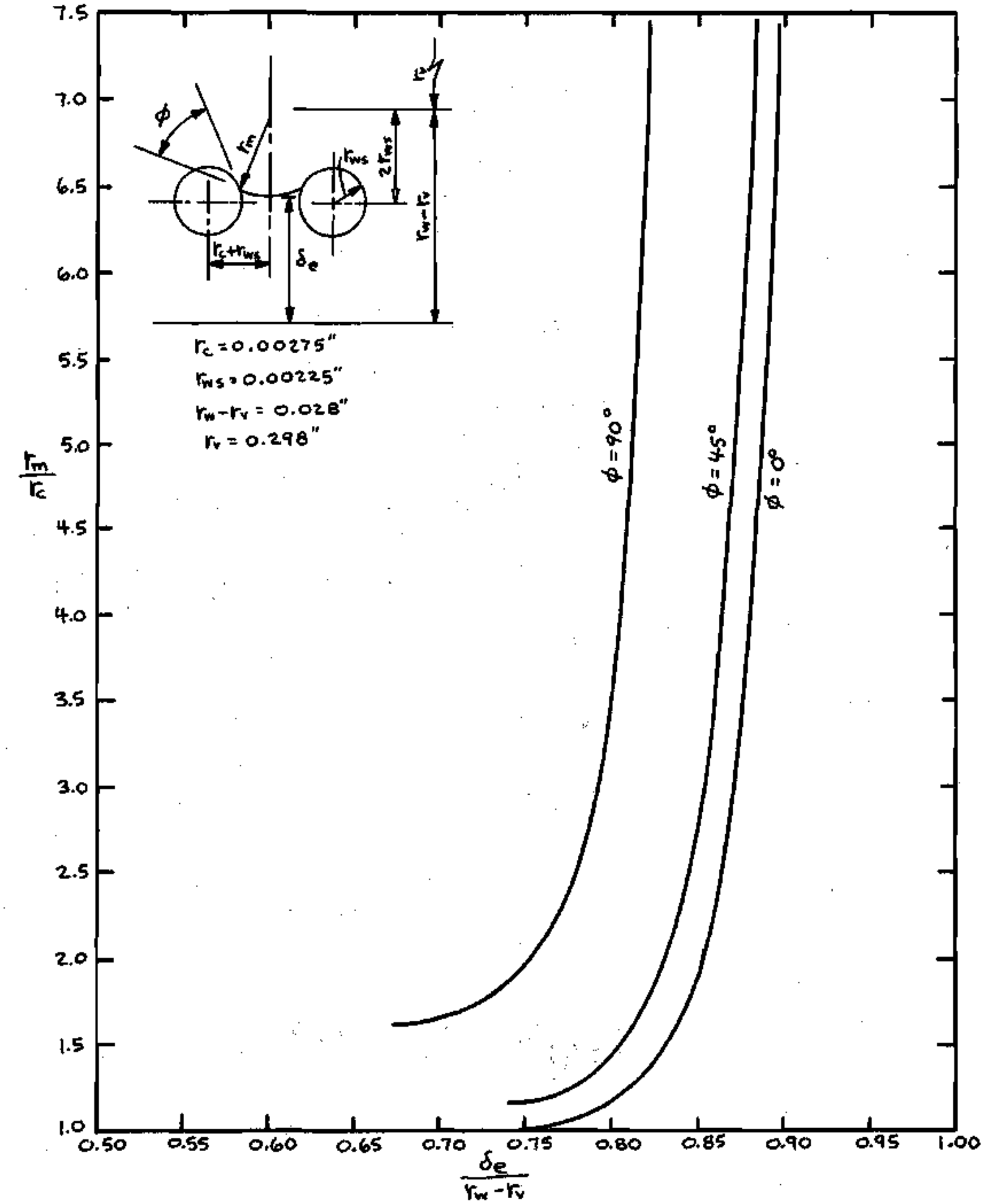

Figure 24. Evaporator Effective Wick Thickness Ratio Versus Meniscus Radius Ratio.

combination of axial and radial conduction in the heat pipe shell, see Appendix S. The temperature $\overline{T}_{aw}$ of Equation (V.10) is interpreted as a self adjusting parameter depending on the chosen power delivered to the evaporator and the condenser environmental parameters. Hence the evaporator contribution to Equation (V.10) is not written in the form of a thermal resistance, as for the case of the condenser (see Equation (V.18)), but by specification of the independent parameter of power

$$\dot{Q}_e = \dot{Q}_{\text{supplied to evaporator}} \quad . \tag{V.34}$$

5. System of Equations

The relations of Chapter V, Sections 1, 2, 3, and 4 form a system of solvable equations.

A. Dimensional Equations

The governing primary dimensional equations are

overall pressure balance

$$r_m = 2\,\frac{\left(\frac{\rho_\ell \sigma h_{v\ell}}{\mu_\ell}\right)\left(\frac{\pi(r_w^2 - r_v^2)}{\dot{Q}_e}\right)}{K_1\left(\frac{1}{2}L_e + \ell_a + \frac{1}{2}L_c\right)} \quad , \tag{V.35}$$

condenser heat transfer

$$T_o - T_c = \dot{Q}_e\left[\frac{\ln\left(\frac{r_w}{r_v}\right)}{2\pi X_{eff} L_c} + \frac{1}{U_c 2\pi r_w L_c}\right] \quad , \tag{V.36}$$

condenser active length

$$L_c = \ell_c\left[f_1\left(\frac{2}{\pi}\frac{\dot{Q}_e}{h_{v\ell}r_v\mu_v}\right)\right] , \tag{V.37}$$

evaporator active length

$$L_e = \ell_e\left[f_2\left(\frac{r_m}{r_c}\right)\right] , \tag{V.38}$$

evaporator meniscus retreat

$$\delta_e = \bar{f}_3(r_w, r_v, r_{ws}, r_c, r_m, \phi), \text{ and} \tag{V.39}$$

wick effective thermal conductivity

$$K_{eff} = \bar{f}_4(K_s, K_\ell, r_w, r_v, r_{ws}, r_c, n) . \tag{V.40}$$

The governing secondary dimensional equations are material property relations, evaluated at the heat pipe operating temperature. These equations are

heat pipe fluid parameter

$$\frac{\rho_\ell \sigma h_{v\ell}}{\mu_\ell} = \bar{f}_7(T_o) , \tag{V.41}$$

vapor viscosity

$$\mu_v = \mu_v(T_o) \tag{V.42}$$

liquid thermal conductivity

$$K_\ell = K_\ell(T_o) \tag{V.43}$$

wick-solid thermal conductivity

$$\chi_s = \chi_s(T_0) = \bar{f}_8(T_0)\ , \text{ and} \tag{V.44}$$

fluid heat of vaporization

$$h_{v\ell} = h_{v\ell}(T_0)\ , \tag{V.45}$$

B. <u>Dimensionless Equations</u>

Equations (V.35) through (V.45) are written in dimensionless form as

$$\left[\frac{r_m}{r_c}\right] = \frac{2\left[\frac{\rho_\ell \sigma h_{v\ell}}{\mu_\ell}\frac{\pi r_c^2}{\dot{Q}_e}\right]\dfrac{\left(\left[\frac{r_w}{r_v}\right]^2-1\right)}{\left[\frac{r_c}{r_v}\right]^2}}{\left[K_1 r_c \ell_c\right]\left(\frac{1}{2}\left[\frac{L_e}{\lambda_e}\right]\left[\frac{\ell_e}{\ell_c}\right]+\left[\frac{\ell_a}{\lambda_c}\right]+\frac{1}{2}\left[\frac{L_c}{\lambda_c}\right]\right)}\ , \tag{V.46}$$

$$\left[\frac{T_0}{T_c}\right] = 1 + \left[\frac{\dot{Q}_e}{2\pi r_w \ell_c U_c T_c}\right]\left[\frac{\ell_c}{L_c}\right]\left\{1+\left[\frac{U_c \ell_c}{\chi_s}\right]\left[\frac{r_w}{r_v}\right]\left[\frac{r_v}{\lambda_c}\right]\left[\frac{\chi_s}{\chi_\ell}\right]\left[\frac{\chi_\ell}{\chi_{eff}}\right]\ln\left(\left[\frac{r_w}{r_v}\right]\right)\right\}, \tag{V.47}$$

$$\left[\frac{L_c}{\lambda_c}\right] = f_1\left(\left[\frac{2}{\pi}\frac{\dot{Q}_e}{h_{v\ell} r_v \mu_v}\right]\right)\ , \tag{V.48}$$

$$\left[\frac{L_e}{\lambda_e}\right] = f_2\left(\left[\frac{r_m}{r_c}\right]\right)\ , \tag{V.49}$$

$$\left[\frac{\delta_e}{r_w - r_v}\right] = f_3\left(\left[\frac{r_m}{r_c}\right], \left[\frac{r_w}{r_v}\right], \left[\frac{r_{ws}}{r_c}\right], \left[\frac{r_c}{r_v}\right], [\phi_0]\right)\ , \tag{V.50}$$

$$\left[\frac{X_\ell}{X_{eff}}\right] = f_4\left(\left[\frac{r_w}{r_v}\right], \left[\frac{r_{ws}}{r_c}\right], \left[\frac{r_c}{r_v}\right], \left[\frac{X_s}{X_\ell}\right], [n]\right) , \tag{V.51}$$

$$\left[\frac{X_s}{X_\ell}\right] = f_5(T_o) , \tag{V.52}$$

$$\left[\frac{2\dot{Q}_e}{\pi r_v h_{v\ell} \mu_v}\right] = \frac{2}{\pi} \frac{\dot{Q}_e}{r_v f_6(T_o)} , \tag{V.53}$$

$$\left[\frac{\rho_\ell \sigma h_{v\ell}}{\mu_\ell} \frac{\pi r_c^2}{\dot{Q}_e}\right] = \frac{\pi r_c^2 f_7(T_o)}{\dot{Q}_e} , \text{ and} \tag{V.54}$$

$$\left[\frac{U_c \ell_c}{X_s}\right] = \frac{U_c \ell_c}{f_8(T_o)} . \tag{V.55}$$

C. Dimensionless Groups

Equations (V.35) through (V.45) contain 24 parameters. With the four dimensions of length, mass, time, and temperature, Equations (V.46) through (V.55) contain 20 dimensionless groups. These groups are listed in Table 10. Each group is assigned a numbered π symbol and interpreted as independent or dependent.

Since the dimensional parameters of wick and shell geometry and environmental coupling $(T_c, U_c, \dot{Q}_e)$ are independent, groups containing only these parameters are also independent.

Since the groups on the left hand side of Equations (V.46) through (V.50) are internal self adjusting terms, these groups are interpreted as dependent. Since the group X_ℓ/X_{eff} of Equation (V.51) is determinable in terms of other dimensionless groups, see also

Equation (V.19), the group χ_ℓ/χ_{eff} is interpreted as dependent.

The groups of Equations (V.52) through (V.55) contain two types of dimensional parameters either wick and shell geometry and environmental coupling (independent) or material property (dependent). If particular heat pipe materials are specified, i.e. stainless steel and water, these groups would be dependent; dependent due to change of material property with change of operating temperature. If the heat pipe materials are not specified, the material properties would be free to take on any value, making the groups independent. This latter interpretation (independent) is taken for Table 10. This choice permits general solutions of the equations for any combination of materials.

D. Dimensionless Equations in Terms of π Symbols

With the interpretation of independent material properties, Equations (V.46) through (V.55) from a system of six independent equations with six dependent parameters and 14 independent parameters. These equations, in terms of the π symbols are

$$\pi_{15} = f_1(\pi_{12}) , \tag{V.56}$$

$$\pi_{16} = f_2(\pi_{17}) , \tag{V.57}$$

$$\pi_{17} = \frac{2\pi_{11}(\pi_3^2 - 1)}{\pi_5^2 \pi_7 \left(\frac{1}{2}\pi_{16}\pi_2 + \pi_1 + \frac{1}{2}\pi_{15}\right)} , \tag{V.58}$$

$$\pi_{18} = f_3(\pi_{17}, \pi_3, \pi_6, \pi_5, \pi_9) , \tag{V.59}$$

$$\pi_{19} = f_4(\pi_3, \pi_6, \pi_5, \pi_{10}, \pi_8) , \text{ and} \tag{V.60}$$

Table 10. Correlation Dimensionless Group Listing

Dependency	Term Definition	Remarks
Independent Groups	$\pi_1 = \frac{\ell_a}{\ell_c}$	adiabatic length / condenser length
	$\pi_2 = \frac{\ell_e}{\ell_c}$	evaporator length / condenser length
	$\pi_3 = \frac{r_w}{r_v}$	outer wick radius / vapor radius
	$\pi_4 = \frac{r_v}{\ell_c}$	vapor radius / condenser length
	$\pi_5 = \frac{r_c}{r_v}$	wick pore radius / vapor radius
	$\pi_6 = \frac{r_{ws}}{r_c}$	wick solid radius / wick pore radius
	$\pi_7 = K_1 r_c \ell_c$	wick friction no.
	$\pi_8 = n$	number of screen layers
	$\pi_9 = \phi_o$	fluid contact angle
	$\pi_{10} = \frac{\chi_s}{\chi_\ell}$	wick solid thermal conductivity / liquid thermal conductivity
	$\pi_{11} = \frac{\rho_\ell \sigma h_{v\ell}}{\mu_\ell} \frac{\pi r_c^2}{Q_e}$	heat pipe number

(Continued)

Table 10. (Continued)

Dependency	Term Definition	Remarks
Independent Groups	$\Pi_{12} = \frac{2}{\pi} \frac{\dot{Q}_e}{h_{v\ell} r_v \mu_v}$	vapor Reynolds no.
	$\Pi_{13} = \frac{\dot{Q}_e}{2\pi r_w \ell_c U_c T_c}$	condenser environment no.
	$\Pi_{14} = \frac{U_c \ell_c}{\chi_s}$	condenser Biot number.
Dependent Groups	$\Pi_{15} = \frac{L_c}{\ell_c}$	active condenser length / design condenser length
	$\Pi_{16} = \frac{L_e}{\ell_e}$	active evaporator length / design evaporator length
	$\Pi_{17} = \frac{r_m}{r_c}$	evaporator meniscus radius / wick pore radius
	$\Pi_{18} = \frac{\delta_e}{r_w - r_v}$	evaporator wick thickness / nominal wick thickness
	$\Pi_{19} = \frac{\chi_\ell}{\chi_{eff}}$	liquid thermal conductivity / wick effective thermal conductivity
	$\Pi_{20} = \frac{T_o}{T_c}$	heat pipe operating temperature / condenser sink temperature

$$\pi_{20} = 1 + \frac{\pi_{13}}{\pi_{15}}\left(1 + \pi_4 \pi_{10} \pi_{14} \pi_{19} \pi_3 \ln(\pi_3)\right) , \qquad (V.61)$$

where the functions f_i for i = 1, 2, 3, and 4 are known functions. f_1 is given by Equation (V.13). f_2 is given by Equation (V.28). is the implicit function described in Appendix T. f_4 is given by Equation (V.19) with Equation (V.20).

6. Results and Discussion

A. Solutions to Correlation Equations

General solutions to Equations (V.56) through (V.61) are made by specifying values of the independent groups and solving algebraically for the dependent groups, explicitly or implicitly. For description of the independent groups governing each dependent group, Equations (V.56) through (V.61) are written as

$$\pi_{15} = \pi_{15}(\pi_{12}) , \qquad (V.62)$$

$$\pi_{16} = \pi_{16}(\pi_1, \pi_2, \pi_3, \pi_5, \pi_7, \pi_{11}, \pi_{12}), \qquad (V.63)$$

$$\pi_{17} = \pi_{17}(\pi_1, \pi_2, \pi_3, \pi_5, \pi_7, \pi_{11}, \pi_{12}), \qquad (V.64)$$

$$\pi_{18} = \pi_{18}(\pi_1, \pi_2, \pi_3, \pi_5, \pi_6, \pi_7, \pi_9, \pi_{11}, \pi_{12}), \qquad (V.65)$$

$$\pi_{19} = \pi_{19}(\pi_3, \pi_5, \pi_6, \pi_8, \pi_{10}) \text{ , and} \qquad (V.66)$$

$$\pi_{20} = \pi_{20}(\pi_3, \pi_4, \pi_5, \pi_6, \pi_8, \pi_{19}, \pi_{12}, \pi_{13}, \pi_{14}) . \qquad (V.67)$$

With the large number of independent variables, e.g. eight for π_{18}, there exist many solutions for the dependent variables. A sample of these solutions is represented graphically by plotting the dependent group vs. the more significant independent group. Consequences of variation of the less significant groups is indicated by varying these groups in blocks of two.

Figure 25, π_{15} vs. π_{12}, indicates the variation of condenser length with vapor Reynolds number. This length increases with increasing Reynolds number. For high Reynolds number, the length ratio approaches unity, reaches unity, and remains at unity.

Figure 26, π_{16} vs. π_{11}, shows the variation of evaporator active length with heat pipe number. This length is shown to increase with increased pipe number and to decrease slightly with increased vapor Reynolds number. Increases in design length and radius groups and the wick friction number cause a decrease in the active length ratio.

Figure 27, π_{17} vs. π_{11}, indicates variation of evaporator meniscus radius with heat pipe numbers. The radius is shown to increase with increased pipe number and to decrease with increased vapor Reynolds number. Increases in design length and wick radius ratios and the wick friction number cause a significant decrease in the meniscus radius ratio.

Figure 28, π_{18} vs. π_{11}, describes variation of evaporator wick thickness ratio with heat pipe numbers. This thickness increases sharply for low pipe numbers and increases slowly for large pipe numbers. An increase in vapor Reynolds number produces a slight decrease in thickness ratio. An increase in contact wetting angle produces a slight decrease in thickness ratio. Increases in length and wick radius ratios in addition to the wick friction number indicate an increase in thickness ratio.

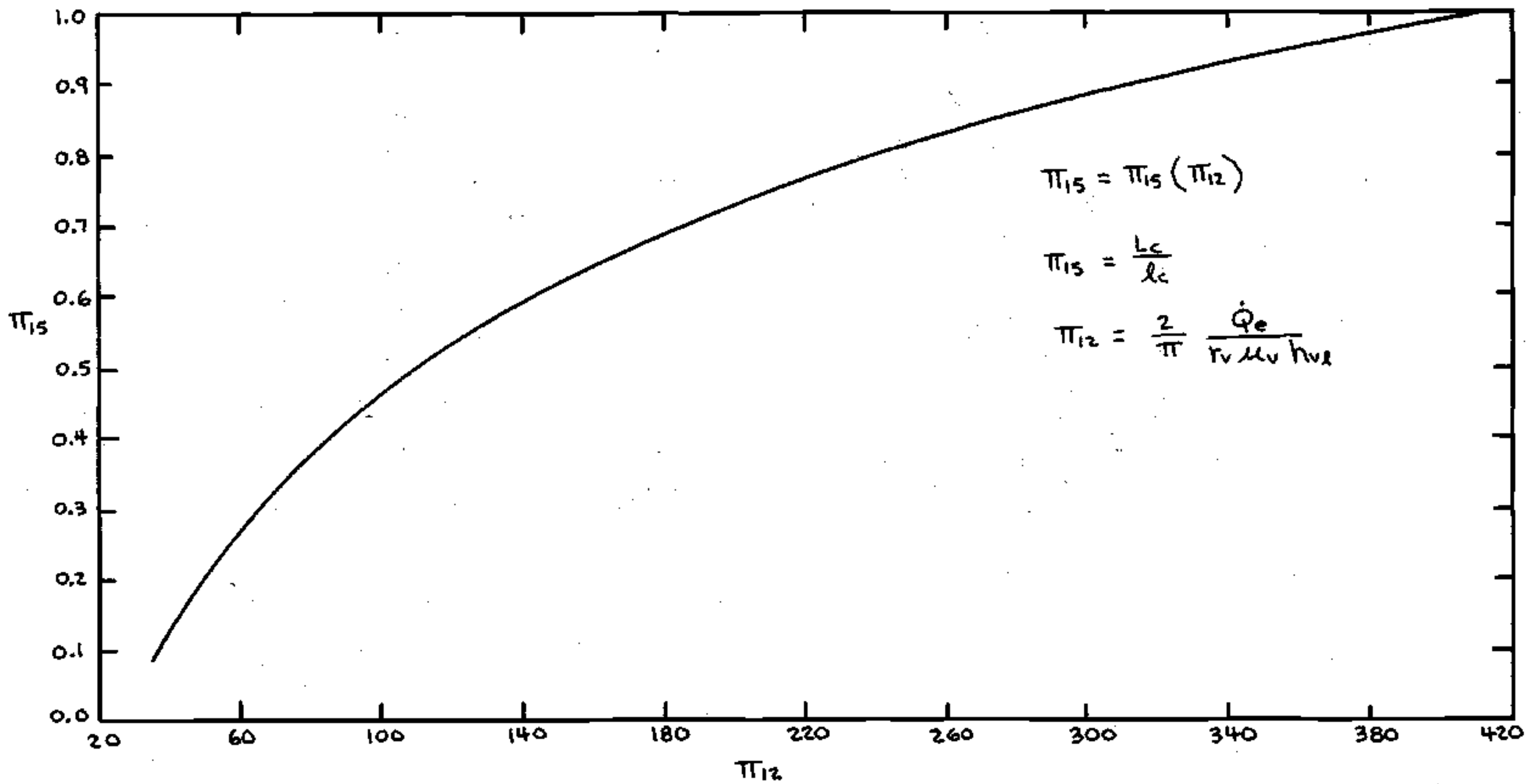

Figure 25. Predicted Values of Condenser Active Length Ratio Versus Axial Vapor Reynolds Number.

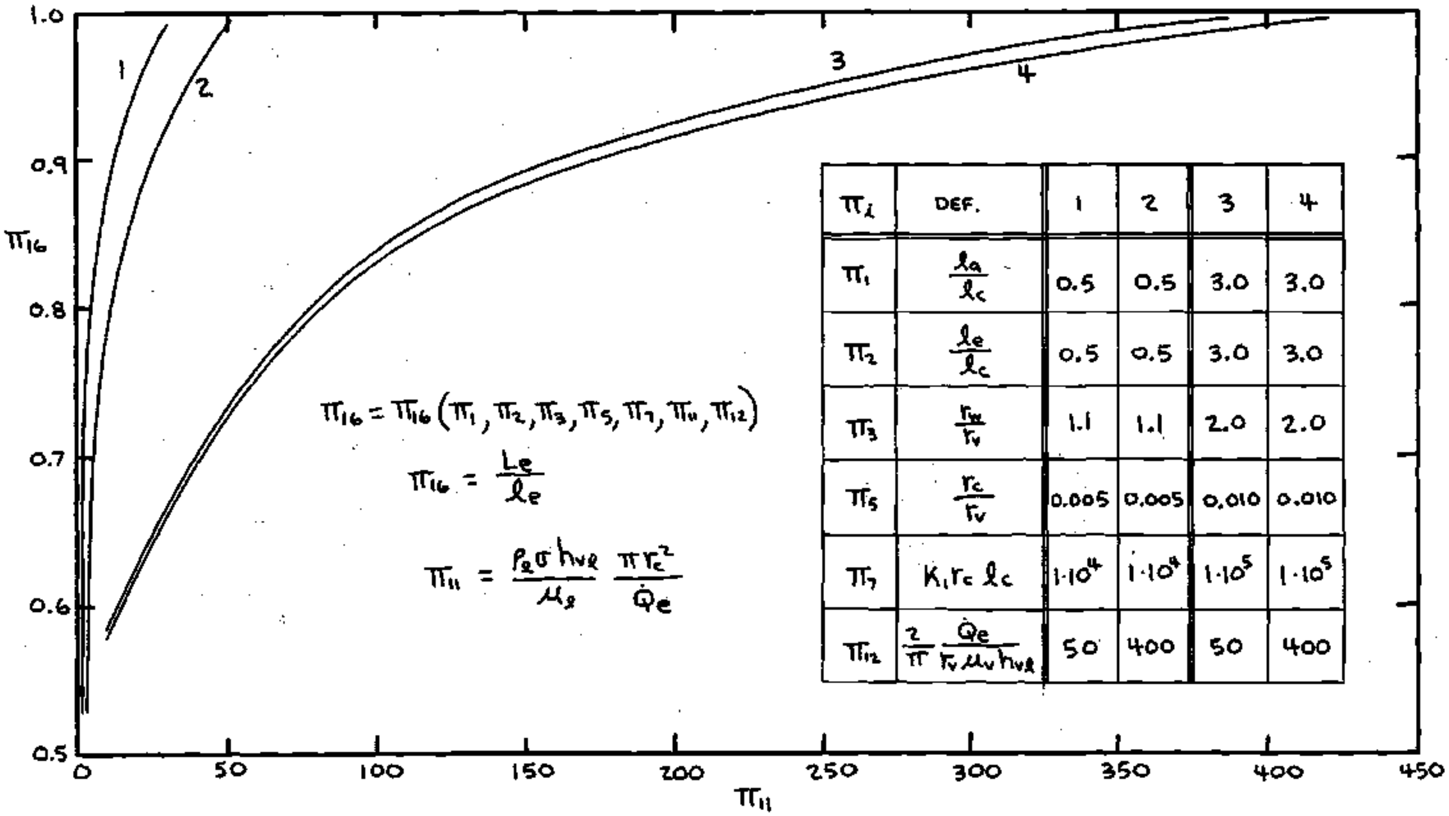

π_i	DEF.	1	2	3	4
π_1	$\frac{l_a}{l_c}$	0.5	0.5	3.0	3.0
π_2	$\frac{l_e}{l_c}$	0.5	0.5	3.0	3.0
π_3	$\frac{r_w}{r_v}$	1.1	1.1	2.0	2.0
π_5	$\frac{r_c}{r_v}$	0.005	0.005	0.010	0.010
π_7	$K_1 r_c l_c$	$1 \cdot 10^4$	$1 \cdot 10^4$	$1 \cdot 10^5$	$1 \cdot 10^5$
π_{12}	$\frac{2}{\pi} \frac{\dot{Q}_e}{r_v \mu_v h_{vl}}$	50	400	50	400

Figure 26. Predicted Values of Evaporator Active Length Ratio Versus Heat Pipe Number.

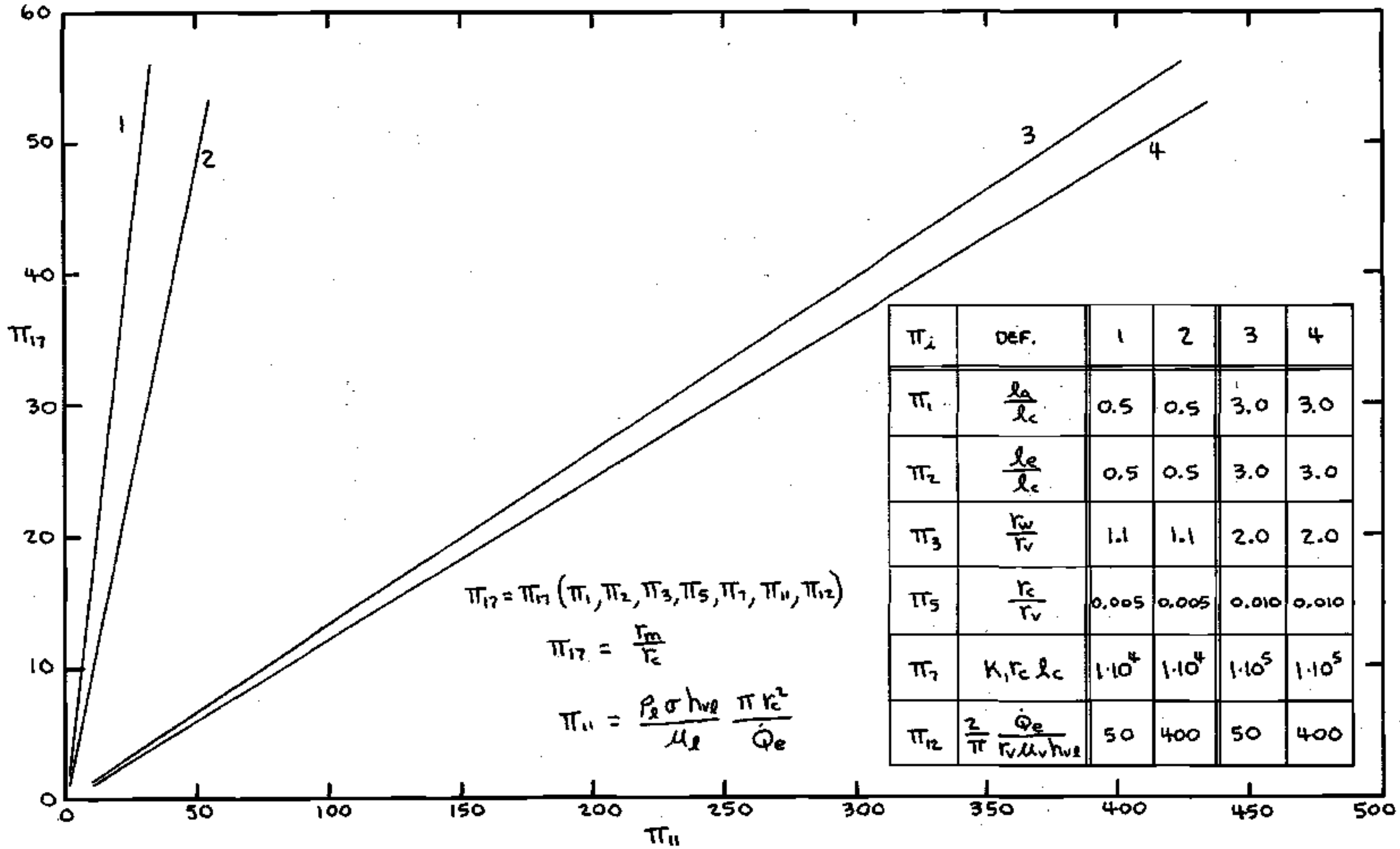

π_i	DEF.	1	2	3	4
π_1	$\frac{\ell_a}{\ell_c}$	0.5	0.5	3.0	3.0
π_2	$\frac{\ell_e}{\ell_c}$	0.5	0.5	3.0	3.0
π_3	$\frac{r_w}{r_v}$	1.1	1.1	2.0	2.0
π_5	$\frac{r_c}{r_v}$	0.005	0.005	0.010	0.010
π_7	$K_1 r_c \ell_c$	$1 \cdot 10^4$	$1 \cdot 10^4$	$1 \cdot 10^5$	$1 \cdot 10^5$
π_{12}	$\frac{2}{\pi} \frac{\dot{Q}_e}{r_v \mu_v h_{v\ell}}$	50	400	50	400

Figure 27. Predicted Values of Evaporator Meniscus Radius Ratio Versus Heat Pipe Number.

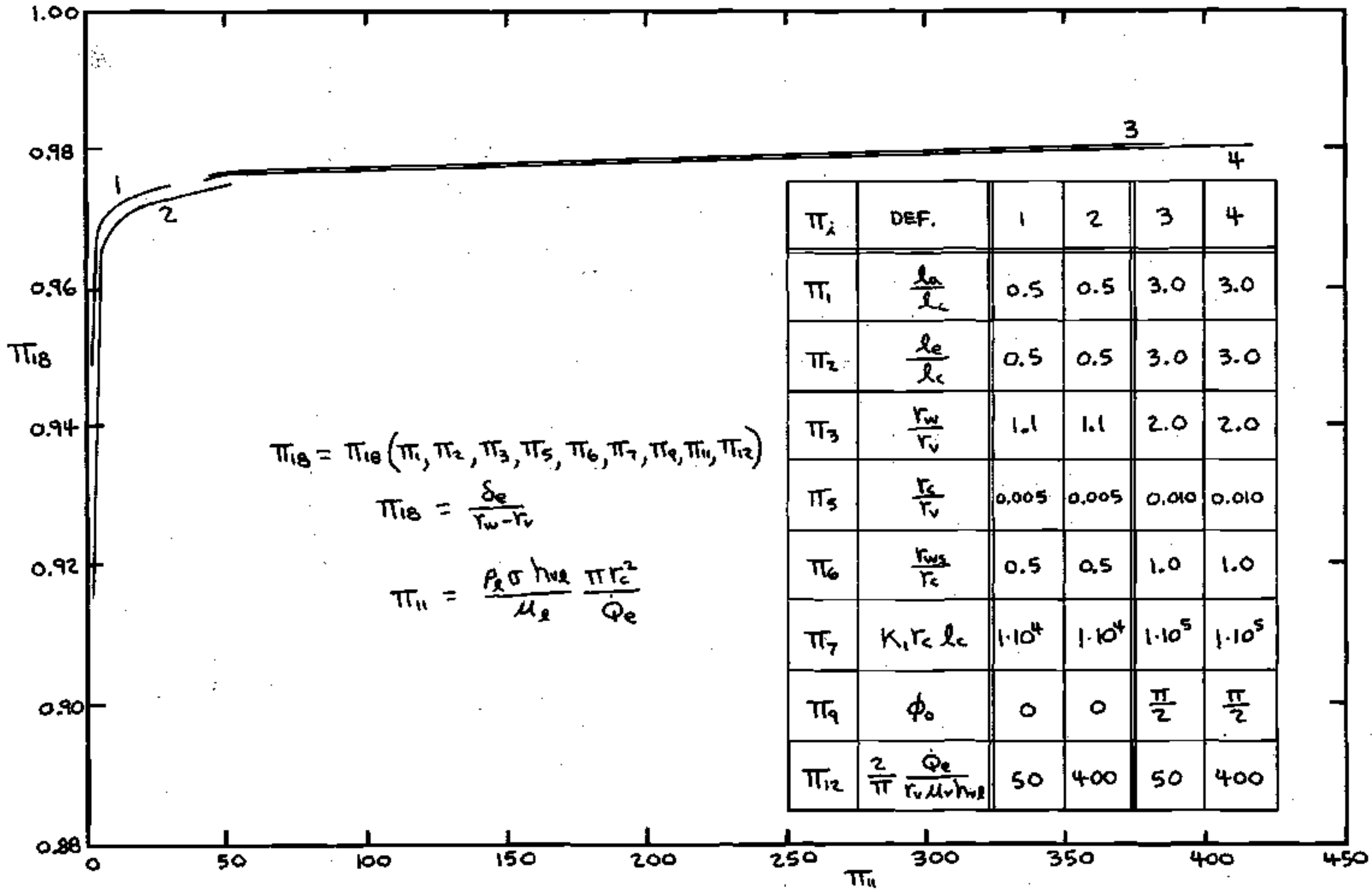

Π_i	DEF.	1	2	3	4
Π_1	$\frac{\ell_a}{\ell_c}$	0.5	0.5	3.0	3.0
Π_2	$\frac{\ell_e}{\ell_c}$	0.5	0.5	3.0	3.0
Π_3	$\frac{r_w}{r_v}$	1.1	1.1	2.0	2.0
Π_5	$\frac{r_c}{r_v}$	0.005	0.005	0.010	0.010
Π_6	$\frac{r_{ws}}{r_c}$	0.5	0.5	1.0	1.0
Π_7	$K_1 r_c \ell_c$	$1\cdot10^4$	$1\cdot10^4$	$1\cdot10^5$	$1\cdot10^5$
Π_9	ϕ_o	0	0	$\frac{\pi}{2}$	$\frac{\pi}{2}$
Π_{12}	$\frac{2}{\pi}\frac{\dot{Q}_e}{r_v \mu_v h_{v\ell}}$	50	400	50	400

Figure 28. Predicted Values of Evaporator Effective Wick Thickness Ratio Versus Heat Pipe Number.

Figure 29, π_{19} vs. π_{10}, illustrates the dependency of the thermal conductivity ratio of liquid/wick effective on the conductivity ratio of wick solid material/liquid. The liquid/effective ratio decreases gradually with increased solid/liquid ratio. The liquid-effective ratio decreases with increases in wick solid/pore radius ratios. The liquid/effective ratio increases with combined increase in wick radius ratio and decrease in wick-pore/vapor space radius ratios.

Figure 30, π_{20} vs. π_{13}, shows the variation of heat pipe operating temperature with condenser environment number. The vapor temperature ratio increases with increased condenser environment number. The vapor temperature ratio decreases with increased heat sink number (π_{14}). The vapor temperature ratio decreases with increased wick radius number.

B. <u>Comparison of Experimental Values to Predicted Values</u>

Comparisons between predicted and measured parameters are indicated in Figures 31, 32, 33, and 34. Since predictions for conditions tested in this investigation are made for specified materials, the full set of Equations (V.42) through (V.51) are solved. This requires solving for the operating temperature prior to evaluation of material properties as expressed in Equations (V.48) through (V.51). For comparisons to the experimental works of others, material properties are evaluated at the measured operating temperature. This is necessary since reported data are incomplete, with insufficient information to permit solution of the operating temperature. Deviations less than ± 10 per cent between measured and predicted values are interpreted as random deviations. Deviations greater than ± 10 per cent are interpreted

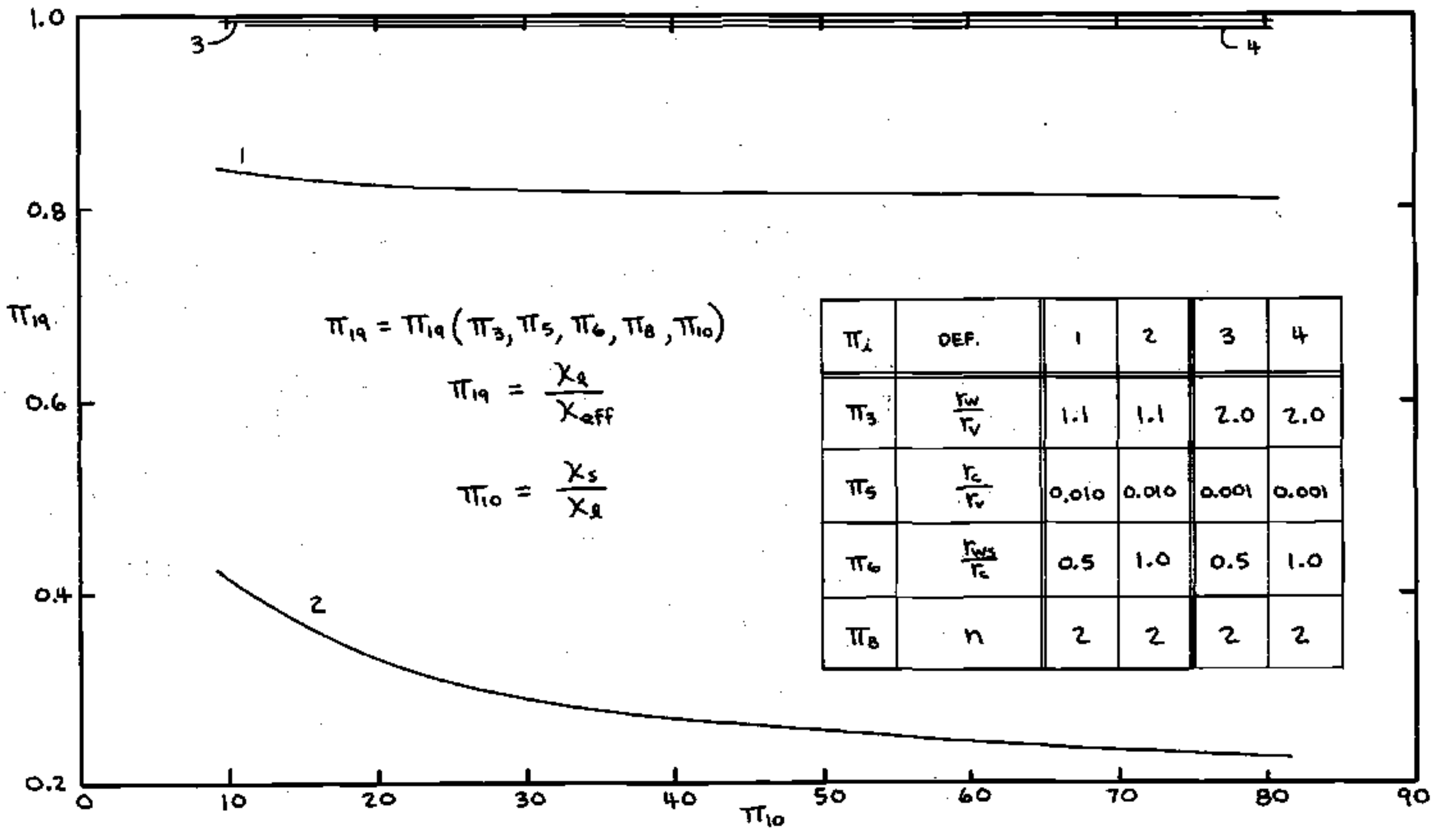

Figure 29. Predicted Values of Wick Effective Thermal Conductivity Ratio Versus Wick Solid-Liquid Thermal Conductivity Ratio.

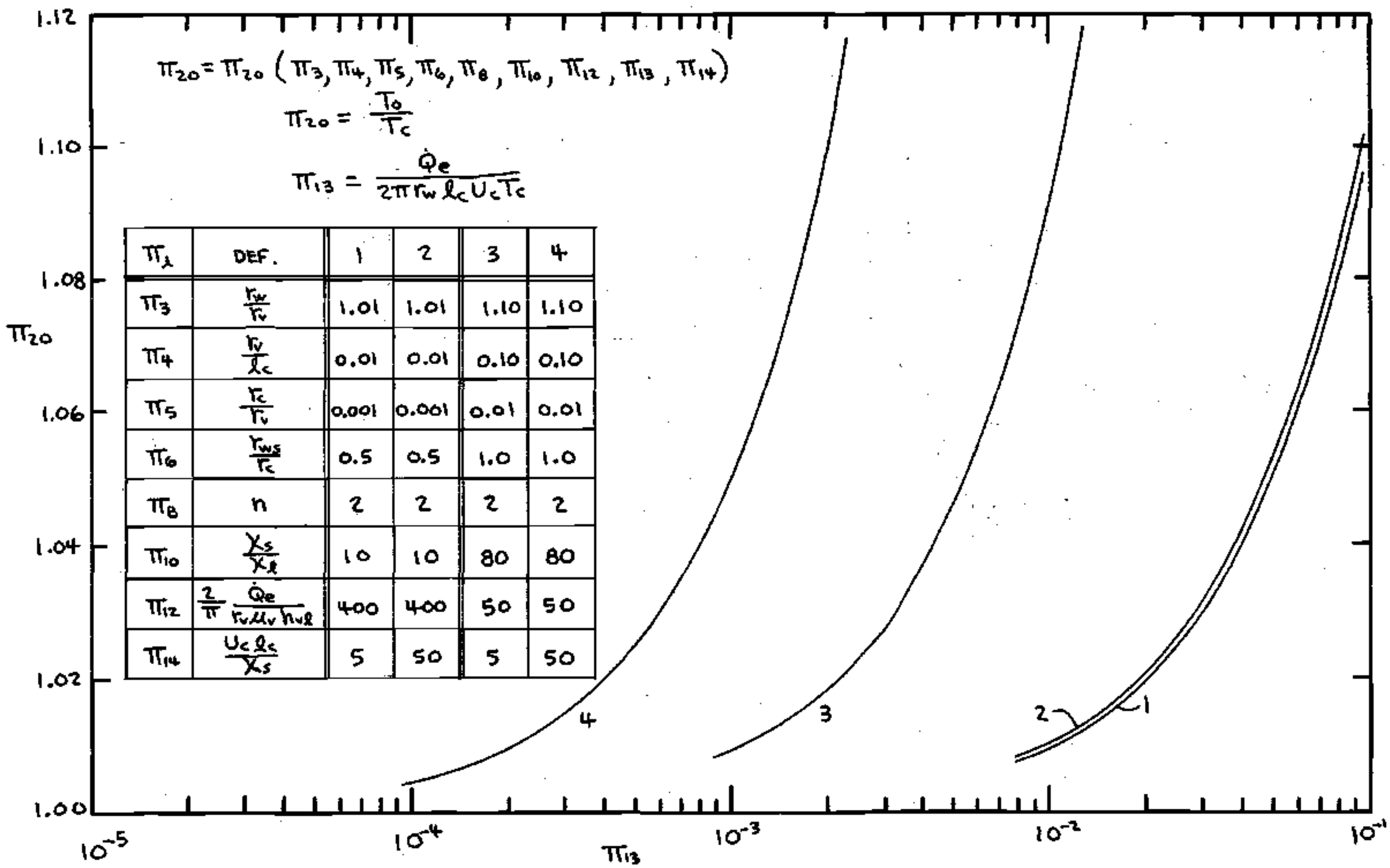

Π_i	DEF.	1	2	3	4
Π_3	$\frac{r_w}{r_v}$	1.01	1.01	1.10	1.10
Π_4	$\frac{r_v}{\ell_c}$	0.01	0.01	0.10	0.10
Π_5	$\frac{r_c}{r_v}$	0.001	0.001	0.01	0.01
Π_6	$\frac{r_{ws}}{r_c}$	0.5	0.5	1.0	1.0
Π_8	n	2	2	2	2
Π_{10}	$\frac{X_s}{X_\ell}$	10	10	80	80
Π_{12}	$\frac{2}{\pi}\frac{\dot{Q}_e}{r_v \mu_v h_{v\ell}}$	400	400	50	50
Π_{14}	$\frac{U_c \ell_c}{X_s}$	5	50	5	50

Figure 30. Predicted Values of Heat Pipe Operating Temperature Ratio Versus Condenser Heat Sink Number.

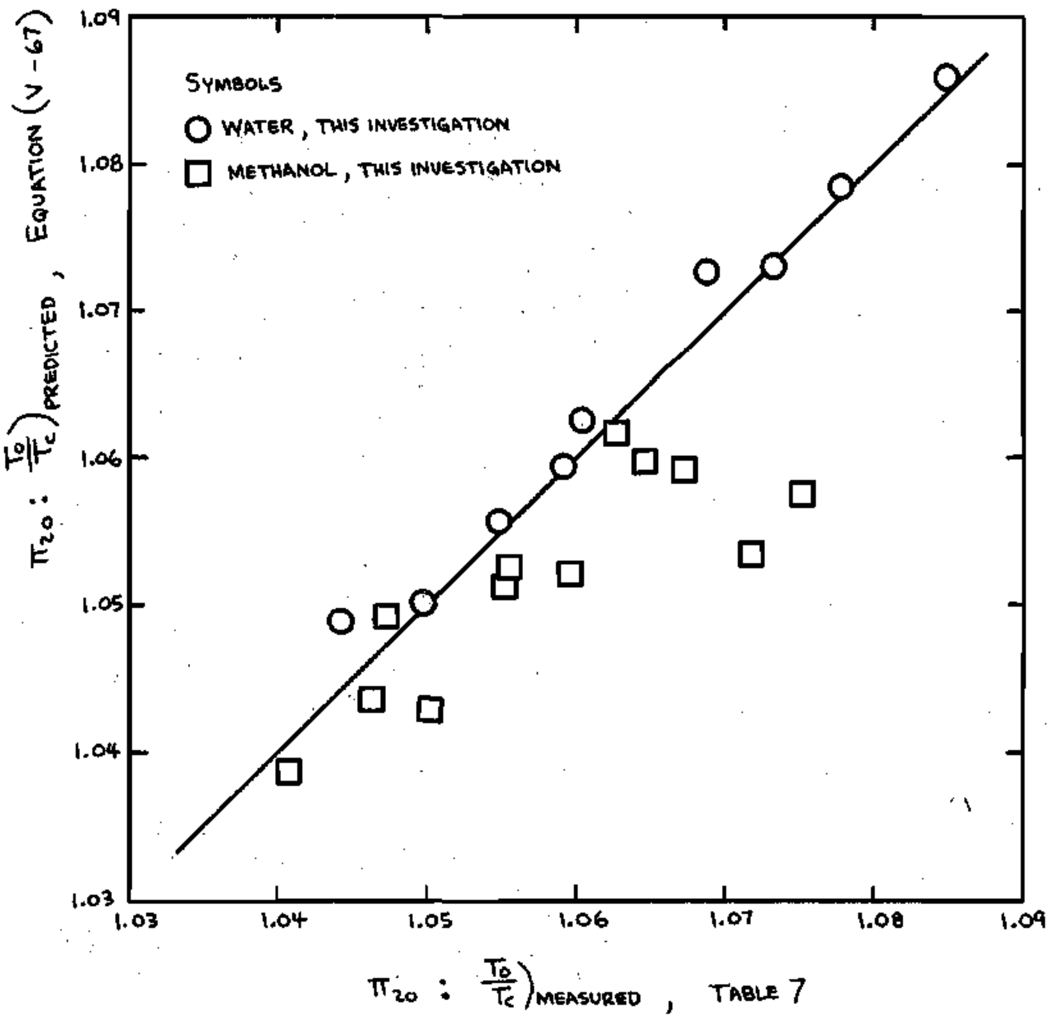

Figure 31. Comparison of Predicted and Measured Values of Heat Pipe Operating Temperature Ratio.

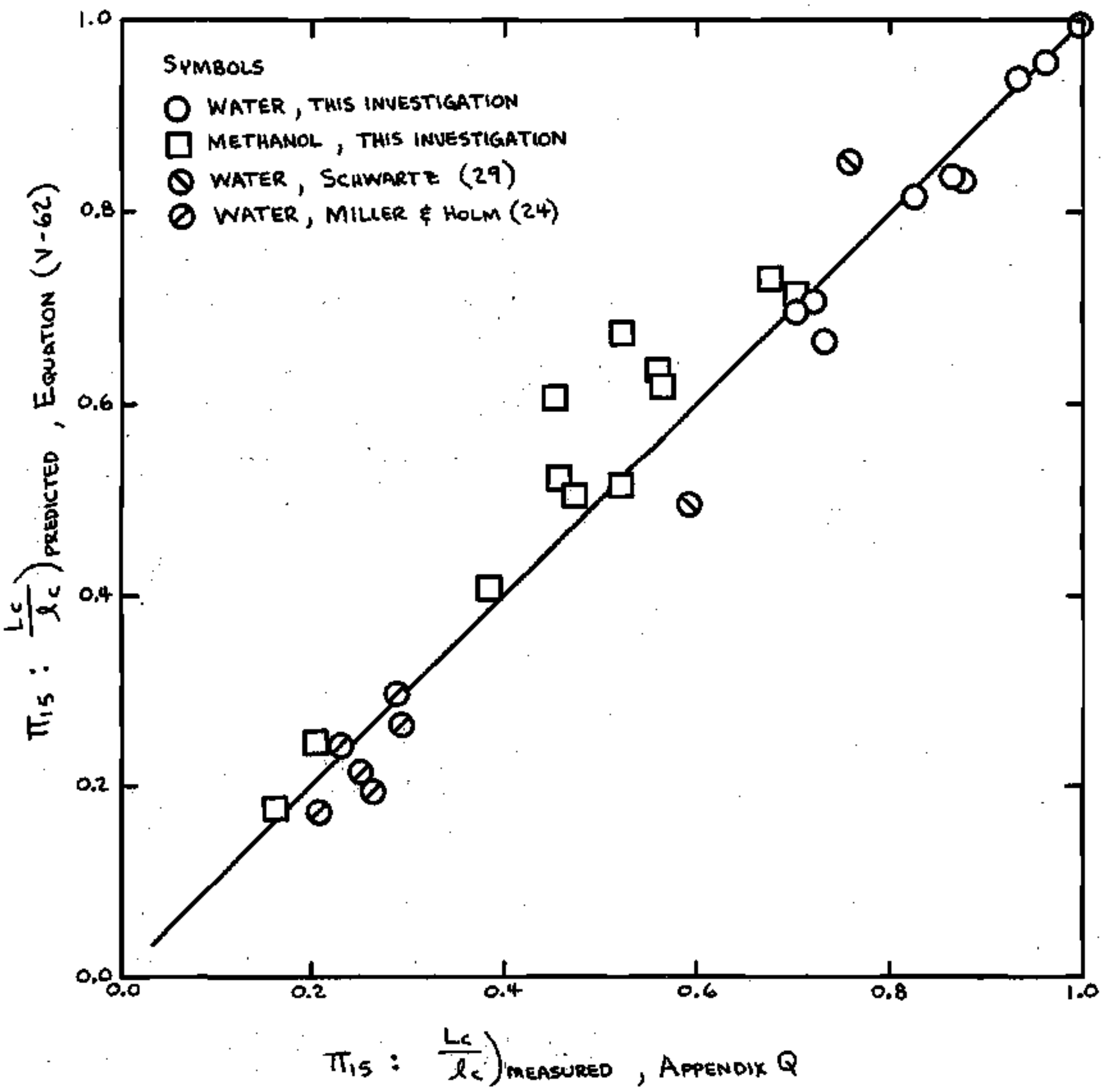

Figure 32. Comparison of Predicted and Measured Values of Condenser Active Length Ratio.

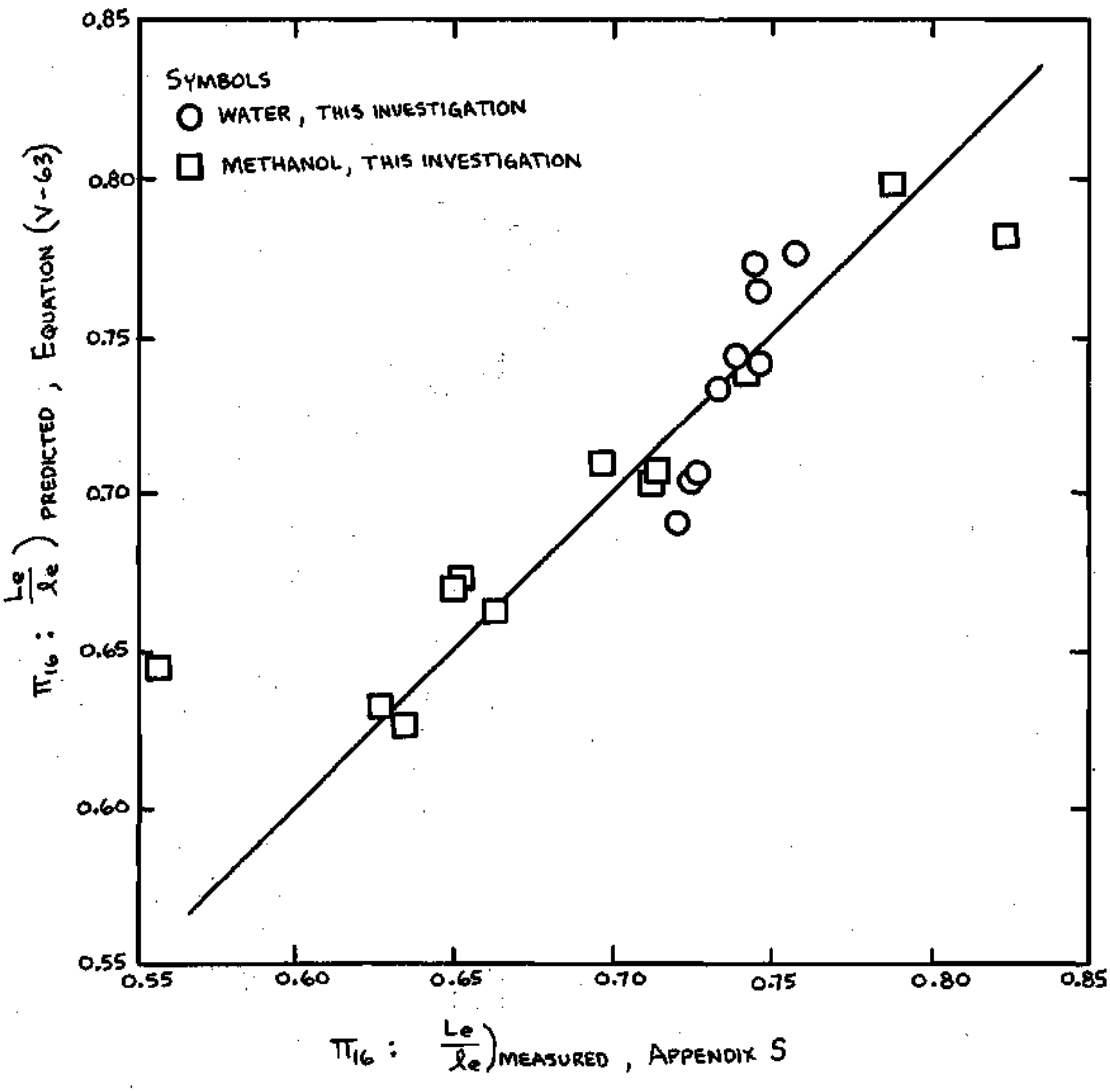

Figure 33. Comparison of Predicted and Measured Values of Evaporator Active Length Ratio.

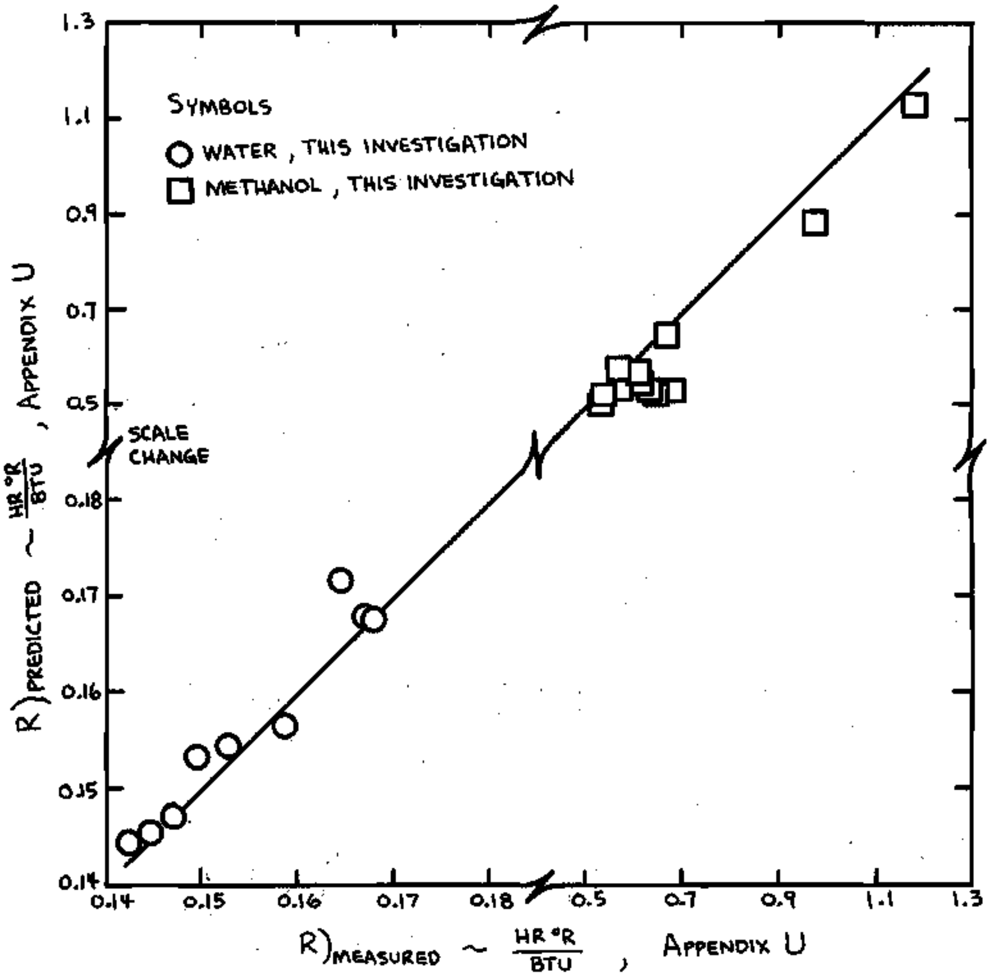

Figure 34. Comparison of Predicted and Measured Values of Overall Heat Pipe Thermal Resistance.

as inherent deviations due to uncertainties of the measured heat pipe heat transfer rate at low operating power levels, or small residue deposits in the wick and on the wick surface. These impurity deposits are suspected to be the result of deterioration of the enamel insulation of the wick thermocouples.

Figure 31 indicates agreement between measured and predicted values of π_{20}, the ratio of heat pipe operating temperature to condenser sink temperature. All of the predicted values deviate less than 10 per cent from measured values.

Figure 32 shows agreement of π_{15}, the ratio of condenser active length to design length. Included are data reduced from the experimental measurements of Miller and Holm (24) and Schwartz (29). Sixty five per cent of the predicted values deviate less than 10 per cent from measured values.

Figure 33 depicts the agreement of π_{16}, the ratio of evaporator active length to design length. Data of other investigators are not indicated due to incomplete data reporting and employment of wick wrapping geometry different from that tested in this investigation. Sufficient data is reported by Fox, et al. (10) to indicate that a variable evaporator length does exist, although Fox failed to deduce this conclusion, see Appendix V. Ninety five per cent of the predicted values deviate less than 10 per cent from measured values.

Comparison between predicted and measured values of internal overall thermal resistance is indicated in Figure 34. This resistance, see Equation (V.9) is given by

$$R = \frac{\bar{T}_{ew} - \bar{T}_{cw}}{\dot{Q}_e} \tag{V.68}$$

Evaluation of the measured value of R is accomplished by using the measured values of the temperatures in Equation (V.68). See Appendix U for evaluation details on measured and predicted values of the resistance R. Eighty five per cent of the predicted values are within 10 per cent of the measured values.

CHAPTER VI

CONCLUSIONS AND RECOMMENDATIONS

Results of this investigation provide a basis for conclusions and recommendations in the three areas of General Theory, Experimentation, and Correlation Theory.

1. Conclusions

Based on the analysis of the General Theory it is concluded that, in addition to the dimensionless groups described or implied by others, the ratio of the wick-solid radius to the wick pore radius (r_{ws}/r_c) may be a significant group.

From the experimentation the following conclusions are obtained.

1) Stable heat pipe operation is possible even when a fraction of the evaporator wick is void of liquid.

2) The independent variables, in addition to materials and fixed geometry, are T_c, the temperature of the condenser heat sink, U_c, the unit conductance between the condenser sink and the outer surface of the wick, and $\dot{Q}_e$, the heat rate supplied to the heat pipe evaporator.

Based on the Correlation Theory for the ranges of variables studied in this investigation, the significant conclusions are as follows

1) Although the axial pressure drop of the vapor is negligible, vapor dynamics are important. Variation of the axial vapor Reynolds number effects the active length of condensation. Corresponding to these length changes are variations in the overall thermal resistance of the heat pipe.

2) Variation of the evaporator meniscus for different heat pipe operating points reflects variation of the active length of evaporation. This dependency should exist only when nonisotropic wick geometrical configurations are employed, e.g. when pore radii within the wick are larger than the pore radii on the wicks surface. Corresponding to the length change there exists a fraction of the wick which is void of liquid where axial heat conductions exists in the pipe shell. The length change results in variation of the overall thermal resistance of the heat pipe.

3) Extensions of the active lengths of condensation or evaporation into the adiabatic section as introduced by consideration of shell or wick axial heat conduction are negligible.

4) The significance of the wick-solid radius, r_{ws}, is reflected in variation of the effective thickness of the wick, δ_e. For different operating points, employment of different values of r_{ws} would cause different levels of recess of the liquid-vapor interface into the wick. Variation of this thickness results in variation of the overall thermal resistance of the heat pipe.

5) It is sufficient to model the evaporator liquid-vapor interface as a spherical surface of radius r_m.

6) Darcy's law for liquid flow in porous media is a suitable model for analysis of liquid flow in heat pipe performance computations.

7) Beginning with the dimensionless groups obtained in the General Theory, the groups explicitly insignificant include vapor Prandtl number, liquid Prandtl number, density ratio of liquid to vapor, Kutateladze number, liquid pore Reynolds number, and vapor Eckert number.

2. Recommendations

Future investigations of heat pipe performance should include studies on 1) the range of validity for describing the evaporator liquid-vapor interface as being composed of spherical surfaces and 2) measurements of the retreating liquid-vapor interface and the variation of wick thickness with meniscus geometry.

Further testing of the correlation models and conclusions of this investigation should include use of wider ranges of the variables. Such studies would include 1) working fluids, for high and low operating temperatures, 2) shell materials, for high and low thermal conductivities, 3) shell geometry, for variations of thickness and design lengths, 4) wick geometrical configurations, both isotropic and non isotropic, and 5) environmental parameters of T_c, U_c, and $\dot{Q}_e$.

APPENDIX A

GENERAL THEORY EQUATIONS IN DIMENSIONLESS FORM

Equations of the general theory are written in dimensionless form by first expanding the vector equations into the component equations and then using the reference parameters to obtain dimensionless coefficients of the dimensionless equations. The spatial boundaries, spatial locations, and constitutive equations are written in dimensionless form as necessary. Equations are presented for functions previously written in words (e.g. radius of curvature $R_m = R_m$(surface geometry).

A-1. Vapor Region

A. Spatial Boundaries

The equations are

$$0 \le \bar{z} < \left[\frac{l_e}{l_c}\right] + \left[\frac{l_a}{l_c}\right] + 1 , \tag{A.1}$$

$$0 \le \bar{r} \le 1 + \left[\frac{r_c}{r_v}\right] \bar{\eta} \text{, and} \tag{A.2}$$

$$0 \le \bar{\theta} \le 1 . \tag{A.3}$$

B. Field Equations

The equations are

equation of continuity

$$\frac{\partial(\bar{r}\bar{\rho}_v\bar{u}_v)}{\partial\bar{r}} + \frac{1}{2\pi}\frac{\partial(\bar{\rho}_v\bar{v}_v)}{\partial\bar{\theta}} + 2\frac{\partial(\bar{\rho}_v\bar{w}_v)}{\partial\bar{z}} = 0 , \qquad \text{(A.4)}$$

equation of motion in radial direction

$$\bar{\rho}_v\left[\bar{u}_v\frac{\partial\bar{u}_v}{\partial\bar{r}} + \frac{1}{2\pi}\bar{v}_v\frac{\partial\bar{u}_v}{\partial\bar{\theta}} + 2\bar{w}_v\frac{\partial\bar{u}_v}{\partial\bar{z}} - \frac{\bar{v}_v^2}{\bar{r}}\right] = -\frac{\partial\bar{P}_v}{\partial\bar{r}} + \qquad \text{(A.5)}$$

$$+\left[\frac{\mu_v}{\rho_v r_v u_v}\right]\left\{2\frac{\partial}{\partial\bar{r}}\left(\bar{\mu}_v\frac{\partial\bar{u}_v}{\partial\bar{r}}\right) + \right.$$

$$+\frac{2}{3}\frac{\partial}{\partial\bar{r}}\left(\bar{\lambda}_v\left(\frac{1}{\bar{r}}\frac{\partial(\bar{r}\bar{u}_v)}{\partial\bar{r}} + \frac{1}{2\pi}\frac{\partial\bar{v}_v}{\partial\bar{\theta}} + 2\frac{\partial\bar{w}_v}{\partial\bar{z}}\right)\right) +$$

$$+\frac{1}{4\pi^2}\frac{1}{\bar{r}}\frac{\partial}{\partial\bar{\theta}}\left(\bar{\mu}_v\left(\frac{1}{\bar{r}}\frac{\partial\bar{u}_v}{\partial\bar{\theta}} + \frac{\partial\bar{v}_v}{\partial\bar{r}} - \frac{\bar{v}_v}{\bar{r}}\right)\right) +$$

$$+\left[\frac{r_v}{l_c}\right]^2\frac{\partial}{\partial\bar{z}}\left(\bar{\mu}_v\frac{\partial\bar{u}_v}{\partial\bar{z}}\right) + 2\frac{\partial}{\partial\bar{z}}\left(\bar{\mu}_v\frac{\partial\bar{w}_v}{\partial\bar{r}}\right) +$$

$$\left. + 2\frac{\bar{\mu}_v}{\bar{r}}\left(\frac{\partial\bar{u}_v}{\partial\bar{r}} - \frac{1}{2\pi}\frac{1}{\bar{r}}\frac{\partial\bar{v}_v}{\partial\bar{\theta}} - \frac{\bar{u}_v}{\bar{r}}\right)\right\} ,$$

equation of motion in angular direction

$$\bar{\rho}_v\left[\bar{u}_v\frac{\partial\bar{v}_v}{\partial\bar{r}} + \frac{1}{2\pi}\bar{v}_v\frac{1}{\bar{r}}\frac{\partial\bar{v}_v}{\partial\bar{\theta}} + 2\bar{w}_v\frac{\partial\bar{v}_v}{\partial\bar{z}} + \frac{\bar{u}_v\bar{v}_v}{\bar{r}}\right] = -\frac{1}{2\pi}\frac{\partial\bar{P}_v}{\partial\bar{\theta}} + \qquad \text{(A.6)}$$

$$+\left[\frac{\mu_v}{\rho_v r_v u_v}\right]\left\{\frac{1}{4\pi^2}\frac{2}{\bar{r}}\frac{\partial}{\partial\bar{\theta}}\left(\bar{\mu}_v\frac{1}{\bar{r}}\frac{\partial\bar{v}_v}{\partial\bar{\theta}}\right) + \right.$$

$$+\frac{1}{2\pi}\frac{2}{3}\frac{1}{\bar r}\frac{\partial}{\partial\bar\theta}\left(\bar\lambda_v\left(\frac{1}{\bar r}\frac{\partial(\bar r\bar u_v)}{\partial\bar r}+\frac{1}{2\pi}\frac{1}{\bar r}\frac{\partial\bar v_v}{\partial\bar\theta}+2\frac{\partial\bar w_v}{\partial\bar z}\right)\right)+$$

$$+\frac{2\epsilon}{2\pi}\frac{\partial}{\partial\bar z}\left(\bar\mu_v\frac{1}{\bar r}\frac{\partial\bar w_v}{\partial\bar\theta}+\left[\frac{r_v}{l_c}\right]^2\frac{\partial}{\partial\bar z}\left(\bar\mu_v\frac{\partial\bar u_v}{\partial\bar z}\right)\right)+$$

$$+\frac{\partial}{\partial\bar r}\left(\bar\mu_v\left(\frac{1}{2\pi}\frac{1}{\bar r}\frac{\partial\bar u_v}{\partial\bar\theta}+\frac{\partial\bar v_v}{\partial\bar r}-\frac{\bar v_v}{\bar r}\right)\right)+$$

$$+\frac{2\bar\mu_v}{\bar r}\left(\frac{1}{2\pi}\frac{1}{\bar r}\frac{\partial\bar u_v}{\partial\bar\theta}+\frac{\partial\bar v_v}{\partial\bar r}-\frac{\bar v_v}{\bar r}\right)\Bigg\}\ ,$$

equation of motion in axial direction

$$\bar\rho_v\left[2\bar u_v\frac{\partial\bar w_v}{\partial\bar r}+\frac{2}{2\pi}\left[\frac{l_c}{r_v}\right]\frac{\bar v_v}{\bar r}\frac{\partial\bar w_v}{\partial\bar\theta}+4\left[\frac{l_c}{r_v}\right]\bar w_v\frac{\partial\bar w_v}{\partial\bar z}\right]=-\left[\frac{r_v}{l_c}\right]\frac{\partial\bar P_v}{\partial\bar z}+\qquad(A.7)$$

$$+\left[\frac{\mu_v}{\rho_v r_v u_v}\right]\Bigg\{2\left[\frac{r_v}{l_c}\right]\frac{\partial}{\partial\bar z}\left(2\bar\mu_v\frac{\partial\bar w_v}{\partial\bar z}\right)+$$

$$+\left[\frac{r_v}{l_c}\right]\frac{\partial}{\partial\bar z}\left(\frac{2}{3}\bar\lambda_v\left(\frac{1}{\bar r}\frac{\partial(\bar r\bar u_v)}{\partial\bar r}+\frac{1}{2\pi}\frac{1}{\bar r}\frac{\partial\bar v_v}{\partial\bar\theta}+2\frac{\partial\bar w_v}{\partial\bar z}\right)\right)+$$

$$+\left[\frac{r_v}{l_c}\right]\frac{1}{\bar r}\frac{\partial}{\partial\bar r}\left(\bar r\bar\mu_v\frac{\partial\bar u_v}{\partial\bar z}\right)+\left[\frac{l_c}{r_v}\right]\frac{2}{\bar r}\frac{\partial}{\partial\bar r}\left(\bar r\frac{\partial\bar w_v}{\partial\bar r}\right)+$$

$$+\frac{2}{4\pi^2}\left[\frac{l_c}{r_v}\right]\frac{1}{\bar r}\frac{\partial}{\partial\bar\theta}\left(\bar\mu_v\frac{1}{\bar r}\frac{\partial\bar w_v}{\partial\bar\theta}\right)+\frac{1}{2\pi}\left[\frac{r_v}{l_c}\right]\frac{1}{\bar r}\frac{\partial}{\partial\bar\theta}\left(\frac{\partial\bar v_v}{\partial\bar z}\right)\Bigg\}\ ,\text{ and}$$

equation of energy

$$\bar\rho_v\left[\bar u_v\frac{\partial\bar h_v}{\partial\bar r}+\frac{1}{2\pi}\bar v_v\frac{\partial\bar h_v}{\partial\bar\theta}+2\frac{\partial\bar h_v}{\partial\bar z}\right]=\left[\left(\frac{\mu_v}{\rho_v r_v u_v}\right)\left(\frac{\chi_v}{\mu_v c_{pv}}\right)\right]\times\qquad(A.8)$$

$$\times\left\{\frac{1}{\bar r}\frac{\partial}{\partial\bar r}\left(\bar r\bar\chi_v\frac{\partial\bar T}{\partial\bar r}\right)+\frac{1}{2\pi}\frac{1}{\bar r^2}\frac{\partial}{\partial\bar\theta}\left(\bar\chi_v\frac{\partial\bar T}{\partial\bar\theta}\right)+\left[\frac{r_v}{l_c}\right]^2\frac{\partial}{\partial\bar z}\left(\bar\chi_v\frac{\partial\bar T}{\partial\bar z}\right)\right\}+$$

$$+\left[\frac{u_v^2}{c_{pv}T_c}\right]\left\{\bar u_v\frac{\partial\bar P_v}{\partial\bar r}+\frac{1}{2\pi}\frac{\bar v_v}{\bar r}\frac{\partial\bar P_v}{\partial\bar\theta}+2\frac{\partial\bar P_v}{\partial\bar z}\right\}\ .$$

A-2. Liquid Region

A. Spatial Boundaries

The equations are

$$0 \leq \bar{z} \leq \left[\frac{\ell_e}{\ell_c}\right] + \left[\frac{\ell_a}{\ell_c}\right] + 1 \quad , \tag{A.9}$$

$$1 + \left[\frac{r_c}{r_v}\right]\bar{\eta} < \bar{r} < \left[\frac{r_w}{r_v}\right] \quad \text{, and} \tag{A.10}$$

$$0 \leq \bar{\theta} \leq 1 \quad . \tag{A.11}$$

B. Field Equations

The equations are

equation of continuity

$$\frac{1}{\bar{r}}\frac{\partial(\bar{r}\bar{u}_\ell)}{\partial \bar{r}} + \frac{1}{2\pi}\frac{1}{\bar{r}}\frac{\partial \bar{v}_\ell}{\partial \bar{\theta}} + \left(\frac{2}{\epsilon_o\left(\left[\frac{r_w}{r_v}\right]^2 - 1\right)}\right)\frac{\partial \bar{w}_\ell}{\partial \bar{z}} = 0 \quad , \tag{A.12}$$

equation of motion in radial direction

$$\bar{u}_\ell\frac{\partial \bar{u}_\ell}{\partial \bar{r}} + \frac{1}{2\pi}\frac{\bar{v}_\ell}{\bar{r}}\frac{\partial \bar{u}_\ell}{\partial \bar{\theta}} + \left(\frac{2}{\epsilon_o\left(\left[\frac{r_w}{r_v}\right]^2 - 1\right)}\right)\bar{w}_\ell\frac{\partial \bar{u}_\ell}{\partial \bar{z}} - \frac{\bar{v}_\ell^2}{\bar{r}} = -\frac{1}{\bar{\rho}_\ell}\frac{\partial \bar{P}_\ell}{\partial \bar{r}} + \tag{A.13}$$

$$+ \left[\frac{r_v}{r_c}\right]\left[K_1 r_c^2\right]\left[\frac{\mu_\ell}{\rho_\ell u_\ell r_c}\right]\epsilon_o \, \bar{K}\bar{\epsilon}\frac{\bar{\mu}_\ell}{\bar{\rho}_\ell}\bar{u}_\ell \quad ,$$

equation of motion in angular direction

$$\bar{u}_\ell \frac{\partial \bar{v}_\ell}{\partial \bar{r}} + \frac{1}{2\pi}\frac{\bar{v}_\ell}{\bar{r}}\frac{\partial \bar{v}_\ell}{\partial \bar{\theta}} + \left(\frac{2}{\epsilon_o\left(\left[\frac{r_w}{r_v}\right]^2-1\right)}\right)\bar{w}_\ell \frac{\partial \bar{v}_\ell}{\partial \bar{z}} + \frac{\bar{u}_\ell \bar{v}_\ell}{\bar{r}} = -\frac{1}{\bar{\rho}_\ell}\frac{1}{2\pi}\frac{\partial \bar{P}_\ell}{\partial \bar{\theta}} + \tag{A.14}$$

$$+ \quad \epsilon_o\left[\frac{r_v}{r_c}\right]\left[\frac{\mu_\ell}{\rho_\ell u_\ell r_c}\right]\left[K_1 r_c^2\right]\frac{\bar{\mu}_\ell}{\bar{\rho}_\ell}\,\frac{\bar{\epsilon}}{\bar{K}}\,\bar{v}_\ell \quad ,$$

equation of motion in axial direction

$$\bar{u}_\ell \frac{\partial \bar{w}_\ell}{\partial \bar{r}} + \frac{1}{2\pi}\,\frac{\bar{v}_\ell}{\bar{r}}\,\frac{\partial \bar{w}_\ell}{\partial \bar{\theta}} + \left(\frac{2}{\epsilon_o\left(\left[\frac{r_w}{r_v}\right]^2-1\right)}\right)\bar{w}_\ell \frac{\partial \bar{w}_\ell}{\partial \bar{z}} = \tag{A.15}$$

$$= \left(\left[\frac{r_w}{r_v}\right]^2-1\right)\frac{\epsilon_o}{2}\left[\frac{r_v}{\ell_c}\right]^2\frac{1}{\bar{\rho}_\ell}\,\frac{\partial \bar{P}_\ell}{\partial \bar{z}} + \left[\frac{\mu_\ell}{\rho_\ell u_\ell r_c}\right]\left[K_1 r_c^2\right]\left[\frac{r_v}{r_c}\right]\times$$

$$\times\, \epsilon_o\,\frac{\bar{K}\bar{\epsilon}}{1}\,\frac{\bar{\mu}_\ell}{\bar{\rho}_\ell}\,\bar{w}_\ell \quad , \text{ and}$$

equation of energy

$$\bar{\rho}_\ell\left[\bar{u}_\ell \frac{\partial \bar{h}_\ell}{\partial \bar{r}} + \frac{1}{2\pi}\,\frac{\bar{v}_\ell}{\bar{r}}\,\frac{\partial \bar{h}_\ell}{\partial \bar{\theta}} + \left(\frac{2}{\epsilon_o\left(\left[\frac{r_w}{r_v}\right]^2-1\right)}\right)\bar{w}_\ell \frac{\partial \bar{h}_\ell}{\partial \bar{z}}\right] = \tag{A.16}$$

$$= \left[\frac{r_c}{r_v}\right]\left[\frac{\mu_\ell}{\rho_\ell u_\ell r_c}\right]\left[\frac{\chi_\ell}{\mu_\ell C_{p\ell}}\right]\left[\frac{\chi_{eff}}{\chi_\ell}\right]\times$$

$$\times\left\{\frac{1}{\bar{r}}\frac{\partial}{\partial \bar{r}}\left(\bar{r}\,\bar{\chi}_{eff}\frac{\partial \bar{T}}{\partial \bar{r}}\right) + \frac{1}{4\pi^2}\frac{1}{\bar{r}^2}\frac{\partial}{\partial \bar{\theta}}\left(\bar{\chi}_{eff}\frac{\partial \bar{T}}{\partial \bar{\theta}}\right) + \right.$$

$$\left. + \left[\frac{r_v}{\ell_c}\right]^2\frac{\partial}{\partial \bar{z}}\left(\bar{\chi}_{eff}\frac{\partial \bar{T}}{\partial \bar{z}}\right)\right\} \;+$$

$$+\left[\frac{u_\ell^2}{C_{p_\ell}T_c}\right]\left\{\bar{u}_\ell\frac{\partial\bar{P}_\ell}{\partial\bar{r}}+\frac{1}{2\pi}\frac{\bar{v}_\ell}{\bar{r}}\frac{\partial\bar{P}_\ell}{\partial\bar{\theta}}+\left(\frac{2}{\epsilon_o\left(\left[\frac{r_w}{r_v}\right]^2-1\right)}\right)\bar{w}_\ell\frac{\partial\bar{P}_\ell}{\partial\bar{z}}\right\} .$$

C. Constitutive Equations

The necessary equations are

equation of wick friction parameter

$$\bar{K} \equiv \frac{K}{K_1} = \bar{K}\left(\left[\frac{r_w}{r_v}\right],\left[\frac{r_c}{r_v}\right],\left[\frac{r_{ws}}{r_c}\right],\ \text{wick configuration}\right),\ \text{and} \quad (A.17)$$

equation of effective wick thermal conductivity

$$\bar{\chi}_{eff} \equiv \frac{\chi_{eff}}{\chi_{eff\ \text{at}\ T_o}} = \bar{\chi}_{eff}\left(\left[\frac{\chi_\ell}{\chi_s}\right]\bar{\chi}_\ell,\ \bar{\chi}_s,\ \left[\frac{r_w}{r_v}\right],\left[\frac{r_c}{r_v}\right],\left[\frac{r_{ws}}{r_c}\right],\ n\right) . \quad (A.18)$$

A-3. Liquid-Vapor Interface

A. Spatial Location

The equations are

$$0 \le \bar{z} \le \left[\frac{\ell_e}{\ell_c}\right]+\left[\frac{\ell_a}{\ell_c}\right]+1 , \quad (A.19)$$

$$\bar{r} = 1+\left[\frac{r_c}{r_v}\right]\bar{\eta} ,\ \text{and} \quad (A.20)$$

$$0 \le \bar{\theta} \le 1 . \quad (A.21)$$

B. Boundary Conditions

The equations are

equation of continuity

$$\left(\bar{\rho}_v \bar{u}_v - \left[\frac{\rho_\ell u_\ell}{\rho_v u_v}\right] \bar{\rho}_\ell \bar{u}_\ell\right)\left(\left(\left(1+\left[\frac{r_c}{r_v}\right]\right)\bar{\eta}_s \frac{\partial \bar{\theta}_s}{\partial \bar{p}} \frac{\partial \bar{\xi}_s}{\partial \bar{q}} - \left(1+\left[\frac{r_c}{r_v}\right]\bar{\eta}_s\right)\frac{\partial \bar{\theta}_s}{\partial \bar{q}} \frac{\partial \bar{\xi}_s}{\partial \bar{p}}\right) + \quad \text{(A.22)}$$

$$+ \left(\bar{\rho}_v \bar{v}_v - \left[\frac{\rho_\ell u_\ell}{\rho_v u_v}\right] \bar{\rho}_\ell \bar{v}_\ell\right)\left(\frac{\partial \bar{\eta}_s}{\partial \bar{q}} \frac{\partial \bar{\xi}_s}{\partial \bar{p}} - \frac{\partial \bar{\eta}_s}{\partial \bar{p}} \frac{\partial \bar{\xi}_s}{\partial \bar{q}}\right) +$$

$$+ 2\left[\frac{\ell_c}{r_v}\right]\left(\bar{\rho}_v \bar{\omega}_v - \left(\frac{1}{\epsilon_o\left(\left[\frac{r_w}{r_v}\right]^2-1\right)}\right)\left[\frac{\rho_\ell u_\ell}{\rho_v u_v}\right] \bar{\rho}_\ell \bar{\omega}_\ell\right)\left\{\left(1+\left[\frac{r_c}{r_v}\right]\bar{\eta}_s\right)\frac{\partial \bar{\theta}_s}{\partial \bar{q}} \frac{\partial \bar{\eta}_s}{\partial \bar{p}} -\right.$$

$$\left. - \left(1+\left[\frac{r_c}{r_v}\right]\bar{\eta}_s\right)\frac{\partial \bar{\eta}_s}{\partial \bar{q}} \frac{\partial \bar{\theta}_s}{\partial \bar{p}}\right\} = 0 \quad ,$$

no slip conditions

$$\left(\bar{u}_v - \bar{u}_i\right)\frac{\partial \bar{\eta}_s}{\partial \bar{p}} + \left(\bar{v}_v - \bar{v}_i\right)\left(1+\left[\frac{r_c}{r_v}\right]\bar{\eta}_s\right)\frac{\partial \bar{\theta}_s}{\partial \bar{p}} + 2\left[\frac{\ell_c}{r_v}\right]\left(\bar{\omega}_v - \bar{\omega}_i\right)\frac{\partial \bar{\xi}_s}{\partial \bar{p}} = 0, \quad \text{(A.23)}$$

$$\left(\bar{u}_v - \bar{u}_i\right)\frac{\partial \bar{\eta}_s}{\partial \bar{q}} + \left(\bar{v}_v - \bar{v}_i\right)\left(1+\left[\frac{r_c}{r_v}\right]\bar{\eta}_s\right)\frac{\partial \bar{\theta}_s}{\partial \bar{q}} + 2\left[\frac{\ell_c}{r_v}\right]\left(\bar{\omega}_v - \bar{\omega}_i\right)\frac{\partial \bar{\xi}_s}{\partial \bar{q}} = 0, \quad \text{(A.24)}$$

$$\left(\bar{u}_\ell - \left[\frac{\rho_v u_v}{\rho_\ell u_\ell}\right]\left[\frac{\rho_\ell}{\rho_v}\right]\bar{u}_i\right)\frac{\partial \bar{\eta}_s}{\partial \bar{p}} + \left(\bar{v}_\ell - \left[\frac{\rho_v u_v}{\rho_\ell u_\ell}\right]\left[\frac{\rho_\ell}{\rho_v}\right]\bar{v}_i\right)\frac{\partial \bar{\theta}_s}{\partial \bar{p}} + \quad \text{(A.25)}$$

$$+ 2\left[\frac{\ell_c}{r_v}\right]\left\{\left(\frac{1}{\epsilon_o\left(\left[\frac{r_w}{r_v}\right]^2-1\right)}\right)\bar{\omega}_\ell - \left[\frac{\rho_v u_v}{\rho_\ell u_\ell}\right]\left[\frac{\rho_\ell}{\rho_v}\right]\bar{\omega}_i\right\}\frac{\partial \bar{\xi}_s}{\partial \bar{p}} = 0, \text{ and}$$

$$\left(\bar{u}_\ell - \left[\frac{\rho_v u_v}{\rho_\ell u_\ell}\right]\left[\frac{\rho_\ell}{\rho_v}\right]\bar{u}_i\right)\frac{\partial\bar{\eta}_s}{\partial\bar{q}} + \left(\bar{v}_\ell - \left[\frac{\rho_v u_v}{\rho_\ell u_\ell}\right]\left[\frac{\rho_\ell}{\rho_v}\right]\bar{v}_i\right)\frac{\partial\bar{\theta}_s}{\partial\bar{q}} + \tag{A.26}$$

$$+ 2\left[\frac{\ell_c}{r_v}\right]\left\{\left(\frac{1}{\epsilon_o\left(\left[\frac{r_w}{r_v}\right]^2-1\right)}\right)\bar{\omega}_\ell - \left[\frac{\rho_v u_v}{\rho_\ell u_\ell}\right]\left[\frac{\rho_\ell}{\rho_v}\right]\bar{\omega}_i\right\}\frac{\partial\bar{\zeta}_s}{\partial\bar{q}} = 0 ,$$

equation of motion in radial direction

$$\left(1+\left[\frac{r_c}{r_v}\right]\bar{\eta}_s\right)\left(\frac{\partial\bar{\theta}_s}{\partial\bar{p}}\frac{\partial\bar{\zeta}_s}{\partial\bar{q}} - \frac{\partial\bar{\theta}_s}{\partial\bar{q}}\frac{\partial\bar{\zeta}_s}{\partial\bar{p}}\right)\left\{\bar{\rho}_v\bar{u}_v^2 - \left[\frac{\rho_\ell u_\ell}{\rho_v u_v}\right]^2\left[\frac{\rho_v}{\rho_\ell}\right]\bar{\rho}_\ell\bar{u}_\ell^2 + \bar{P}_v - \right. \tag{A.27}$$

$$- \left[\frac{\rho_\ell u_\ell}{\rho_v u_v}\right]^2\left[\frac{\rho_v}{\rho_\ell}\right]\bar{P}_\ell - 2\left[\frac{\rho_\ell u_\ell}{\rho_v u_v}\right]^2\left[\frac{\rho_v}{\rho_\ell}\right]^2\left[\frac{\sigma}{\rho_\ell u_\ell^2 r_c}\right]\bar{\sigma}\left[\frac{r_c}{R_m}\right] +$$

$$\left. + \left[\frac{\mu_v}{\rho_v r_v u_v}\right]\left[\frac{r_v}{r_c}\right]\overline{\tau_v)}_{rr} - \left[\frac{\rho_\ell u_\ell}{\rho_v u_v}\right]^2\left[\frac{\rho_v}{\rho_\ell}\right]\left[\frac{\mu_\ell}{\rho_\ell u_\ell r_c}\right]\overline{\tau_\ell)}_{rr}\right\} +$$

$$+ \left(\frac{\partial\bar{\eta}_s}{\partial\bar{q}}\frac{\partial\bar{\zeta}_s}{\partial\bar{p}} - \frac{\partial\bar{\eta}_s}{\partial\bar{p}}\frac{\partial\bar{\zeta}_s}{\partial\bar{q}}\right)\left\{\bar{\rho}_v\bar{u}_v\bar{v}_v - \left[\frac{\rho_\ell u_\ell}{\rho_v u_v}\right]^2\left[\frac{\rho_v}{\rho_\ell}\right]\bar{\rho}_\ell\bar{u}_\ell\bar{v}_\ell + \right.$$

$$\left. + \left[\frac{\mu_v}{\rho_v r_v u_v}\right]\left[\frac{r_v}{r_c}\right]\overline{\tau_v)}_{r\theta} - \left[\frac{\rho_\ell u_\ell}{\rho_v u_v}\right]^2\left[\frac{\rho_v}{\rho_\ell}\right]\left[\frac{\mu_\ell}{\rho_\ell u_\ell r_c}\right]\overline{\tau_\ell)}_{r\theta}\right\} +$$

$$+ \left(1+\left[\frac{r_c}{r_v}\right]\bar{\eta}_s\right)\left(\frac{\partial\bar{\eta}_s}{\partial\bar{q}}\frac{\partial\bar{\theta}_s}{\partial\bar{q}} - \frac{\partial\bar{\eta}_s}{\partial\bar{q}}\frac{\partial\bar{\theta}_s}{\partial\bar{p}}\right)\left\{2\left[\frac{\ell_c}{r_v}\right]\left(\bar{\rho}_v\bar{u}_v\bar{\omega}_v - \left[\frac{\rho_\ell u_\ell}{\rho_v u_v}\right]^2\left[\frac{\rho_v}{\rho_\ell}\right]\left(\frac{1}{\epsilon_o\left(\left[\frac{r_w}{r_v}\right]^2-1\right)}\right)\bar{u}_\ell\bar{\omega}_\ell\right) + \right.$$

$$\left. + \left[\frac{\mu_v}{\rho_v r_v u_v}\right]\left[\frac{r_v}{r_c}\right]\overline{\tau_v)}_{rz} - \left[\frac{\rho_\ell u_\ell}{\rho_v u_v}\right]^2\left[\frac{\rho_v}{\rho_\ell}\right]\left[\frac{\mu_\ell}{\rho_\ell u_\ell r_c}\right]\overline{\tau_\ell)}_{rz}\right\} +$$

$$+ \left[\frac{\rho_\ell u_\ell}{\rho_v u_v}\right]^2\left[\frac{\rho_v}{\rho_\ell}\right]^2\left[\frac{\sigma}{\rho_\ell u_\ell^2 r_c}\right]\bar{a}^{1/2}\,\overline{(\nabla_s\sigma)}_r = 0 ,$$

equation of motion in angular direction

$$
\begin{aligned}
&\left(1+\left[\frac{r_c}{r_v}\right]\bar{\eta}_s\right)\left(\frac{\partial\bar{\theta}_s}{\partial\bar{p}}\frac{\partial\bar{\xi}_s}{\partial\bar{q}}-\frac{\partial\bar{\theta}_s}{\partial\bar{q}}\frac{\partial\bar{\xi}_s}{\partial\bar{p}}\right)\Bigg\{\bar{\rho}_v\bar{u}_v\bar{v}_v-\left[\frac{\rho_\ell u_\ell}{\rho_v u_v}\right]^2\left[\frac{\rho_v}{\rho_\ell}\right]\bar{\rho}_\ell\bar{u}_\ell\bar{v}_\ell \;+ \qquad \text{(A.28)}\\
&+\left[\frac{\mu_v}{\rho_v r_v u_v}\right]\left[\frac{r_v}{r_c}\right]\left(\overline{T_v}\right)_{r\theta}-\left[\frac{\rho_\ell u_\ell}{\rho_v u_v}\right]^2\left[\frac{\rho_v}{\rho_\ell}\right]\left[\frac{\mu_\ell}{\rho_\ell r_c u_\ell}\right]\left(\overline{T_\ell}\right)_{r\theta}\Bigg\} \;+\\
&+\left(\frac{\partial\bar{\eta}_s}{\partial\bar{q}}\frac{\partial\bar{\xi}_s}{\partial\bar{p}}-\frac{\partial\bar{\eta}_s}{\partial\bar{p}}\frac{\partial\bar{\xi}_s}{\partial\bar{q}}\right)\Bigg\{\bar{\rho}_v\bar{v}_v^2-\left[\frac{\rho_\ell u_\ell}{\rho_v u_v}\right]^2\left[\frac{\rho_v}{\rho_\ell}\right]\bar{\rho}_\ell\bar{v}_\ell^2+\bar{P}_v \;-\\
&-\left[\frac{\rho_\ell u_\ell}{\rho_v u_v}\right]^2\left[\frac{\rho_v}{\rho_\ell}\right]\bar{P}_\ell-2\left[\frac{\rho_\ell u_\ell}{\rho_v u_v}\right]\left[\frac{\rho_v}{\rho_\ell}\right]^2\left[\frac{\sigma}{\rho_\ell u_\ell^2 r_c}\right]\bar{\sigma}\left[\frac{r_c}{R_m}\right] \;+\\
&+\left[\frac{\mu_v}{\rho_v r_v u_v}\right]\left[\frac{r_v}{r_c}\right]\left(\overline{T_v}\right)_{\theta\theta}-\left[\frac{\rho_\ell u_\ell}{\rho_v u_v}\right]^2\left[\frac{\rho_v}{\rho_\ell}\right]\left[\frac{\mu_\ell}{\rho_\ell r_c u_\ell}\right]\left(\overline{T_\ell}\right)_{\theta\theta}\Bigg\} \;+\\
&+\left(1+\left[\frac{r_c}{r_v}\right]^2\right)\left(\frac{\partial\bar{\eta}_s}{\partial\bar{p}}\frac{\partial\bar{\theta}_s}{\partial\bar{q}}-\frac{\partial\bar{\eta}_s}{\partial\bar{q}}\frac{\partial\bar{\theta}_s}{\partial\bar{p}}\right)\Bigg\{2\left[\frac{\ell_c}{r_v}\right]\left(\bar{\rho}_v\bar{v}_v\bar{\omega}_v-\left[\frac{\rho_\ell u_\ell}{\rho_v u_v}\right]^2\left[\frac{\rho_v}{\rho_\ell}\right]\left(\frac{1}{\epsilon_o\left(\left[\frac{r_w}{r_v}\right]^2-1\right)}\right)\bar{v}_\ell\bar{\omega}_\ell\right)+\\
&+\left[\frac{\mu_v}{\rho_v r_v u_v}\right]\left[\frac{r_v}{r_c}\right]\left(\overline{T_v}\right)_{z\theta}-\left[\frac{\rho_\ell u_\ell}{\rho_v u_v}\right]^2\left[\frac{\rho_v}{\rho_\ell}\right]\left[\frac{\mu_\ell}{\rho_\ell r_c u_\ell}\right]\left(\overline{T_\ell}\right)_{z\theta}\Bigg\} \;+\\
&+\left[\frac{\rho_\ell u_\ell}{\rho_v u_v}\right]^2\left[\frac{\rho_v}{\rho_\ell}\right]^2\left[\frac{\sigma}{\rho_\ell u_\ell^2 r_c}\right]\bar{a}^{1/2}\;\overline{(\nabla_s\sigma)_\theta} \;=\; 0\;,
\end{aligned}
$$

equation of motion in axial direction

$$\left(1+\left[\frac{r_c}{r_v}\right]\bar{\eta}_s\right)\left(\frac{\partial\bar{\theta}_s}{\partial\bar{p}}\frac{\partial\bar{\zeta}_s}{\partial\bar{q}}-\frac{\partial\bar{\theta}_s}{\partial\bar{q}}\frac{\partial\bar{\zeta}_s}{\partial\bar{p}}\right)\left\{\bar{\rho}_v\bar{u}_v\bar{w}_v-\left[\frac{\rho_\ell u_\ell}{\rho_v u_v}\right]^2\left[\frac{\rho_v}{\rho_\ell}\right]\left(\frac{1}{\epsilon_0\left(\left[\frac{r_w}{r_v}\right]-1\right)}\right)\bar{\rho}_\ell\bar{u}_\ell\bar{w}_\ell+\right. \tag{A.29}$$

$$\left.+\frac{1}{2}\left[\frac{r_v}{\ell_c}\right]\left[\frac{\mu_v}{\rho_v r_v u_v}\right]\left[\frac{r_v}{r_c}\right]\overline{\tau_v)}_{rz}-\left[\frac{\rho_\ell u_\ell}{\rho_v u_v}\right]^2\left[\frac{\rho_v}{\rho_\ell}\right]\left[\frac{\mu_\ell}{\rho_\ell r_c u_\ell}\right]\overline{\tau_\ell)}_{rz}\right\}+$$

$$+\left(\frac{\partial\bar{\eta}_s}{\partial\bar{q}}\frac{\partial\bar{\zeta}_s}{\partial\bar{p}}-\frac{\partial\bar{\eta}_s}{\partial\bar{p}}\frac{\partial\bar{\zeta}_s}{\partial\bar{q}}\right)\left\{\bar{\rho}_v\bar{v}_v\bar{w}_v-\left[\frac{\rho_\ell u_\ell}{\rho_v u_v}\right]^2\left[\frac{\rho_v}{\rho_v}\right]\left(\frac{1}{\epsilon_0\left(\left[\frac{r_w}{r_v}\right]^2-1\right)}\right)\bar{\rho}_\ell\bar{v}_\ell\bar{w}_\ell+\right.$$

$$\left.+\frac{1}{2}\left[\frac{r_v}{\ell_c}\right]\left[\frac{\mu_v}{\rho_v r_v u_v}\right]\left[\frac{r_v}{r_c}\right]\overline{\tau_v)}_{z\theta}-\left[\frac{\rho_\ell u_\ell}{\rho_v u_v}\right]^2\left[\frac{\rho_v}{\rho_\ell}\right]\left[\frac{\mu_\ell}{\rho_\ell u_\ell r_c}\right]\overline{\tau_\ell)}_{z\theta}\right\}+$$

$$+\left(1+\left[\frac{r_c}{r_v}\right]\bar{\eta}_s\right)\left(\frac{\partial\bar{\eta}_s}{\partial\bar{p}}\frac{\partial\bar{\theta}_s}{\partial\bar{q}}-\frac{\partial\bar{\eta}_s}{\partial\bar{q}}\frac{\partial\bar{\theta}_s}{\partial\bar{p}}\right)\left\{4\left[\frac{\ell_c}{r_v}\right]^2\left(\bar{\rho}_v\bar{w}_v^2-\left[\frac{\rho_\ell u_\ell}{\rho_v u_v}\right]^2\left[\frac{\rho_v}{\rho_\ell}\right]\left(\frac{1}{\epsilon_0\left(\left[\frac{r_w}{r_v}\right]^2-1\right)}\right)^2\bar{\rho}_\ell\bar{w}_\ell^2\right)+\right.$$

$$+\bar{P}_v-\left[\frac{\rho_\ell u_\ell}{\rho_v u_v}\right]^2\left[\frac{\rho_v}{\rho_\ell}\right]\bar{P}_\ell-2\left[\frac{\rho_\ell u_\ell}{\rho_v u_v}\right]^2\left[\frac{\rho_v}{\rho_\ell}\right]\left[\frac{\sigma}{\rho_\ell u_\ell^2 r_c}\right]\bar{\sigma}\left[\frac{r_c}{R_m}\right]+$$

$$\left.+\left[\frac{\mu_v}{\rho_v u_v r_v}\right]\left[\frac{r_v}{r_c}\right]\overline{\tau_v)}_{zz}-\left[\frac{\rho_\ell u_\ell}{\rho_v u_v}\right]^2\left[\frac{\rho_v}{\rho_\ell}\right]^2\left[\frac{\mu_\ell}{\rho_\ell u_\ell r_c}\right]\overline{\tau_\ell)}_{zz}\right\}+$$

$$+\left[\frac{\rho_\ell u_\ell}{\rho_v u_v}\right]^2\left[\frac{\rho_v}{\rho_\ell}\right]^2\left[\frac{\sigma}{\rho_\ell u_\ell^2 r_c}\right]\bar{a}^{1/2}\,\overline{(\nabla_s\sigma)}_z=0\,,$$

equation of energy, with substitution of equation of continuity

$$\left(1+\left[\frac{r_c}{r_v}\right]^2\bar{\eta}_s\right)\left(\frac{\partial\bar{\theta}_s}{\partial\bar{p}}\frac{\partial\bar{\xi}_s}{\partial\bar{q}}-\frac{\partial\bar{\theta}_s}{\partial\bar{q}}\frac{\partial\bar{\xi}_s}{\partial\bar{p}}\right)\Big\{\bar{\rho}_v\bar{u}_v\Big(\left[\frac{h_{v\ell}}{u_v^2}\right]\bar{h}_{v\ell}+\frac{1}{2}\left(\bar{u}_v^2-\left[\frac{\rho_\ell u_\ell}{\rho_v u_v}\right]^2\left[\frac{\rho_v}{\rho_\ell}\right]^2\bar{u}_\ell^2\right)+ \tag{A.30}$$

$$+\frac{1}{2}\left(\bar{v}_v^2-\left[\frac{\rho_\ell u_\ell}{\rho_v u_v}\right]^2\left[\frac{\rho_v}{\rho_\ell}\right]^2\bar{v}_\ell^2\right)+\frac{1}{2}\left(4\left[\frac{\ell_c}{r_v}\right]^2\right)\left(\bar{\omega}_v^2-\left[\frac{\rho_\ell u_\ell}{\rho_v u_v}\right]^2\left[\frac{\rho_v}{\rho_\ell}\right]^2\left(\frac{1}{\epsilon_o\left(\left[\frac{r_w}{r_v}\right]^2-1\right)}\right)^2\bar{\omega}_\ell^2\right)\Big)-$$

$$-\left[\frac{\mu_v}{\rho_v r_v u_v}\right]\left[\frac{\chi_v}{\mu_v C_{p_v}}\right]\left[\frac{C_{p_v}T_c}{u_v^2}\right]\bar{X}_v\left(\frac{\partial\bar{T}}{\partial\bar{r}_s}\right)_{\bar{r}_s=\left(1+\left[\frac{r_c}{r_v}\right]\bar{\eta}_s\right)^-}+$$

$$+\left[\frac{r_c}{r_v}\right]\left[\frac{\mu_\ell}{\rho_\ell u_\ell r_c}\right]\left[\frac{\chi_\ell}{\mu_\ell C_{p_\ell}}\right]\left[\frac{C_{p_\ell}T_c}{u_\ell^2}\right]\left[\frac{\rho_\ell u_\ell}{\rho_v u_v}\right]^2\left[\frac{\rho_v}{\rho_\ell}\right]\bar{X}_\ell\left(\frac{\partial\bar{T}}{\partial\bar{r}_s}\right)_{\bar{r}_s=\left(1+\left[\frac{r_c}{r_v}\right]\bar{\eta}_s\right)^+}+$$

$$+\left(\bar{u}_v-\bar{u}_i\right)\left(\left[\frac{\mu_v}{\rho_v r_v u_v}\right]\left[\frac{r_v}{r_c}\right]\overline{T_v)}_{rr}-\left[\frac{\rho_\ell u_\ell}{\rho_v u_v}\right]^2\left[\frac{\rho_v}{\rho_\ell}\right]^2\left[\frac{\mu_\ell}{\rho_\ell u_\ell r_c}\right]\frac{\bar{\rho}_v}{\bar{\rho}_\ell}\overline{T_\ell)}_{rr}\right)+$$

$$+\left(\bar{v}_v-\bar{v}_i\right)\left(\left[\frac{\mu_v}{\rho_v r_v u_v}\right]\left[\frac{r_v}{r_c}\right]\overline{T_v)}_{r\theta}-\left[\frac{\rho_\ell u_\ell}{\rho_v u_v}\right]^2\left[\frac{\rho_v}{\rho_\ell}\right]^2\left[\frac{\mu_\ell}{\rho_\ell u_\ell r_c}\right]\frac{\bar{\rho}_v}{\bar{\rho}_\ell}\overline{T_\ell)}_{r\theta}\right)+$$

$$+\left(\bar{\omega}_v-\bar{\omega}_i\right)\left(2\left[\frac{\ell_c}{r_v}\right]\right)\left(\left[\frac{\mu_v}{\rho_v r_v u_v}\right]\left[\frac{r_v}{r_c}\right]\overline{T_v)}_{r\xi}-\left[\frac{\rho_\ell u_\ell}{\rho_v u_v}\right]^2\left[\frac{\rho_v}{\rho_\ell}\right]^2\left[\frac{\mu_\ell}{\rho_\ell u_\ell r_c}\right]\frac{\bar{\rho}_v}{\bar{\rho}_\ell}\overline{T_\ell)}_{r\xi}\right)\Big\}+$$

$$+\left(\frac{\partial\bar{\eta}_s}{\partial\bar{q}}\frac{\partial\bar{\xi}_s}{\partial\bar{p}}-\frac{\partial\bar{\eta}_s}{\partial\bar{p}}\frac{\partial\bar{\xi}_s}{\partial\bar{q}}\right)\Big\{\bar{\rho}_v\bar{v}_v\Big(\left[\frac{h_{v\ell}}{u_v^2}\right]\bar{h}_{v\ell}+\frac{1}{2}\left(\bar{u}_v^2-\left[\frac{\rho_\ell u_\ell}{\rho_v u_v}\right]^2\left[\frac{\rho_v}{\rho_\ell}\right]^2\bar{u}_\ell^2\right)+$$

$$+\frac{1}{2}\left(\bar{v}_v^2-\left[\frac{\rho_\ell u_\ell}{\rho_v u_v}\right]^2\left[\frac{\rho_v}{\rho_\ell}\right]^2\bar{v}_\ell^2\right)+\frac{1}{2}\left(4\left[\frac{\ell_c}{r_v}\right]^2\right)\left(\bar{\omega}_v^2-\left[\frac{\rho_\ell u_\ell}{\rho_v u_v}\right]^2\left[\frac{\rho_v}{\rho_\ell}\right]^2\left(\frac{1}{\epsilon_o\left(\left[\frac{r_w}{r_v}\right]^2-1\right)}\right)^2\bar{\omega}_\ell^2\right)\Big)-$$

$$-\left[\frac{\mu_v}{\rho_v r_v u_v}\right]\left[\frac{\chi_v}{\mu_v C_{p_v}}\right]\left[\frac{C_{p_v}T_c}{u_v^2}\right]\left(\frac{1}{1+\left[\frac{r_c}{r_v}\right]\bar{\eta}_s}\right)\bar{X}_v\left(\frac{\partial\bar{T}}{\partial\bar{\theta}_s}\right)_{\bar{r}_s=\left(1+\left[\frac{r_c}{r_v}\right]\bar{\eta}_s\right)^-}+$$

$$+\left[\frac{r_c}{r_v}\right]\left[\frac{\mu_\ell}{\rho_\ell u_\ell r_c}\right]\left[\frac{\chi_\ell}{\mu_\ell C_{p_\ell}}\right]\left[\frac{C_{p_\ell}T_c}{u_\ell^2}\right]\left[\frac{\rho_\ell u_\ell}{\rho_v u_v}\right]^2\left[\frac{\rho_v}{\rho_\ell}\right]\left(\frac{1}{1+\left[\frac{r_c}{r_v}\right]\bar{\eta}_s}\right)\bar{X}_\ell\left(\frac{\partial\bar{T}}{\partial\bar{\theta}_s}\right)_{\bar{r}_s=\left(1+\left[\frac{r_c}{r_v}\right]\bar{\eta}_s\right)^+}+$$

$$+\left(\bar{u}_v-\bar{u}_i\right)\left(\left[\frac{\mu_v}{\rho_v u_v r_v}\right]\left[\frac{r_v}{r_c}\right]\overline{T_v)}_{r\theta}-\left[\frac{\rho_\ell u_\ell}{\rho_v u_v}\right]^2\left[\frac{\rho_v}{\rho_\ell}\right]^2\left[\frac{\mu_\ell}{\rho_\ell u_\ell r_c}\right]\frac{\bar{\rho}_v}{\bar{\rho}_\ell}\overline{T_\ell)}_{r\theta}\right)+$$

$$+\left(\bar{v}_v-\bar{v}_i\right)\left(\left[\frac{\mu_v}{\rho_v u_v r_v}\right]\left[\frac{r_v}{r_c}\right]\overline{T_v)}_{\theta\theta}-\left[\frac{\rho_\ell u_\ell}{\rho_v u_v}\right]^2\left[\frac{\rho_v}{\rho_\ell}\right]^2\left[\frac{\mu_\ell}{\rho_\ell u_\ell r_c}\right]\frac{\bar{\rho}_v}{\bar{\rho}_\ell}\overline{T_\ell)}_{\theta\theta}\right)+$$

$$+\left(\bar{\omega}_v-\bar{\omega}_i\right)\left(2\left[\frac{\ell_c}{r_v}\right]\right)\left(\left[\frac{\mu_v}{\rho_v u_v r_v}\right]\left[\frac{r_v}{r_c}\right]\overline{T_\ell)}_{z\theta}-\left[\frac{\rho_\ell u_\ell}{\rho_v u_v}\right]^2\left[\frac{\rho_v}{\rho_\ell}\right]^2\left[\frac{\mu_\ell}{\rho_\ell u_\ell r_c}\right]\frac{\bar{\rho}_v}{\bar{\rho}_\ell}\overline{T_\ell)}_{z\theta}\right)\Bigg\}+$$

$$+\left(1+\left[\frac{r_c}{r_v}\right]\bar{\eta}_s\right)\left(\frac{\partial\bar{\eta}_s}{\partial\bar{p}}\frac{\partial\bar{\theta}_s}{\partial\bar{q}}-\frac{\partial\bar{\eta}_s}{\partial\bar{q}}\frac{\partial\bar{\theta}_s}{\partial\bar{p}}\right)\Bigg\{\bar{\rho}_v\bar{\omega}_v\left(2\left[\frac{\ell_c}{r_v}\right]\right)\left(\left[\frac{h_{v\ell}}{u_v^2}\right]\bar{h}_{v\ell}+\frac{1}{2}\left(\bar{u}_v^2-\left[\frac{\rho_\ell u_\ell}{\rho_v u_v}\right]^2\left[\frac{\rho_v}{\rho_\ell}\right]^2\bar{u}_\ell^2\right)+\right.$$

$$\left.+\frac{1}{2}\left(\bar{v}_v^2-\left[\frac{\rho_\ell u_\ell}{\rho_v u_v}\right]^2\left[\frac{\rho_v}{\rho_\ell}\right]^2\bar{v}_\ell^2\right)+\frac{1}{2}\left(4\left[\frac{\ell_c}{r_v}\right]^2\right)\left(\bar{\omega}_v^2-\left[\frac{\rho_\ell u_\ell}{\rho_v u_v}\right]^2\left[\frac{\rho_v}{\rho_\ell}\right]^2\left(\frac{1}{\epsilon_o\left(\left[\frac{r_{co}}{r_{ci}}\right]^2-1\right)}\right)^2\bar{\omega}_\ell^2\right)\right)-$$

$$-\left[\frac{\mu_v}{\rho_v u_v r_v}\right]\left[\frac{k_v}{\mu_v c_{p_v}}\right]\left[\frac{c_{p_v}T_c}{u_v^2}\right]\bar{k}_v\left(\frac{\partial\bar{T}}{\partial\bar{\zeta}_s}\right)_{\bar{r}_s=\left(1+\left[\frac{r_c}{r_v}\right]\bar{\eta}_s\right)^-}+$$

$$+\left[\frac{r_c}{r_v}\right]\left[\frac{\mu_\ell}{\rho_\ell u_\ell r_c}\right]\left[\frac{k_\ell}{\mu_\ell c_{p_\ell}}\right]\left[\frac{c_{p_\ell}T_c}{u_\ell^2}\right]\left[\frac{\rho_\ell u_\ell}{\rho_v u_v}\right]^2\left[\frac{\rho_v}{\rho_\ell}\right]^2\bar{k}_\ell\left(\frac{\partial\bar{T}}{\partial\bar{\zeta}_s}\right)_{\bar{r}_s=\left(1+\left[\frac{r_c}{r_v}\right]\bar{\eta}_s\right)^+}+$$

$$+ \left(\bar{u}_v - \bar{u}_i\right)\left(\left[\frac{\mu_v}{\rho_v u_v r_v}\right]\left[\frac{r_v}{r_c}\right] \overline{\tau_v)}_{rz} - \left[\frac{\rho_\ell u_\ell}{\rho_v u_v}\right]^2 \left[\frac{\rho_v}{\rho_\ell}\right]^2 \left[\frac{\mu_\ell}{\rho_\ell u_\ell r_c}\right] \frac{\bar{\rho}_v}{\bar{\rho}_\ell} \overline{\tau_\ell)}_{rz}\right) +$$

$$+ \left(\bar{v}_v - \bar{v}_i\right)\left(\left[\frac{\mu_v}{\rho_v u_v r_v}\right]\left[\frac{r_v}{r_c}\right] \overline{\tau_v)}_{z\theta} - \left[\frac{\rho_\ell u_\ell}{\rho_v u_v}\right]^2 \left[\frac{\rho_v}{\rho_\ell}\right]^2 \left[\frac{\mu_\ell}{\rho_\ell u_\ell r_c}\right] \frac{\bar{\rho}_v}{\bar{\rho}_\ell} \overline{\tau_\ell)}_{z\theta}\right) +$$

$$+ \left(\bar{w}_v - \bar{w}_i\right)\left(2\left[\frac{l_c}{r_v}\right]\right)\left(\left[\frac{\mu_v}{\rho_v u_v r_v}\right]\left[\frac{r_v}{r_c}\right] \overline{\tau_v)}_{zz} - \left[\frac{\rho_\ell u_\ell}{\rho_v u_v}\right]^2 \left[\frac{\rho_v}{\rho_\ell}\right]^2 \left[\frac{\mu_\ell}{\rho_\ell u_\ell r_c}\right] \frac{\bar{\rho}_v}{\bar{\rho}_\ell} \overline{\tau_\ell)}_{zz}\right)\Bigg\} +$$

$$+ \bar{a}^{1/2} \left[\frac{\rho_\ell u_\ell}{\rho_v u_v}\right]^2 \left[\frac{\rho_v}{\rho_\ell}\right] \left[\frac{\sigma}{\rho_\ell u_\ell^2 r_c}\right] \left(\overline{\nabla_s \cdot \left(\sigma \bar{V}_i\right)}\right) = 0 .$$

C. <u>Constitutive Equations</u>

The necessary equations are

rheological equations

$$\overline{\tau_v)}_{rr} \equiv \frac{\tau_v)_{rr}}{\left(\frac{\mu_v u_v}{r_c}\right)} = -2\bar{\mu}_v \frac{\partial \bar{u}_v}{\partial \bar{r}_s} - \frac{2}{3}\bar{\lambda}_v \left\{\left(\frac{1}{1+\left[\frac{r_c}{r_v}\right]\eta_s}\right)\frac{\partial\left(\left(1+\left[\frac{r_c}{r_v}\right]\eta_s\right)\bar{u}_v\right)}{\partial \bar{r}_s} + \right. \quad \text{(A.31)}$$

$$\left. + \left(\frac{1}{1+\left[\frac{r_c}{r_v}\right]\eta_s}\right)\frac{\partial \bar{v}_v}{\partial \bar{\theta}_s} + 2\left[\frac{l_c}{r_v}\right]\frac{\partial \bar{w}_v}{\partial \bar{z}_s}\right\} ,$$

$$\overline{T_v)}_{\theta\theta} \equiv \frac{T_v)_{\theta\theta}}{\left(\frac{\mu_v u_v}{r_c}\right)} = -2\,\bar{\mu}_v\left(\left(\frac{1}{1+\left[\frac{r_c}{r_v}\right]\bar{\eta}_s}\right)\frac{\partial \bar{v}_v}{\partial \bar{\theta}_s} + \left[\frac{r_c}{r_v}\right]\left(\frac{1}{1+\left[\frac{r_c}{r_v}\right]\bar{\eta}_s}\right)\bar{u}_v\right) - \tag{A.32}$$

$$- \frac{2}{3}\,\bar{\lambda}_v\left\{\left(\frac{1}{1+\left[\frac{r_c}{r_v}\right]\bar{\eta}_s}\right)\frac{\partial\left(\left(1+\left[\frac{r_c}{r_v}\right]\bar{\eta}_s\right)\bar{u}_v\right)}{\partial \bar{r}_s} + \right.$$

$$\left. + \left(\frac{1}{1+\left[\frac{r_c}{r_v}\right]\bar{\eta}_s}\right)\frac{\partial \bar{v}_v}{\partial \bar{\theta}_s} + 2\left[\frac{l_c}{r_v}\right]\frac{\partial \bar{w}_v}{\partial \bar{z}_s}\right\} ,$$

$$\overline{T_v)}_{zz} \equiv \frac{T_v)_{zz}}{\left(\frac{\mu_v u_v}{r_c}\right)} = -2\,\bar{\mu}_v\left(2\left[\frac{l_c}{r_v}\right]\right)\frac{\partial \bar{w}_v}{\partial \bar{z}_s} - \frac{2}{3}\,\bar{\lambda}_v * \tag{A.33}$$

$$\left. + \left(\frac{1}{1+\left[\frac{r_c}{r_v}\right]}\right)\frac{\partial \bar{v}_v}{\partial \bar{\theta}_s} + 2\left[\frac{l_c}{r_v}\right]\frac{\partial \bar{w}_v}{\partial \bar{z}_s}\right\} ,$$

$$\overline{T_v)}_{r\theta} \equiv \frac{T_v)_{r\theta}}{\left(\frac{\mu_v u_v}{r_c}\right)} = -\bar{\mu}_v\left\{\left(1+\left[\frac{r_c}{r_v}\right]\bar{\eta}_s\right)\frac{\partial\left(\frac{\bar{v}_v}{\left(1+\left[\frac{r_c}{r_v}\right]\bar{\eta}_s\right)}\right)}{\partial \bar{r}_s} + \right. \tag{A.34}$$

$$\left. + \left(\frac{1}{1+\left[\frac{r_c}{r_v}\right]\bar{\eta}_s}\right)\frac{\partial \bar{u}_v}{\partial \bar{\theta}_s}\right\} ,$$

$$\overline{T_v)}_{\theta z} \equiv \frac{T_v)_{\theta z}}{\left(\frac{\mu_v u_v}{r_c}\right)} = -\bar{\mu}_v\left\{\frac{\partial \bar{v}_v}{\partial \bar{z}_s} + \left(\frac{1}{1+\left[\frac{r_c}{r_v}\right]\bar{\eta}_s}\right)2\left[\frac{l_c}{r_v}\right]\frac{\partial \bar{w}_v}{\partial \bar{\theta}_s}\right\} , \tag{A.35}$$

$$\overline{T_v)}_{rz} \equiv \frac{T_v)_{rz}}{\left(\frac{\mu_v u_v}{r_c}\right)} = -\bar{\mu}_v\left\{2\left[\frac{l_c}{r_v}\right]\frac{\partial \bar{w}_v}{\partial \bar{r}_s} + \frac{\partial \bar{u}_v}{\partial \bar{z}_s}\right\} , \tag{A.36}$$

$$\overline{\tau_\ell)}_{rr} \equiv \frac{\tau_\ell)_{rr}}{\left(\frac{\mu_\ell u_\ell}{r_c}\right)} = -2\,\bar{\mu}_\ell \frac{\partial \bar{u}_\ell}{\partial \bar{r}_s} \quad , \tag{A.37}$$

$$\overline{\tau_\ell)}_{\theta\theta} \equiv \frac{\tau_\ell)_{\theta\theta}}{\left(\frac{\mu_\ell u_\ell}{r_c}\right)} = -2\,\bar{\mu}_\ell \left\{ \left(\frac{1}{1+\left[\frac{r_c}{r_v}\right]\bar{\eta}_s}\right) \frac{\partial \bar{v}_\ell}{\partial \bar{\theta}_s} + \left[\frac{r_c}{r_v}\right]\left(\frac{1}{1+\left[\frac{r_c}{r_v}\right]\bar{\eta}_s}\right)\bar{u}_\ell \right\} \quad , \tag{A.38}$$

$$\overline{\tau_\ell)}_{zz} \equiv \frac{\tau_\ell)_{zz}}{\left(\frac{\mu_\ell u_\ell}{r_c}\right)} = -2\,\bar{\mu}_\ell \left\{ \frac{2}{\epsilon_o}\left[\frac{\ell_c}{r_v}\right]\left(\frac{1}{\left[\frac{r_w}{r_v}\right]^2-1}\right) \frac{\partial \bar{w}_\ell}{\partial \bar{z}_s} \right\} \quad , \tag{A.39}$$

$$\overline{\tau_\ell)}_{r\theta} \equiv \frac{\tau_\ell)_{r\theta}}{\left(\frac{\mu_\ell u_\ell}{r_c}\right)} = -\bar{\mu}_\ell \left\{ \left(1+\left[\frac{r_c}{r_v}\right]\bar{\eta}_s\right) \frac{\partial\left(\frac{\bar{v}_\ell}{1+\left[\frac{r_c}{r_v}\right]\bar{\eta}_s}\right)}{\partial \bar{r}_s} + \left(\frac{1}{1+\left[\frac{r_c}{r_v}\right]\bar{\eta}_s}\right)\frac{\partial \bar{u}_\ell}{\partial \bar{\theta}_s} \right\} , \tag{A.40}$$

$$\overline{\tau_\ell)}_{\theta z} \equiv \frac{\tau_\ell)_{\theta z}}{\left(\frac{\mu_\ell u_\ell}{r_c}\right)} = -\bar{\mu}_\ell \left\{ \left(\frac{2}{1+\left[\frac{r_c}{r_v}\right]\bar{\eta}_s}\right)\left[\frac{\ell_c}{r_v}\right]\frac{1}{\epsilon_o}\left(\frac{1}{\left[\frac{r_w}{r_v}\right]^2-1}\right)\frac{\partial \bar{w}_\ell}{\partial \bar{\theta}_s} + \frac{\partial \bar{v}_\ell}{\partial \bar{z}_s} \right\} , \text{ and} \tag{A.41}$$

$$\overline{\tau_\ell)}_{rz} \equiv \frac{\overline{\tau_\ell)}_{rz}}{\left(\frac{\mu_\ell u_\ell}{r_c}\right)} = -\bar{\mu}_\ell \left\{ \left(\frac{2}{\epsilon_o\left(\left[\frac{r_w}{r_v}\right]^2-1\right)}\right)\left[\frac{\ell_c}{r_v}\right] \frac{\partial \bar{w}_\ell}{\partial \bar{r}_s} + \frac{\partial \bar{u}_\ell}{\partial \bar{z}_s} \right\} \quad , \tag{A.42}$$

equation of latent heat of vaporization

$$\bar{h}_{v\ell} = \left[\frac{C_{p_v} T_c}{h_{v\ell}}\right]\bar{h}_v - \left[\frac{C_{p_\ell} T_c}{h_{v\ell}}\right]\bar{h}_\ell \quad , \tag{A.43}$$

unit normal vectors

$$\vec{n}_2 = -\vec{n}_1 = \hat{r}\left(\bar{a}^{-1/2}\right)\left\{\left(1+\left[\frac{r_c}{r_v}\right]\bar{\eta}_s\right)\frac{\partial\bar{\theta}_s}{\partial\bar{p}}\frac{\partial\bar{\zeta}_s}{\partial\bar{q}} - \left(1+\left[\frac{r_c}{r_v}\right]\bar{\eta}_s\right)\frac{\partial\bar{\theta}_s}{\partial\bar{q}}\frac{\partial\bar{\zeta}_s}{\partial\bar{p}}\right\} + \tag{A.44}$$

$$+ \hat{\theta}\left(\bar{a}^{-1/2}\right)\left\{\frac{\partial\bar{\eta}_s}{\partial\bar{q}}\frac{\partial\bar{\zeta}_s}{\partial\bar{p}} - \frac{\partial\bar{\eta}_s}{\partial\bar{p}}\frac{\partial\bar{\zeta}_s}{\partial\bar{q}}\right\} +$$

$$+ \hat{\zeta}\left(\bar{a}^{-1/2}\right)\left\{\left(1+\left[\frac{r_c}{r_v}\right]\bar{\eta}_s\right)\frac{\partial\bar{\eta}_s}{\partial\bar{p}}\frac{\partial\bar{\theta}_s}{\partial\bar{q}} - \left(1+\left[\frac{r_c}{r_v}\right]\bar{\eta}_s\right)\frac{\partial\bar{\eta}_s}{\partial\bar{q}}\frac{\partial\bar{\theta}_s}{\partial\bar{p}}\right\},$$

where

$$\bar{a} = \left\{\left(\frac{\partial\bar{\eta}_s}{\partial\bar{p}}\right)^2 + \left(1+\left[\frac{r_c}{r_v}\right]\bar{\eta}_s\right)^2\left(\frac{\partial\bar{\theta}_s}{\partial\bar{p}}\right)^2 + \left(\frac{\partial\bar{\zeta}_s}{\partial\bar{p}}\right)^2\right\}\left\{\left(\frac{\partial\bar{\eta}_s}{\partial\bar{q}}\right)^2 + \left(1+\left[\frac{r_c}{r_v}\right]\bar{\eta}_s\right)^2 \times \right. \tag{A.45}$$

$$\left.\times\left(\frac{\partial\bar{\theta}_s}{\partial\bar{q}}\right)^2 + \left(\frac{\partial\bar{\zeta}_s}{\partial\bar{q}}\right)^2\right\} - \left\{\left(\frac{\partial\bar{\eta}_s}{\partial\bar{p}}\right)\left(\frac{\partial\bar{\eta}_s}{\partial\bar{q}}\right) + \left(1+\left[\frac{r_c}{r_v}\right]\bar{\eta}_s\right)^2\left(\frac{\partial\bar{\theta}_s}{\partial\bar{p}}\right)\left(\frac{\partial\bar{\theta}_s}{\partial\bar{q}}\right) + \left(\frac{\partial\bar{\zeta}_s}{\partial\bar{p}}\right)\left(\frac{\partial\bar{\zeta}_s}{\partial\bar{q}}\right)\right\}^2,$$

unit tangent vectors

$$\vec{t}_1 = \left\{\left(\frac{\partial\bar{\eta}_s}{\partial\bar{p}}\right)^2 + \left(1+\left[\frac{r_c}{r_v}\right]\bar{\eta}_s\right)^2\left(\frac{\partial\bar{\theta}_s}{\partial\bar{p}}\right)^2 + \left(\frac{\partial\bar{\zeta}_s}{\partial\bar{p}}\right)^2\right\}^{-1/2}\left\{\hat{r}\left(\frac{\partial\bar{\eta}_s}{\partial\bar{p}}\right) + \right. \tag{A.46}$$

$$\left. + \hat{\theta}\left(1+\left[\frac{r_c}{r_v}\right]\bar{\eta}_s\right)\left(\frac{\partial\bar{\theta}_s}{\partial\bar{p}}\right) + \hat{\zeta}\left(\frac{\partial\bar{\zeta}_s}{\partial\bar{p}_s}\right)\right\}, \text{ and}$$

$$\vec{t}_2 = \left\{\left(\frac{\partial\bar{\eta}_s}{\partial\bar{q}}\right)^2 + \left(1+\left[\frac{r_c}{r_v}\right]\bar{\eta}_s\right)^2\left(\frac{\partial\bar{\theta}_s}{\partial\bar{q}}\right)^2 + \left(\frac{\partial\bar{\zeta}_s}{\partial\bar{q}}\right)^2\right\}^{-1/2}\left\{\hat{r}\left(\frac{\partial\bar{\eta}_s}{\partial\bar{q}}\right) + \right. \tag{A.47}$$

$$\left. + \hat{\theta}\left(1+\left[\frac{r_c}{r_v}\right]\bar{\eta}_s\right)\left(\frac{\partial\bar{\theta}_s}{\partial\bar{q}}\right) + \hat{\zeta}\left(\frac{\partial\bar{\zeta}_s}{\partial\bar{q}}\right)\right\},$$

two-dimensional surface orthogonal coordinate system parameters

$$\bar{p} = \bar{p}\left(\left[\frac{r_c}{r_v}\right], \left[\frac{r_{ws}}{r_c}\right], \frac{\phi}{\phi_o}\right) \text{, and} \tag{A.48}$$

$$\bar{q} = \bar{q}\left(\left[\frac{r_c}{r_v}\right], \left[\frac{r_{ws}}{r_c}\right], \frac{\phi}{\phi_o}\right) , \tag{A.49}$$

radius of curvature (Rm)

$$\left[\frac{r_c}{R_m}\right] = \frac{1}{2}\,\bar{a}^{-3/2}\left[\left\{\left(\frac{\partial\bar{\eta}_s}{\partial\bar{q}}\right)^2 + \left(1+\left[\frac{r_c}{r_v}\right]\bar{\eta}_s\right)^2\left(\frac{\partial\bar{\theta}_s}{\partial\bar{q}}\right)^2 + \left(\frac{\partial\bar{\xi}_s}{\partial\bar{q}}\right)^2\right\}\left\{\left(1+\left[\frac{r_c}{r_v}\right]\bar{\eta}_s\right)\times\right.\right. \tag{A.50}$$

$$\times\left(\frac{\partial^2\bar{\eta}_s}{\partial\bar{p}^2}\right)\left(\frac{\partial\bar{\theta}_s}{\partial\bar{p}}\frac{\partial\bar{\xi}_s}{\partial\bar{p}} - \frac{\partial\bar{\theta}_s}{\partial\bar{q}}\frac{\partial\bar{\xi}_s}{\partial\bar{q}}\right) + \left(1+\left[\frac{r_c}{r_v}\right]\bar{\eta}_s\right)\frac{\partial\bar{\eta}_s}{\partial\bar{p}}\left(\frac{\partial\bar{\theta}_s}{\partial\bar{q}}\frac{\partial^2\bar{\xi}_s}{\partial\bar{p}^2} - \right.$$

$$\left. - \frac{\partial^2\bar{\theta}_s}{\partial\bar{p}^2}\frac{\partial\bar{\xi}_s}{\partial\bar{q}}\right) + \left(1+\left[\frac{r_c}{r_v}\right]\bar{\eta}_s\right)\frac{\partial\bar{\eta}_s}{\partial\bar{q}}\left(\frac{\partial^2\bar{\theta}_s}{\partial\bar{p}^2}\frac{\partial\bar{\xi}_s}{\partial\bar{p}} - \frac{\partial\bar{\theta}_s}{\partial\bar{p}}\frac{\partial^2\bar{\xi}_s}{\partial\bar{p}^2}\right) +$$

$$\left. + 2\left[\frac{r_c}{r_v}\right]\left(\frac{\partial\bar{\theta}_s}{\partial\bar{q}}\frac{\partial\bar{\xi}_s}{\partial\bar{q}} - \frac{\partial\bar{\theta}_s}{\partial\bar{p}}\frac{\partial\bar{\xi}_s}{\partial\bar{p}}\right)\right\} + \left\{\left(\frac{\partial\bar{\eta}_s}{\partial\bar{p}}\right)^2 + \right.$$

$$\left. + \left(1+\left[\frac{r_c}{r_v}\right]^2\bar{\eta}_s\right)^2\left(\frac{\partial\bar{\theta}_s}{\partial\bar{p}}\right)^2 + \left(\frac{\partial\bar{\xi}_s}{\partial\bar{p}}\right)^2\right\}\left\{\left(1+\left[\frac{r_c}{r_v}\right]\bar{\eta}_s\right)\frac{\partial^2\bar{\eta}_s}{\partial\bar{q}^2}\left(\frac{\partial\bar{\theta}_s}{\partial\bar{p}}\frac{\partial\bar{\xi}_s}{\partial\bar{p}} - \right.\right.$$

$$\left. - \frac{\partial\bar{\theta}_s}{\partial\bar{q}}\frac{\partial\bar{\xi}_s}{\partial\bar{q}}\right) + \left(1+\left[\frac{r_c}{r_v}\right]\bar{\eta}_s\right)\frac{\partial\bar{\eta}_s}{\partial\bar{q}}\left(\frac{\partial^2\bar{\theta}_s}{\partial\bar{q}^2}\frac{\partial\bar{\xi}_s}{\partial\bar{p}} - \frac{\partial\bar{\theta}_s}{\partial\bar{p}}\frac{\partial^2\bar{\xi}_s}{\partial\bar{q}^2}\right) +$$

$$+\left(1+\left[\frac{r_c}{r_v}\right]\bar{\eta}_s\right)\frac{\partial\bar{\eta}_s}{\partial\bar{p}}\left(\frac{\partial\bar{\theta}_s}{\partial\bar{q}}\frac{\partial^2\bar{\zeta}_s}{\partial\bar{q}^2}-\frac{\partial^2\bar{\theta}_s}{\partial\bar{q}^2}\frac{\partial\bar{\zeta}_s}{\partial\bar{q}}\right)+2\left[\frac{r_c}{r_v}\right]\times$$

$$\times\left(\frac{\partial\bar{\theta}_s}{\partial\bar{q}}\frac{\partial\bar{\zeta}_s}{\partial\bar{q}}-\frac{\partial\bar{\theta}_s}{\partial\bar{p}}\frac{\partial\bar{\zeta}_s}{\partial\bar{p}}\right)\Bigg\}+2\left\{\frac{\partial\bar{\eta}_s}{\partial\bar{p}}\frac{\partial\bar{\eta}_s}{\partial\bar{q}}+\right.$$

$$+\left(1+\left[\frac{r_c}{r_v}\right]\bar{\eta}_s\right)^2\frac{\partial\bar{\theta}_s}{\partial\bar{p}}\frac{\partial\bar{\theta}_s}{\partial\bar{q}}+\left.\frac{\partial\bar{\zeta}_s}{\partial\bar{p}}\frac{\partial\bar{\zeta}_s}{\partial\bar{q}}\right\}\left\{\left(1+\left[\frac{r_c}{r_v}\right]\bar{\eta}_s\right)\frac{\partial\bar{\eta}_s}{\partial\bar{p}}\frac{\partial\bar{\eta}_s}{\partial\bar{q}}\times\right.$$

$$\times\left(\frac{\partial\bar{\theta}_s}{\partial\bar{p}}\frac{\partial\bar{\zeta}_s}{\partial\bar{p}}-\frac{\partial\bar{\theta}_s}{\partial\bar{q}}\frac{\partial\bar{\zeta}_s}{\partial\bar{q}}\right)+\left(1+\left[\frac{r_c}{r_v}\right]\bar{\eta}_s\right)\frac{\partial\bar{\eta}_s}{\partial\bar{q}}\left(\frac{\partial^2\bar{\theta}_s}{\partial\bar{p}\,\partial\bar{q}}\frac{\partial\bar{\zeta}_s}{\partial\bar{p}}-\right.$$

$$-\left.\frac{\partial\bar{\theta}_s}{\partial\bar{p}}\frac{\partial^2\bar{\zeta}_s}{\partial\bar{p}\,\partial\bar{q}}\right)+\left(1+\left[\frac{r_c}{r_v}\right]\bar{\eta}_s\right)\frac{\partial\bar{\eta}_s}{\partial\bar{p}}\left(\frac{\partial\bar{\theta}_s}{\partial\bar{q}}\frac{\partial^2\bar{\zeta}_s}{\partial\bar{p}\,\partial\bar{q}}-\right.$$

$$-\left.\left.\left.\frac{\partial^2\bar{\theta}_s}{\partial\bar{p}\,\partial\bar{q}}\frac{\partial\bar{\zeta}_s}{\partial\bar{q}}\right)+2\left[\frac{r_c}{r_v}\right]\left(\frac{\partial\bar{\theta}_s}{\partial\bar{q}}\frac{\partial\bar{\zeta}_s}{\partial\bar{q}}-\frac{\partial\bar{\theta}_s}{\partial\bar{p}}\frac{\partial\bar{\zeta}_s}{\partial\bar{p}}\right)\right\}\right],$$

surface gradient of σ

$$\overline{\nabla_s\sigma}=\frac{\nabla_s\sigma}{\left(\frac{\sigma}{r_c}\right)}=\hat{r}\left(\bar{a}^{-1}\right)\left[\frac{\partial\bar{\sigma}}{\partial\bar{p}}\frac{\partial\bar{\eta}_s}{\partial\bar{p}}\left\{\left(\left(\frac{\partial\bar{\eta}_s}{\partial\bar{q}}\right)^2+\left(1+\left[\frac{r_c}{r_v}\right]\bar{\eta}_s\right)^2\times\right.\right.\right. \tag{A.51}$$

$$\times\left(\frac{\partial\bar{\theta}_s}{\partial\bar{q}}\right)^2+\left(\frac{\partial\bar{\zeta}_s}{\partial\bar{q}}\right)^2\right)-\left(\frac{\partial\bar{\eta}_s}{\partial\bar{p}}\frac{\partial\bar{\eta}_s}{\partial\bar{q}}+\left(1+\left[\frac{r_c}{r_v}\right]\bar{\eta}_s\right)^2\frac{\partial\bar{\theta}_s}{\partial\bar{p}}\frac{\partial\bar{\theta}_s}{\partial\bar{q}}+\right.$$

$$+\left.\left.\frac{\partial\bar{\zeta}_s}{\partial\bar{p}}\frac{\partial\bar{\zeta}_s}{\partial\bar{q}}\right)\right\}+\frac{\partial\bar{\sigma}}{\partial\bar{q}}\frac{\partial\bar{\eta}_s}{\partial\bar{q}}\left\{\left(\left(\frac{\partial\bar{\eta}_s}{\partial\bar{p}}\right)^2+\left(1+\left[\frac{r_c}{r_v}\right]\bar{\eta}_s\right)^2\left(\frac{\partial\bar{\theta}_s}{\partial\bar{p}}\right)^2+\right.\right.$$

$$+\left(\frac{\partial\bar{\zeta}_s}{\partial\bar{p}}\right)^2\Big) - \Big(\frac{\partial\bar{\eta}_s}{\partial\bar{p}}\frac{\partial\bar{\eta}_s}{\partial\bar{q}} + \left(1+\left[\frac{r_c}{r_v}\right]\bar{\eta}_s\right)^2\frac{\partial\bar{\theta}_s}{\partial\bar{p}}\frac{\partial\bar{\theta}_s}{\partial\bar{q}} +$$

$$+\frac{\partial\bar{\zeta}_s}{\partial\bar{p}}\frac{\partial\bar{\zeta}_s}{\partial\bar{q}}\Big)\Big\}\Big] + \hat{\theta}\left(\bar{a}^{-1}\right)\Big[\frac{\partial\bar{\sigma}}{\partial\bar{p}}\left(1+\left[\frac{r_c}{r_v}\right]\bar{\eta}_s\right)\frac{\partial\bar{\theta}_s}{\partial\bar{p}}\Big\{\Big(\left(\frac{\partial\bar{\eta}_s}{\partial\bar{q}}\right)^2 +$$

$$+\left(1+\left[\frac{r_c}{r_v}\right]\bar{\eta}_s\right)^2\left(\frac{\partial\bar{\theta}_s}{\partial\bar{q}}\right)^2 + \left(\frac{\partial\bar{\zeta}_s}{\partial\bar{q}}\right)^2\Big) - \Big(\frac{\partial\bar{\eta}_s}{\partial\bar{p}}\frac{\partial\bar{\eta}_s}{\partial\bar{q}} + \left(1+\left[\frac{r_c}{r_v}\right]\bar{\eta}_s\right)^2\frac{\partial\bar{\theta}_s}{\partial\bar{p}}\frac{\partial\bar{\theta}_s}{\partial\bar{q}} +$$

$$+\frac{\partial\bar{\zeta}_s}{\partial\bar{p}}\frac{\partial\bar{\zeta}_s}{\partial\bar{q}}\Big)\Big\} + \frac{\partial\bar{\sigma}}{\partial\bar{q}}\left(1+\left[\frac{r_c}{r_v}\right]\bar{\eta}_s\right)\frac{\partial\bar{\theta}_s}{\partial\bar{q}}\Big\{\Big(\left(\frac{\partial\bar{\eta}_s}{\partial\bar{p}}\right)^2 + \left(1+\left[\frac{r_c}{r_v}\right]\bar{\eta}_s\right)^2\left(\frac{\partial\bar{\theta}_s}{\partial\bar{p}}\right)^2 +$$

$$+\left(\frac{\partial\bar{\zeta}_s}{\partial\bar{p}}\right)^2\Big) - \Big(\frac{\partial\bar{\eta}_s}{\partial\bar{p}}\frac{\partial\bar{\eta}_s}{\partial\bar{q}} + \left(1+\left[\frac{r_c}{r_v}\right]\bar{\eta}_s\right)^2\frac{\partial\bar{\theta}_s}{\partial\bar{p}}\frac{\partial\bar{\theta}_s}{\partial\bar{q}} + \frac{\partial\bar{\zeta}_s}{\partial\bar{p}}\frac{\partial\bar{\zeta}_s}{\partial\bar{q}}\Big)\Big\}\Big] +$$

$$+\hat{\zeta}\left(\bar{a}^{-1}\right)\Big[\frac{\partial\bar{\sigma}}{\partial\bar{p}}\frac{\partial\bar{\zeta}_s}{\partial\bar{p}}\Big\{\Big(\left(\frac{\partial\bar{\eta}_s}{\partial\bar{q}}\right)^2 + \left(1+\left[\frac{r_c}{r_v}\right]\bar{\eta}_s\right)^2\left(\frac{\partial\bar{\theta}_s}{\partial\bar{q}}\right)^2 + \left(\frac{\partial\bar{\zeta}_s}{\partial\bar{q}}\right)^2\Big) -$$

$$-\Big(\frac{\partial\bar{\eta}_s}{\partial\bar{p}}\frac{\partial\bar{\eta}_s}{\partial\bar{q}} + \left(1+\left[\frac{r_c}{r_v}\right]\bar{\eta}_s\right)^2\frac{\partial\bar{\theta}_s}{\partial\bar{p}}\frac{\partial\bar{\theta}_s}{\partial\bar{q}} + \frac{\partial\bar{\zeta}_s}{\partial\bar{p}}\frac{\partial\bar{\zeta}_s}{\partial\bar{q}}\Big)\Big\} +$$

$$+\frac{\partial\bar{\sigma}}{\partial\bar{q}}\frac{\partial\bar{\zeta}_s}{\partial\bar{q}}\Big\{\Big(\left(\frac{\partial\bar{\eta}_s}{\partial\bar{p}}\right)^2 + \left(1+\left[\frac{r_c}{r_v}\right]\bar{\eta}_s\right)^2\left(\frac{\partial\bar{\theta}_s}{\partial\bar{p}}\right)^2 + \left(\frac{\partial\bar{\zeta}_s}{\partial\bar{p}}\right)^2\Big) - \Big(\frac{\partial\bar{\eta}_s}{\partial\bar{p}}\frac{\partial\bar{\eta}_s}{\partial\bar{q}} +$$

$$+\left(1+\left[\frac{r_c}{r_v}\right]\bar{\eta}_s\right)^2\frac{\partial\bar{\theta}_s}{\partial\bar{p}}\frac{\partial\bar{\theta}_s}{\partial\bar{q}} + \frac{\partial\bar{\zeta}_s}{\partial\bar{p}}\frac{\partial\bar{\zeta}_s}{\partial\bar{q}}\Big)\Big\}\Big] \quad , \text{ and}$$

surface divergence of $\sigma\vec{V}_i$

$$\overline{\nabla_s \cdot \sigma \vec{V}_i} = \frac{\nabla_s \cdot \sigma \vec{V}_i}{\left(\frac{\sigma u_v}{r_c}\right)} = \bar{a}^{-1/2} \frac{\partial}{\partial \bar{p}}\Bigg[\bar{a}^{1/2} \bar{\sigma} \Bigg\{ \Bigg(\left(\frac{\partial \bar{\eta}_s}{\partial \bar{p}}\right)^2 + \tag{A.52}$$

$$+ \left(1 + \left[\frac{r_c}{r_v}\right]\bar{\eta}_s\right)^2 \left(\frac{\partial \bar{\theta}_s}{\partial \bar{p}}\right)^2 + \left(\frac{\partial \bar{\xi}_s}{\partial \bar{p}}\right)^2 \Bigg) \Bigg(\frac{\partial \bar{\eta}_s}{\partial \bar{p}} \bar{u}_i + \left(1 + \left[\frac{r_c}{r_v}\right]\bar{\eta}_s\right) \frac{\partial \bar{\theta}_s}{\partial \bar{p}} \bar{v}_i +$$

$$+ 2\left[\frac{l_c}{r_v}\right] \frac{\partial \bar{\xi}_s}{\partial \bar{p}} \bar{\omega}_i \Bigg) + \Bigg(\frac{\partial \bar{\eta}_s}{\partial \bar{p}} \frac{\partial \bar{\eta}_s}{\partial \bar{q}} + \left(1 + \left[\frac{r_c}{r_v}\right]\bar{\eta}_s\right)^2 \frac{\partial \bar{\theta}_s}{\partial \bar{p}} \frac{\partial \bar{\theta}_s}{\partial \bar{q}} +$$

$$+ \frac{\partial \bar{\xi}_s}{\partial \bar{p}} \frac{\partial \bar{\xi}_s}{\partial \bar{q}} \Bigg) \Bigg(\frac{\partial \bar{\eta}_s}{\partial \bar{q}} \bar{u}_i + \left(1 + \left[\frac{r_c}{r_v}\right]\bar{\eta}_s\right) \frac{\partial \bar{\theta}_s}{\partial \bar{q}} \bar{v}_i + 2\left[\frac{l_c}{r_v}\right] \times$$

$$\times \frac{\partial \bar{\xi}_s}{\partial \bar{q}} \bar{\omega}_i \Bigg) \Bigg\} \Bigg] + \bar{a}^{-1/2} \frac{\partial}{\partial \bar{q}} \Bigg[\bar{a}^{1/2} \bar{\sigma} \Bigg\{ \Bigg(\left(\frac{\partial \bar{\eta}_s}{\partial \bar{q}}\right)^2 + \left(1 + \left[\frac{r_c}{r_v}\right]\bar{\eta}_s\right)^2 \times$$

$$\times \left(\frac{\partial \bar{\theta}_s}{\partial \bar{q}}\right)^2 + \left(\frac{\partial \bar{\xi}_s}{\partial \bar{q}}\right)^2 \Bigg) \Bigg(\frac{\partial \bar{\eta}_s}{\partial \bar{q}} \bar{u}_i + \left(1 + \left[\frac{r_c}{r_v}\right]\bar{\eta}_s\right) \frac{\partial \bar{\theta}_s}{\partial \bar{q}} \bar{v}_i +$$

$$+ 2\left[\frac{l_c}{r_v}\right] \frac{\partial \bar{\xi}_s}{\partial \bar{q}} \bar{\omega}_i \Bigg) + \Bigg(\frac{\partial \bar{\eta}_s}{\partial \bar{p}} \frac{\partial \bar{\eta}_s}{\partial \bar{q}} + \left(1 + \left[\frac{r_c}{r_v}\right]\bar{\eta}_s\right)^2 \frac{\partial \bar{\theta}_s}{\partial \bar{p}} \frac{\partial \bar{\theta}_s}{\partial \bar{q}} +$$

$$+ \frac{\partial \bar{\xi}_s}{\partial \bar{q}} \frac{\partial \bar{\xi}_s}{\partial \bar{p}} \Bigg) \Bigg(\frac{\partial \bar{\eta}_s}{\partial \bar{p}} \bar{u}_i + \left(1 + \left[\frac{r_c}{r_v}\right]\bar{\eta}_s\right) \frac{\partial \bar{\theta}_s}{\partial \bar{p}} \bar{v}_i + 2\left[\frac{l_c}{r_v}\right] \frac{\partial \bar{\xi}_s}{\partial \bar{p}} \bar{\omega}_i \Bigg) \Bigg\} \Bigg] .$$

A-4. Environmental Boundary Conditions

A. Spatial Location

The necessary equations are

radius of axial sections

$$\bar{r} = \left[\frac{r_w}{r_v}\right] , \tag{A.53}$$

radii at ends of axial sections

$$0 \leq \bar{r} < \left[\frac{r_w}{r_v}\right] , \tag{A.54}$$

angular coordinate

$$0 \leq \bar{\theta} \leq 1 \quad , \text{ and} \tag{A.55}$$

axial sections

$$0 < \bar{z} \leq \left[\frac{l_e}{l_e}\right] , \tag{A.56}$$

$$\left[\frac{l_e}{l_c}\right] < \bar{z} < \left[\frac{l_e}{l_c}\right] + \left[\frac{l_a}{l_c}\right] , \text{ and} \tag{A.57}$$

$$\left[\frac{l_e}{l_c}\right] + \left[\frac{l_a}{l_c}\right] \leq \bar{z} < \left[\frac{l_e}{l_c}\right] + \left[\frac{l_a}{l_c}\right] + 1 . \tag{A.58}$$

B. Boundary Conditions

The equations are

liquid equation of continuity for all axial sections

$$\bar{u}_\ell = 0, \tag{A.59}$$

liquid equation of continuity for ends of axial sections

$$\bar{\omega}_\ell = 0 , \tag{A.60}$$

vapor equation of continuity for ends of axial sections

$$\bar{\omega}_v = 0 , \tag{A.61}$$

liquid no slip conditions for all axial sections

$$\bar{\omega}_\ell = 0 \text{ , and} \tag{A.63}$$

$$\bar{v}_\ell = 0 , \tag{A.64}$$

vapor no slip conditions for ends of axial sections

$$\bar{u}_v = 0 \text{ , and} \tag{A.65}$$

$$\bar{v}_v = 0 , \tag{A.66}$$

equations of energy for axial sections with substitution of continuity, no slip, and constitutive equations

evaporator:

$$-\int_0^1 \int_0^{\left[\frac{\ell_e}{\ell_c}\right]} \overline{K_{eff}} \frac{\partial \bar{T}}{\partial \bar{r}} \, d\bar{z} \, d\bar{\theta} = \frac{1}{2\pi} \left[\frac{r_v}{r_w}\right] \left[\frac{\dot{Q}_e}{K_{eff} \, \ell_c T_c}\right] , \tag{A.67}$$

adiabatic:

$$\frac{\partial \bar{T}}{\partial \bar{r}} = 0 \quad , \text{ and} \tag{A.68}$$

condenser:

$$-\int_0^1 \int_{\left[\frac{l_e}{l_c}\right]+\left[\frac{l_a}{l_c}\right]}^{\left[\frac{l_e}{l_c}\right]+\left[\frac{l_a}{l_c}\right]+1} \bar{K}_{eff} \frac{\partial \bar{T}}{\partial \bar{r}} \, d\bar{z} \, d\bar{\theta} = \left[\frac{U_c r_v}{K_{eff}}\right] \int_0^1 \int_{\left[\frac{l_e}{l_c}\right]+\left[\frac{l_a}{l_c}\right]}^{\left[\frac{l_e}{l_c}\right]+\left[\frac{l_a}{l_c}\right]+1} \bar{U}_c (\bar{T}-1) \, d\bar{z} \, d\bar{\theta} \, , \text{ and} \tag{A.69}$$

equations of energy for ends of axial sections

vapor:

$$\frac{\partial \bar{T}}{\partial \bar{z}} = 0 \quad , \text{ and} \tag{A.70}$$

liquid:

$$\frac{\partial \bar{T}}{\partial \bar{z}} = 0 \quad . \tag{A.71}$$

C. <u>Constitutive Equations</u>

The necessary equation is

$$\bar{K}_{eff} = \frac{K_{eff}}{K_{eff \text{ at } T_o}} = \bar{K}_{eff} \left(\left[\frac{K_l}{K_s}\right] \frac{\bar{K}_l}{\bar{K}_s} \, , \left[\frac{r_w}{r_v}\right] , \left[\frac{r_c}{r_v}\right] , \left[\frac{r_{ws}}{r_c}\right] , n \right) . \tag{A.72}$$

APPENDIX B

VACUUM LEAK TESTING

A. Purpose

The purpose of the vacuum leak testing is to insure that only negligible amounts of room air leak into the heat pipe during operation.

B. Procedure

The procedure consists of evacuating the heat pipe over a twenty four hour period, closing the valve to the pump, and recording the Alphatron pressure over a thirty minute period.

C. Typical Results

Typical results are

date: 7/31/71

room conditions:

pressure response:

Time (minutes)	Pressure (microns Hg)
0	9.0
1	9.2
2	9.6
3	9.8
4	9.8
5	10.0
6	10.0
7	10.1
8	10.2
9	10.4
10	10.6
15	11.2
20	12.0
25	12.6
30	13.4
35	14.0

initial leak rate:

from Figure B-1

initial leak rate = 0.14 microns/minute

projected accumulated air:

for 8 hours of heat pipe testing

final pressure = 67.29 microns Hg

$= 1.3 \times 10^{-3}$ psia at 8 hours

From Reference (6), this is a negligible amount.

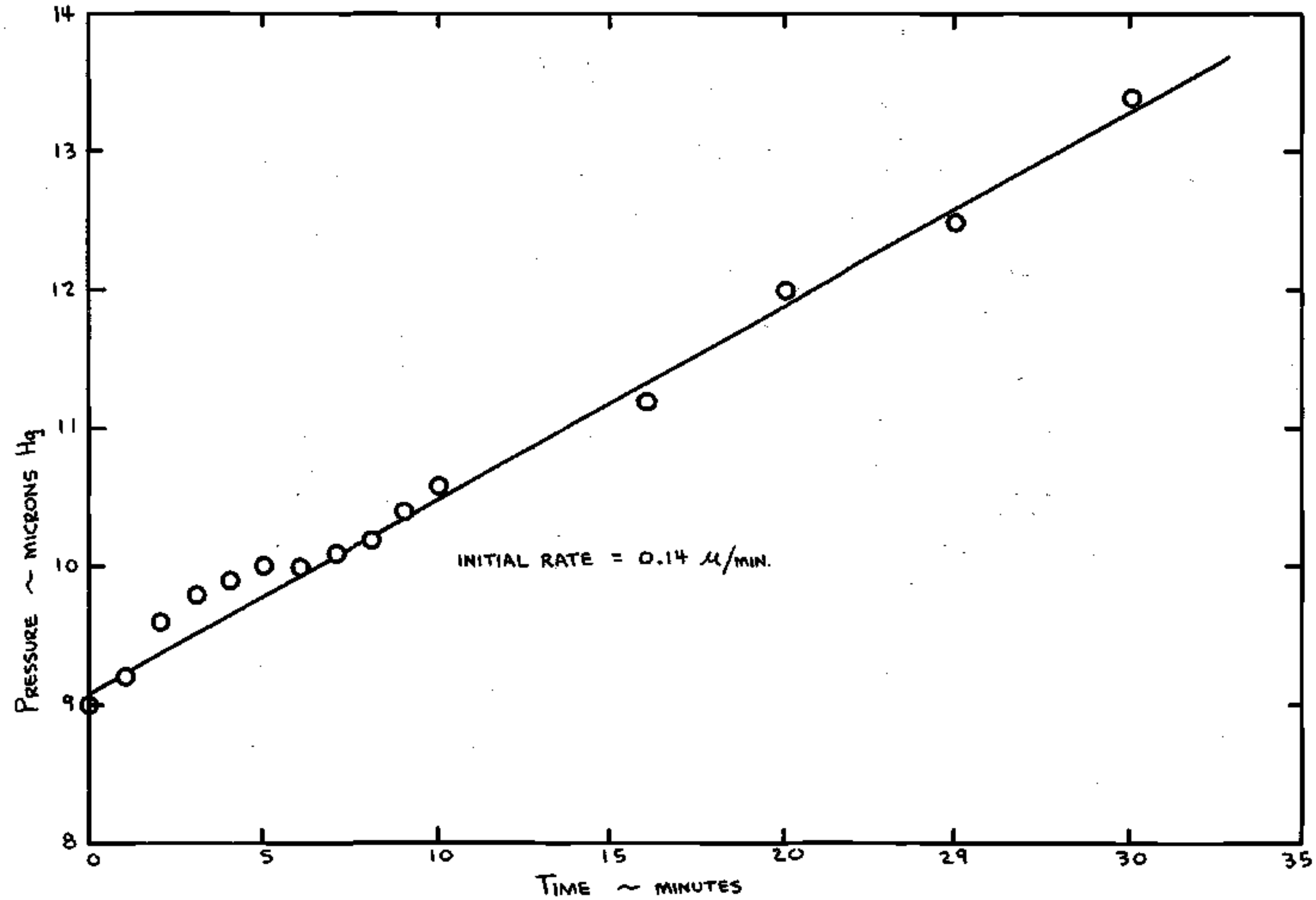

Figure B-1. Vacuum Leak Test.

APPENDIX C

EVALUATION OF FLUID INJECTION VOLUME

A. Purpose

The purpose is to estimate the volume of liquid necessary to saturate the heat pipe wick. This amount is to be injected into the heat pipe during loading of the working fluid.

B. Procedure

The procedure consists of estimating the wick porosity, evaluating the liquid volume required to fill the wick with liquid, evaluating the liquid volume required to fill the vapor space with vapor, estimating the liquid volume required to fill the pipe attachments with liquid, estimating the volume of wick thermocouple wires, and using these estimates to evaluate the injection volume.

C. Results

The results are

wick porosity (see Figure C.1):

$$\epsilon = 1 - \frac{V_{SOLID}}{V_{TOTAL}}$$

$$V_{SOLID} = 4 A_{ws} \ell_{ws} \left(\frac{2\pi \left(\frac{r_v + r_w}{2}\right) (\ell_e + \ell_a + \ell_c)}{(r_c + r_{ws})^2} \right.$$

$$V_{SOLID} = (4)(\pi)(.00225)^2(.011413)(35.2864 \times 10^4) \text{ in}^3$$

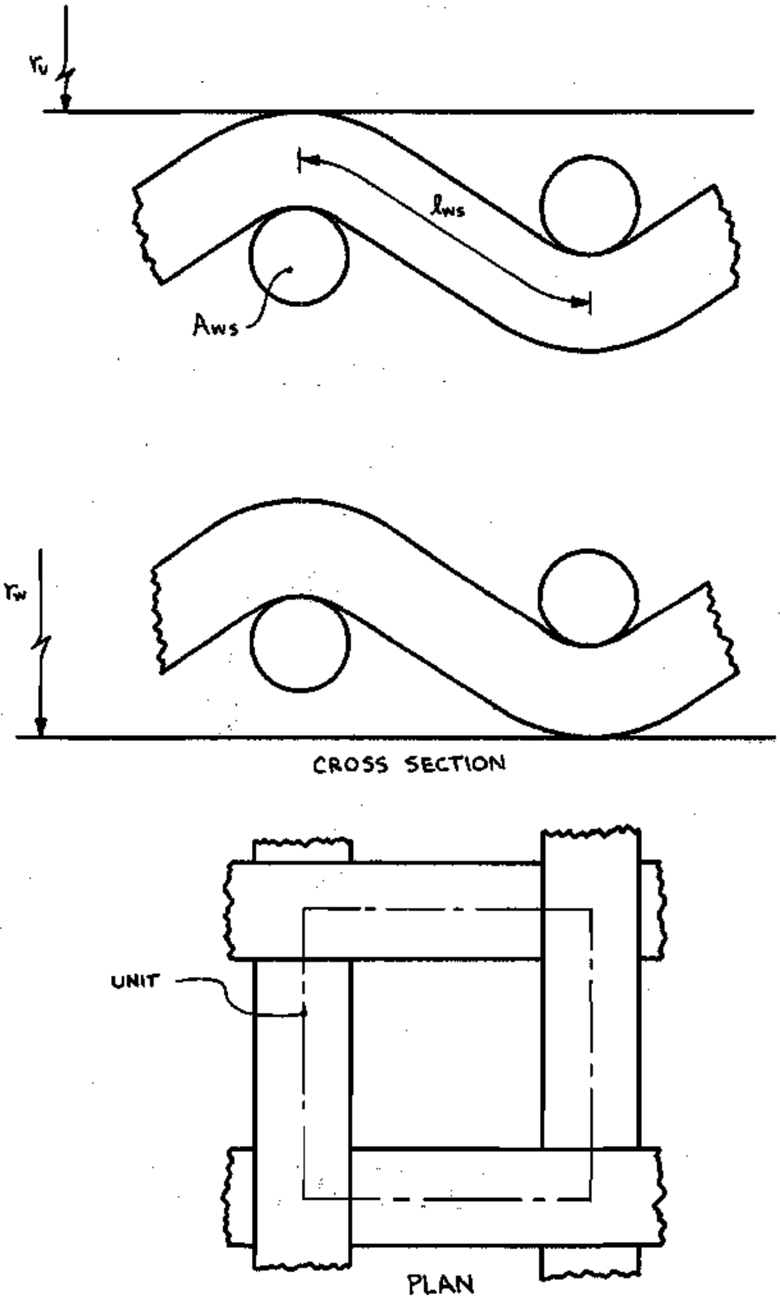

FOR A UNIT:

$$V_{SOLID} = 4\, l_{ws} A_{ws}$$
$$l_{ws}^2 \approx \left(2(r_c + r_{ws})\right)^2 + \left(2r_c\right)^2$$

Figure C-1. Schematic Diagram for Estimation of Wick Porosity.

$$V_{TOTAL} = \pi \left(l_e + l_a + l_c \right) \left(r_w^2 - r_v^2 \right)$$

$$V_{TOTAL} = (\pi)(18)\left((.326)^2 - (.298)^2 \right)$$

$$\epsilon = 1 - 0.259 = 0.741$$

wick liquid:

$$V_l = \epsilon \, V_{TOTAL}$$

$$V_l = (.741)(16.19) \text{ cc.}$$

$$V_l = 12.00 \text{ cc.}$$

liquid for vapor space vapor:

$$V_l = \frac{\rho_v}{\rho_l} V_v$$

$$V_v = \pi r_v^2 \left(l_e + l_a + l_c \right)$$

evaluating at 120°F for water,

$$V_l = \left(\frac{0.01606}{867.9} \right) (\pi) (.298)^2 (18) (2.54)^3 \text{ cc.}$$

$$V_l = 0.00656 \text{ cc}$$

liquid for filling attachments:

condenser transducer	1.6 cc
evaporator transducer	0.7
injection valve	0.5
pipe valve	0.5
$V_l =$	3.3 cc

thermocouple volume:

$$V_{SOLID} = (n) \left(\frac{\pi D^2}{4} \right) \left(l_{AVG.} \right),$$

where

n is the number of wires,

D is wire diameter, and

ℓ_{AVG} is the average length of a wire

$$V_{SOLID} = (14)\left(\frac{\pi(.006)^2}{4}\right)(18)(2.54)^3 \text{ cc.}$$

$$V_{SOLID} = 0.06 \text{ cc.}$$

injection volume:

V_ℓ = sum of liquid volumes - thermocouple solid volume

$V_\ell = 12.00 + .00656 + 3.3 - 0.06$ cc

$V_\ell = 15.2$ cc

This volume, 15.2 cc, is the nominal amount injected in all tests.

APPENDIX D

OPERATING DATA

The operating data consists of $\dot{Q}_E$, the power level delivered to the evaporator heating costs, V, the volume of cooling water collected, and Δt, the time lapse during cooling water collection. For the data indicated in Chapter IV, Table 7, the operating data are

Fluid	Test	$\dot{Q}_E$ watts	V liters	Δt minutes
water	1	48.3	0.858	2.00
	2	74.0	0.816	2.00
	3	108.0	0.822	2.00
	4	133.0	0.839	2.00
	5	54.2	0.800	2.00
	6	79.0	0.798	2.00
	7	112.0	0.800	2.00
	8	52.5	0.597	3.00
	9	79.0	0.590	3.00
methanol	10	19.3	0.850	8.50
	11	40.5	0.647	6.50
	12	13.3	0.796	4.00
	13	19.6	0.792	4.00
	14	29.0	0.782	4.00
	15	41.2	0.786	4.00
	16	19.6	0.396	8.00
	17	29.9	0.392	8.00
	18	41.8	0.390	8.00
	19	5.3	0.632	7.00
	20	28.1	0.804	8.00
	21	5.4	0.810	4.00

APPENDIX E

PRESSURE AND TEMPERATURE EMF DATA

The emf data consists of thermocouple and transducer signals recorded during heat pipe operation. Recorder data (2-46) are given in units of fractions of 5.000 mv as registered on recorder chart paper. Potentiometer data (102-115) are given in units of millivolts as measured. Tests omitted from the data listing are not indicated due to 1) incomplete data recorded during test, 2) operation at too low a power level for reasonable accurate estimation of Q_s (see Appendix I), and 3) operation at too high a cooling water flow rate for reasonable accurate estimation of $\Delta T)$cooling (see Appendix G). Thermocouples omitted from the data listing are not indicated due to 1) suspected thermocouple failure (e.g. insulation deterioration and weld detachment), and 2) considered extraneous (e.g. relay skip-thermocouples and pre-heat temperature of injection fluid).

Thermocouple numbers refer to the locations indicated in Figure 11, Chapter IV. The pressure and temperature emf data are tabulated in the following list.

Emf Data

Test	Thermocouple Number 2	3	4	5	6	7	8	9
1	0.1575	0.2725	0.2245	0.205	0.194	0.205	0.207	0.2125
2	0.1575	0.313	0.2515	0.231	0.211	0.230	0.239	0.241
3	0.158	0.3535	0.2785	0.251	0.2315	0.250	0.268	0.274
4	0.1585	0.3875	0.301	0.285	0.252	0.2805	0.301	0.307
5	0.160	0.289	0.236	0.210	0.2055	0.2225	0.219	0.226
6	0.160	0.3195	0.253	0.2315	0.229	0.2495	0.248	0.2595
7	0.1615	0.366	0.290	0.271	0.255	0.282	0.297	0.297
8	0.155	0.304	0.250	0.2205	0.216	0.234	0.230	0.240
9	0.157	0.348	0.2825	0.260	0.2565	0.271	0.275	0.280
10	0.1475	0.1715	0.204	0.194	0.194	0.169	0.199	0.209
11	0.149	0.309	0.2325	0.2175	0.222	0.218	0.2425	0.248
12	0.148	0.1555	0.190	0.160	0.1755	0.156	0.1605	0.183
13	0.148	0.167	0.1975	0.1815	0.184	0.164	0.1895	0.202
14	0.150	0.2365	0.2105	0.203	0.2005	0.177	0.220	0.226
15	0.1505	0.300	0.2225	0.2125	0.209	0.2195	0.234	0.2405
16	0.080	0.1195	0.1605	0.141	0.1475	0.115	0.1495	0.1615
17	0.0825	0.199	0.1815	0.1725	0.1685	0.138	0.185	0.1965
18	0.0825	0.278	0.200	0.171	0.180	0.1695	0.181	0.2125
19	0.0605	0.0675	0.112	0.069	0.097	0.0695	0.0695	0.100
20	0.057	0.1225	0.1305	0.1245	0.1265	0.094	0.1325	0.158
21	0.045	0.050	0.097	0.050	0.0765	0.050	0.050	0.825

Emf Data

Test	Thermocouple Number							
	10	11	12	14	16	22	25	26
1	0.272	0.272	0.272	0.273	--	0.273	--	0.215
2	0.310	0.310	0.310	0.3145	--	0.3115	--	0.230
3	0.349	0.3495	0.3495	0.354	--	0.3525	--	0.2515
4	0.3795	0.380	0.3805	0.3885	--	0.423	--	0.267
5	0.286	0.287	0.287	0.2895	--	0.287	--	0.224
6	0.318	0.318	0.318	0.320	--	0.316	--	0.240
7	0.365	0.365	0.3655	0.370	--	0.362	--	0.262
8	0.302	0.302	0.3025	0.305	--	0.307	0.254	0.2475
9	0.345	0.3435	0.340	0.350	--	0.347	0.285	0.274
10	0.269	0.269	0.269	--	0.270	0.285	0.1815	0.194
11	0.319	0.319	0.319	--	0.3225	0.413	0.230	0.2225
12	0.246	0.246	0.246	--	0.249	0.258	0.159	0.174
13	0.262	0.262	0.2625	--	0.2645	0.279	0.174	0.180
14	0.290	0.289	0.289	--	0.2925	0.313	0.209	0.193
15	0.316	0.3145	0.3145	--	0.320	0.384	0.2225	0.2105
16	0.234	0.2345	0.235	--	0.2375	0.253	0.1295	0.153
17	0.2655	0.2655	0.265	--	0.270	0.294	0.1755	0.1725
18	0.300	0.300	0.300	--	0.304	0.384	0.196	0.1975
19	0.182	0.182	0.182	--	0.1825	0.192	0.070	0.076
20	0.245	0.246	0.246	--	0.238	0.2625	0.131	0.1305
21	0.172	0.173	0.1735	--	0.173	0.183	0.0485	0.055

Emf Data

Test	Thermocouple Number							
	27	28	29	30	31	32	35	36
1	0.229	0.220	0.264	0.2475	0.2525	0.2675	0.2715	0.158
2	0.252	0.2415	0.304	0.2725	0.286	0.302	0.309	0.1575
3	0.2775	0.260	0.326	0.307	0.318	0.340	0.347	0.1585
4	0.298	0.2785	0.3595	0.330	0.345	0.370	0.380	0.160
5	0.2385	0.2315	0.283	0.250	0.268	--	--	0.173
6	0.2575	0.248	0.310	0.2695	0.2935	--	--	0.173
7	0.2845	0.2795	0.330	0.306	0.3325	--	--	0.176
8	0.255	0.2525	0.296	0.2695	0.286	--	--	0.136
9	0.285	0.280	0.320	0.306	0.322	--	--	0.138
10	0.206	0.202	0.164	0.203	0.244	0.2625	0.269	--
11	0.233	0.230	0.2155	0.239	0.235	0.311	0.320	--
12	0.1875	0.184	0.149	0.164	0.224	0.241	0.246	--
13	0.1955	0.190	0.156	0.189	0.236	0.257	0.263	--
14	0.2075	0.200	0.170	0.210	0.255	0.280	0.2875	--
15	0.2225	0.213	0.211	0.2395	0.280	0.3090	0.315	--
16	0.167	0.1615	0.104	0.146	0.208	0.230	0.2355	0.1285
17	0.1855	0.179	0.141	0.1795	0.2325	0.259	0.265	0.128
18	0.211	0.1995	0.190	0.223	0.263	0.294	0.3015	0.135
19	0.110	0.111	0.064	0.0715	0.145	0.179	0.1825	0.127
20	0.1475	0.1415	0.0925	0.138	0.1995	0.230	0.236	0.127
21	0.090	0.0905	0.046	0.052	0.130	0.167	0.171	0.1285

Emf Data

Test	Thermocouple Number 37	38	39	40	41	42	43	44
1	0.167	0.169	0.175	0.158	0.2285	0.1985	0.170	0.170
2	0.167	0.1675	0.183	0.1635	0.281	0.235	0.171	0.171
3	0.1675	0.1675	0.1875	0.1675	0.346	0.287	0.174	0.1675
4	0.169	0.167	0.195	0.173	0.413	0.328	0.190	0.1835
5	0.183	0.179	0.2095	0.170	0.314	0.215	0.1945	--
6	0.186	0.180	0.216	0.1735	0.387	0.245	0.1995	--
7	0.190	0.182	0.231	0.182	0.515	0.303	0.2125	--
8	0.150	0.1515	0.1645	0.126	0.243	0.184	0.1505	--
9	0.154	0.154	0.1725	0.133	0.3085	0.2225	0.157	--
10	0.1485	0.1495	0.153	--	0.180	--	0.146	0.151
11	0.151	0.151	0.160	--	0.237	--	0.151	0.1575
12	0.144	0.1475	0.149	--	0.1655	--	0.144	0.147
13	0.144	0.148	0.1495	--	0.1795	--	0.148	0.149
14	0.1455	0.1475	0.1525	--	0.2025	--	0.149	0.150
15	0.150	0.150	0.159	--	0.235	--	0.149	0.1525
16	0.139	0.1395	0.148	0.127	0.178	0.148	0.1455	0.1305
17	0.140	0.140	0.150	0.130	0.195	0.158	0.148	0.1365
18	0.146	0.143	0.1595	0.137	0.233	0.179	0.1505	0.143
19	0.135	0.136	0.143	0.121	0.1565	0.1355	0.143	0.1135
20	0.136	0.1365	0.1495	0.127	0.194	0.156	0.148	0.1175
21	0.1325	0.1325	0.142	0.1245	0.1585	0.140	0.141	0.103

Emf Data

Test	Thermocouple Number 45	46	47	102	103	104	106	107
1	0.1815	0.2175	0.1745	0.064	0.470	0.410	1.695	2.046
2	0.1865	0.240	0.1725	0.094	0.521	0.584	2.073	2.758
3	0.188	0.263	0.1715	0.131	0.586	0.812	2.460	3.483
4	0.191	0.2835	0.170	0.157	0.645	1.034	2.745	3.986
5	0.203	0.265	0.1825	0.076	0.496	0.445	--	--
6	0.209	0.310	0.1845	0.102	0.546	0.595	--	--
7	0.219	0.3635	0.189	0.1455	0.621	0.866	--	--
8	0.168	0.222	0.150	0.142	0.525	0.556	--	--
9	0.174	0.251	0.150	0.206	0.600	0.791	--	--
10	0.162	0.210	0.1515	0.080	1.195	3.177	--	--
11	0.169	0.239	0.151	0.170	1.532	4.407	--	--
12	0.1475	0.1985	0.150	0.025	1.086	2.755	--	--
13	0.1605	0.2075	0.150	0.039	1.171	3.080	--	--
14	0.163	0.2225	0.1485	0.065	1.326	3.617	--	--
15	0.1685	0.2385	0.1495	0.090	1.505	4.267	--	--
16	0.153	0.1925	0.149	0.178	1.029	2.555	--	--
17	0.1585	0.210	0.149	0.282	1.205	3.159	--	--
18	0.1625	0.2285	0.1495	0.405	0.414	3.909	--	--
19	0.1485	0.166	0.1495	0.039	0.786	1.741	--	--
20	0.153	0.196	0.148	0.154	1.039	2.589	--	--
21	0.155	0.206	0.149	0.020	0.751	1.640	--	--

Emf Data

Test	Thermocouple Number							
	108	109	110	111	112	113	114	115
1	2.235	2.445	2.689	1.830	2.409	2.590	2.450	1.940
2	2.960	3.650	3.595	2.389	3.567	4.028	3.124	2.429
3	3.826	5.398	4.508	2.991	4.930	6.249	6.171	3.324
4	5.080	7.241	5.660	3.400	5.966	7.753	8.045	3.936
5	--	--	--	--	--	3.189	--	--
6	--	--	--	--	--	4.864	--	--
7	--	--	--	--	--	6.989	--	--
8	--	--	--	--	--	3.092	--	--
9	--	--	--	--	--	4.020	--	--
10	--	--	--	--	--	2.188	--	--
11	--	--	--	--	--	3.746	--	--
12	--	--	--	--	--	1.829	--	--
13	--	--	--	--	--	2.186	--	--
14	--	--	--	--	--	2.820	--	--
15	--	--	--	--	--	3.699	--	--
16	--	--	--	--	--	2.025	--	--
17	--	--	--	--	--	2.740	--	--
18	--	--	--	--	--	3.670	--	--
19	--	--	--	--	--	1.210	--	--
20	--	--	--	--	--	2.514	--	--
21	--	--	--	--	--	1.179	--	--

APPENDIX F

PRESSURE TRANSDUCER DATA REDUCTION

A sample calculation is provided for transducer data reduction for Test 2 (Chapter IV, Table 7).

A. <u>Absolute Pressure Transducer</u>

emf: 0.584 mv

pressure, from calibration: <u>P = 1.66 in Hg absolute</u>

B. <u>Differential Pressure Transducer</u>

transducer emf = 0.521 mv.

room temperature (TC-47) = 71.69°F (from method of Appendix H)

barometric pressure, indicated = 29.75 in Hg

barometric pressure, corrected = 29.25 $\mp$ 0.114 (from correction curve) in Hg

= 29.36 in Hg abs.

transducer pressure differential = 26.39 in Hg (from calibration curve)

transducer absolute pressure = 29.25 - 26.39 = <u>2.86 in Hg absolute</u>

APPENDIX G

POTENTIOMETER DATA REDUCTION

Sample calculations are provided for emf data measured with the potentiometer for Test 2 (Chapter IV, Table 7).

A. Pressure Transducer EMF

See Appendix F.

B. Cooling Water Temperature Differential

emf = 0.094 mv. (from Appendix E)

$\Delta T = 4.37\ F^{\circ}$ (from Figure G-1)

Figure G-1 is based on NBS Circular S61 calibrations for Cu-Cn, where an emf of 0.215 mb ($42^{\circ}F$) corresponds to a temperature differential of $10^{\circ}F$.

C. Typical Thermocouple

TC-113: emf = 4.028 mv.

$T_{ind} = 208.90^{\circ}F$ (from NBS Cir. 561 tables)

correction factor = $2.00^{\circ}F$ (from calibration curve)

$T_{actual} = 208.90 + 2.00 = \underline{210.90^{\circ}F}$

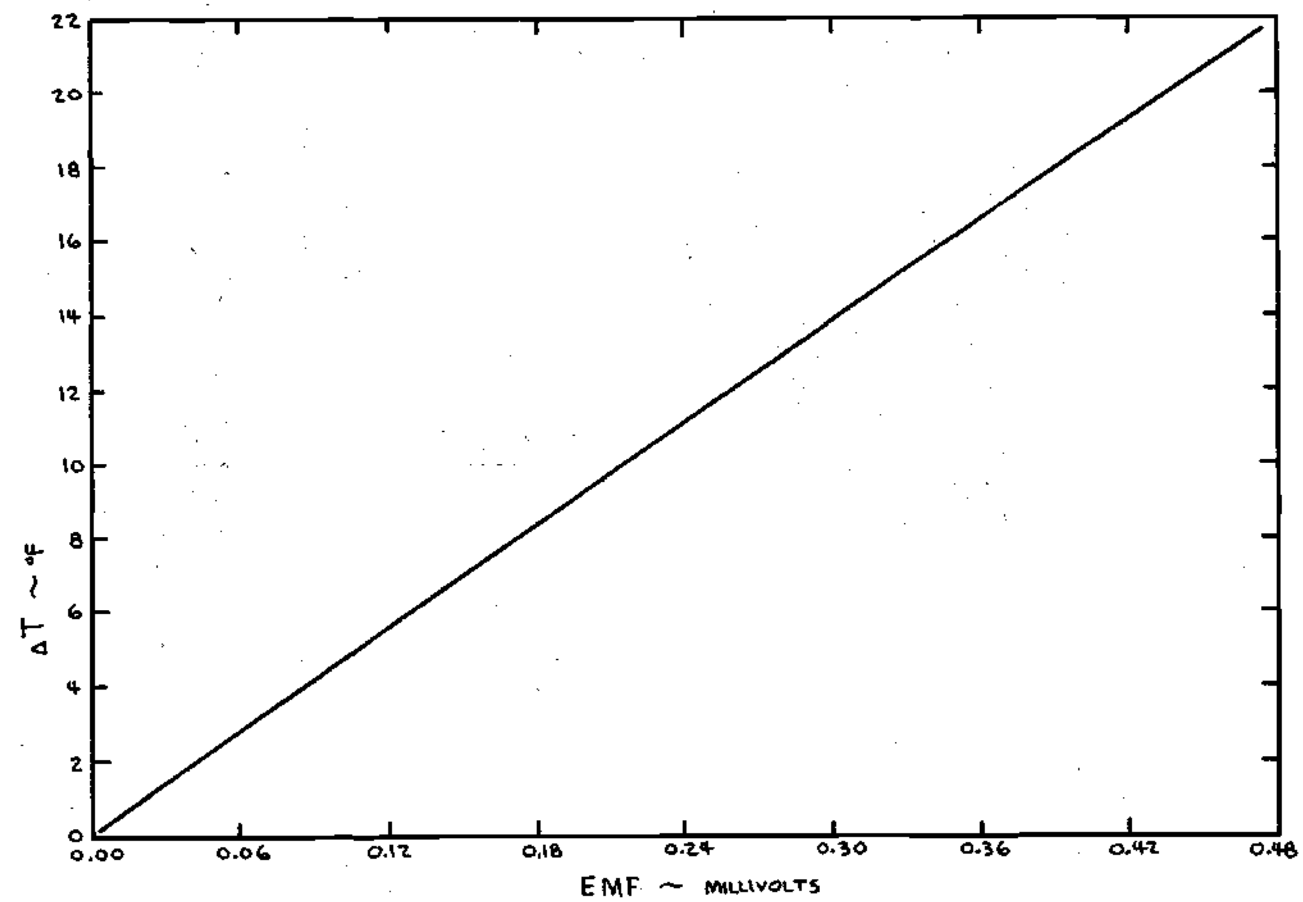

Figure G-1. Cooling Water Temperature Difference Versus EMF.

APPENDIX H

RECORDER DATA REDUCTION

A sample calculation is made for emf data measured with the recorder for Test 2 (Chapter IV, Table 7).

Typical Thermocouple:

TC-47: emf fraction = 0.1725

$T_{indicated} = 71.35^{\circ}F$ (from Figure H-1)

correction factor = + $0.34^{\circ}F$ (from calibration curve)

$T_{actual} = 71.35 + 0.34 = \underline{71.69^{\circ}F}$

Figure H-1 is based on the NBS Circular 561 calibration tables for Cu-Cn with an emf fraction of 1.000 equal to 5.000 mv.

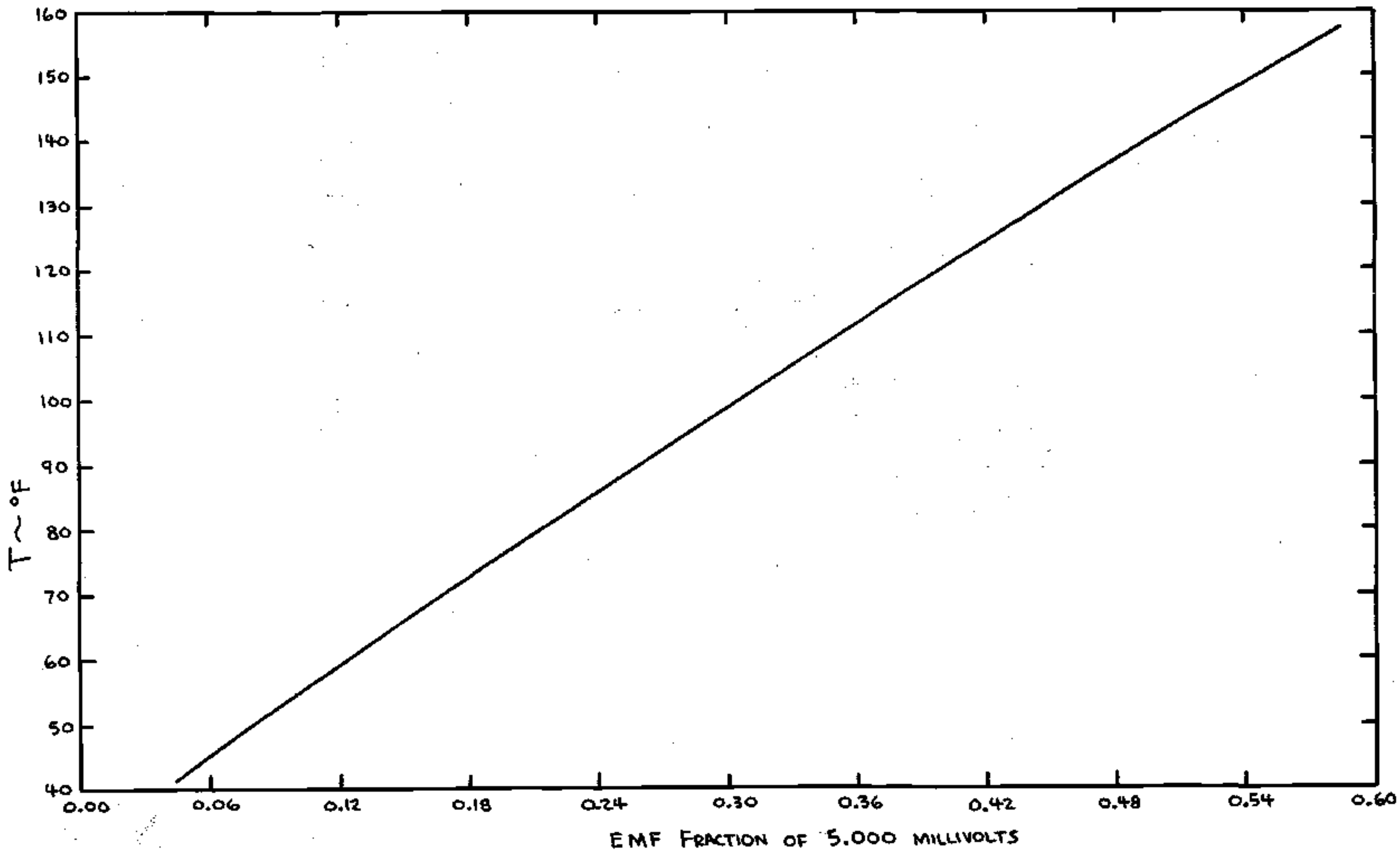

Figure H-1. Recorder EMF Fraction Versus Temperature.

APPENDIX I

HEAT TRANSFER RATE DATA REDUCTION

The heat pipe heat transfer rate data reduction consists of four parts 1) measurement of evaporator coil power, 2) evaluation of cooling water heat transfer rate, 3) estimation of heat rate to the surroundings, and 4) calculation of heat pipe heat transfer rate. A sample reduction is made for Test 2 (Chapter IV, Table 7).

1. Evaporator Coil Power (Q_E)

The coil power is that value recorded in Operating Data (Appendix D):

$$\dot{Q}_E = 74.0 \text{ WATTS} = 252.50 \text{ BTU/HR}.$$

2. Cooling Water Heat Transfer Rate (Q_C)

The rate of heat transfer to the cooling water is calculated by the expression

$$\dot{Q}_c = \left(\rho_\ell C_{p\ell}\right)\left(V\right)\left(\Delta T_c\right)\left(\frac{1}{\Delta t}\right), \tag{I.1}$$

where

V is the volume of cooling water collected,

ΔT_c is the measured temperature difference between inlet and out,

Δt is the time lapse for water collection, and

$\rho_\ell C_{p\ell}$ is the volume heat capacity evaluated at T_c.

For Test 2 from Appendix D,

$$V = 0.816 \text{ liters, and}$$

$$\Delta t = 2.00 \text{ minutes.}$$

From Appendix I, the average cooling water temperature is

$$T_c = 70.43^{\circ}F.$$

Evaluating material properties (40, 44) and using Figure I-1, gives

$$\rho_\ell C_{p_\ell} = 131.850 \ \frac{BTU}{HR\ ^{\circ}R} \ \frac{MIN.}{LIT.} \ .$$

From Appendix E, with the method of Appendix G,

$$\Delta T_c = 4.37\ ^{\circ}F$$

Substituting these values into Equation (I.1) gives

$$Q_c = (131.850)(0.816)(4.37)\left(\frac{1}{2.0}\right) \ \frac{BTU}{HR} \text{ , or}$$

$$Q_c = 235.55 \ \frac{BTU}{HR} \ .$$

3. <u>Heat Transfer to the Surroundings</u>

Circulation of ventilation air in the room surrounding the test equipment causes the convective film coefficient (h_i) to differ from values calculated from free convection models. This coefficient h_i is taken to be expressed by the relation

$$\dot{Q}_s = h_i A_s (\Delta T)_s \ , \qquad (I.2)$$

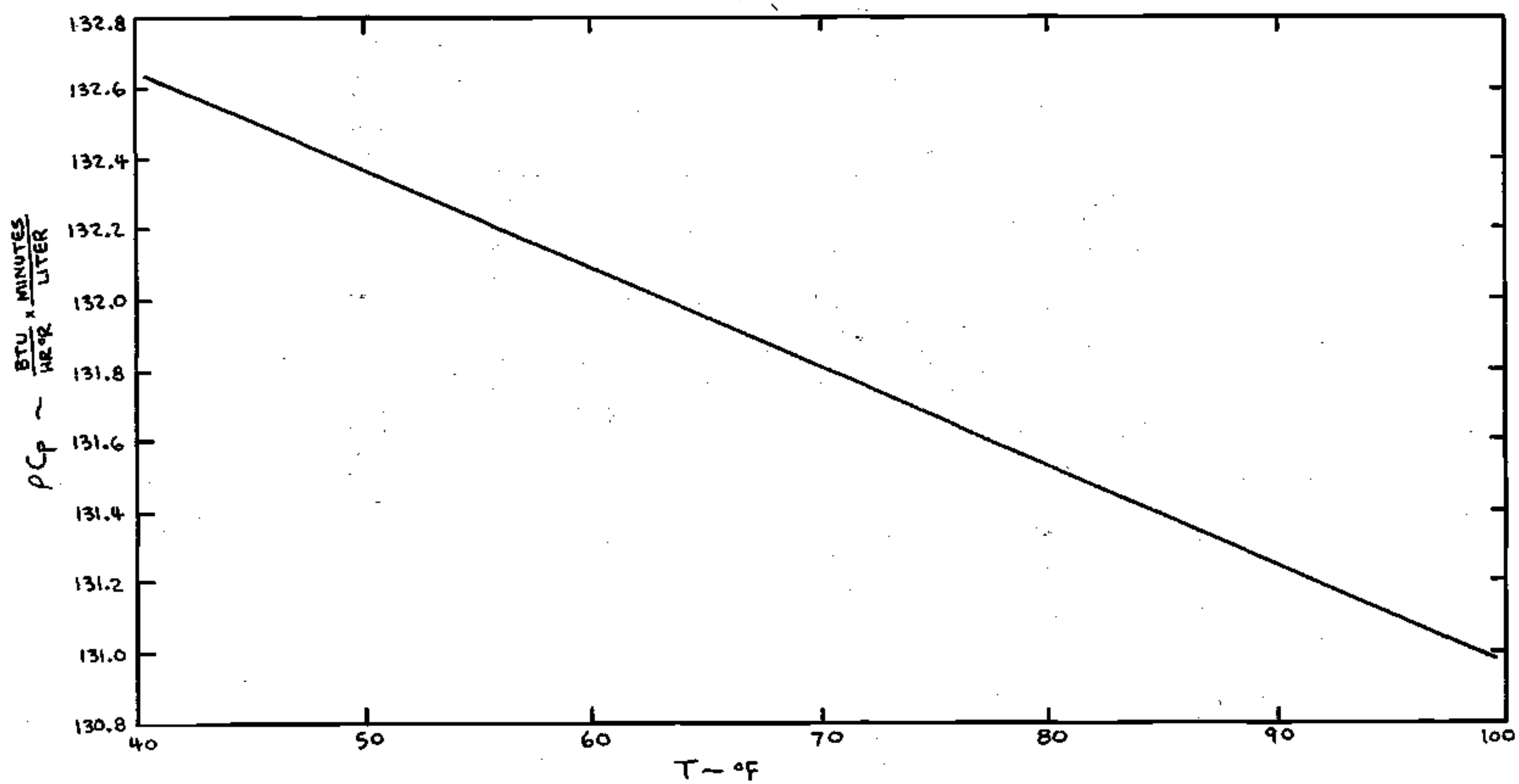

Figure I-1. Cooling Water Heat Capacity Versus Temperature.

where

$\dot{Q}_s$ is the heat transfer rate to the surroundings,

A_s is the area exposed to the surroundings, and

ΔT_s is the temperature difference between the surface in question and the surroundings.

The coefficient (h), used for final data reduction, is taken as the average value of h_i for a series of n tests, where

$$h = \frac{1}{n} \sum_{i=1}^{n} h_i \quad . \tag{I.3}$$

Considering an overall heat balance for a single test, gives

$$\dot{Q}_E = \dot{Q}_c + \sum_{j=1}^{m} h_i A_j (\Delta T_s)_j \quad , \tag{I.4}$$

where m is the number of surfaces considered. Solving Equation (I.4) for h_i gives

$$h_i = \frac{\dot{Q}_E - \dot{Q}_c}{\sum_{j=1}^{m} A_j (\Delta T_s)_j} \quad . \tag{I.5}$$

The respective areas are

$A_{C,I}$ = condenser insulation area on the outside of the aluminum foil cover,

$A_{A,I}$ = adiabatic insulation area on the outside of the foil cover,

$A_{A,CT}$ = adiabatic area contribution from the condenser transducer,

$A_{E,I}$ = evaporator insulation area on the outside of the foil cover, and

$A_{E,ET}$ = evaporator area contribution from the evaporator transducer.

The respective temperature differences are taken as the difference between the surface temperature (averaged over the respective area) and room temperature. In terms of thermocouple numbers, see Figure 11, these differences are

$$\text{for } A_{C,I},\ \Delta T_s = \tfrac{1}{3}(TC36 + TC37 + TC38) - TC47\,, \tag{I.6}$$

$$\text{for } A_{A,I},\ \Delta T_s = \tfrac{1}{2}(TC39 + TC40) - TC47\,, \tag{I.7}$$

$$\text{for } A_{A,CT},\ \Delta T_s = TC45 - TC47\,, \tag{I.8}$$

$$\text{for } A_{E,I},\ \Delta T_s = \tfrac{1}{3}(TC41 + TC42 + TC43) - TC47\,, \text{ and} \tag{I.9}$$

$$\text{for } A_{E,ET},\ \Delta T_s = TC46 - TC47\,. \tag{I.10}$$

From surface geometry, the values of the respective areas are:

$A_{C,I}$ = 267.8 in. sq.

$A_{A,I}$ = 138.2 in. sq.

$A_{A,CT}$ = 19.2 in. sq.

$A_{E,I}$ = 285.0 in. sq.

$A_{E,ET}$ = 5.3 in. sq.

Temperatures are evaluated from Appendix E, with the method of Appendix H.

Sample calculation is made for Test 2 of the series Tests 1, 2, 3, and 4 (Chapter IV, Table 7), where h_i is evaluated from Equation (I.5), and Equation (I.6) through (I.10) are used for temperature differences. The calculation table is as follows.

h_i calculation table

Test No	$\dot{Q}_E$ BTU/hr	$\dot{Q}_C$ BTU/hr	$A\ T_s)_{C,I}$ $in^2\ R^o$	$A\ T_s)_{A,I}$ $in^2\ R^o$	$A\ T_s)_{A,CT}$ $in^2\ R^o$	$A\ T_s)_{E,I}$ $in^2\ R^o$	$A\ T_s)_{E,ET}$ $in^2\ R^o$	$A_j(\ T_s)_j$ $ft^2\ R^o$	h_i $\frac{BTU}{hr\ ft^2 R^o}$
1	164.80	169.66	- 600.76	- 252.22	30.53	1578.90	- 1.27	5.244	0.9591
2	252.50	235.55	- 516.85	17.28	61.06	3612.85	80.61	22.604	0.8132
3	368.51	329.96	- 424.91	190.72	72.19	6249.10	108.92	43.028	0.9161
4	453.81	404.95	- 284.76	440.17	91.97	8897.70	134.73	64.443	0.7703

Using these values of h_i, Equation (I.5) indicates

$$h = \frac{1}{4}\left(0.9591 + 0.8132 + 0.9161 + 0.7703\right) \text{, or}$$

$$h = 0.865 \ \frac{\text{BTU}}{\text{HR FT}^2 \text{ R}^\circ} \ .$$

The respective heat transfer terms are calculated from Equation (I.2) for Test 2

$$\left.\dot{Q}_S\right)_{\text{CONDENSER}} = 0.865\left(-516.85\right)\left(\frac{1}{144}\right) = -3.10 \ \frac{\text{BTU}}{\text{HR}} ,$$

$$\left.\dot{Q}_S\right)_{\text{ADIABATIC}} = 0.865\left(17.28 + 61.06\right)\left(\frac{1}{144}\right) = 1.30 \ \frac{\text{BTU}}{\text{HR}} ,$$

$$\left.\dot{Q}_S\right)_{\text{EVAPORATOR}} = 0.865\left(3612.85 + 80.61\right)\left(\frac{1}{144}\right) = 22.18 \ \frac{\text{BTU}}{\text{HR}} .$$

The overall balance is checked using the expression

$$\dot{Q}_E \overset{?}{=} \dot{Q}_C + \sum \dot{Q}_S \ . \tag{I.11}$$

For Test 2 in BTU/hr

$$252.50 \overset{?}{=} 235.55 - 3.10 + 1.30 + 22.18 \text{ , or}$$

$$252.50 \overset{?}{=} 255.93, \quad 1.4\% \text{ off} \ .$$

4. Heat Pipe Heat Transfer Rate ($\dot{Q}_e$)

The heat pipe heat transfer rate is taken as the difference between evaporator coil power and the loss to the surroundings from the evaporator section, i.e.

$$\dot{Q}_e = \dot{Q}_E - \left.\dot{Q}_S\right)_{\text{EVAPORATOR}} . \tag{I.12}$$

For Test 2 in BTU/hr

$$\dot{Q}_e = 252.50 - 22.18 = 230.32 \ \frac{\text{BTU}}{\text{HR}}$$

5. Accuracy

The least accurate numbers used in heat rate data reduction are the film coefficients between insulation and room air. The effect of this uncertainty is exhibited in the overall heat balance of Equation (I.11). Typical data indicate the balance is in agreement to within $\pm$ 5 per cent. For a typical heat rate of 300 BTU/hr, this represents an uncertainty of $\pm$ 15 BTU/hr.

APPENDIX J

HEAT SINK TEMPERATURE DATA REDUCTION

A sample calculation is provided for the sink temperature of Test 2 (Chapter IV, Table 7). The sink temperature (T_c) is taken as the arithmetic average of inlet and exit cooling water temperatures, hence

$$T_c = T_{inlet} + 0.5 \; (\Delta T \text{ cooling water}),$$

$$T_{inlet} = 68.24^{\circ}F \text{ (from method of Appendix H)},$$

$$T = 4.37 \text{ (from method of Appendix G)},$$

$$T_c = 68.24 + 0.5(4.37) = \underline{70.43^{\circ}F}.$$

APPENDIX K

CONDENSER EXTERNAL UNIT CONDUCTANCE DATA REDUCTION

Evaluation of the unit conductance between the heat sink and the outer wick wall $(r = r_w)$ is accomplished by dividing the heat pipe heat transfer rate by the product of heat flow area and the temperature difference between wick wall and heat sink. The expression is

$$\dot{Q}_e = U_c \left(2\pi r_w L_c\right)\left(T_w - T_c\right) . \qquad \text{(K.1)}$$

Using the radial heat flow data reduction model of Appendix S, Equation (K.1) is re-expressed in terms of measured parameters as

$$U_c \left(2\pi r_w L_c\right) = \frac{1}{\dfrac{T_p - T_c}{\dot{Q}_e} + \dfrac{\ln\left(\frac{r_p}{r_w}\right)}{2\pi K_p L_c}} , \qquad \text{(K.2)}$$

where

T_p is the average measured temperature along the outer pipe shell wall,

K_p is the thermal conductivity of the pipe shell material, and

L_c is the length of heat transfer along the condenser section.

Solving Equation (K.2) for U_c gives

$$U_c = \left[\frac{r_w \ln\left(\frac{r_p}{r_w}\right)}{K_p} + \left[\frac{L_c}{\ell_c}\right]\left(2\pi r_w \ell_c\right)\left(\frac{T_p - T_c}{\dot{Q}_e}\right)\right]^{-1} . \qquad \text{(K.3)}$$

For a sample calculation for Test 2 (Chapter IV, Table 7), the parameter values are:

$\dot{Q}_e = 230.32 \ \frac{BTU}{HR}$ (from Appendix I),

$T_P = 85.57 \ °F$ (from Appendix E, with methods of Appendix H and Appendix Q),

$T_c = 70.43 \ °F$ (from Appendix J),

$K_P = 8.42 \ \frac{BTU}{HR\ FT\ °R}$ (from method of Appendix Q),

$\frac{L_c}{\ell_c} = 0.814$ (from Appendix Q),

$r_p = 0.375$ inches,

$r_w = 0.326$ inches, and

$\ell_c = 5.00$ inches.

Substitution of these values into Equation (K.3) gives the measured value of the condenser external unit conductance in BTU/hr ft^{2}R^o as

$$U_c = \left[\frac{(0.326)\ln\left(\frac{.375}{.326}\right)}{(8.42)}\left(\frac{1}{12}\right) + (0.814)(2\pi)(0.326)(5)\left(\frac{85.57-70.43}{230.32}\right)\left(\frac{1}{144}\right)\right]^{-1},$$

or

$$U_c = 234.89 \ \frac{BTU}{HR\ FT^2\ °R} .$$

APPENDIX L

ESTIMATION OF INTERFACIAL INERTIAL FORCES

The pressure change across an evaporative interface with inertial forces included is given by (14)

$$P_v - P_\ell = \frac{2\sigma}{r_m} - \frac{(\rho_v u_v)^2}{\rho_v}\left(1 - \frac{\rho_v}{\rho_\ell}\right), \text{ or} \qquad \text{(N.1)}$$

$$(P_v - P_\ell) = \frac{2\sigma}{r_m}\left[1 - \frac{r_m}{2\sigma}\frac{(\rho_v u_v)^2}{\rho_v}\left(1 - \frac{\rho_v}{\rho_\ell}\right)\right]. \qquad \text{(N.2)}$$

Using the pore radius, r_c, as an estimation of magnitude of the meniscus radius, r_m, estimating u_v from Equation (III.2), and using typical experimental data taken in this investigation, the relative magnitude of the inertial term is calculated.

For water at 100°F, $\dot{Q}_e$ = 300 BTU/hr, the estimation is

$$\rho_v u_v = \frac{\dot{Q}_e}{2\pi r_v L_e h_{v\ell}} = \frac{300}{(2\pi)(.298)(2)(1037.2)}\left(\frac{144}{3600}\right)\frac{\text{LBM}}{\text{FT}^2\text{ SEC}}$$

$$\rho_v u_v = 3.10 \times 10^{-4}\ \frac{\text{LBM}}{\text{FT}^2\text{ SEC}}$$

$$\left(\frac{r_c}{2\sigma}\right)\frac{(\rho_v u_v)^2}{\rho_v}\left(1 - \frac{\rho_v}{\rho_\ell}\right) = \frac{.00275}{(2)(4.793\times10^{-3})}\frac{(3.10\times10^{-4})^2}{(350.4)^{-1}}\left(1 - \frac{(350.4)^{-1}}{(.01613)^{-1}}\right)\left(\frac{1}{12(32.2)}\right),$$

or

$$\left(\frac{r_c}{2\sigma}\right)\frac{(\rho_v u_v)^2}{\rho_v}\left(1 - \frac{\rho_v}{\rho_\ell}\right) = 2.52\times10^{-8},$$

hence the magnitude of the inertial term is negligible compared to unity.

APPENDIX M

ESTIMATION OF VAPOR PRESSURE DROP

The relative magnitude of the vapor axial pressure drop is estimated using Cotter's (8) Equations (II.6) and (II.7), typical water data taken in this investigation, the meniscus pressure term and Equation (II.30) for mass flow rate. This gives

$$\left|\Delta P_v\right| = \left(\ell_{TOTAL}\right)\left(\frac{8\,\mu_v\,\dot{m}_v}{\pi\,\rho_v\,r_v^4}\right)\left(1 + \frac{3}{4}\gamma - \frac{11}{270}\gamma^2\right), \qquad \text{(M.1)}$$

$$\dot{m}_v = \frac{\dot{Q}_e}{h_{v\ell}}, \text{ and} \qquad \text{(M.2)}$$

$$\left|\gamma\right| = \frac{\rho_v\,u_v\,r_v}{\mu_v}.$$

For water at 100°F, $\dot{Q}_e$ = 300 BTU/hr ,

$$\rho_v u_v = \frac{\dot{Q}_e}{2\pi r_v L_c h_{v\ell}} = \frac{300\,(144)}{(2\pi)(.298)(4)(1037.2)(3600)} = 1.55\times10^{-4}\ \frac{\text{LBM}}{\text{FT}^2\text{SEC}},$$

$$\gamma = \frac{(1.55\times10^{-4})(.298)}{(64.31\times10^{-7})}\left(\frac{1}{12}\right) = 0.598,$$

$$\frac{8\,\mu_v\,\dot{Q}_e}{\pi\rho_v r_v^4 h_{v\ell}} = \frac{(8)(64.31\times10^{-7})(300)}{(\pi)(350.4)^{-1}(.298)^4(1037.2)}\ \frac{12}{(3600)(32.2)}\ \text{PSI/INCH},$$

$$\frac{8\,\mu_v\,\dot{Q}_e}{\pi\rho_v r_v^4 h_{v\ell}} = 2.18\times10^{-5}\ \text{PSI/INCH},$$

$$|\Delta P_v| = (18)(2.18\times10^{-5})(1+(.75)(.598) - (.0408)(.598)^2 = 5.36\times10^{-4} \text{ psi} \quad ,$$

$$\frac{|\Delta P_v|}{\frac{2\sigma}{r_c}} = \frac{5.36\times10^{-4}}{\frac{2(4.793\times10^{-3})}{(.00275)}}\left(\frac{12}{1}\right) = 1.93\times10^{-3} \, ,$$

hence the vapor pressure drop is negligible.

APPENDIX N

EVALUATION OF WICK FRICTION FACTOR

Darcy's law for liquid flow in porous media (27) expresses the pressure gradient as

$$\frac{dP}{dz} = K \frac{\mu}{\rho} \frac{\dot{m}}{A_{TOTAL}} , \tag{N.1}$$

where K, the friction factor, is experimentally determined. For a porous media consisting of tightly packed layers of 100 mesh screen (0.0045 inch wire diameter), Kunz, et al. (17) report the experimental value of

$$K = 6.1 \times 10^{8} \ 1/FT^{2} . \tag{N.2}$$

For a wick, as employed in this investigation, with two layers of 100 mesh screen separated by a liquid gap, the value of the wick friction factor, K_1, is different from that given by Equation (N.2). Since K is based on the area through which the liquid flows for tight wicks, K_1 is also based on the liquid flow area. From Figure N-1, the relation is described by

$$K_1 = (K) \times \frac{A_{\ell\, wick}}{A_{\ell\, wick} + A_{\ell\, GAP}} , \tag{N.3}$$

where $A_{\ell\ wick}$ is the cross sectional area of liquid flow in the wick and $A_{\ell\ gap}$ is the cross sectional area of liquid flow in the gap. Using the data from Figure N-1, Equation (N.3) reduces to

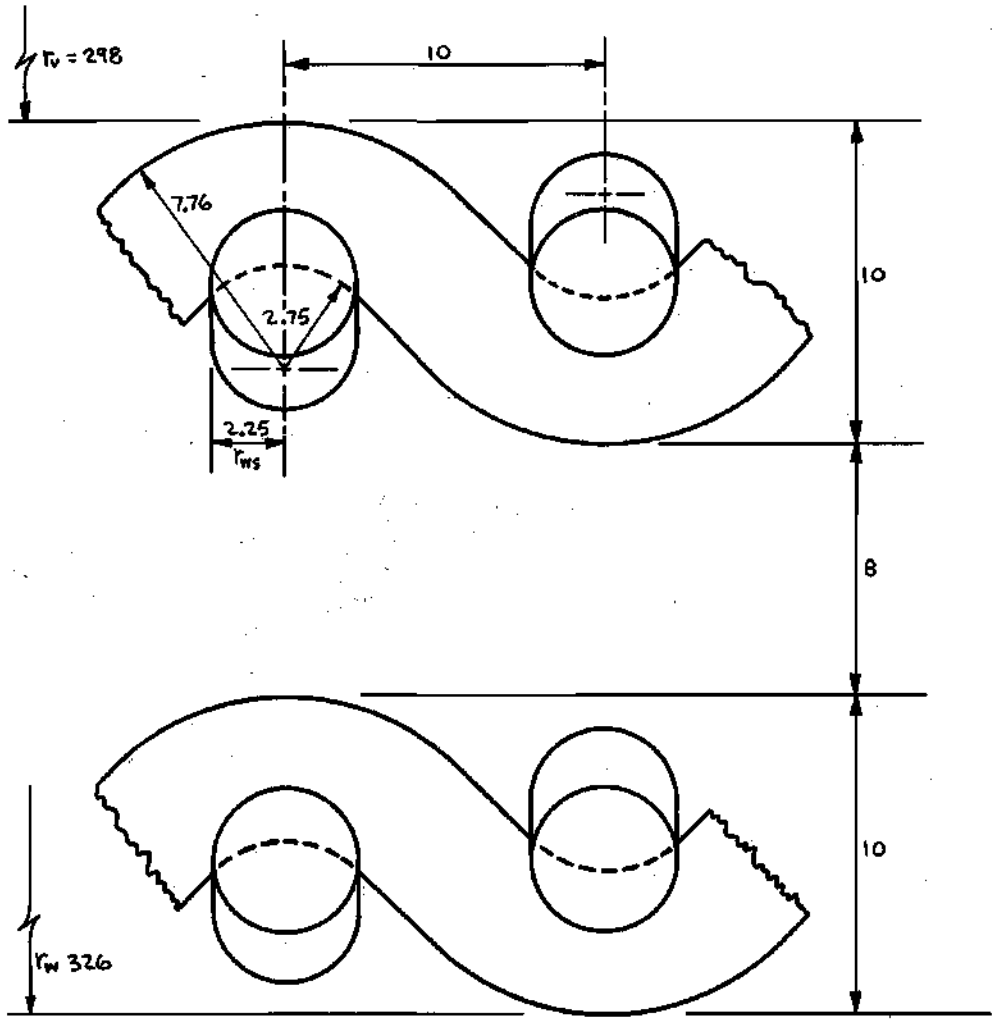

NOTE:
DIMENSIONS IN MILS (THOUSANDTHS OF AN INCH)

FROM GEOMETRY:

$$A_{\text{LIQUID, WICK}} = 59.73 \text{ MIL}^2$$

$$A_{\text{LIQUID, GAP}} = 80.00 \text{ MIL}^2$$

$$A_{\text{TOTAL}} = 280.00 \text{ MIL}^2$$

$$\epsilon = \text{AREA POROSITY} = \frac{A_{\text{LIQUID TOTAL}}}{A_{\text{TOTAL}}} = \frac{139.73}{280} = 0.499$$

Figure N-1. Wick Cross Section for Evaluation of Wick Friction Factor.

$$K_1 = \left(6.1 \times 10^{+8}\right)\left(\frac{59.73}{139.73}\right) \ 1/\mathrm{FT}^2 \quad \text{, or}$$

$$K_1 = 2.61 \times 10^{+8} \ 1/\mathrm{FT}^2 \ . \tag{N.4}$$

This is the value of wick friction factor used in this investigation.

APPENDIX O

ESTIMATION OF LIQUID INERTIA TERM

The pressure drop term due to changes in inertia of axially flowing liquid is given by

$$|\Delta P| = \int_0^{l_{TOTAL}} \left(\rho\, w \left(\frac{dw}{dz}\right)\right) dz \quad \text{, where} \tag{O.1}$$

$$w = \frac{\dot{Q}_e}{\rho_l\, \epsilon\, A_w\, h_{vl}} \left(\frac{z}{l_c}\right) \quad \text{, for} \tag{O.2}$$

$$0 \le z \le l_c \quad , \tag{O.3}$$

$$w = \frac{\dot{Q}_e}{\rho_l\, \epsilon\, A_w\, h_{vl}} (1) \quad \text{, for} \tag{O.4}$$

$$l_c < z < l_c + l_a \text{ , and} \tag{O.5}$$

$$w = \frac{\dot{Q}_e}{\rho_l\, \epsilon\, A_w\, h_{vl}} \left(\frac{l_c + l_a + l_e - z}{l_e}\right) \text{, for} \tag{O.6}$$

$$l_c + l_a \le z \le l_c + l_a + l_e \quad . \tag{O.7}$$

These velocity relations are based on the model of uniform injection and rejection of liquid along the condenser and evaporator sections respectively. Equations (O.2), (O.4), and (O.6) are simplified by

$$w(z) = w_l \; \Psi(z) \quad \text{, where} \tag{O.8}$$

$$\omega_\ell = \frac{\dot{Q}_e}{\rho_\ell \epsilon A_w h_{v\ell}} ,$$

and $\Psi(z)$ is a linear function, piece-wise continuous. Substituting Equation (0.8) into (0.1) gives

$$|\Delta P| = \rho_\ell \omega_\ell^2 \int_0^{\ell_{TOTAL}} \left(\Psi \frac{d\Psi}{dz} \right) dz . \qquad (0.9)$$

The integral in Equation (0.9) is evaluated piece wise:

for $\quad 0 \le z \le \ell_c ,$

$$\Psi(z) = \frac{z}{\ell_c} ,$$

$$\int_0^{\ell_c} \left(\frac{z}{\ell_c} \right) \left(\frac{1}{\ell_c} \right) dz = +\frac{1}{2} ,$$

for $\quad \ell_c < z < \ell_c + \ell_a ,$

$$\Psi(z) = 1 ,$$

$$\int_{\ell_c}^{\ell_c+\ell_a} (1)(0)\, dz = 0 ,$$

for $\quad \ell_c + \ell_a \le z \le \ell_c + \ell_a + \ell_e ,$

$$\Psi(z) = \frac{\ell_c + \ell_a + \ell_e - z}{\ell_e} ,$$

$$\int_{\ell_e+\ell_a}^{\ell_c+\ell_a+\ell_e} \left(\frac{\ell_c+\ell_a+\ell_e-z}{\ell_e} \right) \left(\frac{-1}{\ell_e} \right) dz = -\frac{1}{2} ,$$

hence

$$\int_0^{l_{TOTAL}} \Psi(z)\frac{d\Psi}{dz}\,dz = \frac{1}{2} + 0 - \frac{1}{2} = 0 \ , \text{ or}$$

the net change in inertia is zero. This could have been deduced from the fact that the initial and final velocities are zero, hence no net change in inertia.

Comparison is made of the relative magnitude of inertial to frictional pressure drop only over the condenser section:

$$\frac{|\Delta P|_{INERTIA}}{|\Delta P|_{FRICTION}} = \frac{\left[\left(\frac{1}{2}\right)\rho_l\,\omega_l^2\right]}{\left[K_1\frac{\mu_l}{\rho_l}\frac{\dot{Q}_e}{h_{vl}A_w}\left(\frac{1}{2}l_c\right)\right]} \ , \text{ or} \tag{0.10}$$

$$\frac{|\Delta P|_{INERTIA}}{|\Delta P|_{FRICTION}} = \frac{\dot{Q}_e}{\epsilon^2 A_w h_{vl} K_1 \mu_l l_c} \ . \tag{0.11}$$

Equation (0.11) is evaluated using the wick parameters of the investigation and conditions of water at 100°F, $\dot{Q}_e$ = 300 BTU/hr. Equation (0.11) is evaluated as

$$\frac{|\Delta P|_{INERTIA}}{|\Delta P|_{FRICTION}} = \frac{300}{(.499)^2\left(\pi(.326^2-.298^2)\right)(1037.2)\left(2.94\times10^{8}\right)\left(142\times10^{-7}\right)(5)}\times\left(\frac{1728}{(3600)(32.2)}\right),$$

$$\frac{|\Delta P|_{INERTIA}}{|\Delta P|_{FRICTION}} = 1.51\times10^{-5} \ ,$$

hence the inertia term is negligible compared to the frictional term.

APPENDIX P

ESTIMATION OF MAGNITUDE OF THERMAL RESISTANCES

From Equation (V. 8) the total thermal resistance is

$$R_{TOTAL} = R_{ew} + R_{ei} + R_v + R_{ci} + R_{cw} \ . \tag{P.1}$$

Dividing by the condenser wick term provides a nondimensional comparison

$$\frac{R_{TOTAL}}{R_{cw}} = 1 + \frac{R_{ew}}{R_{cw}} + \frac{R_{ei}}{R_{cw}} + \frac{R_v}{R_{cw}} + \frac{R_{ci}}{R_{cw}} \ . \tag{P.2}$$

The wick resistance magnitudes are estimated by the conduction model of

$$R_{cw} = \frac{\ln\left(\frac{r_w}{r_v}\right)}{2\pi X_{eff}\, l_c} \ , \text{ and} \tag{P.3}$$

$$R_{ew} = \frac{\ln\left(\frac{r_w}{r_v}\right)}{2\pi X_{eff}\, l_e} \ . \tag{P.4}$$

The vapor resistance magnitude is estimated by using the Clapeyron equation and the estimated vapor axial pressure drop

$$\left(\frac{\Delta P}{\Delta T}\right)_{SAT.} = \frac{h_{vl}}{T_o\left(\frac{1}{\rho_v} - \frac{1}{\rho_l}\right)} \ , \tag{P.5}$$

$$\Delta P = \left(\ell_{TOTAL}\right)\left(\frac{8\mu_v \dot{m}_v}{\pi \rho_v r_v^4}\right)\left(1 + \frac{3}{4}\gamma - \frac{11}{270}\gamma^2\right), \quad (P.6)$$

where

$$\gamma = \frac{\rho_v u_v r_v}{\mu_v}, \text{ and} \quad (P.7)$$

$$\dot{m}_v = \frac{\dot{Q}_e}{h_{v\ell}} = \rho_v u_v (2\pi r_v \ell_e) . \quad (P.8)$$

Substituting Equations (P.6), (P.7), and (P.8) into Equation (P.5) gives

$$R_v = \frac{\Delta T}{\dot{Q}_e} = \frac{8\mu_v T_o \ell_{TOTAL}}{\pi \rho_v^2 r_v^4 h_{v\ell}^2}\left(1 - \frac{\rho_v}{\rho_\ell}\right)\left(1 + \frac{3}{4}\gamma - \frac{11}{270}\gamma^2\right) . \quad (P.9)$$

The interfacial thermal resistances are estimating using the model theory of Wilcox and Rohsenow (37) which is an extension of the Schrage (30) theory and with an accumulation coefficient of unity. This model gives

$$R_{ci} = \frac{(\Delta T)_i}{\dot{Q}_e} = \frac{1}{2}\left(\frac{1}{2\pi r_v \ell_c}\right)\left[\frac{(2\pi R)^{1/2}\, T_o^{5/2}\, R}{P_o\, h_{v\ell}^2}\right], \quad (P.10)$$

$$R_{ei} = \frac{(\Delta T)_i}{\dot{Q}_e} = \frac{1}{2}\left(\frac{1}{2\pi r_v \ell_e}\right)\left[\frac{(2\pi R)^{1/2}\, T_o^{5/2}\, R}{P_o\, h_{v\ell}^2}\right], \quad (P.11)$$

where T_o and P_o are the saturation temperature and pressure respectively, and R is the gas constant of the vapor.

Using typical data taken in this investigation for water at 100°F, $\dot{Q}_e$ = 300 BTU/hr, the ratios of thermal resistances are estimated as

$$\frac{R_{ew}}{R_{cw}} = \frac{l_c}{l_e} = 1.49 \quad , \tag{P.12}$$

$$\frac{R_v}{R_{cw}} = \frac{16\,\mu_v T_o l_c (l_c + l_a + l_e) X_{eff}}{\ln\left(\frac{r_w}{r_v}\right) \rho_v^2 \cdot r_v^4 \, h_{vl}^2}\left(1 - \frac{\rho_v}{\rho_o}\right)\left(1 + \frac{3}{4}\gamma - \frac{11}{270}\gamma^2\right) = 1.32 \times 10^{-4} , \tag{P.13}$$

$$\frac{R_{ci}}{R_{cw}} = \frac{(2\pi)^{1/2} R^{3/2} T_o^{5/2} X_{eff}}{2 r_v \ln\left(\frac{r_w}{r_v}\right) P_o \, h_{vl}^2} = 3.23 \times 10^{-4} \quad \text{, and} \tag{P.14}$$

$$\frac{R_{ei}}{R_{cw}} = \frac{(2\pi)^{1/2} R^{3/2} T_o^{5/2} X_{eff}}{2 r_v \ln\left(\frac{r_w}{r_v}\right) P_o \, h_{vl}^2} = 3.23 \times 10^{-4} \quad . \tag{P.15}$$

Hence the wick resistances are retained and the vapor and interfacial resistances are neglected.

APPENDIX Q

EVALUATION OF CONDENSER ACTIVE LENGTH FROM MEASURED PARAMETERS

Evaluation of the measured active length of condensation (L_C) is accomplished by use of a data reduction model based on 1) radial heat conduction through the wick and pipe shell, 2) measured vapor and outer shell wall temperatures, and 3) the measured heat pipe heat transfer rate. A sample calculation is provided for Test 2 (Chapter IV, Table 7).

For radial conduction of heat from inner wick surface ($r = r_v$), through the outer wick surface ($r = r_w$), and to the outer pipe shell surface ($r = r_p$), the heat flow expression is .

$$\dot{Q}_e = \frac{T_v - T_p}{\dfrac{\ln\left(\frac{r_p}{r_w}\right)}{2\pi X_p L_c} + \dfrac{\ln\left(\frac{r_w}{r_v}\right)}{2\pi X_{eff} L_c}} \qquad \text{(Q.1)}$$

Solving for the value of the condenser active length ratio gives

$$\left[\frac{L_c}{\ell_c}\right] = \left(\frac{\dot{Q}_e}{T_o - T_p}\right)\left[\frac{\ln\left(\frac{r_p}{r_w}\right)}{2\pi X_p \ell_c} + \left[\frac{X_\ell}{X_{eff}}\right]\frac{\ln\left(\frac{r_w}{r_v}\right)}{2\pi X_\ell \ell_c}\right], \qquad \text{(Q.2)}$$

where $\dot{Q}_e$ is the measured heat pipe heat transfer rate,

T_o is the measured heat pipe operating temperature (equal to the vapor and adiabatic wall temperature),

T_p is the average measured temperature along the condenser at the outer pipe shell wall ($r = r_p$); in terms of thermocouple numbers:

$$T_p = \frac{1}{12}\Big[2(TC\text{-}4) + 3(TC\text{-}5) + 1(TC\text{-}6) + \qquad (Q.3)$$

$$+ \quad 3(TC\text{-}26) + 2(TC\text{-}27) + 1(TC\text{-}28)\Big],$$

χ_p is the thermal conductivity of the pipe shell material, evaluated at T_o,

χ_ℓ is the thermal conductivity of the liquid working fluid evaluated at T_o, and

χ_ℓ/χ_{eff} is the thermal conductivity ratio of liquid to effective evaluated at T_o and using Equations (V.19) and (V.20), see Appendix R.

For Test 2, the parameter values are:

$\dot{Q}_e$ = 230.32 BTU/hr (from Appendix I),

T_o = TC-14 = 102.37°F (from Appendix E, with method of Appendix H),

T_p = 85.57°F (from Equation (Q.3), using data from Appendix E, with method of Appendix H),

χ_p = 8.42 BTU/hr ft R° (for 304 stainless steel using data of Reference (16)),

χ_ℓ = 0.3621 BTU/hr ft R° (for water using data of Reference (40), methanol (43)),

$\frac{\chi_\ell}{\chi_{eff}}$ = 0.5593 (from Equations (V.19) and (V.20), with the wick solid material as 316 stainless steel using data of Reference (16)),

r_p = 0.375 inches,

r_w = 0.326 inches,

r_v = 0.298 inches, and

$\ell_c \quad = 5.00$ inches.

Substitution of these values into Equation (Q.2) gives the value of the condenser active length ratio as

$$\frac{L_c}{\ell_c} = \frac{230.32}{(102.37-85.57)}\left[\frac{\ln\left(\frac{.375}{.326}\right)(12)}{2\pi(8.42)(5)} + (0.5593)\frac{\ln\left(\frac{.326}{.298}\right)(12)}{2\pi(0.3621)(5)}\right], \text{ or}$$

$$\frac{L_c}{\ell_c} = 0.814 \quad .$$

APPENDIX R

DERIVATION OF EQUATION FOR EFFECTIVE WICK THERMAL CONDUCTIVITY

The effective thermal conductivity of the wick in this investigation depends on the wick geometry and the conductivities of the liquid and wick-solid materials. An expression for the effective conductivity is derived in two steps 1) the effective conductivity for a single layer of screen, K_w, is modeled by combined series and parallel conduction, and 2) the overall wick effective conductivity, K_{eff}, is modeled by series conduction through two layers of screen separated by a liquid gap.

A. Thermal Conductivity of a Single Layer of Screen (K_w)

The wick is modeled by considering a typical section of screen, see Figure R-1. Each section is composed of liquid and/or solid. The conduction area for each section is different, but each total length (screen thickness) of conduction is the same. Defining the thermal resistance as

$$R = \frac{\text{length of conduction}}{(\text{thermal conductivity})(\text{conduction area})} \tag{R.1}$$

and using the geometry indicated in Figure R-1, the respective resistances are

$$R_1 = \frac{4\, r_{ws}}{K_s\, r_{ws}^2} + \frac{2r_c - 2r_{ws}}{K_\ell\, r_{ws}^2} \quad , \tag{R.2}$$

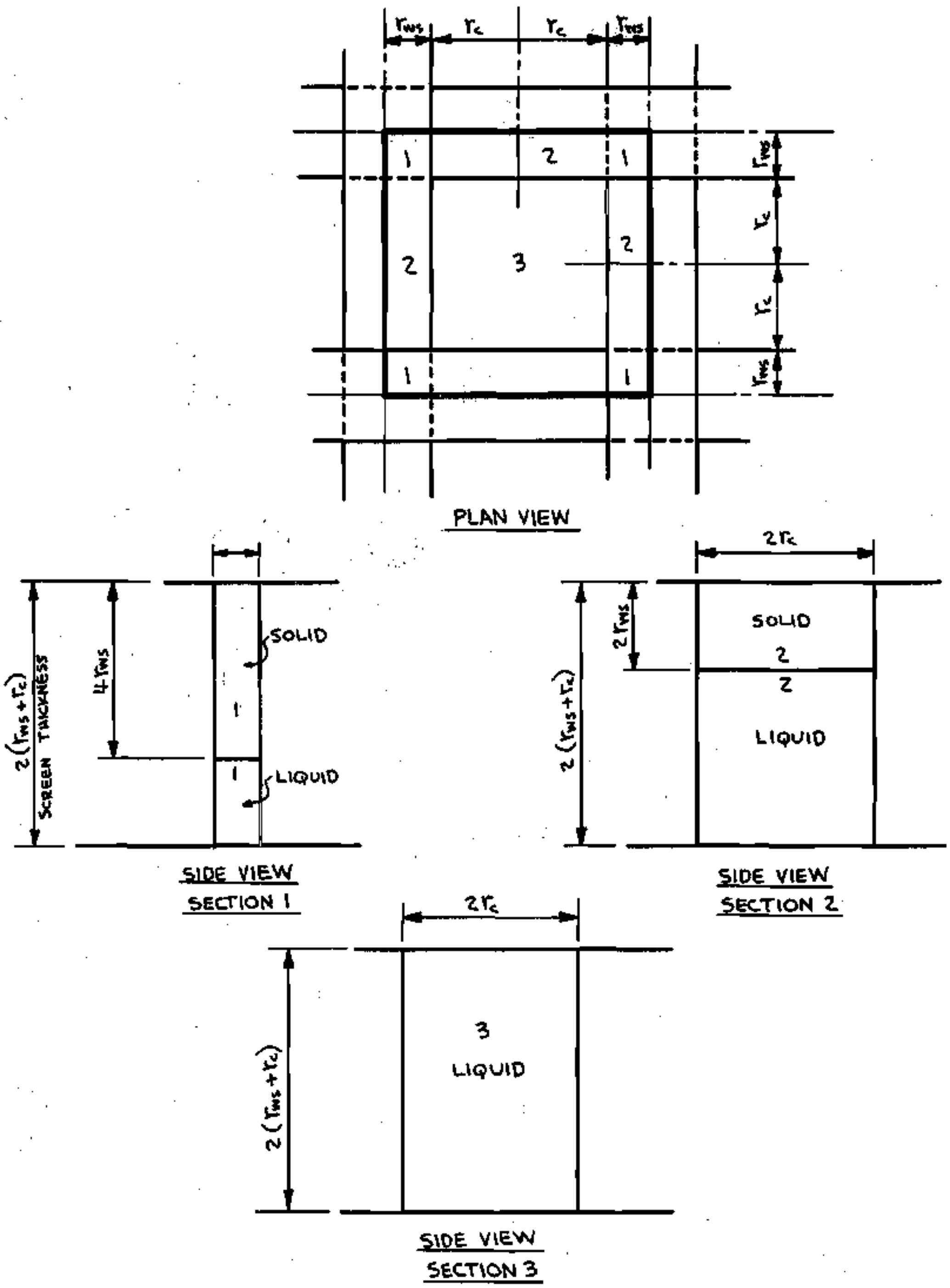

Figure R-1. Geometry Model for Conduction Through One Layer of Screen.

$$R_2 = \frac{2r_{ws}}{\chi_s 2r_{ws}r_c} + \frac{2r_c}{\chi_\ell 2r_{ws}r_c} \quad \text{, and} \tag{R.3}$$

$$R_3 = \frac{2(r_{ws}+r_c)}{\chi_\ell 4r_c^2} \quad . \tag{R.4}$$

Combining these resistances in parallel gives

$$\frac{1}{R_W} = \frac{4}{R_1} + \frac{4}{R_2} + \frac{1}{R_3} \quad , \tag{R.5}$$

where R_W is the thermal resistance of one layer of screen given by

$$R_w = \frac{2r_{ws} + 2r_c}{\chi_w\left(2(r_{ws}+r_c)\right)^2} \quad . \tag{R.6}$$

Combining Equations (R.2) through (R.6), and expressing in nondimensional form gives

$$\frac{\chi_w}{\chi_\ell} = \frac{1}{\left(\frac{r_c}{r_{ws}}+1\right)\left(2\frac{\chi_\ell}{\chi_s}+\left(\frac{r_c}{r_{ws}}-1\right)\right)} + \frac{2}{\left(\frac{r_c}{r_{ws}}+1\right)\left(\frac{\chi_\ell}{\chi_s}\frac{r_{ws}}{r_c}+1\right)} + \frac{1}{\left(\frac{r_{ws}}{r_c}+1\right)^2} \quad . \tag{R.7}$$

B. <u>Effective Wick Thermal Conductivity</u>

The two layers of screen and their separating liquid gap, see Figure R-2, form a series of concentric cylinders. Defining the thermal resistance as

$$R = \frac{\ln\left(\frac{\text{outer radius}}{\text{inner radius}}\right)}{(2\pi)(\text{thermal conductivity})(\text{axial length})} \quad , \tag{R.8}$$

the respective resistances of each annulus is

$$R_A = \frac{\ln\left(\frac{r_w}{r_w-(2)(r_{ws}+r_c)}\right)}{2\pi\chi_w \ell} \quad , \tag{R.9}$$

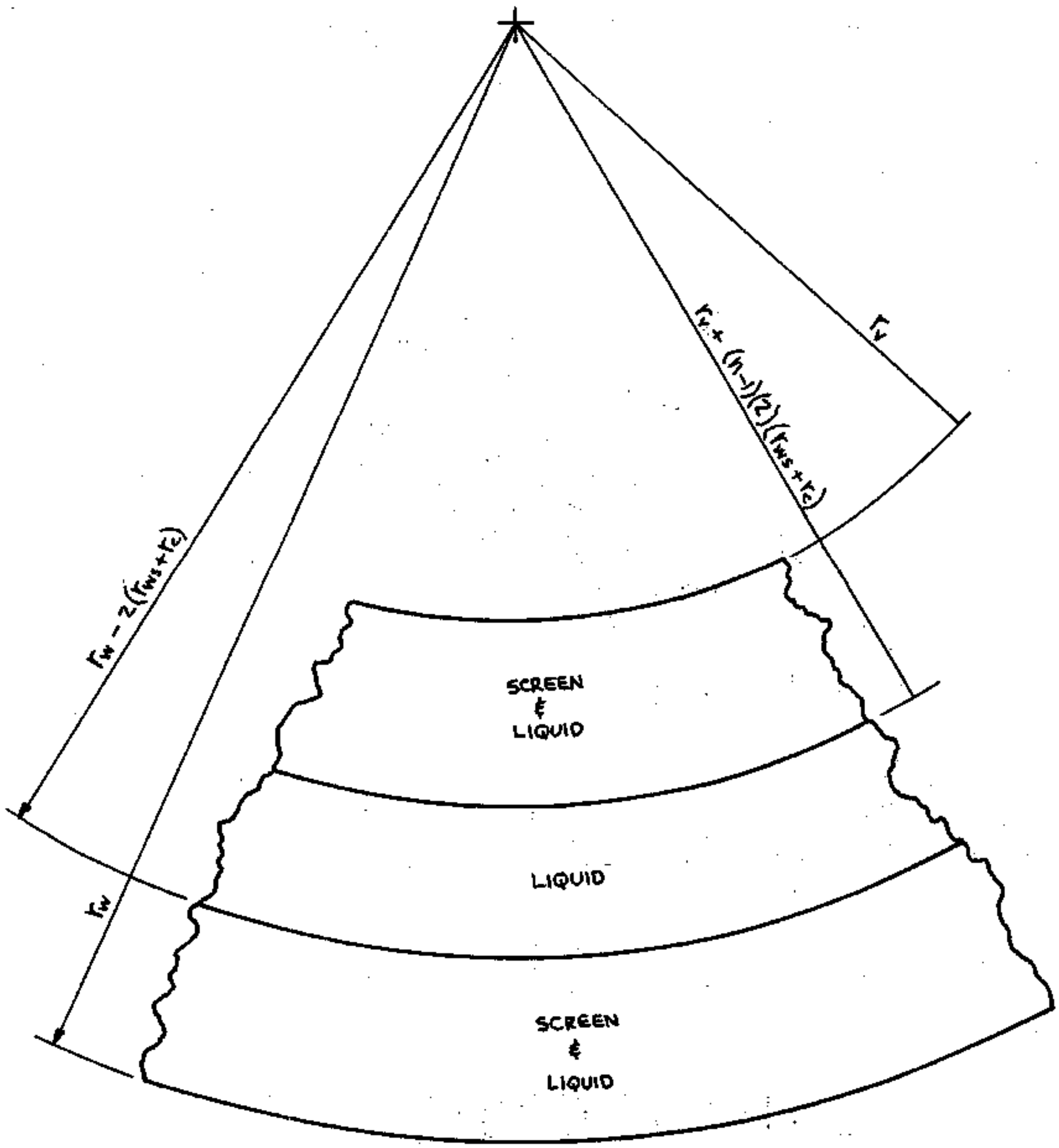

Figure R-2. Annular Cross Section for Conduction Through Screen Layers with Liquid Gap.

$$R_B = \frac{\ln\left(\dfrac{r_w - 2(r_{ws}+r_c)}{r_v + 2(r_{ws}+r_c)}\right)}{2\pi \chi_\ell \ell} \text{, and} \qquad (R.10)$$

$$R_c = \frac{\ln\left(\dfrac{r_v + 2(r_{ws}+r_c)}{r_v}\right)}{2\pi \chi_w \ell} \, . \qquad (R.11)$$

Combining the resistances in series gives

$$R_{eff} = R_A + R_B + R_c \, , \qquad (R.12)$$

where R_{eff} is the effective thermal resistance of the wick given by

$$R_{eff} = \frac{\ln\left(\dfrac{r_w}{r_v}\right)}{2\pi \chi_{eff} \ell} \, . \qquad (R.13)$$

Combining Equations (R.9) through (R.13) and expressing in nondimensional form gives

$$\frac{\chi_\ell}{\chi_{eff}} = \frac{1}{\ln\left(\frac{r_w}{r_v}\right)} \left\{ \left(\frac{\chi_\ell}{\chi_w}\right)\left[\ln\left(\frac{r_w}{r_w - 2r_c - 2r_{ws}}\right) + \right.\right. \qquad (R.14)$$

$$\left.\left. + \ln\left(\frac{r_v + 2(n-1)\, r_c \left(1 + \frac{r_{ws}}{r_c}\right)}{r_v}\right)\right] + \ln\left(\frac{r_w - 2r_c\left(1 + \frac{r_{ws}}{r_c}\right)}{r_v + 2(n-1) r_c \left(1 + \frac{r_{ws}}{r_c}\right)}\right)\right\} ,$$

where n is the number of screen layers (two for this investigation) forming a wick with one layer of screen at the outer annulus, a liquid gap at the second annulus, and other screen layers constituting the inner annulus.

Equations (R.7) and (R.14) together express the effective thermal conductivity of the wick used in this investigation.

APPENDIX S

EVALUATION OF EVAPORATOR ACTIVE LENGTH FROM MEASURED PARAMETERS

Evaluation of the evaporator active length from experimental data is based on a data reduction model in which the pipe shell is a fin with 1) axial heat flow within the fin, 2) heat addition along the outside of the fin from the evaporator heating coils, and 3) heat rejection along a fraction of the inside of the fin to the heat pipe wick (see Figure S-1). For this model, the necessary experimental data include the healing coil power, the heat loss rate to the surroundings from the evaporator, the heat pipe operating temperature (vapor temperature), and the temperature at an axial location along the designed evaporator length. The equations necessary for this data reduction model are developed and solved, and a sample calculation made for Test 2 (Chapter IV, Table 7).

1. Development of Expression for L_e

The energy balance for the differential control volume of length dx shown in Figure S-1 is described by the diagram of

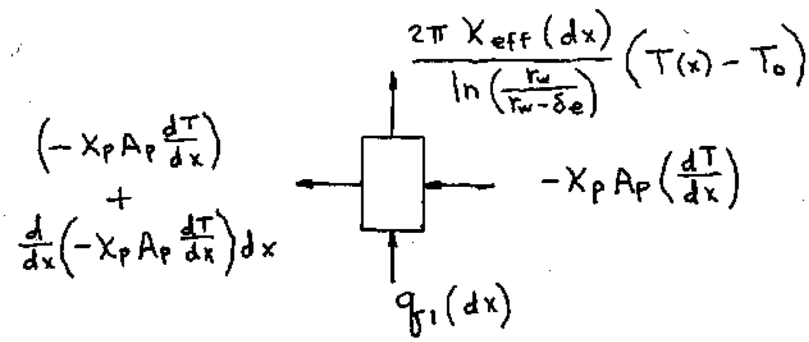

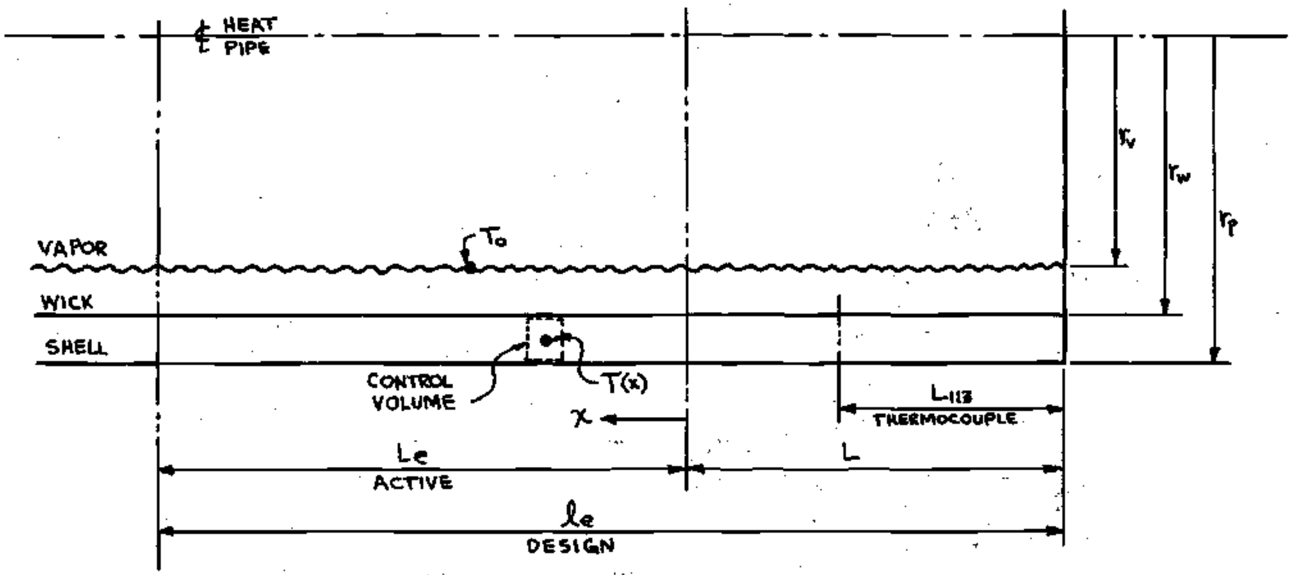

Figure S-1. Shell Diagram for Evaporator.

where

$$q_1 = \frac{\dot{Q}_E}{l_e} \quad , \text{ and} \tag{S.1}$$

$$A_p = \pi\left(r_p^2 - r_w^2\right) \quad . \tag{S.2}$$

Balancing these energy terms gives

$$-\chi_p A_p \left(\frac{dT}{dx}\right) + \frac{d}{dx}\left(-\chi_p A_p \frac{dT}{dx}\right) dx + \frac{2\pi \chi_{eff}\, dx}{\ln\left(\frac{r_w}{r_w - \delta_e}\right)}\left(T(x) - T_o\right) = \tag{S.3}$$

$$= \frac{\dot{Q}_E}{l_e}(dx) - \chi_p A_p \frac{dT}{dx} \quad .$$

Cancelling terms and assuming constant pipe shell thermal conductivity gives

$$-\chi_p A_p \frac{d^2T}{dx^2} + \frac{2\pi \chi_{eff}}{\ln\left(\frac{r_w}{r_w - \delta_e}\right)}\left(T(x) - T_o\right) = \frac{\dot{Q}_E}{l_e} \quad , \text{ or} \tag{S.4}$$

$$\frac{d^2T}{dx^2} - \frac{1}{l_e^2}\frac{R_p}{R_w} T = -\left[\frac{R_p}{R_w}\frac{1}{l_e^2} T_o + \frac{1}{l_e^2} R_p \dot{Q}_E\right] , \tag{S.5}$$

where

$$R_p = \frac{l_e}{\chi_p A_p} \quad , \text{ and} \tag{S.6}$$

$$R_w = \frac{\ln\left(\frac{r_w}{r_w - \delta_e}\right)}{2\pi \chi_{eff}\, l_e} \quad . \tag{S.7}$$

The boundary conditions for Equation (S.5) are

$$\text{B.C. 1)} \qquad x = 0 \quad , \quad -\chi_p A_p \frac{dT}{dx} = \dot{Q}_E \frac{L}{l_e} - \dot{Q}_{s,e} \quad , \tag{S.8}$$

where $\dot{Q}_{s,e}$ is the heat rate from the evaporator section to the surroundings (see Appendix I),

$$\text{B.C. 2)} \qquad X = L_{113} - L \,, \qquad T = T_{113} \,, \tag{S.9}$$

where T_{113} is the temperature measured by thermocouple number 113. (TC-113), and

$$\text{B.C. 3)} \qquad X = L_e \,, \qquad \frac{dT}{dx} = 0 \,, \tag{S.10}$$

i.e., no further axial conduction along the shell. Three boundary conditions are required for solving Equation (S.5) since Equation (S.5) is of second order, and the origin of the coordinate (describing the position of L_e) is unknown.

The general solution to Equation (S.5) is

$$T(x) = C_1 \cosh(\lambda x) + C_2 \sinh(\lambda x) + T_o + R_w \dot{Q}_E \,, \tag{S.11}$$

where

$$\lambda = \frac{1}{\ell_e} \left(\frac{R_P}{R_W}\right)^{1/2} . \tag{S.12}$$

Substitution of the boundary conditions, Equations (S.8) and (S.9) gives the solution of

$$T(x) = \left[\frac{(T_{113} - T_o) - R_W \dot{Q}_E}{\cosh(\lambda(L_{113} - L))} + \left(Q_E \frac{L}{\ell_e} - \dot{Q}_{s,e}\right) \times \right. \tag{S.13}$$

$$\left. \times (R_P R_W)^{1/2} \frac{\sinh(\lambda(L_{113} - L))}{\cosh(\lambda(L_{113} - L))} \right] \times \cosh(\lambda X) - (R_P R_W)^{1/2} \times$$

$$\times \left(Q_E \frac{L}{\ell_e} - \dot{Q}_{s,e}\right) \sinh(\lambda X) + T_o + R_W \dot{Q}_E \, .$$

Substitution of the boundary condition of Equation (S.10), Equation (S.12), and the identities

$$L_e + L = \ell_e \quad , \text{ and} \tag{S.14}$$

$$\left(\cosh A\right)\left(\cosh B\right) - \left(\sinh A\right)\left(\sinh B\right) = \cosh\left(A-B\right) \tag{S.15}$$

gives the solution for L_e as

$$\frac{L_e}{\ell_e} = \left(1 - \frac{\dot{Q}_{s,e}}{\dot{Q}_E}\right) - \left[\frac{T_{113} - T_o}{\dot{Q}_E\left(R_p R_w\right)^{1/2}} - \left(\frac{R_w}{R_p}\right)^{1/2}\right]\left[\frac{\sinh\left(\left(\frac{R_p}{R_w}\right)^{1/2}\frac{L_e}{\ell_e}\right)}{\cosh\left(\left(\frac{R_p}{R_w}\right)^{1/2}\left(1 - \frac{L_{113}}{\ell_e}\right)\right)}\right] . \tag{S.16}$$

The position of thermocouple number 113 is given by

$$\frac{L_{113}}{\ell_e} = \frac{1}{4} . \tag{S.17}$$

For typical heat pipe operation in this investigation,

$$\frac{L_e}{\ell_e} > 0.5 \quad , \text{ and} \tag{S.18}$$

$$\left(\frac{R_p}{R_w}\right)^{1/2}\frac{L_e}{\ell_e} > 10 \quad , \text{ hence} \tag{S.19}$$

$$\frac{\sinh\left(\left(\frac{R_p}{R_w}\right)^{1/2}\left(\frac{L_e}{\ell_e}\right)\right)}{\cosh\left(\frac{3}{4}\left(\frac{R_p}{R_w}\right)^{1/2}\right)} = \frac{\frac{1}{2}\, e^{\left(\frac{R_p}{R_w}\right)^{1/2}\frac{L_e}{\ell_e}}\left[1 - e^{-2\left(\frac{R_p}{R_w}\right)^{1/2}\frac{L_e}{\ell_e}}\right]}{\frac{1}{2}\, e^{\frac{3}{4}\left(\frac{R_p}{R_w}\right)^{1/2}}\left[1 + e^{-\frac{3}{2}\left(\frac{R_p}{R_w}\right)^{1/2}}\right]} , \tag{S.20}$$

hence the bracket terms may be approximated as unity. This approximation, and Equation (S.16) gives

$$\frac{L_e}{\ell_e} = \left(1 - \frac{\dot{Q}_{s,e}}{\dot{Q}_E}\right) - \left[\frac{T_{113}-T_o}{Q_E\,(R_p R_w)^{1/2}} - \left(\frac{R_w}{R_p}\right)^{1/2}\right] e^{\left(\frac{R_p}{R_w}\right)^{1/2}\left(\frac{L_e}{\ell_e}-0.75\right)} . \qquad (S.21)$$

Equation (S.21) is the expression used to reduce experimental data to obtain the evaporator active length ratio.

2. Sample Calculation

For Test 2 (Chapter IV, Table 7) the values of the variables are:

$Q_{s,e}$ = 22.18 BTU/hr (from Appendix I),

Q_E = 252.50 BTU/hr (from Appendix I),

T_o = 102.37°F (from Appendix E with method of Appendix H),

T_{113} = 210.90°F (from Appendix E with method of Appendix H),

ℓ_e = 3.36 inches,

r_w = 0.326 inches

r_v = 0.298 inches, and

r_p = 0.375 inches.

The value of the evaporator wick thickness parameter $\frac{\delta_e}{r_w - r_v}$ is approximated by using Equation (V.33), re-written as

$$\left(\frac{\delta_e}{r_w - r_v}\right) = f_3\left(\frac{r_w}{r_v}, \frac{r_{ws}}{r_c}, \frac{r_c}{r_v}, \frac{r_m}{r_c}, \phi\right), \qquad (S.22)$$

where the function f_3 is plotted in Figure 24 for parameter values used in this investigation (see Appendix T). The meniscus radius ratio, Equation (V.46), re-written as

$$\frac{r_m}{r_c} = \frac{2\left[\frac{\rho_\ell \sigma h_{v\ell}}{\mu_\ell}\frac{\pi r_c^2}{\dot{Q}_e}\right]\frac{\left(\left(\frac{r_w}{r_v}\right)^2-1\right)}{\left(\frac{r_c}{r_v}\right)^2}}{\left[K_1 r_c \ell_c\right]\left(\frac{1}{2}\frac{L_e}{\ell_e}\frac{\ell_e}{\ell_c} + \frac{\ell_a}{\ell_c} + \frac{1}{2}\frac{L_c}{\ell_c}\right)}, \qquad (S.23)$$

is first evaluated with the additional parameters of

r_c = .00275 inches,

$K_1 \equiv 2.61 \times 10^8$ 1/ft^2 (from Appendix N),

Q_e = 230.32 BTU/hr (from Appendix I), and

$\frac{\rho_\ell \sigma h_{v\ell}}{\mu_\ell} = 7.976 \times 10^{10}$ BTU/hr ft^2, where

ρ_ℓ = 61.966 lbm/ft^3 (for water (40), methanol (33)),

$\sigma = 4.778 \times 10^{-3}$ lbf/ft (for water (42), methanol (42)),

$h_{v\ell}$ = 1035.7 BTU/lbm (for water (40), methanol (33)),

$\mu_\ell = 138.4 \times 10^{-7}$ lbf/sec/ft^2 (for water (40), methanol (41)).

Substitution of these values into Equation (S.23) gives

$$\frac{r_m}{r_c} = 4.10 \quad .$$

From Figure 24, at = 45°,

$$\frac{\delta_e}{r_w - r_v} = 0.865 \quad .$$

Hence the remaining parameters are

δ_e = 0.865(.028) = 0.02422 inches,

χ_p = 9.39 BTU/hr ft$^\circ$R (from Reference (16), at temperature of TC-113), and

χ_{eff} = 0.6474 BTU/hr ft$^\circ$R (by method of Appendix R, and References (40) and (16), at temperature T_o).

The resistance terms are

$$R_p = \frac{\ell_e}{\chi_p \pi (r_p^2 - r_w^2)} = 39.792 \ \frac{HR\ R^\circ}{BTU} \quad ,$$

$$R_w = \frac{\ln\left(\frac{r_w}{r_w - \delta_e}\right)}{2\pi \chi_{eff} \ell_e} = 0.06178 \ \frac{HR\ R^\circ}{BTU} \quad , \text{ and}$$

$$\left(\frac{R_p}{R_w}\right)^{1/2} = 24.230 \quad .$$

Substitution of these values into Equation (S.21) gives

$$\frac{L_e}{l_e} = 0.91216 - \frac{0.2204}{e^{24.23\left(0.75 - \frac{L_e}{l_e}\right)}} \quad .$$

Using Newton's method of approximation for an iterative solution gives

$$\frac{L_e}{l_e} = 0.740 \quad .$$

APPENDIX T

DERIVATION OF RELATION FOR EVAPORATOR EFFECTIVE WICK THICKNESS

The retreat, in the radial direction, of the liquid-vapor interface into the wick of the evaporator section is modeled by a spherical surface, radius r_m, attached, with contact angle ϕ, to a solid torus, inside radius r_c and solid radius r_{ws}, see Figure T-1. The effective thickness is taken as the height from the bounding surface below to the minimum point of the spherical surface. For given values of r_v, r_w, r_{ws}, r_m, and ϕ, the thickness δ_e is implicitly determined with the aid of the generating angle α. From Figure T-1, the geometrical relations are

$$r_m \cos(\alpha+\phi) + r_{ws}\cos\alpha = r_{ws} + r_c \text{ , and} \tag{T.1}$$

$$\delta_e = (r_w - r_v) - 2r_{ws} + r_{ws}\sin\alpha + r_m \sin(\alpha+\phi) - r_m . \tag{T.2}$$

Expressing in dimensionless form gives

$$\frac{r_m}{r_c} = \frac{1 + \frac{r_{ws}}{r_c}(1-\cos\alpha)}{\cos(\alpha+\phi)} \text{ , and} \tag{T.3}$$

$$\left(\frac{\delta_e}{r_w - r_v}\right) = \left(1 - \frac{2r_{ws}}{r_w - r_v}\right) + \left(\frac{r_{ws}}{r_w - r_v}\right)\sin\alpha - \left(\frac{r_c}{r_w - r_v}\right)\frac{r_m}{r_c}\left(1 - \sin(\alpha+\phi)\right). \tag{T.4}$$

Eliminating the generating parameter α by combining Equations (T.3) and (T.4) results in the function form of

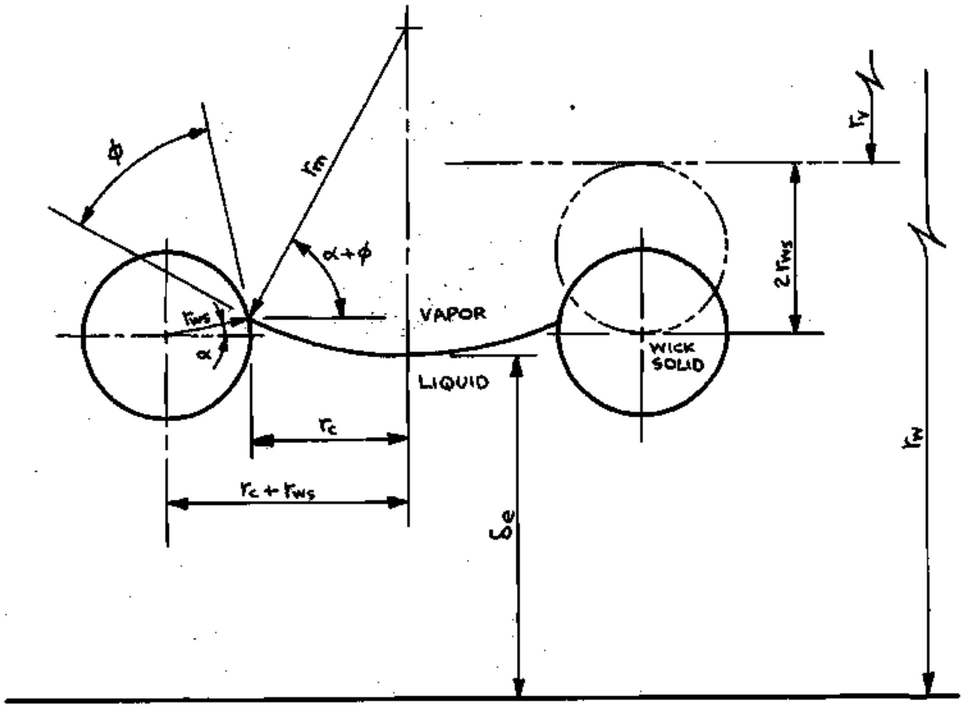

PARAMETER VALUES (THIS INVESTIGATION)

r_w = 0.326 in.
r_v = 0.298 in.
r_c = 0.00275 in.
r_{ws} = 0.00225 in.

Figure T-1. Interface Model for Derivation of δ_e.

$$\left(\frac{\delta_e}{r_w - r_v}\right) = f_3\left(\frac{r_w}{r_v}, \frac{r_{ws}}{r_c}, \frac{r_c}{r_v}, \frac{r_m}{r_c}, \phi\right). \tag{T.5}$$

From algebra and simple trigonometric identities, the explicit form of δ_e is found to be

$$\begin{aligned}
\left(\frac{\delta_e}{r_w - r_v}\right) = 1 - \Bigg\{ \Bigg[& \frac{\frac{r_c}{r_v}\left(\frac{r_{ws}}{r_c} + \frac{r_m}{r_c}\right)}{\left(\frac{r_w}{r_v} - 1\right)} + \Bigg\{\left(\frac{r_m}{r_c}\cos\phi + \frac{r_{ws}}{r_c}\right)^2 + \\
& + \left(\frac{r_m}{r_c}\sin\phi\right)^2\Bigg\}^{-1} \Bigg\{ \Bigg[\left(\frac{r_m}{r_c}\sin\phi\right)\left(\frac{\frac{r_c}{r_v}\left(\frac{r_{ws}}{r_c} + \frac{r_m}{r_c}\cos\phi\right)}{\left(\frac{r_w}{r_v} - 1\right)}\right) - \\
& - \Bigg[\Bigg\{ \left(\left(\frac{r_m}{r_c}\sin\phi\right)\left(\frac{\frac{r_c}{r_v}\left(\frac{r_{ws}}{r_c} + \frac{r_m}{r_c}\cos\phi\right)}{\left(\frac{r_w}{r_v} - 1\right)}\right) - \left(\frac{r_{ws}}{r_c} + \frac{r_m}{r_c}\cos\phi\right) \times \right. \\
& \left. \times \left(\frac{\frac{r_c}{r_v}\frac{r_m}{r_c}\sin\phi}{\frac{r_w}{r_v} - 1}\right)\right]\Bigg\}^2 - \left\{\left(\frac{r_{ws}}{r_c} + \frac{r_m}{r_c}\cos\phi\right)^2 + \left(\frac{r_m}{r_c}\sin\phi\right)^2\right\} \times \\
& \times \Bigg\{ \left(\frac{\frac{r_c}{r_v}\frac{r_m}{r_c}\sin\phi}{\frac{r_w}{r_v} - 1}\right)^2 + \left(\frac{\frac{r_c}{r_v}\left(\frac{r_{ws}}{r_c} + \frac{r_m}{r_c}\cos\phi\right)}{\frac{r_w}{r_v} - 1}\right)^2 - \\
& - \left\{ \frac{\frac{r_c}{r_v}\left(\frac{r_{ws}}{r_c} + \frac{r_m}{r_c}\cos\phi\right)^2}{\left(\frac{r_w}{r_v} - 1\right)} + \frac{\frac{r_c}{r_v}\left(\frac{r_m}{r_c}\sin\phi\right)^2}{\left(\frac{r_w}{r_v} - 1\right)} \right\}^2 \Bigg\}^2 \Bigg]^{1/2} \Bigg] \Bigg\} \Bigg\} \Bigg].
\end{aligned} \tag{T.6}$$

Chapter V, Figure 24 indicates a plot of $\frac{\delta_e}{r_w - r_v}$ vs. $\frac{r_m}{r_c}$ for the values of r_c, r_{ws}, r_w, and r_v used in this investigation.

APPENDIX U

EVALUATION OF INTERNAL THERMAL RESISTANCE

The internal overall thermal resistance is given by Equation (V-68) as

$$R = \frac{\bar{T}_{ew} - \bar{T}_{cw}}{\dot{Q}_e} , \qquad \text{(U.1)}$$

where $\bar{T}_{ew}$ and $\bar{T}_{cw}$ are the average temperatures at r_w along the active lengths of evaporator (L_e) and condenser (L_c) respectively. Evaluation of measured and predicted values of the resistance R, used in Figure 34, is accomplished by substituting measured and predicted wall temperatures into Equation (U.1). A sample calculation is made for Test 2 (Chapter IV, Table 7).

1. Evaluation of R from Predicted Parameters

The predicted values of the average wall temperatures are evaluated from simple conduction models through the active lengths of the wick. For the condenser,

$$\bar{T}_{cw} = T_o - \dot{Q}_e \frac{\ln\left(\frac{r_w}{r_{vc}}\right)}{2\pi \chi_{eff} L_c} , \text{ or} \qquad \text{(U.2)}$$

$$\bar{T}_{cw} = T_o - \dot{Q}_e \frac{\ln\left(\frac{r_w}{r_v}\right)}{2\pi \chi_\ell \ell_c} \left(\frac{\chi_\ell}{\chi_{eff}}\right)\left(\frac{\ell_c}{L_c}\right) . \qquad \text{(U.3)}$$

For the evaporator,

$$\bar{T}_{ew} = T_o + \dot{Q}_e \frac{\ln\left(\frac{r_w}{r_{ve}}\right)}{2\pi \chi_{eff} L_e}, \text{ or} \tag{U.4}$$

$$\bar{T}_{ew} = T_o + \dot{Q}_e \frac{\ln\left(\frac{r_w}{r_w - \delta_e}\right)}{2\pi \chi_\ell \ell_e} \left(\frac{\chi_\ell}{\chi_{eff}}\right)\left(\frac{\ell_e}{L_e}\right). \tag{U.5}$$

For Test 2 of Table 7, the solution of the system of Equations (V-46) through (V-55) with the independent parameter values of

$\dot{Q}_e$ = 230.32 BTU/hr,

U_c = 234.89 BTU/hr ft^2 $^\circ$R,

T_c = 70.43°F,

gives the predicted parameter values of

T_o = 102.55°F,

χ_ℓ = 0.3622 BTU/hr ft $^\circ$R,

$\frac{\chi_\ell}{\chi_{eff}}$ = 0.5593,

$\delta_e = (r_w - r_v)\left[\frac{\delta_e}{r_w - r_v}\right]$ = (0.028)(0.865) = 0.02422 inches,

$\frac{L_c}{\ell_c}$ = 0.809,

$\frac{L_e}{\ell_e}$ = 0.743.

Substitution of these values into Equations (U.3) and (U.5) gives

$$\bar{T}_{cw} = 87.47^\circ F,$$

$$\bar{T}_{ew} = 123.55^\circ F.$$

Substitution of these values into Equation (U.1) gives the predicted value of thermal resistance as

$$R = 0.1567 \frac{hr\ ^\circ R}{BTU} .$$

2. Evaluation of R from Measured Parameters

The measured values of the average wall temperatures along the active lengths are evaluated from simple heat transfer models based on thermocouple measurements of the shell temperature. For the condenser,

$$\bar{T}_{cw} = \bar{T}_p + \dot{Q}_e \frac{\ln\left(\frac{r_p}{r_w}\right)}{2\pi K_p L_c} , \quad \text{or} \tag{U.6}$$

$$\bar{T}_{cw} = \bar{T}_p + \dot{Q}_e \frac{\ln\left(\frac{r_p}{r_w}\right)}{2\pi K_p \ell_c} \left(\frac{\ell_c}{L_c}\right) , \tag{U.7}$$

where $\bar{T}_p$ is the average measured temperature at $r = r_p$ along L_c. For the evaporator, the data reduction technique of Appendix S is used to evaluate $\bar{T}_{ew}$ from measured parameters. This average temperature is given by

$$\bar{T}_{ew} = \frac{1}{L_e} \int_0^{L_e} T(x)\, dx , \tag{U.8}$$

where T(x) is given by Equation (S.13). Substitution of Equation (S.16) into Equation (S.13) and evaluation of the integral of Equation (U.8) gives

$$\bar{T}_{ew} = T_{113} - R_w \dot{Q}_E \left\{ \left[\left(\frac{\ell_e}{L_e}\right)\left(1 - \frac{\dot{Q}_{se}}{\dot{Q}_e}\right) - 1 \right] \left[\left(\frac{L_e}{\ell_e}\right)\left(\frac{R_p}{R_w}\right)^{1/2} \frac{\cosh\left(\frac{3}{4}\left(\frac{R_p}{R_w}\right)^{1/2}\right)}{\sinh\left(\frac{L_e}{\ell_e}\left(\frac{R_p}{R_w}\right)^{1/2}\right)} - 1 \right] \right\}, \quad (U.9)$$

where T_{113} is the temperature measured by thermocouple number 113. For Test 2, Table 7, the term values based on measured parameters are

$\bar{T}_p = 85.57°F$ (from Appendix Q),

$\chi_p = 8.42$ BTU/hr ft°R (from Reference (16)),

$\frac{L_c}{\ell_c} = 0.814$ (from Appendix Q),

$\dot{Q}_e = 230.32$ BTU/hr (from Appendix I),

$T_{113} = 210.90°F$ (from Appendix E with method of Appendix H),

$R_w = 0.06778$ hr°R/BTU (from Appendix S),

$R_p = 39.792$ hr°R/BTU (from Appendix S),

$\dot{Q}_E = 252.50$ BTU/hr (from Appendix I),

$\dot{Q}_{se} = 22.18$ BTU/hr (from Appendix I), and

$\frac{L_e}{\ell_e} = 0.740$ (from Appendix S).

Substitution of these values into Equations (U.7) and (U.9) gives

$\bar{T}_{cw} = 87.37°F$,

$\bar{T}_{ew} = 123.92°F$.

Substitution of these values into Equation (U.1) gives the measured value of thermal resistance as

$$R = 0.1587 \ \frac{HR\ °R}{BTU} .$$

APPENDIX V

DATA AND THEORIES OF OTHER INVESTIGATIONS

1. Kunz, et al., Reference (17)

A calculation is made for Kunz's theory on capillary limited maximum heat transfer rate for the materials and geometries used in this investigation. From Equation (II.33),

$$Q_{MAX.} = \left(\frac{\rho_\ell \sigma h_{v\ell}}{\mu_\ell}\right)\frac{(b\delta)}{1}\frac{4}{K_1(2\ell_{eff})r_{min.}} \quad . \qquad (V.1)$$

For this investigation, typical parameter values are:

$$\frac{\rho_\ell \sigma h_{v\ell}}{\mu_\ell} = 7.82 \times 10^{10} \ \frac{BTU}{HR\ FT^2}$$

(for water at 100°F, see also Appendix U),

$$b = \pi(r_w + r_v) = \pi(.326 + .298) = 1.9604 \text{ in.} \ ,$$

$$\delta = r_w - r_v = .326 - .298 = 0.028 \text{ in.} \ ,$$

$K_1 = 2.61 \times 10^8 \ 1/FT^2$ (see Appendix N),

$$2\ell_{eff} = 2\left(\tfrac{1}{2}\ell_e + \ell_a + \tfrac{1}{2}\ell_c\right) = 3.36 + 2(9.64) + 5.0 = 27.64 \text{ in., and}$$

$$r_{min.} = \frac{r_c}{\cos\phi} = \frac{.00275}{(.707)} = 0.0038897 \text{ in.} \quad .$$

Using these values gives

$$Q_{MAX} = 611.9 \ \frac{BTU}{HR} \quad .$$

2. Sun and Tien, Reference (34)

A calculation is made of the Sun and Tien parameters which indicate the presence of axial heat conduction along wick and pipe shell. From Equations (II.39) and (II.40)

$$M^2 = \frac{2\left(\frac{\chi_{eff}}{\chi_p}\right)\left(\frac{l}{r_w}\right)^2}{\left(\left(\frac{r_p}{r_w}\right)^2 - 1\right)\ \ln\left(\frac{r_w}{r_v}\right)} \quad \text{, and} \tag{V.2}$$

$$B_i = \frac{H\ r_p}{\chi_{eff}}\ \ln\left(\frac{r_w}{r_v}\right) \quad . \tag{V.3}$$

For this investigation, typical parameter values are:

l = 18.0 inches,

r_p = 0.375 inches,

r_w = 0.326 inches,

r_v = 0.298 inches,

χ_p = 8.52 BTU/hr ft °R (for 304 stainless steel at 100°F, from Reference (16)),

χ_{eff} = 0.645 BTU/hr ft °R (by method of Appendix R, and Reference (40) and (16) at 100°F), and

H = 220 BTU/hr ft^2 °R (by methods of Appendix K).

Using these values gives

$$M = 126 \text{ , and}$$
$$B_i = 0.957 \ .$$

Since $M > 100$ and $B_i < 1$ Sun and Tien suggest axial conduction is negligible.

3. Schwartz, Reference (29)

The experimental work of Schwartz provides data for the indication of variation in active condenser long the Schwartz did not refer to an active length, but concluded the effective wick thermal conductivity to be a variable. Schwartz's data is reduced to the present correlation by calculating the active condenser length. For condenser heat transfer, the active length is expressed by

(V.4)

where is the temperature difference across the wick. The vapor axial Reynold's number is given by

$$Re = \frac{\rho V(2r_v)}{\mu} = \frac{2}{\pi}\frac{\dot{Q}_e}{r_v \mu_v h_{vl}} \quad . \tag{V.5}$$

Schwartz's materials and parameter values are

working fluid: water

wick: 100 mesh stainless steel screen,

geometry: $r_w = 0.199$ in.

$r_v = 0.189$ in.

$\ell_c = 2.8$ in. .

From Appendix R

$$\frac{X_l}{X_{eff}} = 0.305 \quad .$$

Using these values and Equations (V.4) and (V.5), Schwartz's data is reduced as:

test	T_o	Q	ΔT	L_c/ℓ_c	Re_v
	^oF	BTU/hr	F^o	~	~
1	98	61.7	3.1	0.592	104.5
2	134	169.3	6.4	0.756	272.0

4. Miller and Holm, Reference (24)

The experimental work of Miller and Holm provides data for the indication of variation in active condenser length. Miller did not recognize this variation. Miller's materials and parameter values for the model heat pipe are

working fluid: water

wick: 200 mesh nickel screen

geometry: $r_w = 0.412$ in.

$r_v = 0.352$ in.

$\ell_c = 5.0$ in.

From Appendix T,

$$\frac{\chi_A}{\chi_{eff}} = 0.061 .$$

Using these values and Equations (V.4) and (V.5), Miller's data is reduced as:

test	T_o ^oF	Q BTU/hr	ΔT F^o	L_c/ℓ_c ~	Re_v ~
1	310	62.8	2.8	0.209	44.5
2	323	68.0	2.4	0.264	47.6
3	336	72.4	2.7	0.250	50.6
4	350	77.9	3.2	0.228	54.1
5	363	83.3	2.7	0.292	57.8
6	380	90.5	3.0	0.288	62.7

5. Fox, et al., Reference (10)

The experimental work of Fox, et al. provides data for the indication of variation of active evaporator length. Fox did not refer to an active length, but concluded that a vapor film was present in sections along the outer region of the evaporator wick and liquid along the inner region. Fox's materials and parameter values are

working fluid: water

wick: 100 mesh stainless steel screen

geometry: $r_w = 0.722$ in.

$r_v = 0.672$ in.

$\ell_c = 6.0$ in.

Although the Fox data was incomplete to permit correlation, Figure (V-1), redrawn from Figure 2 of Reference (34), does indicate a variation in active length. The vapor film concluded by Fox would explain the magnitude of thermal resistance along the evaporator, but not the variation of thermal resistance. From Figure (V.1) it is seen that the slope, expressed by

$$\frac{L_e}{\ell_e} = A \frac{\dot{Q}}{\Delta T} , \qquad (V.6)$$

where A is a constant, does decrease for increased power levels, indicating the active length does decrease.

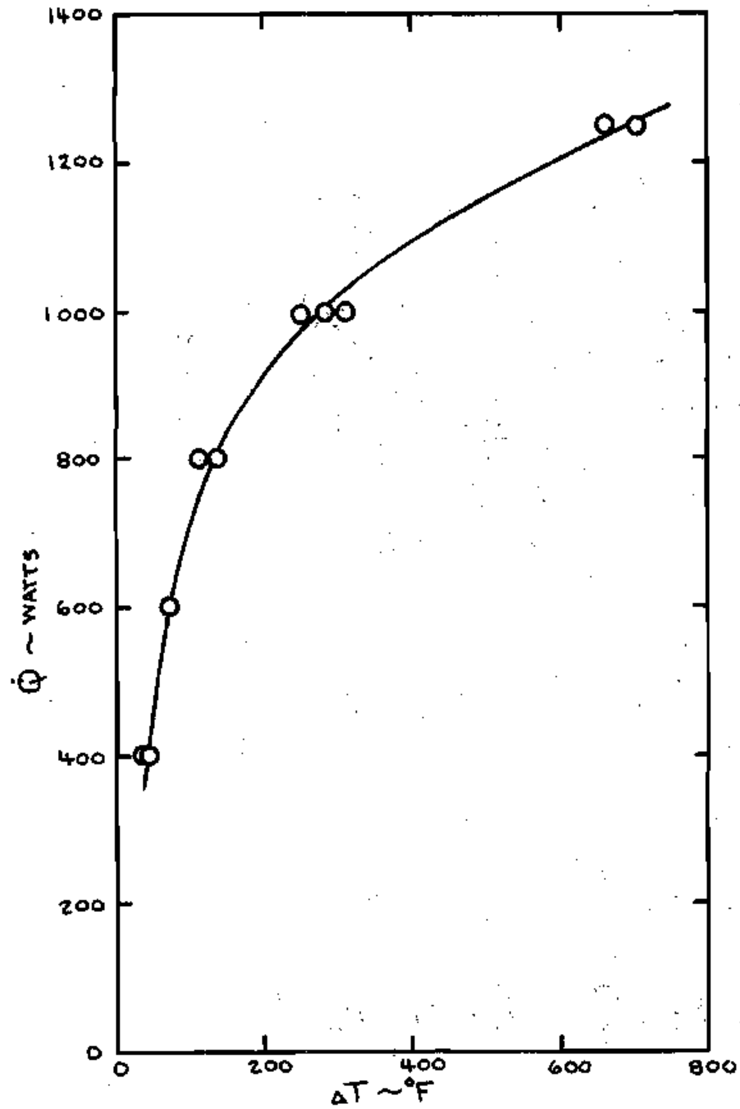

Figure V-1. Power Versus Evaporator Wick Temperature Difference for Data of Fox, et al. (10).

BIBLIOGRAPHY

1. Bankston, C. A. and Smith, H. J., "Incompressible Laminar Vapor Flow in Cylindrical Heat Pipes," A.S.M.E. Winter Annual Meeting, 71-WA/HT-15, Washington, D. C., November 1971.

2. Bienert, W. B. and Brennan, P. J., "Transient Performance of Electrical Feedback-Controlled Variable-Conductance Heat Pipes," S.A.E./A.S.M.E./A.I.E.E. Life Support and Environmental Control Conference, 71-Av-27, San Francisco, California, July 1971.

3. Bird, R. B., Stewart, W. E., and Lightfoot, E. N., Transport Phenomena, John Wiley and Sons, Inc., New York, 1960.

4. Cheung, H., "A Critical Review of Heat Pipe Theory and Applications," Lawrence Radiation Laboratory, UCRL-50453, July 1968.

5. Chi, S. W. and Cygnarowicz, T. A., "Theoretical Analysis of Cryogenic Heat Pipes," A.S.M.E., Space Technology and Heat Transfer Conference, Los Angeles, California, 70-HT/SpT-6, June 1970.

6. Colwell, G. T., Williams, C. L., Hsu, J. C., and Zevallos, G. E., "A Study of Noncondensable Effects in a Heat Pipe," Nuclear Technology, Vol. 10, No. 3, pp. 293-300, March 1971.

7. Cosgrove, J. H., Ferrel, J. K. and Carnesale, A., "Operating Characteristics of Capillarity-Limited Heat Pipes," Journal of Nuclear Technology, Vol. 21, pp. 547-558, 1967.

8. Cotter, T. P., "Theory of Heat Pipes," Los Alamos Scientific Laboratory, LA-3246-MS, March 1965.

9. Edwards, D. K., Fleischman, G. L., and Marcus, B. D. "User's Manual for the TRW Gaspipe Program (A Vapor-Gas Front Analysis Program for Heat Pipes Containing Non-Condensible Gas)," CR-114306, Accession No. N71-29908, April 1971.

10. Fox, R. D., Carothers, K. G., and Thompson, W. J., "Internal Temperature Distributions in an Operational Heat Pipe," Backup Document for A.I.A.A. Synoptic Scheduled for Publication in A.I.A.A. Journal, July 1972, Accession No. N72-18959, March 1972.

11. Grover, G. M., Cotter, T. P., and Erickson, G. F., "Structures of Very High Thermal Conductance," Journal of Applied Physics, Vol. 35, pp. 1900-1991, 1964.

12. Kemme, J. E., "Heat Pipe Capability Experiments," I.E.E.E. Thermionic Conversion Specialist Conference, Conference Records, pp. 159-168, November 1966.

13. Kessler, S. W., Jr., "Transient Thermal Impedance of a Water Heat Pipe," A.S.M.E. Winter Annual Meeting, 71-WA/HT-9, Washington, D. C., November 1971.

14. Kocamustafaogullari, G. and Zuber, N., "The Effects of Heat and Mass Transfer on the Dynamics of Liquid Films," unpublished report, Georgia Instutite of Technology, Atlanta, Georgia, 1970.

15. Knight, B. W. and McInteer, B. B., "Laminar Incompressible Flow in Channels with Porous Walls," Los Alamos Scientific Laboratory, LADC-5309.

16. Kreith, F., Principles of Heat Transfer, International Textbook Company, Scranton, Pennsylvania, 1966.

17. Kunz, H. R., Langston, L. S., Hilton, B. H., Wyde, S. S., and Nashick, G. H., "Vapor-Chamber Fin Studies, Transport Properties and Boiling Characteristics of Wicks," NASA CR-812, June 1967.

18. Kunz, H. R., Wyde, S. S., Nashick, G. H., and Barnes, J. F., "Vapor-Chamber Fin Studies, Operating Characteristics of Fin Models," NASA CR-1139, August 1968.

19. Levy, E. K., "Theoretical Investigation of Heat Pipes Operating at Low Pressures," A.S.M.E. Transactions, Journal of Engineering for Industry, Vol. 90, pp. 547-552, November 1969.

20. Levy, E. K. and Chou, S. F., "Vapor Compressibility Effects in Heat Pipes," Contract AT(30-1)-4095, (NYO-4095-1, PR-1), May 1970.

21. Lyman, F. A. and Huang, Y. S., "Analysis of Temperature Distributions in Heat Pipe Wicks," A.S.M.E.-A.I.Ch.E. Heat Transfer Conference, 69-HT-23, Minneapolis, Minnesota, August 1969.

22. McKinney, B. G., "An Experimental and Analytical Study of Water Heat Pipes for Moderate Temperature Ranges," (Ph.D. Thesis), University of Alabama, June 1969.

23. McSweeney, T. I., "The Performance of a Sodium Heat Pipe," A.I.Ch.E.-A.S.M.E., Eleventh National Heat Transfer Conference, A.I.Ch.E. 7, Minneapolis, Minnesota, August 1969.

24. Miller, P. L. and Holm, F. W., "Investigation of Constraints in Thermal Simlitude, Volume II," AFFDL-TR-69-91, December 1969.

25. Neal, L. G., "An Analytical and Experimental Study of Heat Pipes," TRW Systems, TRW-99900-6114-R000, EM-17-5, January 1967.

26. Parker, G. H. and Hanson, J. P., "Heat Pipe Analysis," I.E.E.E. Thermionic Conversion Specialist Conference, Conference Records, pp. 847-857, 1967.

27. Scheidegger, A. E., The Physics of Flow Through Porous Media, Macmillan, 1960.

28. Schwartz, J., "Performance Map of an Ammonia (NH_3) Heat Pipe," A.S.M.E. Space Technology and Heat Transfer Conference, 70-HT/SpT-5, Los Angeles, California, June 1970.

29. Schwartz, J., "Performance Map of the Water Heat Pipe and the Phenomenon of Noncondensible Gas Generation," A.S.M.E.-A.I.Ch.E. Heat Transfer Conference, 69-HT-15, Minneapolis, Minnesota, August 1969.

30. Schrage, R. W., A Theoretical Study of Interphase Mass Transfer, Columbia University Press, New York, 1950.

31. Seban, R. A. and Abhat, A., "Steady and Maximum Evaporization from Screen Wicks," A.S.M.E. Winter Annual Meeting, 71-WA/HT-12, Washington, D. C., November 1971.

32. Shinnick, W. A., Director, Technology Application Center, University of New Mexico, "Heat Pipe Technology, A Bibliography with Abstracts," Cumulative Volumes, March 1971-September 1972.

33. Smith, J. M., "Thermodynamic Properties of Methyl Alcohol," Chemical Engineering Progress, Vol. 44, No. 7, pp. 521-528, 1948.

34. Sun, K. H. and Tien, C. L., "Simple Conduction Model for Theoretical Steady-State Heat Pipe Performance," A.I.A.A. Journal, Vol. 10, No. 8, August 1972.

35. Watts, J. L., "A Heat Pipe Optimization Code, LAM2," Lawrence Radiation Laboratory, UCID-15462.

36. White, F. M., Jr., "Laminar Flow in Porous Ducts," (Ph.D. Thesis), Georgia Institute of Technology, March 1959.

37. Wilcox, S. and Rohsenow, W., "Film Condensation of Potassium Using Copper Condensing Block for Precise Wall Temperature Measurement," A.S.M.E. Transactions, Journal of Heat Transfer, Vol. 92, No. 3, p. 359, August 1970.

38. Winter, E. R. F. and Borsch, W. O., "The Heat Pipe," Advances in Heat Transfer, Vol. 7, 1971.

39. Yuan, S. W. and Finkelstein, A. B., "Laminar Pipe Flow with Injection and Suction Through a Porous Wall," A.S.M.E. Transactions, Vol. 78, pp. 719-724, 1956.

40. 1967 ASME Steam Tables, Thermodynamic and Transport Properties of Steam, The American Society of Mechanical Engineers, New York, 1968.

41. Handbook of Chemistry and Physics, 51st Edition, The Chemical Rubber Company, Cleveland, Ohio, 1970.

42. International Critical Tables of Numerical Data, Physics, Chemistry and Technology, Volume IV, McGraw-Hill Book Company, New York, 1928.

43. Thermophysical Properties of Matter, Thermal Conductivity, Nonmetallic Liquids and Gases, Vol. 3, Purdue University, IFI/Plenum, New York, 1970.

44. Thermophysical Properties of Matter, Specific Heat-Nonmetallic Liquids and Gases, Vol. 6, Purdue University, IFI/Plenum, New York, 1970.

VITA

Colquitt Lamar Williams was born in Valdosta, Georgia, on June 20, 1944, the son of Mr. and Mrs. Walter H. Williams Jr. He received elementary and high school education in Gulfport, Anona, and Largo, Florida. He attended the Georgia Institute of Technology from 1962 to 1967 on the Co-operative Plan where he won the degree of Bachelor in Mechanical Engineering in June, 1967. In June, 1968, he obtained a Master of Science in Mechanical Engineering and continued work on the Doctor of Philosophy degree at Georgia Tech. His financial support in graduate school was by an NDEA Fellowship and teaching assistantships in thermodynamics and fluid flow.

He married Carrolyn Jo Lovering, a native of Lakeland, Florida in January, 1973.